Design and Synthesis of L-Proline Containing Polymer Assemblies with Tuneable Catalytic Activity

Submitted for the degree of Doctor of Philosophy

August 2013

Annhelen Lu

Department of Chemistry

THE UNIVERSITY OF WARWICK

Table of Contents

Declaration of authorship

This thesis is submitted in to the University of Warwick in support of my application for the degree of Doctor of Philosophy. It has been composed by myself and has not been submitted in any previous application for any degree. The work presented was carried out by the author, except Chapter 4 which was carried out in collaboration with Ms Dafni Moatsou at the University of Warwick. Any data analysis carried out by persons other than the author is clearly labelled.

Acknowledgements

Firstly I would like to thank my supervisor Rachel O'Reilly for the opportunity to work with her, for all her support and invaluable advice. I am grateful to EPSRC for providing me with funding and the Department of Chemistry for the excellent facilities.

I would also like to thank Dr Deborah Longbottom for her expertise in organic chemistry, fruitful discussions and her very kind words of encouragement throughout my PhD. Special thanks also go to Prof. Michael Monteiro for taking such good care of me during my stay in Australia.

A huge thanks to all previous and current O'Reilly group members, without your guidance and awesome company (and snack breaks), finishing my thesis would have been much more difficult. I am particularly grateful to Pepa, Joe, Helen and Dafni for all their advice and support, you guys are awesome. Special thanks to Claire and the O'Reilly triathletes; I have had so much fun learning how to swim (and run!) and I have truly enjoyed our time together.

Finally and most importantly I want to thank my family, friends and my lovely boyfriend for all their support all these years when they watched me get more and more crazy and moody. Thanks to my sisters for becoming my personal psychologists in my darkest moments (i.e. crawled-up-in-a-ball-in-the-corner-in-the-dark-crying). I cannot promise my mood swings are necessarily PhD or thesis related and that they won't come back, but I love you all.

List of publications

- C. Evans, A. Lu, C. Ondeck, D. A. Longbottom, R. K. O'Reilly, Organocatalytic Tuneable Amino Acid Polymers Prepared by Controlled Radical Polymerization, *Macromolecules*, 2010, 43, 6374-6380. DOI: 10.1021/ma1008447
- A. Lu, T. P. Smart, T. H. Epps III, D. A. Longbottom, R. K. O'Reilly, L-Proline functionalized polymers prepared by RAFT polymerization and their assemblies as supported organocatalysts, *Macromolecules*, 2011, 44, 7233-7241. DOI: 10.1021/ma201256m (**Chapter 2**)
- P. Cotanda, A. Lu, J. P. Patterson, N. Petzetakis, R. K. O'Reilly, Functionalized organocatalytic nanoreactors: hydrophobic pockets for acylation reactions in water, *Macromolecules*, 2012, 45, 2377, DOI: 10.1021/ma2027462
- A. Lu, P. Cotanda, J. P. Patterson, D. Longbottom and R. K. O'Reilly, Aldol Reactions Catalyzed by L-Proline Functionalized Polymeric Nanoreactors in Water, *Chem. Commun*. 2012, 48, 9699-9701, DOI: 10.1039/C2CC35170F (**Chapter 3**)
- A. Lu, D. Moatsou, D. A. Longbottom and R. K. O'Reilly, Tuning the Catalytic Activity of L-Proline Functionalized Hydrophobic Nanogel Particles in Water, *Chem. Sci*. 2013, 4, 965-969, DOI: 10.1039/C2SC21300A (**Chapter 4**)
- A. Lu and R. K. O'Reilly, Advances in nanoreactor technology using polymeric nanostructures, *Curr. Opin. Biotech.*, 2013, 24, 639-645, DOI: 10.1016/j.copbio.2012.11.013
- J. P. Patterson, P. Cotanda, E. G. Kelley, A. O. Moughton, A. Lu, T. H. Epps, III and R. K. O'Reilly, Catalytic Y-tailed amphiphilic homopolymers – aqueous

nanoreactors for high activity, low loading SCS pincer catalysts, *Polym. Chem.* 2013, 4, 2033-2039, DOI: 10.1039/C3PY21137A

- B. L. Moore, A. Lu, D. A. Longbottom and R. K. O'Reilly, Immobilization of MacMillan Catalyst *via* Controlled Radical Polymerization: Catalytic Activity and Reuse, *Polym. Chem.* 2013, 4, 2304-2312, DOI: 10.1039/C3PY21125H
- H. A. Zayas, A. Lu, D. Valade, F. Amir, Z. Jia, R. K. O'Reilly and M. J. Monteiro, Thermoresponsive Polymer-Supported L-Proline Micelle Catalysts for the Direct Asymmetric Aldol Reaction in Water, *ACS Macro Lett.*, 2013, 2, 327-331, DOI: 10.1021/mz4000943
- Y. Kang, A. Lu, A. Ellington, M. Jewett and R. K. O'Reilly, Effect of Complementary Nucleobase Interactions in the Copolymer Composition of RAFT copolymerization, *ACS Macro Lett.*, 2013, 2, 581-586, DOI: 10.1021/mz4001833
- J. P. Patterson, E. Kelley, R. Murphy, A. O. Moughton, M. Robin, A. Lu, O. Colombani, C. Chassenieux, D. Cheung, M. Sullivan, R. K. O'Reilly, T. H. Epps, III, Y-Tailed Amphiphilic Homopolymer Micelles: Structural Characterization by Light Scattering, SANS and Cryo-TEM, *Macromolecules*, 2013, 46, 6319-6325, DOI: 10.1021/ma4007544
- H. Willcock, A. Lu, C. F. Hansell, E. Chapman, I. R. Collins, R. K. O'Reilly, One-pot synthesis of responsive sulfobetaine nanoparticles by RAFT polymerisation: the effect of branching on the UCST cloud point, *Polym. Chem.*, 2014, 5, 1023-1030, DOI: 10.1039/c3py00998j
- B. L. Moore, D. Moatsou, A. Lu and R. K. O'Reilly, Studying the activity of the MacMillan catalyst embedded within hydrophobic crosslinked polymeric nanostructures, *Polym. Chem*. 2014, 5, 3487-3494, DOI: 10.1039/C3PY01734F

- C. F. Hansell, A. Lu, J. P. Patterson and R. K. O'Reilly, Exploiting the tetrazine-norbornene reaction for single polymer chain collapse, *Nanoscale*, 2014, 6, 2033-2039, DOI: 10.1039/C3NR06706H
- B. L. Moore, A. Lu, D. Moatsou and R. K. O'Reilly, The effect of polymer nanostructure on diffusion of small molecules using Tryptophan as a FRET probe, Eur. Polym. J, 2015, 62, 380-385, DOI: 10.1016/j.eurpolymj.2014.06.003
- A. Lu, D. Moatsou, I. Hands-Portman, D. A. Longbottom and R. K. O'Reilly, Recyclable L-Proline functional nanoreactors with temperature-tuned activity based on core-shell nanogels, *ACS Macro Lett*., 2014, 3, 1235-1259, DOI: 10.1021/mz500704y

Abbreviations

δ	chemical shift
λ	wavelength
AIBN	2,2'-azo-bis(isobutyronitrile)
AM	ammonium molybdate
ATRP	atom-transfer radical polymerization
Bn	benzyl ester
Boc	di-*tert*-butyl-dicarbonate
BuA	butyl acrylate
^{t}BuA	*tert*-butyl acrylate
^{n}BuMA	*n*-butyl methacrylate
^{t}BuMA	*tert*-butyl methacrylate
CBz	benzyl carbamate
CLD	cross-linking density
CMC	critical micelle concentration
COSY	correlation spectroscopy
CRP	controlled radical polymerization
CS	core-shell
CSC	core-shell-corona
CTA	chain transfer agent
d	doublet
Da	Daltons (g mol^{-1})
D_{av}	average diameter
DIEA	*N*,*N*-diisopropylethylamine
DLS	dynamic light scattering

DMA	dimethylacrylamide
DMAP	dimethylaminopyridine
DMF	dimethyl formamide
DMSO	dimethyl sulfoxide
D_h	hydrodynamic radius
DoF	degree of catalyst functionalization
DP	degree of polymerization
EDCI	*N*-Ethyl-*N'*-(3-dimethylaminopropyl)carbodiimide hydrochloride
ee	enantioselectivity
EMA	ethyl methacrylate
eq	equivalents
GO	graphene oxide
HPLC	high performance liquid chromatography
IR	infrared
J	coupling constant
KPS	potassium persulfate
LMA	lauryl methacrylate
LCST	lower critical solution temperature
m	multiplet
MA	methyl acrylate
MMA	methyl methacrylate
mol%	mole percent
M_n	number average molecular weight
M_w	weight average molecular weight
MW	molecular weight
MWCO	molecular weight cut off

NIPAM	*N*-isopropylacrylamide
NMP	nitroxide mediated polymerization
NMR	nuclear magnetic resonance
NP	nanoparticle
NR	Nile Red
PAA	poly(acrylic acid)
PMAA	poly(methacylic acid)
PMMA	poly(methyl methacrylate)
PS	polystyrene
PVC	polyvinylchloride
q	quartet
RAFT	reversible addition-fragmentation chain transfer agent
RI	refractive index
RT	room temperature
s	singlet
SDS	sodium dodecyl sulfate
SEC	size exclusion chromatography
SEM	scanning electron microscopy
St	styrene
TEA	triethylamine
TEM	transmission electron spectroscopy
TFA	trifluoroacetic acid
THF	tetrahydrofuran
TON	turnover number
UA	uranyl acetate
UCST	upper critical solution temperature

Summary

The general concepts of the thesis are introduced in Chapter 1, including polymerization techniques employed to synthesize our catalytic nanoreactors and our motivations behind the work in this thesis.

In Chapter 2 the catalytic activity of the amino acid L-proline after functionalization onto a polymer backbone was investigated. This was achieved using reversible addition-fragmentation chain transfer (RAFT) polymerization yielding copolymers with predictable molecular weights and catalyst incorporation.

Chapter 3 discusses the synthesis and self-assembly of block copolymers to yield polymer micelles with the catalytic motif contained within the hydrophobic micelle core. The application of polymer micelles as nanoreactors in water was assessed and the influence of core hydrophobicity on catalytic activity investigated. The effect of tethering the catalytic moiety to the micelle shell was also examined.

In Chapter 4 the catalytic motif is incorporated into cross-linked nanogels and the property of the scaffold was investigated more in depth, such as the effect of cross-linking density and degree of functionalization on catalytic activity and selectivity. The hydrophobic nature of the nanogel and its importance in maintaining high selectivity was further examined.

Chapter 5 reviews the possibility of using core-shell nanogels as recyclable nanoreactors. A thermo-responsive shell was introduced and the catalytic dependency of the core-shell nanostructures on temperature was investigated. The morphology of the shell was found to have a significant effect on the catalytic efficiency of the nanostructrues.

1. Introduction

1.1 Polymerization techniques

1.1.1 Living polymerization

Anionic and cationic polymerization have for many years been used to synthesize polymers and block copolymers with well-defined molecular weights and narrow molecular weight distribution.[1] These were categorized as 'living' processes as the polymerization process continues upon addition of a second batch of monomer; thus, all active centers at the chain end must be retained during the time-scale of the experiment. Nevertheless, extremely stringent reaction conditions are required, including high monomer purity and complete removal of oxygen and water from the polymerization.[2,3] Thus, the polymerization is required to meet the following criteria to be considered a 'living' process:[4]

- Monomers must reach 100% conversion and the polymerization must continue upon further monomer additions
- Monomer conversion is directly proportional to final polymer molecular weight
- Concentration of active chains is equal to the concentration of initiator, and the number of active chains must be independent of monomer conversion
- Final polymer molecular weight is controlled by stoichiometry
- Polymers with narrow molecular weight distribution is achieved
- Block copolymers can be synthesized *via* the addition of a second monomer species
- Polymers can be chain end functionalized

Hence, by carefully controlling the polymerization conditions it is possible to synthesize a range of block copolymers with pre-determined molecular weights and active chain ends for further polymerizations or functionalization.[5]

1.1.2 Controlled radical polymerization

In more recent years a number of controlled radical polymerization (CRP) techniques have been developed with advantages from both the living and radical polymerization processes.[6,7] These exhibit the versatility of conventional free radical polymerization as well as the control of traditional living processes. They are more tolerant to trace impurities from the radical process and thus less stringent or vigorous conditions are required.[8,9] Three main steps are typically involved in a CRP polymerization, initiation, propagation and termination. The polymerization is initiated in the first step *via* the formation of a reactive radical, monomer units are subsequently added to the radical in the propagation step resulting in chain growth. Finally, the polymerization is terminated by recombination to remaining radicals or between polymer chain ends.

In order to obtain control over the polymerization process, controlling the propagation step is key. This step is often faster than the initiation step which results in the growth of some polymer chains during the initiation of other chains and can be controlled by maintaining a low concentration of the propagating radicals, reducing inter-chain termination. In CRP, the concentration of propagating radicals is controlled by the establishing a dynamic equilibrium between the propagating species and a deactivated species. This can be achieved by two general mechanisms, by reversible deactivation and degenerative transfer between the propagating chain and dormant polymer species. Atom transfer radical polymerization (ATRP)[10–12] relies on the formation of a dormant species using organometallic compounds which can be catalytically reactivated. Nitroxide mediated polymerization (NMP)[13] relies on a similar process using nitroxyl radicals to stabilize the dormant species and are reversibly deactivated by temperature. Reversible addition-fragmentation chain transfer (RAFT) polymerization relies on a

degenerative transfer process between a chain transfer agent and the growing polymer chain.[14–18]

1.1.2.1 Nitroxide Mediated Polymerization (NMP)

In NMP, the overall radical concentration is reduced by using a nitroxide species such as 2,2,6,6-tetramethylpiperidinyl-1-oxy (TEMPO) to reversibly cap the growing polymer radical chain end to yield a dormant alkoxyamine species (Scheme 1.1, **A**). Crucially, the C-ON bond of (**A**) is homolytically unstable and undergoes thermal fragmentation to yield (**B**), a nitroxide species and (**C**), a polymer radical. It is important that nitroxide species (**B**) cannot initiate polymer growth and is only able to react with carbon-centered free radicals. Polymer radical (**C**) then undergoes polymerization and to yield (**D**), a chain extended polymer radical which recombines with (**B**) to re-form the dormant species (**E**). This cycle is then repeated and control over the polymerization is achieved as termination events have been minimized.[9,19] However, the compatibility of this polymerization process is limited to styrenic monomers as the control over methacryalates and acrylates type polymerizations have been reported to be poor.[9] Moreover, relatively high temperatures are required (*ca.* 125 °C).

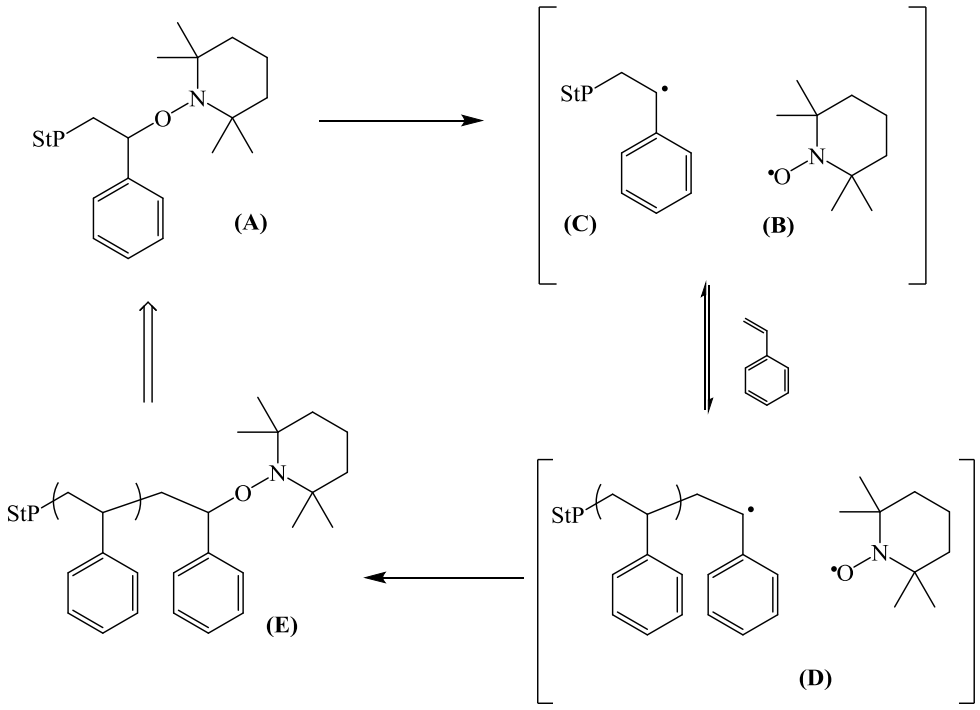

Scheme 1.1. NMP of styrene using TEMPO as the initiator

A more superior initiator to the commonly used TEMPO has been developed by the Hawker group which has enabled the polymerization of acrylates and acrylamides in addition to styrenes (Figure 1.1). This initiator has allowed for the synthesis of chain end functional polymers.[9,19–21]

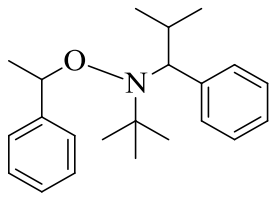

Figure 1.1. Hawker's universal NMP initiator[21]

1.1.2.2 Atom Transfer Radical Polymerization (ATRP)

ATRP was independently developed by Matyjaszewski and co-workers[22] and Sawamoto and co-workers,[23] and follows a reversible deactivation mechanism using a halide (X) and a transition metal complex. A dynamic equilibrium between the dormant and active

species is established through a reversible redox process catalyzed by the metal complex *via* electron exchange with the halide (Scheme 1.2).[22,23] The first step of the polymerization process is the homolytic fission of the P-X bond, with the transition metal complex initially in a low oxidation state. Upon oxidation of the transition metal ion, a carbon centered radical is generated and can react with monomers to produce a polymer radical. The halide is subsequently transferred back onto the growing polymer chain yielding a dormant polymer chain and a reduced transition metal complex. At the end of the polymerization, halide terminated polymers are achieved and these can be re-activated to yield block copolymers.[22] Polymers with narrow molecular weight distribution are achieved by careful selection of the transition metal complex and initiator which dictates the rate of monomer addition and initiation processes respectively.[12,24,25]

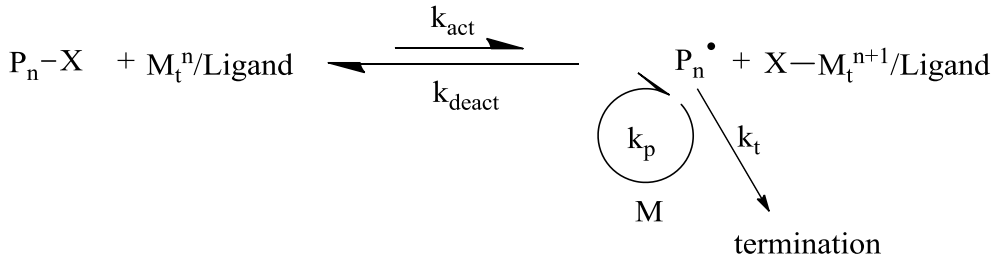

Scheme 1.2. Representation of ATRP polymerization

A range of monomers including acrylonitrile, styrene, acrylate and methacrylates can be polymerized by ATRP.[12] Importantly, the polymer can be easily end group modified with a range of functionalities.[26] Nevertheless, ATRP may not be applicable in the synthesis of polymers for biomedical and catalytic applications, due to the presence of residual transition metals such as Cu and Fe, commonly used metal catalysts.[27]

1.1.2.3 Reversible addition-fragmentation chain transfer (RAFT)

RAFT is the latest CRP technique to be developed and was reported in 1998 by researchers at CSRIO in Australia.[14,28–30] RAFT polymerization utilizes a chain transfer agent (CTA) or RAFT agent to mediate the polymerization *via* a reversible chain transfer process between the active propagating species and a dormant species capped with the RAFT agent. Polymerizations can be carried out in both aqueous and organic media[15] and unlike ATRP does not require the use of metal complexes which is advantages in the synthesis of biocompatible polymers. Moreover, relatively low polymerization are generally used (~65 °C), unlike NMP which requires comparatively higher polymerization temperatures. The polymerization can be initiated thermally or through the use of a suitable initiator, such as AIBN.

The most important feature of RAFT is the CTA, which controls the equilibrium between active and dormant polymer species and hence the resulting polymer molecular weight distribution.[31,32] The CTAs can be divided into four general types, trithiocarbonates, xanthates, dithioesters and dithiocarbamates (Figure 1.2). Although CTAs are prepared using materials such as carbon disulfide, their simple synthetic procedure allows an infinite number of CTAs to be synthesized,[16] which can be readily tailed to polymerized a vast range of monomers, hydrophobic, hydrophilic and those with functionality.[16] This is an advantageous feature of RAFT and explains its evolution since its discovery. Wood *et al.* have made significant contributions in this area, reporting a simply method for the synthesis of CTA using non-toxic materials.[33]

trithiocarbonate

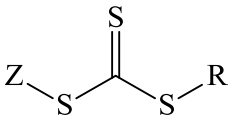

xanthate

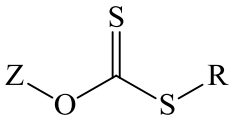

dithioester

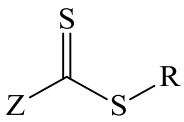

dithiocarbamate

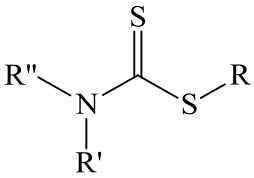

Figure 1.2. Structural representation of the four types of CTAs

The compatibility and efficiency of the CTA to mediate the polymerization of certain monomers is dependent on the nature of the Z and R-group, where the R-group is a free-radical leaving group that must be capable of reinitiating polymerization and the Z-group influences the reactivity of the C=S bond towards radical addition.[14,34] Generally, dithioesters and trithiocarbonates are more susceptible to radical addition as they have high transfer constants and thus tend to polymerize styrenes, acrylates, methacrylates, acrylamides and methacrylamides. Conversely, xanthates and dithiocarbamates are less susceptible towards radical attack due to the formation of the zwitterionic canonical structures (Figure 1.3). These structures reduce the double bond character of the C=S bond, making them less active towards "more activated monomers" (MAMs) such as styrene and methacrylates and more active towards "less activated monomers" (LAMs) such as vinyl acetates and *N*-vinylcarbazole.[35] Nevertheless, if an electron withdrawing substituent or a substituent that facilitates the delocalization of the lone pairs is present, the CTAs are likely to be more effective with a wider range of monomers.[17]

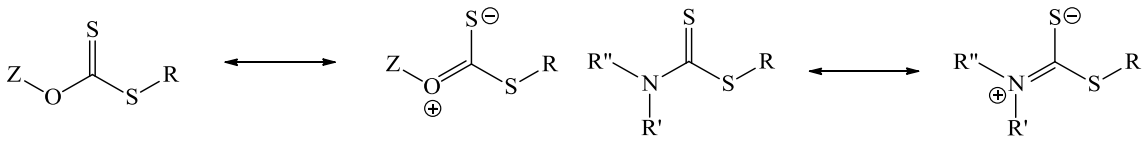

Figure 1.3. Zwitterionic canonical structures of xanthates and dithiocarbamates are represented.

It is important that the Z-group is able to stabilize the radical species but it also needs to be able to fragment for the reversible addition/fragmentation process to occur (Scheme 1.3). As already mentioned, the R-group must be a good leaving group compared to the propagating polymer chain, but must also be able to re-initiate the polymerization (Scheme 1.4). Thus, the R- and Z-groups can be tailored to suit almost any monomers. More recently, universal RAFT agents have been developed which allows efficient polymerization of LAMs followed by chain extension with MAMs and *vice versa*.[35,36]

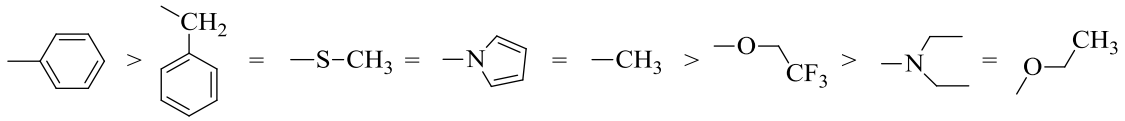

Scheme 1.3. RAFT CTA Z-groups, with decreasing addition rate and increasing fragmentation rates going from left to right

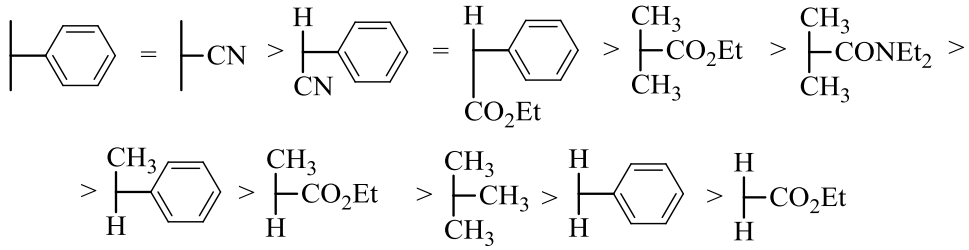

Scheme 1.4. RAFT CTA R-groups, with decreasing fragmentation rates going from left to right.

RAFT mechanism

The polymerization is initiated by the decomposition of the radical initiator to yield the radical species, $I^{\bullet}$ which reacts with the monomer (Scheme 1.5). In the chain transfer

step the growing polymer ($P_n^{\bullet}$) reacts with the CTA, at the C=S bond, forming a radical polymer intermediate. It is important that the C=S bond is reactive, i.e. high k_{add}. The intermediate species can undergo fragmentation to release the R-group or reversibly towards the initial growing polymer chain $P_n^{\bullet}$. The R-group can then reinitiate polymerization to start the growth of a new polymer chain, $P_m^{\bullet}$. Once all the CTA has been consumed, both polymer chains P_n and P_m enter the main chain equilibrium where they will continue to grow. Rapid exchange between the active and dormant polymer chains will ensure both chains will grow equally.[17] Moreover, as a result of the stable nature of the dormant species, the concentration of active radicals in solution is always lower than the concentration of dormant species. This effectively controls the polymerization and yields polymers with pre-determined molecular weights with narrow molecular weight distribution.[37]

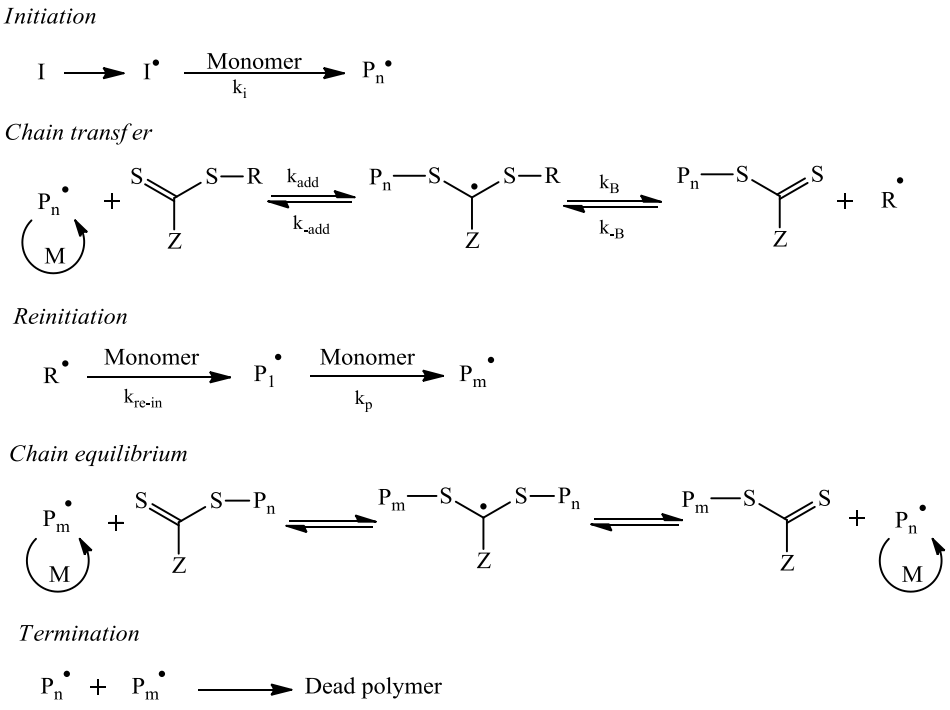

Scheme 1.5. RAFT polymerization mechanism

The success of RAFT is much related to its versatility and compatibility with a range of monomers and reaction conditions.[14–18,38] Nevertheless, RAFT has some drawbacks, one of them being the colour of the resulting polymer as a result of the coloured CTA. However, white polymers can be achieved by post-polymerization modification or removal of the end group.[34,39–42]

1.2 Heterogeneous polymerization techniques

Heterogeneous polymerizations such as suspension, emulsion, precipitation and dispersion polymerizations have been used to prepare a range of polymer particles which can measure from nanometres to millimetres.[43] The type of polymerization is dictated by the characteristics of the heterogeneity such as:

- Two phased system, oil-in-water or water-in-oil
- Monomer and/or resulting polymer is immiscible in the continuous phase
- Initiator is soluble in the continuous or monomer phase
- Monomer droplets and resulting polymer particles are generally stabilized by an additive such as a steric stabilizer or surfactant

Perhaps the most applicable type of polymerization in industry is a typical oil-in-water polymerization, where relatively hydrophobic monomers such as styrene, butadiene, acrylate and methacrylates are stabilized in water by an emulsifier. Ionic and non-ionic surfactants are often used to provide this stabilization through physical adsorption or chemical incorporation onto the particle surface. The final particle size is determined in the nucleation process which is strongly influenced by both surfactant and initiator concentrations.

The four types of heterogeneous polymerizations may be distinguished based on a number of features including initial state and kinetics of the polymerization, mechanism

of particle formation and the final particle size and shape. In suspension polymerization the monomer and initiator are insoluble in the continuous phase and thus initiation occurs within the stabilized microdroplet.[44] After initiation, the monomer droplet is directly converted into the polymer particle with a size comparable to the initial droplet size, commonly in the 20 µm to 2 mm range. This technique is used to synthesize polyvinylchloride (PVC) and specific grades of PS.[45] Both dispersion[46] and precipitation[47] polymerization is homogeneous at the start and the final polymer is insoluble in the continuous phase. In both cases, initiation occurs in the continuous phase and the polymer grows until it reaches a critical length and becomes insoluble. The main difference between the two polymerizations is the stabilization of the insoluble particles where a steric stabilizer is used in the case of dispersion and no surfactant in the precipitation process. As the polymers begin to precipitate out of solution, particles form through aggregation of the nuclei and continue to grow by adsorption and continued polymerization from the continuous phase or by capture of oligomers or other particle nuclei. In order to achieve particles with uniform size and morphology it is important to control the precipitation speed which may be achieved by carefully matching the monomer, solvent and resulting polymer. Particles in the 0.1 to 5 µm size range are often achieved using precipitation and 0.1 to 10 µm for dispersion polymerization.

1.2.1 Emulsion polymerization

Particles in the range of 50 to 300 nm can be synthesized using emulsion polymerization.[48–50] In this case the initiator is soluble, the monomer sparingly soluble and the final polymer insoluble in the continuous phase. Initially, most of the monomers will be contained within a large monomer droplet, stabilized by surfactants, such as sodium dodecyl sulfate (SDS) (Scheme 1.6, **A**). There may also be monomer swollen

surfactant micelles in solution. Initiation will occur in the continuous phase, where the initiator is solubilized. As the growing oligomer reaches a critical length, whereby it can no longer remain in the continuous phase, they will enter surfactant micelles and continue to propagate acquiring monomer from the monomer droplet (Scheme 1.6, **B**). The growing particle is stabilized by surfactants from broken up micelle that did not contribute to particle nucleation or from the monomer droplet as more monomer is removed. When no further surfactant micelles containing growing polymer chains are able to form, the nucleation process is ended. In the particle growth stage, the nucleated particles grow in size by continued propagation of the polymer chain. This stage continues until the monomer droplet is completely depleted from monomer. The final stage involved continued polymerization until almost 100% of the monomer has been used up (Scheme 1.6, **C**).[51]

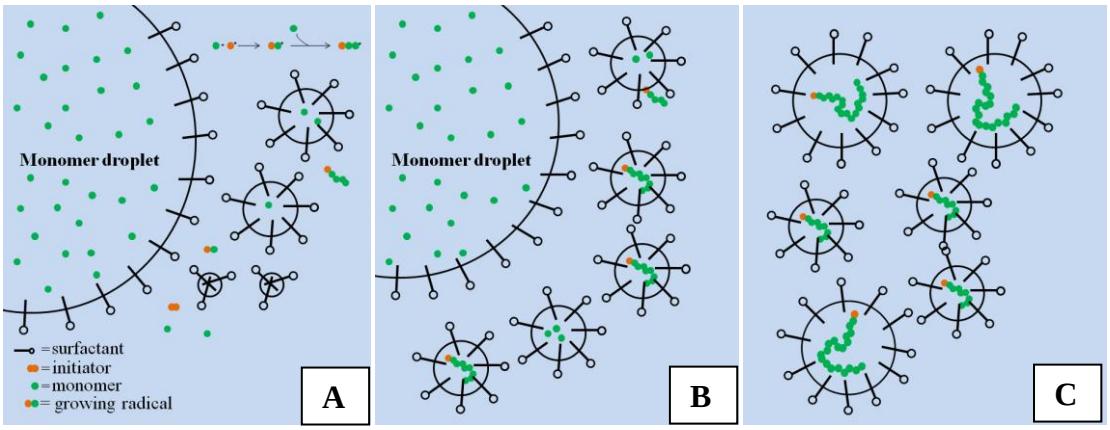

Scheme 1.6. Representation of a heterogeneous emulsion polymerization process

The main advantage of the emulsion process is the high conversion of monomers achieved where the particles achieved at the end of the polymerization can be directly used. This process has been used to polymerize a range of monomers including styrene,[52–54] methacrylates[55,56] and pH-responsive monomers such as 2-vinylpyridine (2VP)[57,58] and 2-(diethylamino)ethyl methacrylate (DEA).[59] The disadvantage of the

process is the remaining surfactant impurities which may be difficult to remove. If a cross-linker is added to the polymerization, cross-linked polymer particles will result[52] and these have additional advantages over non-cross-linked particles with enhanced stability in a range of conditions including changes in solvent, temperature and concentration.[53,60]

1.3 Self-Assembly amphiphilic block copolymers

Core-shell type supramolecular structures formed by the assembly of amphiphilic diblock copolymers are attractive systems due to their high stability and durability compared to small molecule assemblies. This advantageous property has made them relevant in applications such as drug delivery[61] and nanoreactors.[62] The spontaneous assembly of these polymers in selective solvents via non-covalent interactions may be readily tuned by controlling the polymer composition. Recent advances in CRP techniques[14,19,63] has allowed for the synthesis of well-defined polymers which in turn has made it possible to achieve a high level of control over the assembly process. A range of morphologies including spheres, cylinders and vesicles (or polymersomes) may be achieved by controlling the ratio of the hydrophobic and hydrophilic segments of the polymer amphiphile.[64,65] This determines the way the polymer chains pack upon assembly and thus the resulting morphology of the nanostructure. This packing parameter is calculated according to the following equation:[66]

$$p = \frac{v}{a_o l_c}$$

Equation 1.1. Equation to determine the packing parameter, p

where p is the packing parameter, v is the volume of the hydrophobic chains, a_o is the optimal area of the head group and l_c is the length of the hydrophilic tail. It has been

shown that spherical micelles are achieved when $p \leq 1/3$, cylindrical micelles when $1/3 \leq p \leq 1/2$ and finally vesicles when $1/2 \leq p \leq 1$.

The major driving force behind the spontaneous assembly process is a decrease in the overall free energy of the system through the elimination of energetically unfavourable interactions. The most common method for preparing polymer aggregates is *via* a solvent switch method which involves complete dissolution of both blocks in a common solvent and where upon addition of a specific concentration/volume of a non-solvent such as water, the hydrophobic segments will associate to limit unfavourable interactions with the water resulting in the formation of nanostructures. As previously mentioned, the morphology achieved is influenced by the copolymer composition which relates to the following three elements: the degree of stretching of the core-forming block, the surface tension at the core-corona interface and repulsive interactions among corona chains (Figure 1.4).[62,67] The quality of the common solvent is also of great important as it has been theorized by Nagarajan and Ganesh[68] and shown by Yu and Eisenberg[67] that it is possible to attain aggregates of different morphologies from the same initial copolymer by simply changing the common solvent.

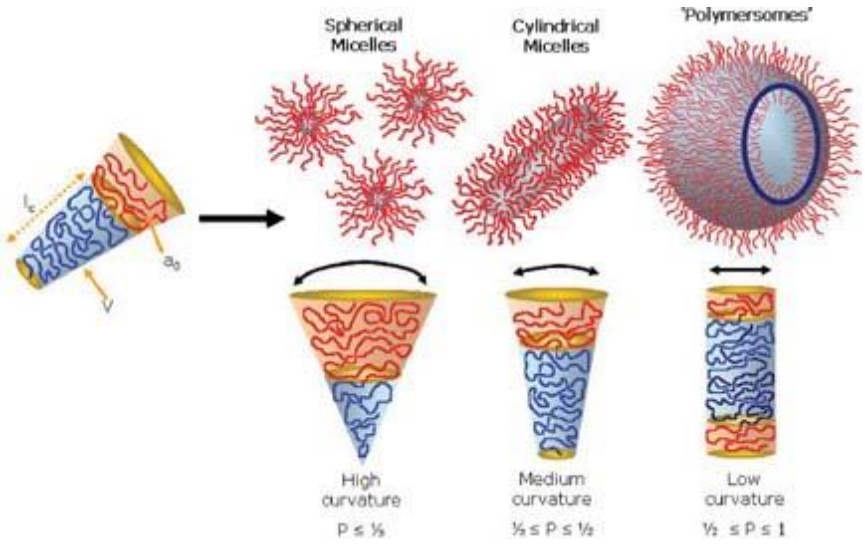

Figure 1.4. The influence of the packing parameter on the morphology of the self-assembled nanostructures[64]

Spherical micelles in water have been extensively studied as a hydrophobic cavity is presented upon assembly which may act as a protective compartment for lipophilic molecules (Figure 1.5). The availability of the compartment or core microenvironment to encapsulate hydrophobic molecules such as drugs and dyes has been shown by functionalizing reactive moieties within the micelle core for fluorescent tagging.[69] The possibility to carry out orthogonal reactions in both the shell and the core[70,71] has also been demonstrated the potential use of micelle scaffolds as vehicles in applications such as imaging. The ability of the micelle core to selectively sequester molecules from the aqueous surroundings based on hydrophobic interactions has been shown by Nagarajan *et al.*[72] and Cotanda and O'Reilly[73] Both groups showed the preferential uptake of hydrophobic molecules in a mixture of molecules with a range of hydrophobicities.

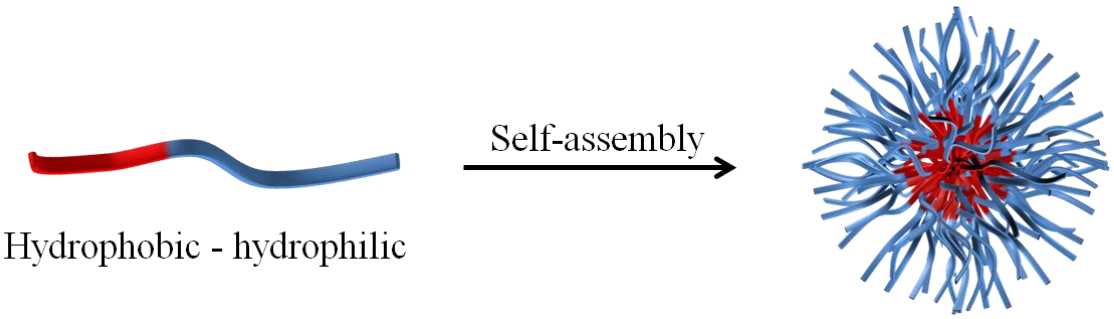

Figure 1.5. Representative self-assembly process of amphiphilic diblock copolymers in water

Furthermore, the functionalization of a catalytic moiety within the core has allowed for highly efficient reactions not conventionally compatible with water to take place within the micelle compartment. Possible destabilization of the micellar structures upon dramatic changes to polymer concentration or addition of core selective solvent can be stabilized by the introduction of core or shell cross-linking. This extends the potential applications of the assembled nanostructures as these are more robust and stable to a greater range of environmental changes compared to the non-cross-linked equivalence.

1.4 Stimuli-responsive polymers

The interest in stimuli-responsive polymer systems has grown immensely in recent years due to their potential applications as 'intelligent'/'smart' materials. Changes in the physical state or properties of polymers triggered by stimuli such as light, temperature and pH have been investigated. For the purpose of this thesis, only temperature-responsive polymers will be discussed.

Many temperature-responsive systems have been reported due to the ease of control and employment. Polymers can exhibit an upper or lower critical solution temperature, UCST and LCST respectively. LCST polymers are fully soluble below and phase separate above the transition temperature, and the opposite behaviour is observed for UCST polymers. This transition is also known as the coil-to-globule transition for LCST polymers which is largely a hydrogen bonding property (Figure 1.6).[74,75] Hydrogen bonding interactions between the solution and the polymer are preferred below the LCST, with increasing temperature these interactions become unfavourable and inter-polymer hydrogen bonding is preferred, increasing the overall entropic gain of the system. Poly(*N*-isopropylacrylamide) (PNIPAM) has been the subject of intensive research in recent years as a result of its sharp phase transition around 32 °C, a physiologically interesting temperature. Additionally, the copolymerization of NIPAM with monomers such as acrylic acid has allowed the transition temperature to be readily tuned.[75,76] NIPAM has also been used to synthesize hydrophobic-hydrophilic, double hydrophobic and double hydrophilic switchable diblock copolymers.[77,78] This has been used to reversibly switch the morphology of nanostructures.

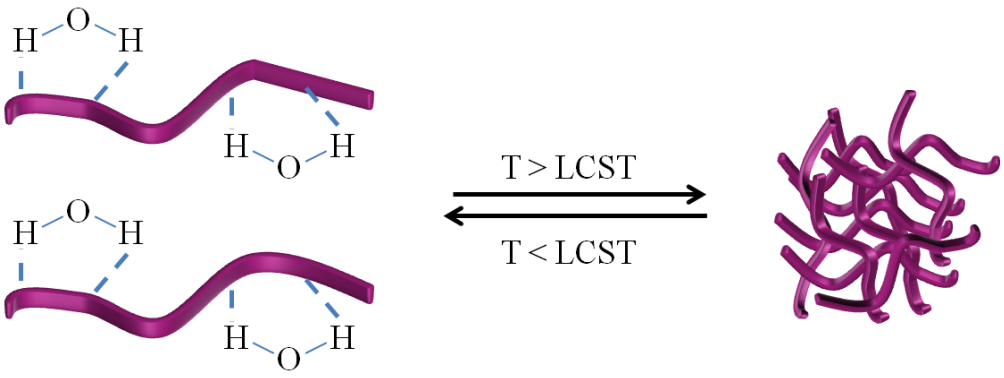

Figure 1.6. The reversible coil-to-globule transition of a LCST polymer

Cross-linked PNIPAM microstructures have also been used as scaffolds for immobilization of a range of catalytic functionalities where the catalytic activity could be turn on and off as a result of the reversible temperature transition property of PNIPAM. The hydrophobic nature of PNIPAM at elevated temperatures has in some cases enhanced substrate uptake and in other cases blocked access and thus the catalytic activity of the system.[79–81]

1.5 Catalytic polymer nanoreactors

The complexity of natural systems such as enzymes is something scientists strive to achieve. Enzymes are highly specific in their function where substrate selectivity is based on features such as hydrophobic and hydrogen bonding interactions as well as the substrate shape and size. The compartmentalized nature of the active site allows several hundreds of reactions to occur simultaneously and is a result of the elegant folding of protein chains placing amino acid residues perfectly within this compartmentalized space. This results in the extremely high and specific catalytic activity observed by enzymes in Nature.[82] Inspired by these complex natural systems, efforts have been focused towards the understanding of these interactions in order to design a

macromolecular scaffold able to mimic the unique environment created by enzymes. Well defined and robust nanostructures such as core-shell micelles,[83] polymer vesicles,[84] star polymers[85] and dendrimers[86] can today be synthesized with great complexity. This is a result of the advances made in CRP techniques and macromolecular chemistry. The confined environment exhibited by these nanostructures has been shown to efficiently increase the local concentration of both the substrates and the catalyst, often resulting in enhanced catalytic activity. The polymeric scaffolds also serve to protect the tethered or encapsulated catalytic functionality from the external environment, thus preventing degradation or deactivation. Additionally, 'smart' or stimuli-responsive polymers may be used to control the activity of the tethered catalyst and the substrate specificity of the system.[87] By taking these features into consideration, we can start to design synthetic nanoreactors which may act as efficient enzyme mimics.

1.5.1 Protective nature of scaffold

The great advantage of using polymeric nanostructures as scaffolds for catalytic functionalities is their superior stability compared to surfactant-based micelles. As the constituents of the polymer can be based on a range of monomers, it is possible to design nanostructures with a dynamic or a frozen nature.[88] This can be used to control the critical micelle concentration (cmc) and the swellability of the structures as well as the level of protection it can provide. Moreover, by further cross-linking the core or the shell of the nanostructure, the stability of the nanostructures is further enhanced in a greater number of environments. These are important features to consider, especially for metal and enzyme catalysts as these are easily deactivated.

Despite the high efficiency of metal catalysts, even at low catalyst loading, it is still desirable to achieve a recovery and reuse protocol due to catalyst cost and leaching problems associated with polymer supported metal catalysis. Dendrimers,[89]

hyperbranched polymers,[90] hollow particles,[91] hydrogels[92] and ionic brushes[93] have been successfully used as scaffolds for the *in situ* preparation, and protection of metal nanoparticles (NPs). The presence of the scaffold significantly reduced NP aggregation and allowed for recovery and reuse of the metal NP immobilized nanoreactor system. Sawamoto and co-workers reported great recovery and reuse of a ruthenium containing microgel star polymers after hydrogenation and oxidation reactions.[94,95] The excellent catalyst stability and thus reusability was attributed to the unique structure of the cross-linked microgel scaffold which encased the metal catalyst and therefore prevented catalyst deactivation and leaching. The successful immobilization of metal NPs such as Au, Ag, Pd and Pt into cross-linked PNIPAM microgels has also been reported. In many cases, the high and prolonged activity and successful reuse have been directly associated with reduced NP aggregation and catalyst deactivation as a result of the polymer scaffold. Liu *et al.* used poly(2-oxazoline) shell cross-linked micelles to stabilize their Co(III)-salen catalyst. The nanoreactor system showed outstanding recycling properties, reporting up to 8 catalytic cycles, highlighting the protective property of the polymer nanoreactor.[96]

Enzymes with enhanced bioavailability, *in vivo* stability, pH and temperature stability have been achieved *via* immobilization or encapsulation within polymer nanostructures. Palivan and co-workers[97–99] have designed an elegant polymer vesicle (poly(2-methyloxazoline)-poly(dimethylsiloxane)-poly(2-methyloxazoline)) system with the ability to protect the encapsulated enzyme mimic and maintain its activity. The nanoreactor system was successfully used to combat oxidative stress by catalyzing the conversion of $O_2^{\cdot -}$ to hydrogen peroxide and oxygen in a number of cycles. The work of Van Dongen *et al.*[100] further highlights how the advances in macromolecular chemistry can be used to design synthetic polymer systems to increase the lifetime of encapsulated or immobilized enzymes. They reported the synthesis of a polystyrene-*b*-poly(L-

isocyanoalanine(2-thiophen-3-yl-ethyl)amide) diblock copolymer, which self-assembled into polymer vesicles able to encapsulate the horseradish peroxidase (HRP) enzyme. To encourage intracellular uptake, the vesicle surface was decorated with the protein Tat. The HRP containing polymer vesicles were able to maintain high activity for a longer period of time compared to free HRP upon incubation with HeLa cells. This was determined to be a direct result of the protective nature of the polymer vesicle.

More recently, the encapsulation of three different enzymes within a single nanostructure for applications in cascade reactions was demonstrated by Bäumler and Georgieva.[101] By using a nanostructure built up of concentric compartments, deactivation of the enzymes was prevented. Moreover, by tuning the distance between each compartment, the distance between the enzymes was controlled. This subsequently influenced the diffusion of substrates between compartments and thus the catalytic activity of the nanoreactor system as a whole. These examples demonstrate the idea of using a polymeric scaffold to effectively protect the active functionality from the surrounding environment or from neighbouring functionalities enhancing the lifetime and reducing degradation of the catalyst.

1.5.2 Isolated reaction space

Enzymes are able to form hydrophobic compartments/cavities making it possible to carry out organic reactions in water. This is highly desirable as Nature achieves this efficiently. Nevertheless, water has many advantageous properties making it a desirable solvent such as its abundance and safety. In addition, water has shown rather unique properties in organic reactions, when added as an additive has improved both the rates and selectivity of the organocatalyst.[102] However, its use is often restricted by its inability to solubilize most of the organic compounds. The great advantage of using polymeric assemblies as nanoreactors is the formation of hydrophobic cavities upon

self-assembly in water. The hydrophobic cavities are able to efficiently concentrate the reaction substrates with the catalyst within it, allowing highly active processes to occur. This phenomenon was first observed many years ago where enhanced activity was observed in the presence of self-assembled surfactants in water.[103,104] However, the dynamic nature of these assemblies can be a disadvantage. In comparison, the polymer based assemblies are much more stable and can be further stabilized by carrying out cross-linking chemistries. Nevertheless, the most important aspect of these polymer assembles is the ability to tether the desired catalytic functionality on the surface, in the shell or within the confined core of the nanostructure.[105–108] This allows a rather hydrophilic catalyst such as L-proline may be incorporated within the hydrophobic core allowing it to catalyze a range of organic reactions not compatible with water.

Rodionov *et al.* introduced two different catalytic functionalities, the amine 4-dimethylaminopyridine (DMAP) and the acid *para*-toluenesulfonic acid into the core of two separate styrenic star polymers (Figure 1.7).[109] A two-step sequential cascade reaction was successfully catalyzed by the two star polymers in one pot. This was accomplished using two normally incompatible catalysts where the presence of the nanostructures allowed discrete reactions to take place within the isolated cores. The presence of soluble arms ensured the catalyst contained cores were unable to interact with each other and thus limiting catalyst deactivation.

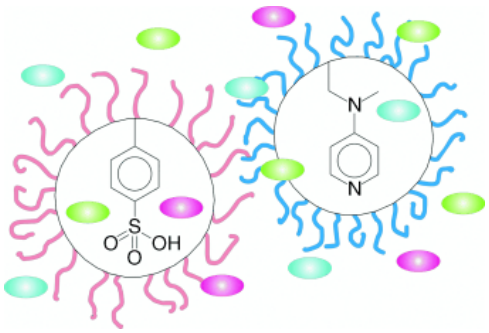

Figure 1.7. The use of star polymers to create individual and isolated reaction spaces allowing cascade reactions with incompatible catalysts to take place.[109]

DMAP has also been successfully incorporated into the core of polymer micelles based on amphiphilic diblock copolymers.[73,107] The micelle-supported organocatalyst showed an unprecedented increase in the rate of reaction as a direct result of the ability of the hydrophobic micelle core to sequester the organic substrates from the surrounding aqueous environment. This truly highlighted the importance of hydrophobic effects or concentrator effect to enhance the activity of the tethered catalyst. Block copolymers,[73,105,107] ionic polymers and brushes,[93,110–112] dendrimers,[113–116] and polymer capsules[117] are other nanostructures that have been used to create a favourable environment to achieve efficient catalysis in water.

This confined reaction cavity has also shown great efficiency for polymerizations of hydrophobic monomers in water.[118–120] Cross-linked microgels with encapsulated ruthenium successfully catalyzed the polymerization of a range of monomers including the unprotected methacrylic acid with good control.[121,122] Sebakhy *et al*. presented an elegant polymer nanoreactor system based on a temperature responsive PNIPAM and a non-responsive poly(dimethylacrylamide) (PNIPAM-*b*-PMDA) diblock copolymer (Figure 1.8).[123] At temperatures below the LCST of PNIPAM, the block copolymer was fully soluble in water; however, above the LCST PNIPAM became hydrophobic and core-shell nanostructures were formed. Subsequently, by allowing the system to cool back down below the LCST, the polymer was again fully soluble in water. Upon addition of a PNIPAM block containing an active RAFT chain end, co-assembly occurred at elevated temperatures. The RAFT chain end was used in the chain extension of the hydrophobic monomer within the assembled nanoreactor. The RAFT mediated polymerization was found to proceed with good control over both molecular weight and molecular weight distribution. Upon polymerization completion, the reaction was

cooled and the thermo-responsive nanoreactor released the PNIPAM-*b*-PS nanoparticles, as schematically shown in Figure 1.8. The resulting PNIPAM-*b*-PS nanoparticle size was readily tuned by controlling the size of the PNIPAM-*b*-PDMA nanoreactor. The same design was recently extended to L-proline catalyzed organic reactions in water where high catalytic activity and selectivity was observed upon formation of the micelles.[124] However, at temperatures below micelle formation, precipitation of the hydrophobic substrates in the surrounding water was observed. The ability of the scaffold to effectively form a confined and favourable reaction space, as demonstrated, is one of the most important features of a nanoreactor system.

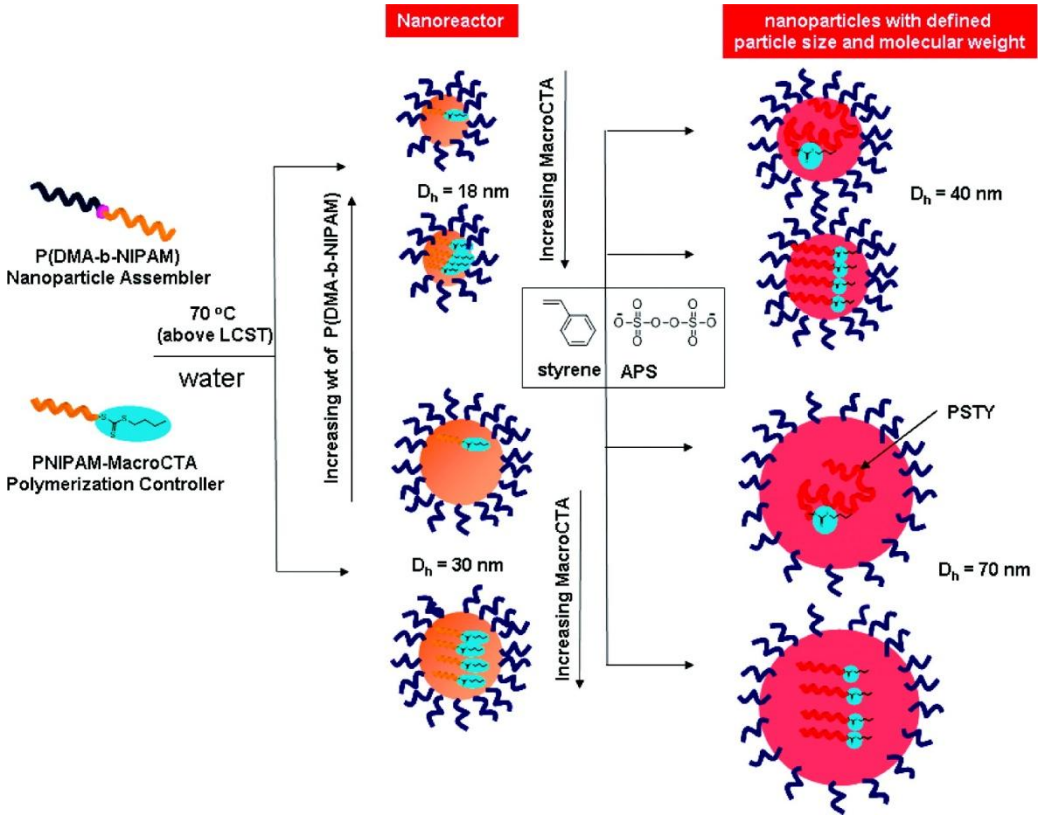

Figure 1.8. Successful polymerization of styrene within thermo-responsive nanoreactors dispersed in water, where control over molecular weight and particle size distribution is a result of the confined nature of the nanoreactor[123]

1.5.3 Substrate selectivity / specificity

It is highly desirable to achieve a substrate selective nanoreactor system, a feature that will allow a specific reaction to take place over others. This may be achieved by introducing specific features within the polymer scaffold to enhance certain interactions or characteristics of the substrates such as hydrophobic, ionic or hydrogen bonding interactions and substrate size. Rodionov *et al.*[109] were able to achieve substrate selectivity based on size by controlling the cross-linking density of their polystyrene based nanoreactor (Figure 1.9). The interior of the nanoreactor was decorated with azide functionalities and the reactivity towards a range of alkyne molecules was demonstrated. At low cross-linking density high accessibility of the azide functionality was achieved for all alkyne molecules. However, at higher cross-linking density, access of the larger alkyne functionalized PEG was significantly lower but all the smaller alkynes were successfully incorporated regardless of the cross-linking density (up to 5 wt% cross-linking). This work illustrates how the cross-linking density may be used to introduce substrate selectivity into a nanoreactor system.

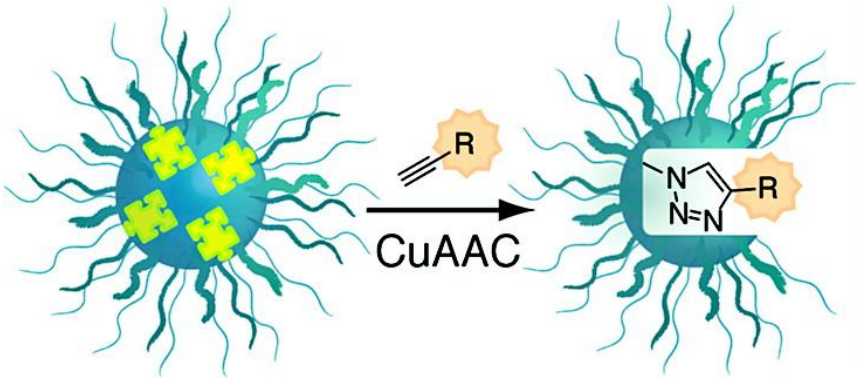

Figure 1.9. Polystyrene particles where the cross-linking density had a significant effect on the accessibility of the internal azide functionalities for the larger alkyne molecules, demonstrating substrate selectivity based on size.[109]

Two different substrate selective polymer nanoreactors based on non-covalent interactions have recently been reported the O'Reilly group.[73,125] Polymer micelles with DMAP functionalities tethered within the hydrophobic core were found to selectively catalyze acylation reactions based on substrate hydrophobicity. It was clear that in competitive reactions with four substrates with different hydrophobicities, catalysis of the two most hydrophobic substrates (> 99%) was preferred. This hydrophobic preference overruled the reactivity observed under homogeneous conditions further highlighting another key aspect that is achieved by nanoreactor technology. In the second nanoreactor system, the micelle core consisted of the nucleobase thymine functionality. The nanoreactor reported efficient polymerization selective towards a monomer containing the adenine functionality as a result of the complementary hydrogen bonding interactions between the nucleobase pairs. The template nanoreactor was able to segregate and protect the propagating radicals within the nanoreactor core allowing control over molecular weight and molecular weight distribution of the daughter polymer. By further exploring interactions similar to those found in nature, more complex synthetic reactors with specific interactions can be designed.

In addition to enhancing interactions between the nanoreactor core and the desired substrates to achieve selectivity, it is also possible to control access to the catalytic site by using stimuli-responsive polymers. Gaitzsch *et al.*[126] controlled the trans-membrane traffic of a polymer vesicle using the pH-responsive poly(diethylaminoethyl methacylate) (PDEAEM) containing the enzyme myoglobin (Figure 1.10). At high pH (*ca.* 8) the membrane was deprotonated and in this hydrophobic and entangled state, reagents were not able to enter the vesicle core. However, at low pH (*ca.* 6) the membrane was protonated and in this hydrated and swollen state the substrates were able to diffuse through the membrane into the core. Thus, at low pH high enzymatic catalysis rates were reported for a model oxidation reaction.

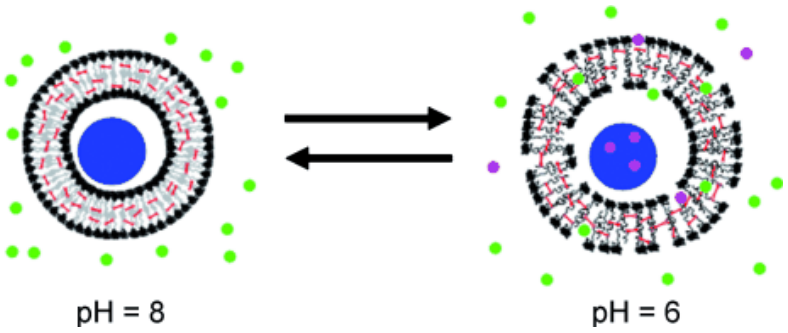

Figure 1.10. Polymersome bioreactor consisting of hydrophilic poly(ethylene glycol) and pH-sensitive diethyl amino ethyl methacrylate (DEAEM) where the pH induced swelling and shrinking controlled the transmembrane trafficking of reagents to the catalytic core.[126]

A similar system using a temperature-responsive polymer to control the permeability of the nanoreactor has been reported by Wang *et al.*[127] Gold nanoparticles were immobilized onto a PNIPAM-*b*-poly(4-vinylpyridine) nanoreactor in water (Figure 1.11). The shrinking and swelling behaviour of the PNIPAM corona, and the corresponding change in hydrophobicity/hydrophilicity of the system upon changes to the temperature was used to achieve an on/off catalytic system. At temperatures above the LCST, the collapsed nature of the PNIPAM corona dramatically inhibited the diffusion of substrates into the catalytic core. However, below the LCST the extended nature of the corona resulted in the significant increase in substrate uptake and thus catalytic activity. A similar effect was also observed by Li *et al.*[128] They also reported a second on/off catalytic system using a temperature-induced cross-linking polymer scaffold.[129] The monomer units formed cross-linking interactions at low temperatures, restricting access to the catalytic functionalities. However, at elevated temperatures, these cross-linking interactions were eliminated and substrates were able to enter the core and high catalytic activity was reported. Inter-polymer interactions of ionic polymer systems have also been used influence nanoreactor activity depending on whether diffusion was permitted or not.[103,130]

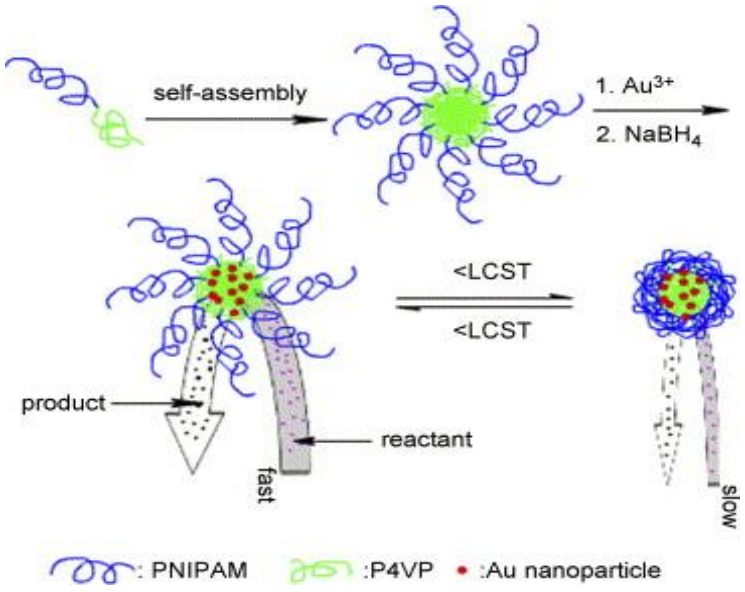

Figure 1.11. Self-assembly of PNIPAM-*b*-P4VP in water where the catalytic activity of the immobilized Au NPs was controlled by the temperature induced swelling and collapse of PNIPAM corona.[127]

Terashima *et al.*[131] reported the formation of a confined pocket in water *via* the folding of a single polymer chain, mimicking the specific folding of proteins. Functionalities on the polymer were designed with specific interactions to encourage the formation of the desired cavity. The catalyst was also functionalized with a ruthenium metal catalyst and demonstrated efficient catalysis for the reduction of cyclohexanone. A similar system was also applied to the organocatalyst L-proline (Figure 1.12).[132] The authors showed that the catalyst retained most of its activity through a model aldol reaction, though a significant drop in selectivity was observed. Although the systems found in nature are more well-defined, this demonstrates the potential of decorating synthetic polymers with motifs to allow for efficient assembly and catalysis in water.

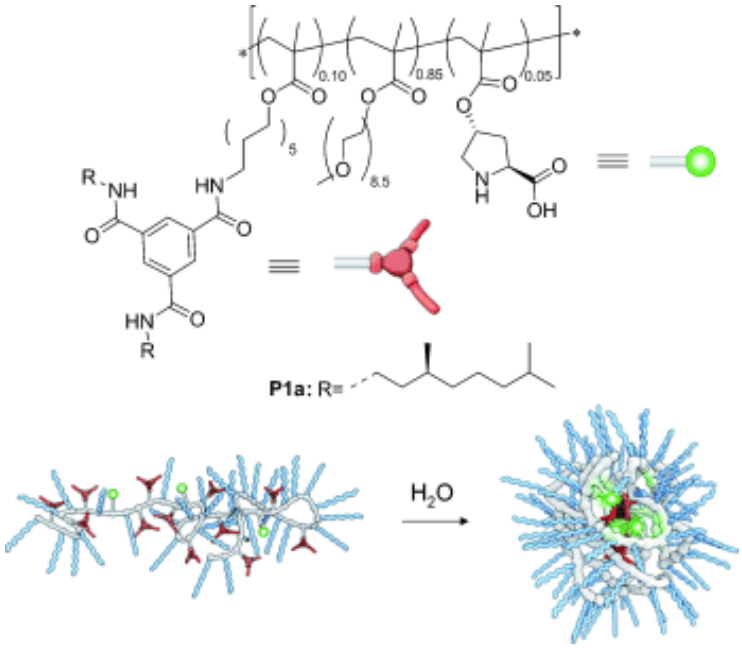

Figure 1.12. Polymer chains decorated with specific functional motifs which efficiently direct the folding process of a single chain forming a catalytic hydrophobic cavity with functionalized L-proline for asymmetric aldol reaction in water, demonstrating the potential of using a single polymer chain for catalysis.[132]

1.5.4 Cross-linked nanogels (and microgels)

Related to polymeric self-assembled nanoreactors are unimolecular structures such as microgels and nanogels that retain their form but may swell and change dimensions in a range of conditions such as changes to temperature, solvent or concentration, due to their cross-linked nature.[133] Structures in the size range 1-100 nm are generally considered nanogels and 0.1-100 μm microgels. In line with these structures are unimolecular branched[134,135] and dendrimeric[136,137] structures which also exhibit some characteristics of nano/microgels. As a result of their stability, these structures have been used as delivery systems and other biomedical applications.[138,139] Their application as nanoreactors has also been well demonstrated, where immobilized metal nanoparticles such Au, Pt, Ag and Pd and enzymes have been used to catalyze reduction (Figure 1.13),[140,141] hydrolysis,[142] carbon-carbon bond forming reactions[141,143] and

polymerization reactions.[121,122] Other applications can be found in fields such as membranes,[144] magnetic resonance imaging,[145] drug delivery,[146,147] biotechnology,[148] biomedical diagnostics (theranostics)[149] and cosmetics.[150]

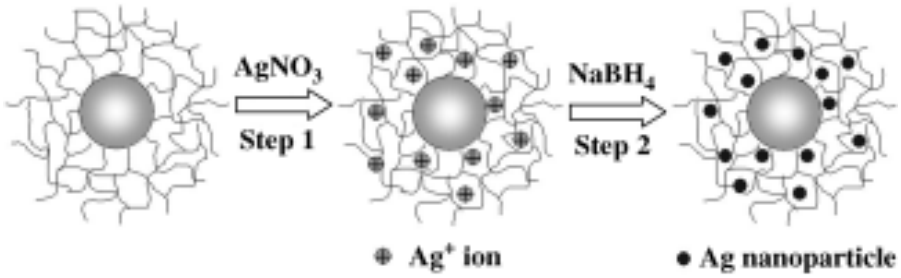

Figure 1.13. Core-shell nanogels as carriers for Ag nanoparticles for the reduction of 4-nitrophenol[140]

Cross-linked PNIPAM microgels have also been used as intelligent microreactors where the reversible nature of PNIPAM as a response to temperature has been used to control access of substrates through the microgel. However, this has mainly been centred around the immobilization of metal NPs and much less work has involved enzyme- and organo-functionalized systems. Several groups have taken advantage of both the hydrophilic and hydrophobic property of PNIPAM, allowing catalysis of hydrophilic and hydrophobic substrates by simply tuning the temperature of the system.[143,151,152] In other cases, high catalytic efficiency has been reported at elevated temperatures where hydrophobic PNIPAM improves substrate uptake.[80,142,153–157] Others have reported the opposite, where the collapse of PNIPAM decreases the pore size of the microgel and reduces substrate uptake, effectively blocking the activity of the immobilized NPs.[81,127,140,141,158–161]

Thayumanavan and co-workers have designed an elegant nanogel system based on random copolymers containing hydrophilic oligoethylene glycol (OEG) and hydrophobic pyridyldisulfide (PDS) functionalities, synthesized by RAFT

polymerization (Figure 1.14).[162] In an aqueous solution, nanoaggregates are formed which are able to sequester lipophilic molecules from the surrounding solution. Dithiothreitol (DTT) was used to cleave the desired amount of PDS functionalities to give thiol group that can subsequently inter- and intrachain cross-link to yield a cross-linked nanogel containing a lipophilic guest molecule (Figure 1.14). Upon cleaving the disulfide bond, the encapsulated molecule was successfully released from the nanogel. Furthermore, the nanogel surface was functionalized with cell penetrating peptides, folic acid, cyclic arginine-glycine-aspartic acid peptide to specifically target receptors overexpressed in cancer cells.[149,163,164]

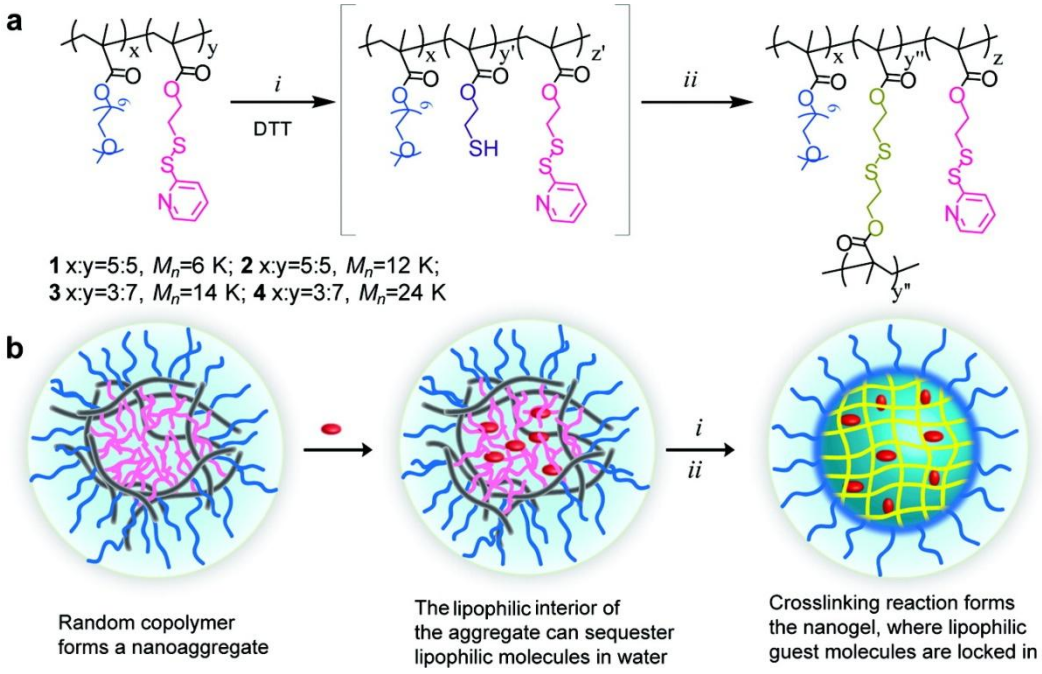

Figure 1.14. Cross-linked nanogels based on RAFT copolymers for targeting and delivery applications, where the desired amount of PDS groups is cleaved in step (i) and inter/intrachain cross-linking occurs in step (ii)[165]

1.6 L-Proline catalysis

Organocatalysis is the use of small organic compounds to catalyze organic transformations and is considered a relatively new concept in the area of asymmetric

synthesis, which has previously been dominated by transition metal- and biocatalysis.[166] The advantage of organocatalysis over the more conventional metal and enzyme based catalyst is their stability in air and water, making them experimentally easy to handle. In addition, they are often cheap and non-toxic as they are mostly based on natural products with a naturally existing chirality, such as sugars, peptides and amino acids.[167] The most popular organocatalyst is the amino acid L-proline and its derivative *trans*-4-hydroxy-L-proline (Figure 1.15), one of the few with a cyclic structure. It is bifunctional, containing a secondary amine and a Brønsted active carboxylic acid and both enantiomeric forms are commercially available.

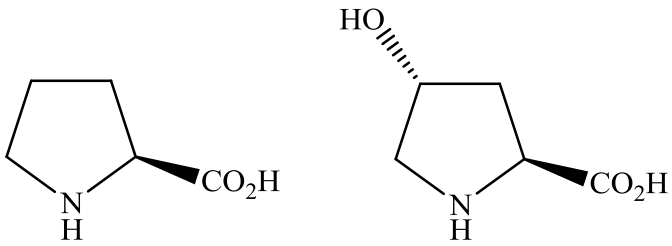

Figure 1.15. The structure of the bifunctional amino acid L-proline and its derivative *trans*-4-hydroxy-L-proline

The first use of L-proline as a small organic catalyst was reported by two research groups in the early 1970s, Hajos and Parrish[168] and Eder *et al*.[169] However, its potential as an organocatalyst was not further explored until the 1990s when List *et al*[170] and Ahrendt *et al*[171] re-introduced enamine and iminium catalysis respectively. This defined organocatalysis which became an intense area of research. L-Proline has been used in range of asymmetric reactions including the Mannich reaction,[167,172] Michael addition,[173,174] aldol reaction[167,175] and Robinson annulations.[176] These reactions are often key steps in the synthesis of natural products,[177,178] as a new chiral carbon-carbon bond is formed. As the catalyst is highly enantioselective, enantio-enriched products are

often efficiently achieved. L-Proline has been named the 'simple enzyme' as it proceeds *via* an enamine type mechanism similar to that of the naturally occurring class I aldolase enzyme.[177,179–181] The proposed mechanism for the asymmetric aldol reaction catalyzed by L-proline is shown in Scheme 1.7. For the shown cross-coupling aldol reaction, the ketone substrate first interacts with the catalyst forming and an iminium ion and then the desired enamine species. As all the steps are reversible, it is important to drive the equilibrium forward, towards formation of the desired enamine species (step 1) and then finally the product. It has been proposed that the presence of a proton or an acid drives the equilibrium forward, favouring the formation of the enamine, releasing water. Secondly, the aldehyde substrate interacts with the enamine species forming an organized transition state where a hydrogen bonding network is formed between the reagents and the carboxylic acid functionality of the catalyst (Figure 1.16).[178,182–184] The catalyst is subsequently regenerated *via* a hydrolysis process, releasing the aldol product. Thus, the balance of water in the reaction is of great importance, as some is required to complete the catalytic cycle. However, if present in a high degree will drive the equilibrium in the first step back towards the catalyst and the starting ketone.

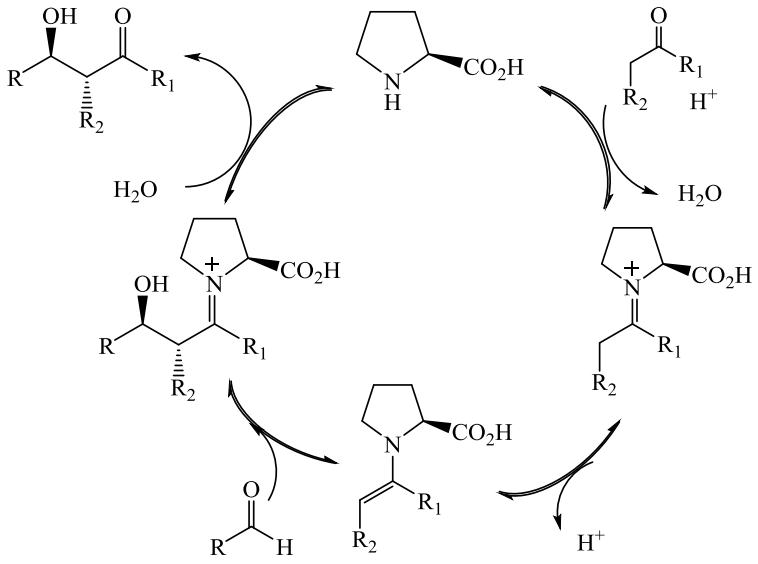

Scheme 1.7. The catalytic cycle of *L*-proline catalyzed aldol reaction

For the reaction of most substrates, up to four different isomers will result. This is due to the formation of two chiral centres, as depicted in Figure 1.16, where the chiral centres have been highlighted with an asterisk (*). The transition states shown in Figure 1.16 may be used to explain the observed diastereomeric and enantiomeric ratios resulting from proline-catalyzed aldol reactions. Attack on the *re*-face of the aldehyde is favoured over *si*-face due to unfavourable interactions between the aldehyde R-group and the carboxylic acid group. Thus, the bulkier R-group is more likely to be positioned away from the carboxylic acid functionality favouring the formation of the anti-isomer for both D- and L-proline.[185–187] This arrangement and its importance for the enantioselectivity of the catalyst has been well documented. When modifications have been made to the catalyst to achieve a more active derivative, functionality with similar characteristics to the carboxylic acid proton has always been preserved. Eliminating this functionality has resulted in reduced enantioselectivity.

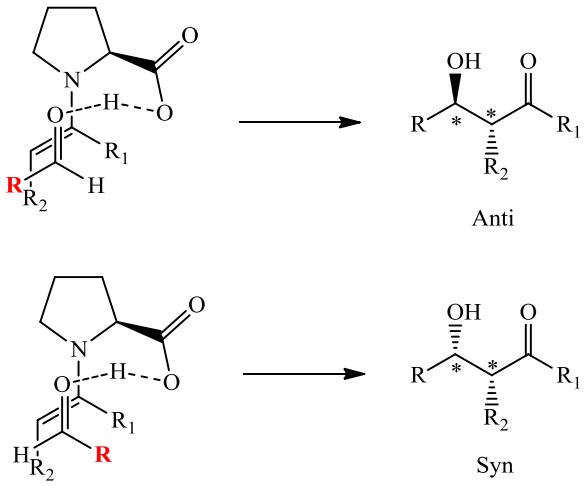

Figure 1.16. The formation of *anti* and *syn* isomers where L-proline is the catalyst

1.6.1 Modified and Solid-supported prolines

With catalyst recycling in mind, research has intensified around the immobilization of L-proline onto a solid support. Although organocatalysts such as L-proline are relatively

cheap, there are modified catalysts and more expensive natural catalysts that would benefit from possible recyclability.[186,188,189]

Furthermore, the potential of using a polymer scaffold to provide a favourable microenvironment for the reaction to occur and enhancing the overall catalyst performace are additional driving forces for the immobilization of these catalysts. Moreover, by forming a favourable confined reaction environment, it may be possible to significantly lower the catalyst concentration without compromising with the catalyst activity.

The first type of polymer supported catalysis was reported already in 1985 by Kondo *et al.*[167] Though the catalytic efficiency and selectivity of this organocatalyst cannot be considered remarkable, the type of support developed has a striking resemblance to the supports used today.[108] The majority of the reported solid-supported L-prolines have involved attaching a derivative of L-proline such as 4-hydroxy-L-proline onto a pre-formed polymer or bead using the hydroxyl group as the anchoring point. The most common supports have been polystyrene,[190–193] poly(ethylene glycol) (PEG)[194,195] (Figure 1.17) and Merrifield resin.[196] Other reported solid supports include dendrimers[197] and ionic liquids.[198,199]

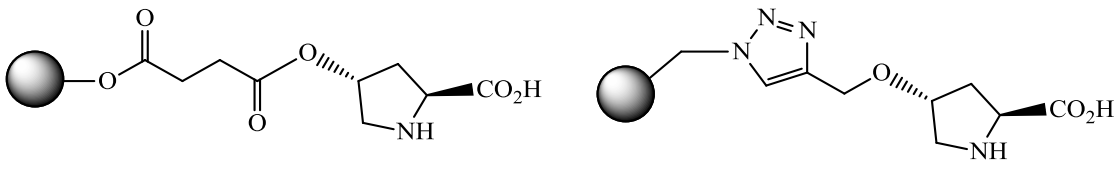

PEG-supported proline[194,195] PS-supported proline[190–193]

Figure 1.17. Examples of polymer-supported L-proline organocatalysts from literature

Most of these involved catalysis under organocatalytic conditions, i.e. in organic solvent where both the support and the reagents were soluble. However, in a few cases some

interesting results and observations were reported when hydrophobically modified prolines were used as catalysts in pure water. The hydrophobic groups were found to interact with the reagents forming a concentrated organic phase in the surrounding water. Gruttadauria *et al.* [194] synthesized a polystyrene supported L-proline for the asymmetric aldol reaction in water. Unexpectedly, the supported catalyst did not show any activity in organic solvents such as DMF, DMSO, $CHCl_3$ or 1,4-dioxane, commonly used to promote the reaction. Instead water and methanol were found to be favourable solvents and the authors proposed this was due to the formation of an organic phase or hydrophobic pocket (Figure 1.18).

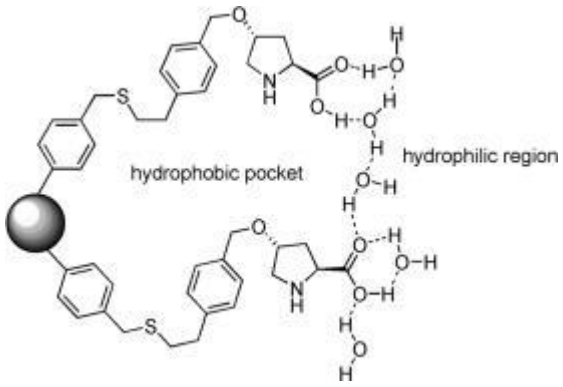

Figure 1.18. The proposed hydrophobic pocket formed by the polystyrene-supported L-proline in water.[194]

The organic phase was able to effectively solubilize the water insoluble reagents and prevented precipitation by protecting them from the bulk water. The lack of activity in organic solvents was proposed to be associated with the solubility of both the polymer and reagents which eliminated the formation of these concentrated organic pockets, i.e. the reagents were not forced to concentrate around the support and catalyst to stay soluble. Moreover, the reaction proceeded with higher selectivity when more hydrophobic reagents were used, further supporting the role of the support and hydrophobic pocket.

Surfactant type supports have also been reported to facilitate L-proline catalyzed reactions in water. Mase *et al.*[181] reported a hydrophobically modified proline bearing long alkyl chains which was found to form an emulsion together with the reagents (Figure 1.19). In the presence of an acid additive, high catalytic activity and selectivity were achieved. In the absence of the hydrophobic alkyl chains, no reaction was observed, not even in the presence of the acid additive. Hayashi *et al.*[200] reported a similar observation with their modified catalyst (Figure 1.19).

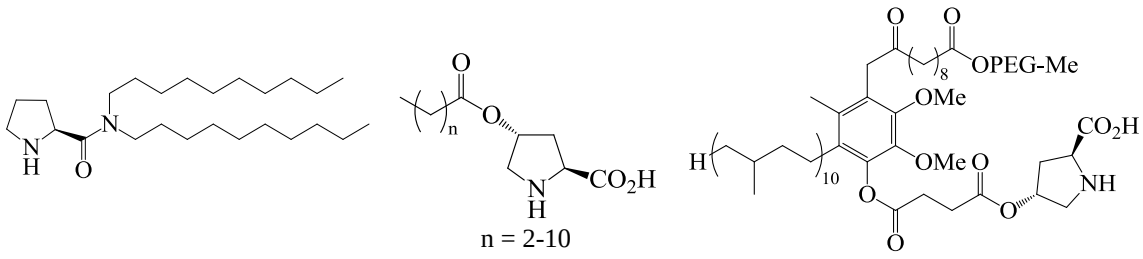

Figure 1.19. Hydrophobically modified L-proline catalysts with successful catalytic activity and selectivity in water, reported by Mase *et al.* (left), Hayashi *et al.* (middle) and Lipshutz and Ghorai(right)

In both cases, enhanced activity was observed in water as a result of the hydrophobic interactions between the catalyst and the reagents forming a concentrated organic phase. Lipshutz and Ghorai[201] reported the use of a large molecule derived from ubiquiol, CoQ_{10}, which consisted of a hydrophobic hydrocarbon chain and a hydrophilic poly(ethylene glycol) component (PQS-proline) (Figure 1.19). PQS-proline was found to spontaneously self-assemble in water to give 79 nm micelles. The authors found that the water insoluble reagents were favoured over more soluble ones suggesting the reaction took place in the lipophilic core rather than the surrounding water. The modified catalyst showed relatively high activity and satisfactory selectivity. More notable is in-flask recyclability of the system where after reaction the catalyst was found to be retained in the aqueous phase allowing extraction of the product using organic

solvents. These were indeed very interesting observations, as this has allowed the modification or support to act in a way similar to that of enzymes in natural systems.

Sanda and Endo [202] reported the synthesis and controlled polymerization of a range of vinyl amino acid monomers including L-phenylalanine and L-proline, widening the variety of methods used for immobilization of these amino acid functionalities (Figure 1.20).[203,204] The L-proline containing RAFT copolymers and diblock copolymers were further studied for their thermo-responsive properties and temperature-induced self-assembly behaviour. This was a step towards synthesizing tailored polymers with unique properties for various applications such as controlled release, biomedical sensing and biocompatible materials.[203,204] More recently the range of vinyl amino acid monomers has been extended to L-leucine, L-alanine L-histidine and L-tryptophan (Figure 1.20), as a result of their interesting properties, providing a chiral environment for asymmetric catalysis, chiral recognition and as optically active materials.[205–209]

However, as previously mentioned, the amine and carboxylic acid functionalities play a key role in the catalytic cycle, ensuring high enantioselectivity, and for the mentioned vinyl amino acids, the amino functionality was used as the anchoring point. Hence, it will be highly desirable to synthesize vinyl monomers leaving both active functionalites free for catalysis.

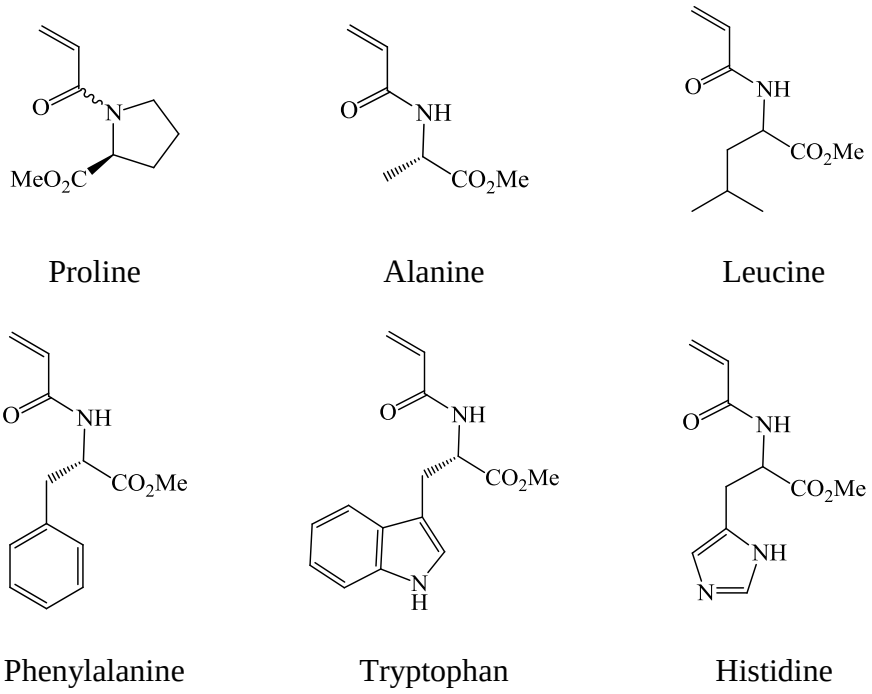

Figure 1.20. A display of vinyl amino acid monomers

More recently, Kristensen *et al.* used suspension polymerization to synthesize copolymer beads containing the L-proline functionality by synthesizing methacylate type monomers using the hydroxyl functionality as the anchoring point (Figure 1.21).[210] Using this polymerization technique, they were able to synthesize a polymer containing only the catalyst functionality. However, the polymer had very limited solubility and showed poor activity and selectivity in a model aldol reaction. The monomer was therefore copolymerized with both styrenic and methacrylic monomers resulting in a variety of copolymer beads in the micron size range (Figure 1.22). The beads showed high catalytic properties in a model aldol reaction carried out in water. The recyclability of the beads was also investigated, with no loss in activity over 5 catalytic cycles.

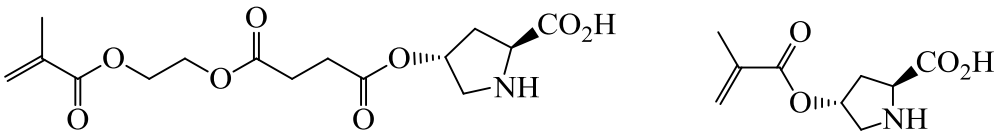

Figure 1.21. Examples of L-proline functionalized methacrylate monomers synthesized by Kristensen *et al.*[210]

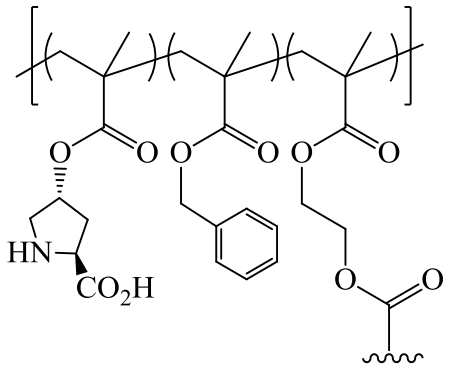

Figure 1.22. An example of a copolymer synthesized by suspension polymerization with a methacrylic support, by Kristensen *et al.*[210]

Other organocatalysts including DMAP and MacMillan have been successfully incorporated into a polymer scaffold and shown comparable or better catalytic activity to the unsupported catalyst.[73,107,188]

In this thesis work we aim to explore a number of polymers and polymer assemblies as potential recyclable scaffolds for the organocatalyst L-proline. The influence of the polymer scaffold to successfully mediate L-proline catalyzed reactions in water will be investigated. A range of functional copolymers and diblock copolymers will be synthesized using a CRP technique such as RAFT polymerization. Using this it will be possible to achieve reproducible control over catalyst incorporation and polymer block length. This will allow us to control the final size of the assembled micelle and its influence on the catalytic activity and selectivity of the incorporated catalyst. Additionally, by employing an emulsion polymerization process, cross-linked particles in water may be prepared in one pot. By investigating effects such as cross-linking

density and catalyst incorporation, the catalyst efficiency may be readily tuned. Moreover, the introduction of cross-linking can further expand the uses of the assembled particles as their increased stability may allow for particle and thus catalyst recycling.

By synthesizing a range of nanoreactors using different polymerization techniques it will be possible to investigate a range of factors that may play a key role in determining the catalytic activity and selectivity of the functionalized catalyst which may be extended to a number of other chiral catalysts.

1.7 References

1. Thurmond, K. B., Kowalewski, T., Wooley, K. L. *J. Am. Chem. Soc.*, 1996, **118,** 7239

2. Szwarc, M., *Nature,* 1956, **178,** 1168

3. Szwarc, M. *J. Polym. Sci. Part A Polym. Chem.*, 1998, **36,** IX

4. Quirk, R. P., Lee, B. *Polym. Int.*, 1992, **27,** 359

5. Levy, M. *Polym. Adv. Technol.*, 2007, **18,** 681.

6. Matyjaszewski, K. *Curr. Opin. Solid State Mater. Sci.*, 1996, **1,** 769.

7. Greszta, D., Mardare, D., Matyjaszewski, K. *Macromolecules*, 1994, **27,** 638.

8. Hawker, C. J. *J. Am. Chem. Soc.*, 1994, **116,** 11185.

9. Hawker, C. J. *Acc. Chem. Res.*, 1997, **30,** 373.

10. Wang, J.-S., Matyjaszewski, K. *Macromolecules*, 1995, **28,** 7901.

11. Kato, M., Kamigaito, M., Sawamoto, M., Higashimura, T. *Macromolecules*, 1995, **28,** 1721.

12. Percec, V., Barboiu, B., Kim, H. J. *J. Am. Chem. Soc.*, 1998, **120,** 305.

13. Hawker, C. J., Barclay, G. G., Orellana, A., Dao, J., Devonport, W. *Macromolecules*, 1996, **29,** 5245.

14. Chiefari, J., Chong, Y. K., Ercole, F., Krstina, J., Jeffery, J., Le, T. P. T., Mayadunne, R. T. A., Meijs, G. F., Moad, C. L., Moad, G., Rizzardo, E., Thang, S. H. *Macromolecules*, 1998, **31,** 5559.

15. Lowe, A. B., McCormick, C. L. *Prog. Polym. Sci.*, 2007, **32,** 283.

16. Perrier, S., Takolpuckdee, P. *J. Polym. Sci. Part a-Polymer Chem.*, 2005, **43,** 5347.

17. Moad, G., Rizzardo, E., Thang, S. H. *Aust. J. Chem.*, 2006, **59,** 669.

18. Moad, G., Rizzardo, E., Thang, S. H. *Polymer*, 2008, **49,** 1079.

19. Hawker, C. J., Bosman, A. W., Harth, E. *Chem. Rev.*, 2001, **101,** 3661.

20. Listigovers, N. A., Georges, M. K., Odell, P. G., Keoshkerian, B. *Macromolecules*, 1996, **29,** 8992.

21. Benoit, D., Chaplinski, V., Braslau, R., Hawker, C. J. *J. Am. Chem. Soc.*, 1999, **121,** 3904.

22. Mueller, L., Jakubowski, W., Tang, W., Matyjaszewski, K. *Macromolecules*, 2007, **40,** 6464.

23. Sawamoto, M., Kamigaito, M. *Macromol. Symp.*, 1995, **98,** 153.

24. Haddleton, D. M., Jasieczek, C. B., Hannon, M. J., Shooter, A. J. *Macromolecules*, 1997, **30,** 2190.

25. Haddleton, D. M., Crossman, M. C., Dana, B. H., Duncalf, D. J., Heming, A. M., Kukulj, D., Shooter, A. J. *Macromolecules*, 1999, **32,** 2110.

26. Jakubowski, W., Min, K., Matyjaszewski, K. *Macromolecules*, 2005, **39,** 39.

27. Jankova, K., Chem, X., Kops, J., Batsberg, W. *Macromolecules*, 1998, **31,** 538.

28. Moad, G., Chong, Y. K., Postma, A., Rizzardo, E., Thang, S. H. *IUPAC World Polym. Congr.*, (2004). in **46,** 8458.

29. Moad, G., Rizzardo, E., Thang, S. H. *Aust. J. Chem.*, 2006, **59,** 669.

30. Moad, G., Rizzardo, E., Thang, S. H. *Aust. J. Chem.*, 2009, **62,** 1402.

31. Chong, Y. K., Krstina, J., Le, T. P. T., Moad, G., Postma, A., Rizzardo, E., Thang, S. H. *Macromolecules*, 2003, **36,** 2256.

32. Chiefari, J., Mayadunne, R. T. A., Moad, C. L., Moad, G., Rizzardo, E., Postma, A., Thang, S. H. *Macromolecules*, 2003, **36,** 2273.

33. Wood, M. R., Duncalf, D. J., Rannard, S. P., Perrier, S. *Org. Lett.*, 2006, **8,** 553.

34. Chong, Y. K., Moad, G., Rizzardo, E., Thang, S. H. *Macromolecules*, 2007, **40,** 4446.

35. Benaglia, M., Chiefari, J., Chong, Y. K., Moad, G., Rizzardo, E., Thang, S. H. *J. Am. Chem. Soc.*, 2009, **131,** 6914.

36. Keddie, D. J., Guerrero-Sanchez, C., Moad, G., Rizzardo, E., Thang, S. H. *Macromolecules*, 2011, **44,** 6738.

37. Moad, G., Chong, Y. K., Postma, A., Rizzardo, E., Thang, S. H. *Polymer*, 2005, **46,** 8458.

38. Moad, G., Rizzardo, E., Thang, S. H. *Aust. J. Chem.*, 2012, **65,** 985.

39. Chong, B., Moad, G., Rizzardo, E., Skidmore, M., Thang, S. H. *Aust. J. Chem.*, 2006, **59,** 755.

40. Moughton, A. O., Stubenrauch, K., O'Reilly, R. K. *Soft Matter*, 2009, **5,** 2361.

41. Postma, A., Davis, T. P., Moad, G., O'Shea, M. S. *Macromolecules*, 2005, **38,** 5371.

42. Moad, G., Chiefari, J., Chong, Y. K., Krstina, J., Mayadunne, R. T. A., Postma, A., Rizzardo, E., Thang, S. H. *Polym. Int.*, 2000, **49,** 993.

43. Arshady, R. *Colloid Polym. Sci.*, 1992, **270,** 717.

44. Brooks, B. *Chem. Eng. Technol.*, 2010, **33,** 1737.

45. Kiparissides, C. *Chem. Eng. Sci.*, 1996, **51,** 1637.

46. Kawaguchi, S., Ito, K. *Polymer Particles*, 2005, **175**, 299, Springer Berlin Heidelberg.

47. Li, G. L., Mohwald, H., Shchukin, D. G. *Chem. Soc. Rev.*, 2013, **42,** 3628.

48. Hansen, F. K., Ugelstad, J. *J. Polym. Sci. Polym. Chem. Ed.*, 1979, **17,** 3047.

49. Chern, C. S. *Prog. Polym. Sci.*, 2006, **31,** 443.

50. Smith, W. V, Ewart, R. H. *J. Chem. Phys.*, 1948, **16,** 592

51. Nomura, M., Tobita, H., Suzuki, K. *Polymer Particles*, 2005, 175, 1, Springer Berlin Heidelberg

52. Tobita, H., Kumagai, M., Aoyagi, N. *Polymer*, 2000, **41,** 481.

53. Dingenouts, N., Norhausen, C., Ballauff, M. *Macromolecules*, 1998, **31,** 8912.

54. Lu, Y., Wittemann, A., Ballauff, M., Drechsler, M. *Macromol. Rapid Commun.*, 2006, **27,** 1137.

55. Cho, I., Lee, K.-W. *J. Appl. Polym. Sci.*, 1985, **30,** 1903.

56. Santos, A. M., Elaïssari, A., Martinho, J. M. G., Pichot, C. *Polymer*, 2005, **46,** 1181.

57. Dupin, D., Fujii, S., Armes, S. P., Reeve, P., Baxter, S. M. *Langmuir*, 2006, **22,** 3381.

58. Ma, G. H., Fukutomi, T. *Macromolecules*, 1992, **25,** 1870.

59. Amalvy, J. I., Wanless, E. J., Li, Y., Michailidou, V., Armes, S. P., Duccini, Y. *Langmuir*, 2004, **20,** 8992.

60. Jones, C. D., Lyon, L. A. *Macromolecules*, 2003, **36,** 1988.

61. Kim, Y., Liemmawal, E. D., Pourgholami, M. H., Morris, D. L., Stenzel, M. H. *Macromolecules*, 2012, **45,** 5451.

62. Mai, Y., Eisenberg, A. *Chem. Soc. Rev.*, 2012, **41,** 5969.

63. Matyjaszewski, K., Xia, J. *Chem. Rev.*, 2001, **101,** 2921.

64. Blanazs, A., Armes, S. P., Ryan, A. J. *Macromol. Rapid Commun.*, 2009, **30,** 267.

65. Read, E. S., Armes, S. P. *Chem. Commun.*, 2007, **29,** 3021.

66. Israelachvili, J. N., Mitchell, D. J., Ninham, B. W. *Biochim. Biophys. Acta*, 1977, **470,** 185.

67. Yu, Y., Eisenberg, A. *J. Am. Chem. Soc.*, 1997, **119,** 8383.

68. Nagarajan, R., Ganesh, K. *Macromolecules*, 1989, **22,** 4312.

69. O'Reilly, R. K., Joralemon, M. J., Hawker, C. J., Wooley, K. L. *Chem. A Eur. J.*, 2006, **12,** 6776.

70. Joralemon, M. J., O'Reilly, R. K., Hawker, C. J., Wooley, K. L. *J. Am. Chem. Soc.*, 2005, **127,** 16892.

71. Hansell, C. F., O'Reilly, R. K. *ACS Macro Lett.*, 2012, **1,** 896.

72. Nagarajan, R., Barry, M., Ruckenstein, E. *Langmuir*, 1986, **2,** 210.

73. Cotanda, P., O'Reilly, R. K. *Chem. Commun.*, 2012, **48,** 10280.

74. Schild, H. G. *Prog. Polym. Sci.*, 1992, **17,** 163.

75. Wu, C., Wang, X. *Phys. Rev. Lett.*, 1998, **80,** 4092.

76. Housni, A., Narain, R. *Eur. Polym. J.*, 2007, **43,** 4344.

77. Schilli, C. M., Zhang, M., Rizzardo, E., Thang, S. H., Chong, Y. K., Edwards, K., Karlsson, G., Müller, A. H. E. *Macromolecules*, 2004, **37,** 7861.

78. Hales, M., Barner-Kowollik, C., Davis, T. P., Stenzel, M. H. *Langmuir*, 2004, **20,** 10809.

79. Lu, Y., Proch, S., Schrinner, M., Drechsler, M., Kempe, R., Ballauff, M. *J. Mater. Chem.*, 2009, **19,** 3955.

80. Welsch, N., Wittemann, A., Ballauff, M. *J. Phys. Chem. B*, 2009, **113,** 16039.

81. Carregal-Romero, S., Buurma, N. J., Pérez-Juste, J., Liz-Marzán, L. M., Hervés, P. *Chem. Mater.*, 2010, **22,** 3051.

82. Chandrawati, R., van Koeverden, M. P., Lomas, H., Caruso, F. *J. Phys. Chem. Lett.*, 2011, **2,** 2639.

83. Monteiro, M. J. *Macromolecules*, 2010, **43,** 1159.

84. Peters, R. J. R. W., Louzao, I., van Hest, J. C. M. *Chem. Sci.*, 2012, **3,** 335.

85. Gao, H. *Macromol. Rapid Commun.*, 2012, **33,** 722.

86. Rasmussen, B., Christensen, J. B. *Org. Biomol. Chem.*, 2012, **10,** 4821.

87. Renggli, K., Baumann, P., Langowska, K., Onaca, O., Bruns, N., Meier, W. *Adv. Funct. Mater.*, 2011, **21,** 1241.

88. Nicolai, T., Colombani, O., Chassenieux, C. *Soft Matter*, 2010, **6,** 3111.

89. Yu, T., Wang, W., Chen, J., Zeng, Y., Li, Y., Yang, G., Li, Y. *J. Phys. Chem. C*, 2012, **116,** 10516.

90. Hu, N., Yin, J.-Y., Tang, Q., Chen, Y. *J. Polym. Sci. A Polym. Chem.*, 2011, **49,** 3826.

91. Deng, J., Yu, Y., Dun, S., Yang, W. *J. Phys. Chem. B*, 2010, **114,** 2593.

92. Sahiner, N., Butun, S., Ilgin, P. *Colloids Surfaces A*, 2011, **386,** 16–24

93. Li, J., Shi, X.-Y., Bi, Y.-Y., Wei, J.-F., Chen, Z.-G. *ACS Catal.*, 2011, **1,** 657.

94. Terashima, T., Ouchi, M., Ando, T., Sawamoto, M. *J. Polym. Sci. A Polym. Chem.*, 2010, **48,** 373.

95. Terashima, T., Ouchi, M., Ando, T., Sawamoto, M. *J. Polym. Sci. A Polym. Chem.*, 2011, **49,** 1061.

96. Liu, Y., Wang, Y., Wang, Y., Lu, J., Piñón, V., Weck, M. *J. Am. Chem. Soc.*, 2011, **133,** 14260.

97. Onaca, O., Hughes, D. W., Balasubramanian, V., Grzelakowski, M., Meier, W., Palivan, C. G. *Macromol. Biosci.*, 2010, **10,** 531.

98. Tanner, P., Onaca, O., Balasubramanian, V., Meier, W., Palivan, C. G. *Chem. A Eur. J.*, 2011, **17,** 4552.

99. Balasubramanian, V., Onaca, O., Ezhevskaya, M., Van Doorslaer, S., Sivasankaran, B., Palivan, C. G. *Soft Matter*, 2011, **7,** 5595.

100. van Dongen, S. F. M., Verdurmen, W. P. R., Peters, R. J. R. W., Nolte, R. J. M., Brock, R., van Hest, J. C. M. *Angew. Chem. Int. Ed.*, 2010, **49,** 7213.

101. Bäumler, H., Georgieva, R. *Biomacromol.*, 2010, **11,** 1480.

102. Narayan, S., Muldoon, J., Finn, M. G., Fokin, V. V, Kolb, H. C., Sharpless, K. B. *Angew. Chem. Int. Ed.*, 2005, **44,** 3275.

103. Mello, R. S., Orth, E. S., Loh, W., Fiedler, H. D., Nome, F. *Langmuir*, 2011, **27,** 15112.

104. Moyano, F., Falcone, R. D., Mejuto, J. C., Silber, J. J., Correa, N. M. *Chem. A Eur. J.*, 2010, **16,** 8887.

105. Lu, A., Cotanda, P., Patterson, J. P., Longbottom, D. a, O'Reilly, R. K. *Chem. Commun.*, 2012, **48,** 9699.

106. Lu, A., Smart, T. P., Epps, T. H., Longbottom, D. A., O'Reilly, R. K. *Macromolecules*, 2011, **44,** 7233.

107. Cotanda, P., Lu, A., Patterson, J. P., Petzetakis, N., O'Reilly, R. K. *Macromolecules*, 2012, **45,** 2377.

108. Kristensen, T. E., Hansen, T. *Eur. J. Org. Chem.*, 2010, **17,** 3179.

109. Rodionov, V., Gao, H., Scroggins, S., Unruh, D. A., Avestro, A.-J., Fréchet, J. M. J. *J. Am. Chem. Soc.*, 2010, **132,** 2570.

110. Korovin, A. N., Sergeyev, V. G., Pyshkina, O. A., Hanske, C., Fery, A., Wittemann, A., Tsarkova, L. *Macromol. Rapid Commun.*, 2011, **32,** 462.

111. Ahn, H., Park, M. J. *Macromol. Rapid Commun.*, 2011, **32,** 1790.

112. Berlamino, A. T. N., Orth, E. S., Mello, R. S., Medeiros, M., Nome, F. *J. Mol. Catal. A Chem.*, 2010, **332,** 7.

113. Garcia, L., Roglans, A., Laurent, R., Majoral, J.-P., Pla-Quintana, A., Caminade, A.-M. *Chem. Commun.*, 2012, **48,** 9248.

114. Goren, K., Portnoy, M. *Chem. Commun.*, 2010, **46,** 1965.

115. Imada, Y., Iida, H., Kitagawa, T., Naota, T. *Chem. A Eur. J.*, 2011, **17,** 5908.

116. Diallo, A. K., Boisselier, E., Liang, L., Ruiz, J., Astruc, D. *Chem. Eur. J.*, 2010, **16,** 11832.

117. Lan, Y., Yang, L., Zhang, M., Zhang, W., Wang, S. *ACS Appl. Mater. Interfaces*, 2009, **2,** 127.

118. Zhang, M., Zhang, W. *J. Polym. Sci. Part A Polym. Chem.*, 2010, **48,** 5446.

119. Zetterlund, P. B. *Polym. Chem.*, 2011, **2,** 534.

120. Valade, D., Jeon, Y., Kessel, S., Monteiro, M. J. *J. Polym. Sci. A Polym. Chem.*, 2012, **50,** 4762.

121. Terashima, T., Nomura, A., Ito, M., Ouchi, M., Sawamoto, M. *Angew. Chemie Int. Ed.*, 2011, **50,** 7892.

122. Terashima, T., Nomura, A., Ouchi, M., Sawamoto, M. *Macromol. Rapid Commun.*, 2012, **33,** 833.

123. Sebakhy, K. O., Kessel, S., Monteiro, M. J. *Macromolecules*, 2010, **43,** 9598.

124. Zayas, H. A., Lu, A., Valade, D., Amir, F., Jia, Z., O'Reilly, R. K., Monteiro, M. J. *ACS Macro Lett.*, 2013, **2,** 327.

125. McHale, R., Patterson, J. P., Zetterlund, P. B., O'Reilly, R. K. *Nat Chem*, 2012, **4,** 491.

126. Gaitzsch, J., Appelhans, D., Wang, L., Battaglia, G., Voit, B. *Angew. Chem. Int. Ed.*, 2012, **51,** 4448.

127. Wang, Y., Wei, G., Zhang, W., Jiang, X., Zheng, P., Shi, L., Dong, A. *J. Mol. Catal. A Chem.*, 2007, **266,** 233.

128. Li, S., Ge, Y., Tiwari, A., Wang, S., Turner, A. P. F., Piletsky, S. A. *J. Catal.*, 2011, **278,** 173.

129. Li, S., Ge, Y., Turner, A. P. F. *Adv. Funct. Mater.*, 2011, **21,** 1194.

130. Li, S., Ge, Y., Tiwari, A., Cao, S. *Small*, 2010, **6,** 2453.

131. Terashima, T., Mes, T., De Greef, T. F. A., Gillissen, M. A. J., Besenius, P., Palmans, A. R. A., Meijer, E. W. *J. Am. Chem. Soc.*, 2011, **133,** 4742.

132. Huerta, E., Stals, P. J. M., Meijer, E. W., Palmans, A. R. A. *Angew. Chem. Int. Ed.*, 2013, 52, 2906.

133. Sanson, N., Rieger, J. *Polym. Chem.*, 2010, **1,** 965.

134. Weaver, J. V. M., Williams, R. T., Royles, B. J. L., Findlay, P. H., Cooper, A. I., Rannard, S. P. *Soft Matter*, 2008, **4,** 985.

135. He, T., Adams, D. J., Butler, M. F., Yeoh, C. T., Cooper, A. I., Rannard, S. P. *Angew. Chem. Int. Ed.*, 2007, **46,** 9243.

136. Hawker, C. J., Wooley, K. L., Fréchet, J. M. J. *J. Chem. Soc. Perkin Trans. 1*, 1993, 1287.

137. Fréchet, J. M. J. *J. Polym. Sci. Part A Polym. Chem.*, 2003, **41,** 3713.

138. Fréchet, J. M. J. *Proc. Natl. Acad. Sci. U.S.A*, 2002, **99,** 4782.

139. Aulenta, F., Hayes, W., Rannard, S. *Eur. Polym. J.*, 2003, **39,** 1741.

140. Lu, Y., Mei, Y., Drechsler, M., Ballauff, M. *Angew. Chem. Int. Ed.*, 2006, **45,** 813.

141. Wang, Y., Wei, G., Wen, F., Zhang, X., Zhang, W., Shi, L. *J. Mol. Catal. A Chem.*, 2008, **280,** 1.

142. Wang, G., Kuroda, K., Enoki, T., Grosberg, A., Masamune, S., Oya, T., Takeoka, Y., Tanaka, T. *Proc. Natl. Acad. Sci. U.S.A*, 2000, **97,** 9861.

143. Wang, Y., Zhang, J., Zhang, W., Zhang, M. *J. Org. Chem.*, 2009, **74,** 1923.

144. Siddique, H., Peeva, L. G., Stoikos, K., Pasparakis, G., Vamvakaki, M., Livingston, A. G. *Ind. Eng. Chem. Res.*, 2012, **52**, 1109.

145. Cho, K. Y., Choi, J.-W., Lee, S.-H., Hwang, S. S., Baek, K.-Y. *Polym. Chem.*, 2013, **4,** 2400.

146. Eichenbaum, G. M., Kiser, P. F., Dobrynin, A. V, Simon, S. A., Needham, D. *Macromolecules*, 1999, **32,** 4867.

147. Qiu, X., Leporatti, S., Donath, E., Möhwald, H. *Langmuir*, 2001, **17,** 5375.

148. Ogawa, K., Wang, B., Kokufuta, E. *Langmuir*, 2001, **17,** 4704.

149. González-Toro, D. C., Ryu, J.-H., Chacko, R. T., Zhuang, J., Thayumanavan, S. *J. Am. Chem. Soc.*, 2012, **134,** 6964.

150. Kim, J.-Y., Song, J.-Y., Lee, E.-J., Park, S.-K. *Colloid Polym. Sci.*, 2003, **281,** 614.

151. Wei, G., Zhang, W., Wen, F., Wang, Y., Zhang, M. *J. Phys. Chem. C*, 2008, **112,** 10827.

152. Wu, S., Dzubiella, J., Kaiser, J., Drechsler, M., Guo, X., Ballauff, M., Lu, Y. *Angew. Chem. Int. Ed.*, 2012, **51,** 2229.

153. Ge, Z., Xie, D., Chen, D., Jiang, X., Zhang, Y., Liu, H., Liu, S. *Macromolecules*, 2007, **40,** 3538.

154. Choi, B. G., Song, R., Nam, W., Jeong, B. *Chem. Commun.*, 2005, **23**, 2960.

155. Pan, G., Guo, Q., Cao, C., Yang, H., Li, B. *Soft Matter*, 2013, **9,** 3840.

156. Gan, D., Lyon, L. A. *Macromolecules*, 2002, **35,** 9634.

157. Li, S., Gong, S. *J. Phys. Chem. B*, 2009, **113,** 16501.

158. Jiang, X., Xiong, D., An, Y., Zheng, P., Zhang, W., Shi, L. *J. Polym. Sci. Part A Polym. Chem.*, 2007, **45,** 2812.

159. Huang, X., Yin, Y., Tang, Y., Bai, X., Zhang, Z., Xu, J., Liu, J., Shen, J. *Soft Matter*, 2009, **5,** 1905.

160. Yan, N., Zhang, J., Yuan, Y., Chen, G.-T., Dyson, P. J., Li, Z.-C., Kou, Y. *Chem. Commun.*, 2010, **46,** 1631.

161. Lu, Y., Yuan, J., Polzer, F., Drechsler, M., Preussner, J. *ACS Nano*, 2010, **4,** 7078.

162. Ryu, J.-H., Chacko, R. T., Jiwpanich, S., Bickerton, S., Babu, R. P., Thayumanavan, S. *J. Am. Chem. Soc.*, 2010, **132,** 17227.

163. Ryu, J.-H., Bickerton, S., Zhuang, J., Thayumanavan, S. *Biomacromol.*, 2012, **13,** 1515.

164. Zhuang, J., Jiwpanich, S., Deepak, V. D., Thayumanavan, S. *ACS Macro Lett.*, 2011, **1,** 175.

165. Ryu, J.-H., Jiwpanich, S., Chacko, R., Bickerton, S., Thayumanavan, S. *J. Am. Chem. Soc.*, 2010, **132,** 8246.

166. MacMillan, D. W. C. *Nature*, 2008, **455,** 304.

167. Kondo, K., Yamano, T., Takemoto, K. *Macromol. Chem. Phys.*, 1985, **186,** 1781.

168. Hajos, Z. G., Parrish, D. R. *J. Org. Chem.*, 1974, **39,** 1615.

169. Eder, U., Sauer, G., Wiechert, R. *Angew. Chem. Int. Ed.*, 1971, **10,** 496.

170. List, B., Lerner, R. A., Barbas III, C. F. *J. Am. Chem. Soc.*, 2000, **122,** 2395.

171. Ahrendt, K. A., Borths, C. J., MacMillan, D. W. C. *J. Am. Chem. Soc.*, 2000, **122,** 4243.

172. Notz, W., Tanaka, F., Watanabe, S., Chowdari, N. S., Turner, J. M., Thayumanavan, R., Barbas, C. F. *J. Org. Chem.*, 2003, **68,** 9624.

173. List, B., Pojarliev, P., Castello, C. *Org. Lett.*, 2001, **3,** 573.

174. Mase, N., Thayumanavan, R., Tanaka, F., Barbas, C. F. *Org. Lett.*, 2004, **6,** 2527.

175. List, B. *Tetrahedron*, 2002, **58,** 5573.

176. Bui, T., Barbas, C. F. *Tetrahedron Lett.*, 2000, **41,** 6951.

177. Hoang, L., Bahmanyar, S., Houk, K. N., List, B. *J. Am. Chem. Soc.*, 2002, **125,** 16.

178. Mukherjee, S., Yang, J. W., Hoffmann, S., List, B. *Chem. Rev.*, 2007, **107,** 5471.

179. Movassaghi, M., Jacobsen, E. N. *Science*, 2002, **298,** 1904.

180. Notz, W., Tanaka, F., Barbas, C. F. *Acc. Chem. Res.*, 2004, **37,** 580.

181. Mase, N., Nakai, Y., Ohara, N., Yoda, H., Takabe, K., Tanaka, F., Barbas, C. F. *J. Am. Chem. Soc.*, 2005, **128,** 734.

182. Liu, X., Basu, A. *J. Am. Chem. Soc.*, 2009, **131,** 5718.

183. List, B., Hoang, L., Martin, H. J. *Proc. Natl. Acad. Sci. USA*, 2004, **101,** 5839.

184. Raj, M., Singh, V. K. *Chem. Commun.*, 2009, **44**, 6687.

185. Tang, Z., Jiang, F., Yu, L.-T., Cui, X., Gong, L.-Z., Mi, A.-Q., Jiang, Y.-Z., Wu, Y.-D. *J. Am. Chem. Soc.*, 2003, **125,** 5262.

186. Raj, M., Vishnumaya, Ginotra, S. K., Singh, V. K. *Org. Lett.*, 2006, **8,** 4097.

187. Gaunt, M. J., Johansson, C. C. C. *Chem. Rev.*, 2007, **107,** 5596.

188. Moore, B. L., Lu, A., Longbottom, D. A., O'Reilly, R. K. *Polym. Chem.*, 2013, **4,** 2304.

189. Gröger, H., Wilken, J. *Angew. Chem. Int. Ed.*, 2001, **40,** 529.

190. Benaglia, M., Celentano, G., Cozzi, F. *Adv. Synth. Catal.*, 2001, **343,** 171.

191. Benaglia, M., Cinquini, M., Cozzi, F., Puglisi, A., Celentano, G. *Adv. Synth. Catal.*, 2002, **344,** 533.

192. Benaglia, M., Cinquini, M., Cozzi, F., Puglisi, A., Celentano, G. *J. Mol. Catal. A Chem.*, 2003, **204–205,** 157.

193. Font, D., Jimeno, C., Pericàs, M. A. *Org. Lett.*, 2006, **8,** 4653.

194. Gruttadauria, M., Salvo, A. M. P., Giacalone, F., Agrigento, P., Noto, R. *Eur. J. Org. Chem.*, 2009, **2009,** 5437.

195. Liu, Y. X., Sun, Y. N., Tan, H. H., Liu, W., Tao, J. C. *Tetrahedron: Asymmetry*, 2007, **18,** 2649.

196. Font, D., Sayalero, S., Bastero, A., Jimeno, C., Pericas, M. A. *Org. Lett.*, 2007, **10,** 337.

197. Torchilin, V. P. *Pharm. Res.*, 2007, **24,** 1.

198. Aprile, C., Giacalone, F., Gruttadauria, M., Marculescu, A. M., Noto, R., Revell, J. D., Wennemers, H. *Greem Chem.*, 2007, **9,** 1328.

199. Miao, W., Chan, T. H. *Adv. Synth. Catal.*, 2006, **348,** 1711.

200. Hayashi, Y., Aratake, S., Okano, T., Takahashi, J., Sumiya, T., Shoji, M. *Angew. Chemie Int. Ed.*, 2006, **45,** 5527.

201. Lipshutz, B. H., Ghorai, S. *Org. Lett.*, 2011, **14,** 422.

202. Sanda, F., Endo, T. *Macromol. Chem. Phys.*, 1999, **200,** 2651.

203. Mori, H., Iwaya, H., Endo, T. *Macromol. Chem. Phys.*, 2007, **208,** 1908.

204. Mori, H., Iwaya, H., Nagai, A., Endo, T. *Chem. Commun.*, 2005, **38**, 4872.

205. Lokitz, B. S., Stempka, J. E., York, A. W., Li, Y., Goel, H. K., Bishop, G. R., McCormick, C. L. *Aust. J. Chem.*, 2006, **59,** 749.

206. Skey, J., Hansell, C. F., O'Reilly, R. K. *Macromolecules*, 2010, **43,** 1309.

207. Skey, J., O'Reilly, R. K. *J. Polym. Sci. Part a-Polymer Chem.*, 2008, **46,** 3690.

208. Casolaro, M., Bottari, S., Cappelli, A., Mendichi, R., Ito, Y. *Biomacromol.*, 2004, **5,** 1325.

209. Sanda, F., Nakamura, M., Endo, T. *Macromolecules*, 1996, **29,** 8064.

210. Kristensen, T. E., Vestli, K., Fredriksen, K. A., Hansen, F. K., Hansen, T. *Org. Lett.*, 2009, **11,** 2968.

2. L-Proline Containing RAFT Polymers: Their Synthesis, Solution Self-Assembly and Catalytic Efficiency

2.1. Abstract

Well-defined copolymers containing the catalytically interesting amino acid L-proline have been successfully synthesized using reversible addition-fragmentation chain transfer (RAFT) polymerization. Their application in supported catalysis was explored in a model asymmetric aldol reaction. Interesting polymer assemblies were found in the mixed solvent system used for catalysis and explain the high catalytic efficiency of the copolymer at low catalyst loading compared to unsupported L-proline. We propose this is a direct effect of the copolymer forming a unique microenvironment which acts as a confined reaction sphere concentrating the catalyst and substrates. The supported catalyst also exhibited recovery and reuse potential which is a great advantage over the unsupported catalyst. The spherical nature of the copolymer assemblies were confirmed by transmission and scanning electron microscopy (TEM and SEM) at a range of tilt angles.

2.2. Introduction

Nature's processes are highly efficient due to the precise placement of functionalities within natural macromolecules allowing them to assemble into well-defined reactors in water. The naturally occurring amino acid L-proline is known as the 'simple enzyme' as it catalyzes asymmetric carbon-carbon bond forming reactions in a similar mechanistic manner to the aldolase enzyme.[1] However, L-proline catalyzed reactions are often carried out in organic solvents such as DMF and chloroform due to the hydrophobic nature of the substrates. Thus, the desire to achieve the precision in macromolecular design and catalytic efficiency observed in Nature, has sparked research into the direction of polymer supported catalysis. In this aspect, L-proline has been modified with a variety of hydrophobic moieties to improve the performance of the catalyst.

Barbas' group,[2, 3] Hayashi *et al.*[4] and others[5, 6] showed improved activity with their catalytic derivatives. The selection of anchoring site and its importance on the activity of the resulting catalyst has also been investigated.[7] The studies highlighted the importance of sterics and electronics around the active site as a number of derivatives with reduced performance have also been reported.[8-10] Most significantly was the observation that a concentrated organic phase was formed in water as a result of the hydrophobic modifications. This allowed catalysis of highly hydrophobic substrates in water to take place.[3, 4, 11]

Polymers have been compared to a peptide backbone and may, in addition to enhancing the hydrophobicity of the catalyst, be a closer resemblance to Nature's macromolecules. Initial studies were dedicated to the immobilization of L-proline onto supports such as polyethylene glycol (PEG),[12-14] polystyrene beads,[15-18] Merrifield resin,[19] ionic liquids[20, 21] and dendrimers.[22] Some of these have been successfully used in multiple catalytic cycles with close to unchanged yields and only relatively small losses in selectivity. Endo and Sanda[23] reported the synthesis of vinyl amino acid monomers and their polymerization widening the variety of methods used for immobilization of these amino acid functionalities (Figure 2.1). More recently the range of amino acid monomers has been extended to L-phenylalanine, L-leucine, L-alanine, L-histidine and L-tryptophan.[24-28]

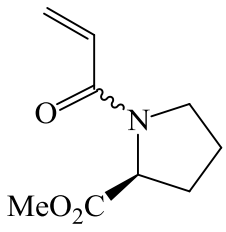

Figure 2.1. Endo and Sanda's vinyl monomer, *N*-acryloyl-L-proline methyl ester[23]

Kristensen *et al.*[29-31] have also chosen this bottom up approach and reported the synthesis of several methacrylic type L-proline monomers. However, rather than synthesizing linear polymers, like the ones discussed above, a range of methacrylic and styrenic cross-linked copolymer beads were synthesized. These micron-sized beads were successfully used in multiple catalytic cycles with high activity and selectivity.

We wanted to take advantage of recent advances made in controlled radical polymerization (CRP) techniques to achieve improved control over polymer molecular weight and dispersity. This level of control allows the synthesis of well-defined polymers with predictable catalyst incorporation which may undergo self-assembly to form higher ordered structures and nanoreactors. Previously our group used nitroxide-mediated polymerization (NMP) and RAFT polymerization to synthesize polystyrene (PS) copolymers containing the L-proline functionality. The retained activity of the catalyst was thoroughly studied in a model aldol reaction in a range of solvent systems. We wanted to further explore the use of RAFT polymerization to access a greater range of polymer supports and more readily achieve block copolymers with tuneable solution properties.

2.3. Results and Discussion

2.3.1. Monomer synthesis

To afford the means to attach organocatalytically active L-proline onto the polymer backbone, whilst leaving both the amino and carboxylic acid functionalities of L-proline available for catalysis, a 4-hydroxy-L-proline functionalized monomer, protected at the amino and acid functionalities was synthesized (Scheme 2.1). The RAFT polymerization technique has been shown to be tolerant to a range of monomers with varying functionalities, including acids and amines.[32, 33] Nevertheless, a monomer

where the amino and acid functionalities were protected was synthesized in order to allow for simple characterization by SEC, as acids and non-substituted amines have been shown to interact with the column.

The monomer synthesis started with the commercially available *Boc*-*O*-benzyl-*trans*-hydroxy-L-proline, protected at the hydroxyl and amine functionalities. The carboxylic acid functionality was first protected with a *tert*-butyl protecting group using *tert*-butanol *via* the Steglich esterification reaction.[34,35] This coupling reaction was carried out with *N*-(3-dimethylaminopropyl)-*N*'-ethylcarbodiimide hydrochloride (EDCI.HCl) as the coupling reagent and 4-dimethylaminopyridine (DMAP) as the catalyst in CH_2Cl_2 (Scheme 2.1). The triply protected product (**2.1**) was afforded after removal of the coupling reagent and catalyst by aqueous washes (87% yield). The hydroxyl functionality of **2.1** was revealed *via* removal of the benzyl protecting group by hydrogenation using Pd/C (Scheme 2.1). The pure ^{t}Bu/Boc protected hydroxy-L-proline (**2.2**) was isolated by flash column chromatography (82% yield).

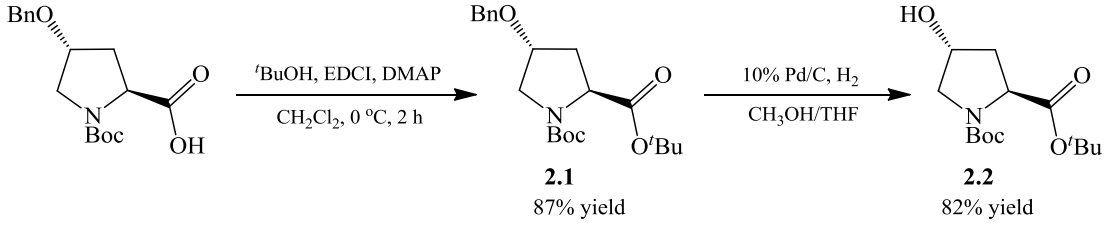

Scheme 2.1. Two step synthesis of amino and acid protected hydroxy-L-proline (1.2) from commercially available *bis*-protected Boc-*O*-benzyl-*trans*-hydroxy-L-proline

Key intermediate **2.2** was then coupled with 4-vinylbenzoic acid (VBA) *via* a Steglich esterification reaction to provide the desired *bis*-protected L-proline functionalized styrenic monomer **2.3** (Scheme 2.2).

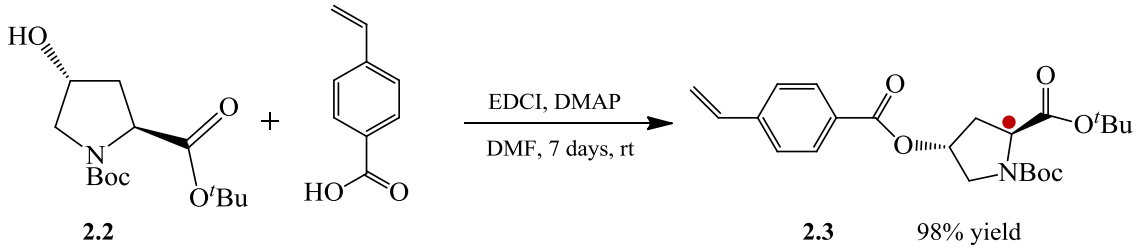

2.2 **2.3** 98% yield

Scheme 2.2. Steglich esterification of 2.2 and VBA to give monomer 2.3, highlighted is the chiral C2 carbon

The catalyst functionality was connected to the polymerizable styrenic functionality *via* an ester linkage rather than an ether linkage, as previously reported by our group.[36] Although the ether linkage may provide a chemically more stable link, it has been shown that the chemistry used caused racemization at the chiral C2 carbon (highlighted in Scheme 2.2). The coupling chemistry used for the ester linkage in previous work[36] and in this work did not result in the racemization of the same carbon centre. Specific rotation of **2.3** in the same direction as the starting L-proline precursor determined by polarimetry suggests no racemization had occurred. The absence of diastereoisomers in the ^{1}H NMR spectrum further supports the successful coupling chemistry.

Previous work in our group utilized the benzyl carbamate (CBz) and benzyl ester (Bn) protecting groups for the amino and acid functionalities respectively. However, this required the use of relatively harsh deprotection chemistries.[36] Therefore, Boc and ^{t}Bu protecting groups were selected: by utilizing an acid catalyzed deprotection strategy, both protecting groups may be easily deprotected simultaneously to reveal both the amino and acid functionalities.[37]

The ^{1}H NMR spectrum of fully protected monomer **2.3** is shown below in Figure 2.2 and 2D COSY NMR spectroscopy was used to confirm the identity of the signals. The

^{1}H NMR spectrum showed the expected chemical shifts and integration. However, a number of signals assigned to the 5-membered ring of L-proline showed unexpected splitting patterns, labelled **g**, **h** and **i** in Figure 2.2. These signals have been assigned to the protons of the proline ring. The splitting pattern observed for diastereotopic protons **g** and **i** were a direct result of their position between the two stereocenters in the 5-membered ring.

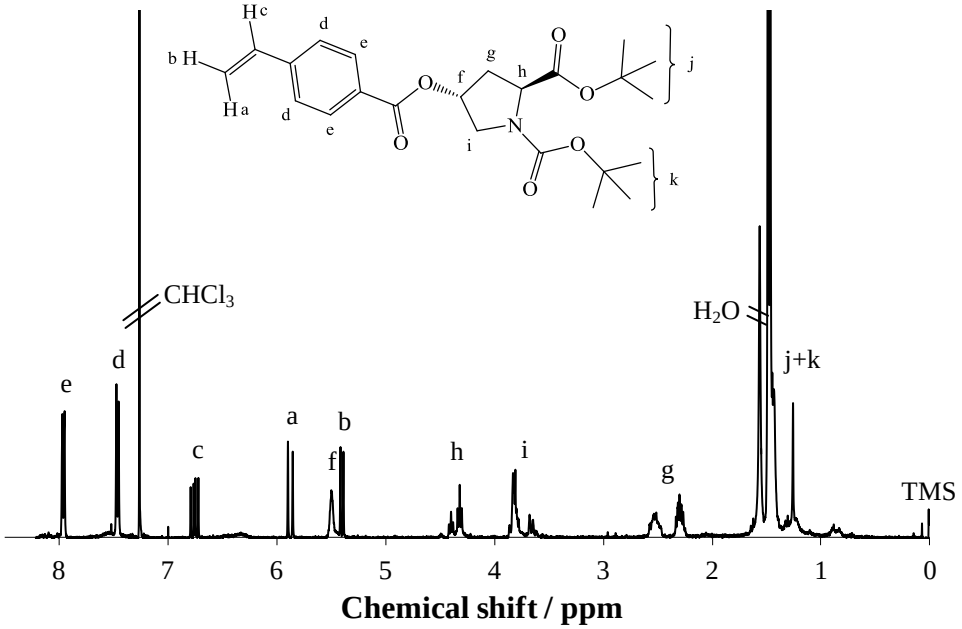

Figure 2.2. ^{1}H NMR spectrum (400 MHz, $CDCl_3$) of 2.3 at 25 °C clearly showing the rotameric effects for proton H_h at 4.35 ppm

The unusual splitting noted at δ 4.30 ppm for proton **h** was believed to be the result of a rotameric effect of the neighbouring *Boc N*-protecting group. Splitting of signals assigned to the L-proline ring was also observed in the ^{13}C NMR spectrum of monomer **2.3**. To elucidate if this was indeed an effect of the presence of rotamers or diastereomers further NMR experiments were carried out. Rotameric effect is a result of restriction in rotation about a single bond leading to different conformations of the molecule. That is to say that the isomerization is not permanent and may be overcome by breaking the rotational energy barrier. Thus, by carrying out NMR experiments at a higher temperature, it is possible to differentiate between diastereomers and rotamers as

equilibration of the rotameric species will result in a more simplified NMR spectrum. Indeed, the splitting pattern observed for H_h was resolved by high temperature ^{1}H NMR spectroscopy (Figure 2.3, Figure 2.4). This was carried out at 60 °C in $CDCl_3$ and showed a single peak for H_h, which verified that no racemization had taken place during the coupling process.

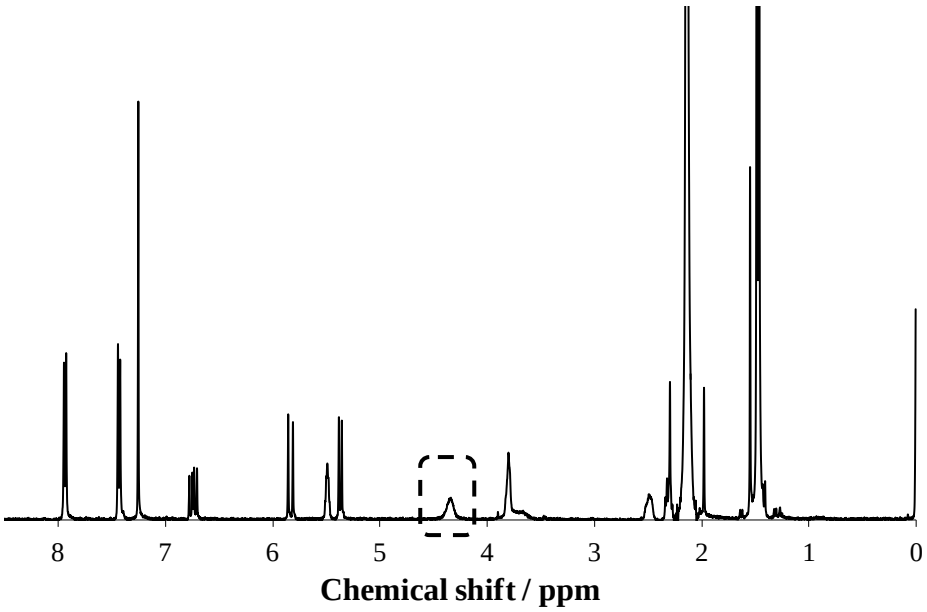

Figure 2.3. ^{1}H NMR spectrum (400 MHz, $CDCl_3$) of 2.3 at 60 °C where the rotameric effect is confirmed by elimination of the unusual splitting previously observed at 4.35 ppm (highlighted)

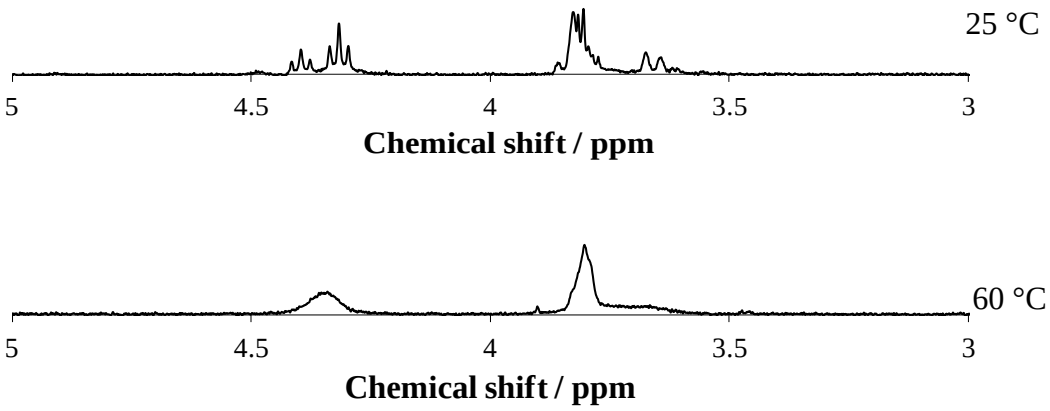

Figure 2.4. ^{1}H NMR spectrum (400 MHz, $CDCl_3$) of 2.3 at 25 °C and 60 °C, showing the signal altered due to the rotameric effects for proton H_h

2.3.2. CTA synthesis

An adapted procedure for the synthesis of RAFT agents or chain transfer agents (CTA) was used to synthesize the desired CTA dodecyl 1-phenylethyl trithiocarbonate (CTA1) (Scheme 2.3).[38-40] A trithiocarbonate type CTA was targeted, as these have been shown to polymerize a range of monomers, including functional monomers, with high efficiency.[32] The desired CTA was synthesized in a relatively quick one-pot reaction starting from 1-dodecanethiol, 1-bromoethyl benzene and carbon disulfide. A yellow viscous liquid was formed in 89% yield after purification by flash column chromatography. The purity of CTA 1 was confirmed by elemental analysis and ^{1}H NMR spectroscopy (Figure 2.5).

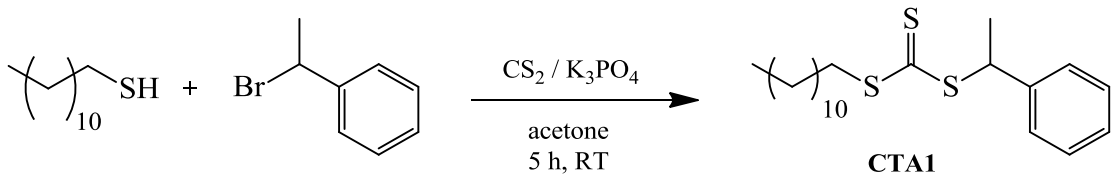

Scheme 2.3. Representative scheme for the synthesis of RAFT agent dodecyl 1-phenylethyl trithiocarbonate (CTA 1)

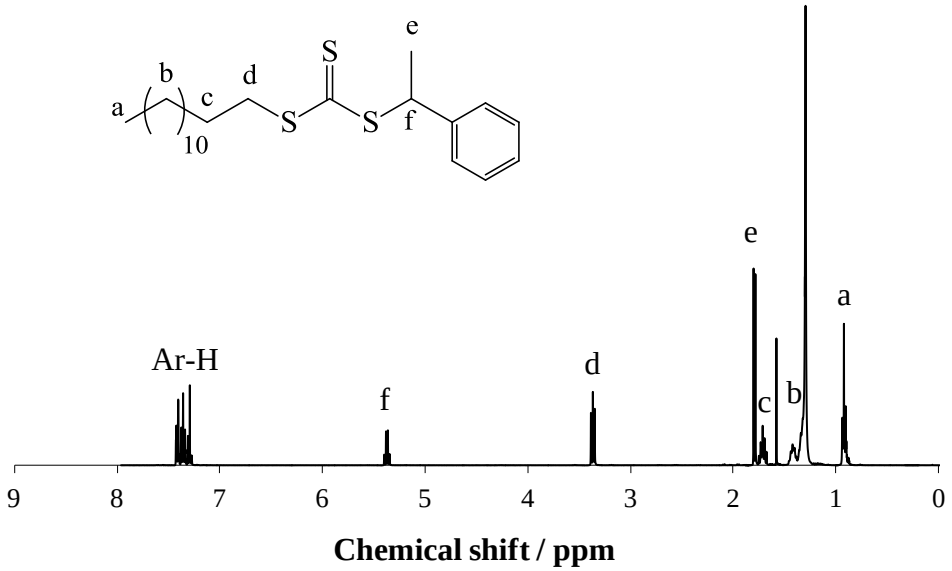

Figure 2.5. ^{1}H NMR (400 MHz, $CDCl_3$) spectrum of CTA1

2.3.3. Homopolymerization of styrene

The synthesized CTA1 was used in the homopolymerization of styrene to evaluate its RAFT efficiency i.e. its ability to achieve the desired molecular weights, polymers with narrow molecular weight distribution and high end group fidelity. The polymerization was carried out under solvent free conditions at 110 °C for 22 hours (Scheme 2.5).

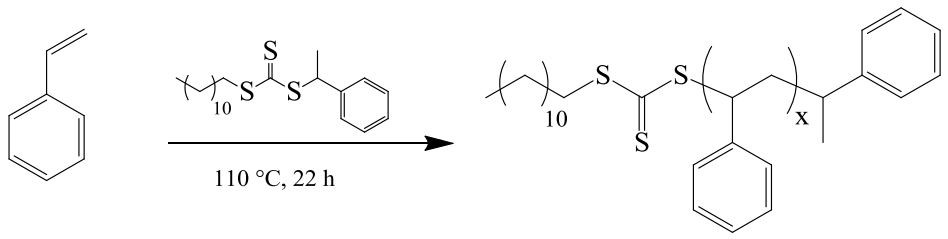

Scheme 2.4. Homopolymerization of styrene using CTA 1, polymerization under solvent free conditions at 110 °C for 22 hours

The polymer was precipitated into cold methanol, collected by filtration and dried in the vacuum oven at 40 °C overnight. The PS polymer was then characterized by ^{1}H NMR spectroscopy and SEC. By comparing ^{1}H NMR signals originating from the CTA end group with those of the polymer, the molecular weight ($M_{n,\mathrm{NMR}}$) and degree of polymerization (DP) were determined ($M_{n,\mathrm{NMR}}$ = 6.6 kDa, $\mathrm{DP_{St}}$ = 60, 63% conversion) and the polymer was additionally analyzed by SEC and compared to a PS calibration (M_n = 6.6 kDa, M_w 7.0 kDa, Đ = 1.06) with a narrow molecular weight distribution, confirming that the RAFT process with CTA1 was indeed efficient. The molecular weights determined by ^{1}H NMR spectroscopy and SEC were found to be comparable, suggesting good end group fidelity and with these results in hand, we were confident to proceed with the copolymerization of styrene and functional monomer **2.3**.

2.3.4. Copolymerization of styrene and 2.3

The RAFT copolymerization of **2.3** and styrene with CTA 1 was similar to the homopolymerization of styrene, carried out under solvent free conditions at high temperature (Scheme 2.5). This was allowed to proceed for 22 hours, after which an aliquot was withdrawn to determine the conversion of the two monomers and the polymer was precipitated into cold methanol. A range of copolymers was synthesized with the aim of achieving statistical copolymers with varying molecular weights and approximately 5% catalyst incorporation. The final DP of the copolymers were tuned by quenching the polymerization after different times; hence, always starting with the same monomer ratios, i.e. 95:5 styrene:**2.3**. It is worth noting that copolymerizations previously carried out in the group suggested that monomer **2.3** polymerized at a faster rate compared with the comonomer styrene under RAFT conditions. Thus, it was hypothesized that the catalytic functionality was not randomly distributed along the polymer backbone, but that diblock copolymers were more likely achieved. This was supported by the fact that greater than the desired 5% incorporation of **2.3** was observed in all copolymerizations, suggesting that in fact only the final ratio of styrene was controlled by quenching the reaction at different times. The reactivity ratio of the two monomers will be discussed later in this chapter.

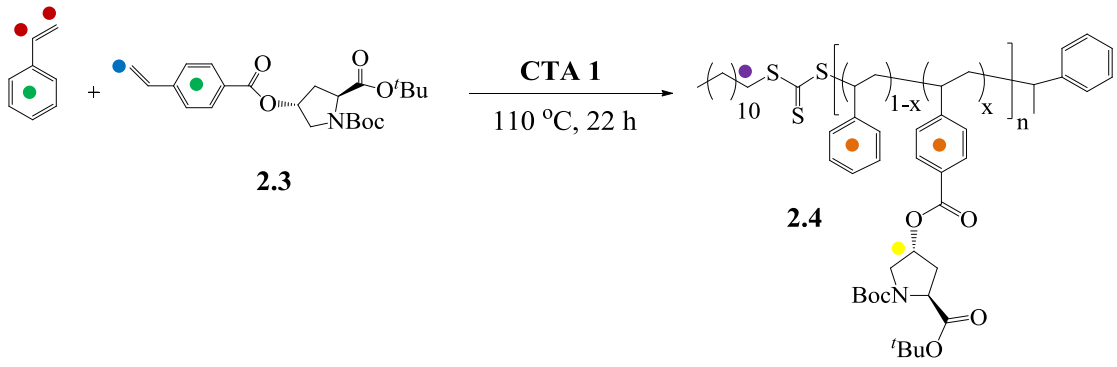

Scheme 2.5. Representative scheme of the copolymerization of 2.3 and styrene using CTA1 under solvent free conditions to give protected copolymers (2.4)

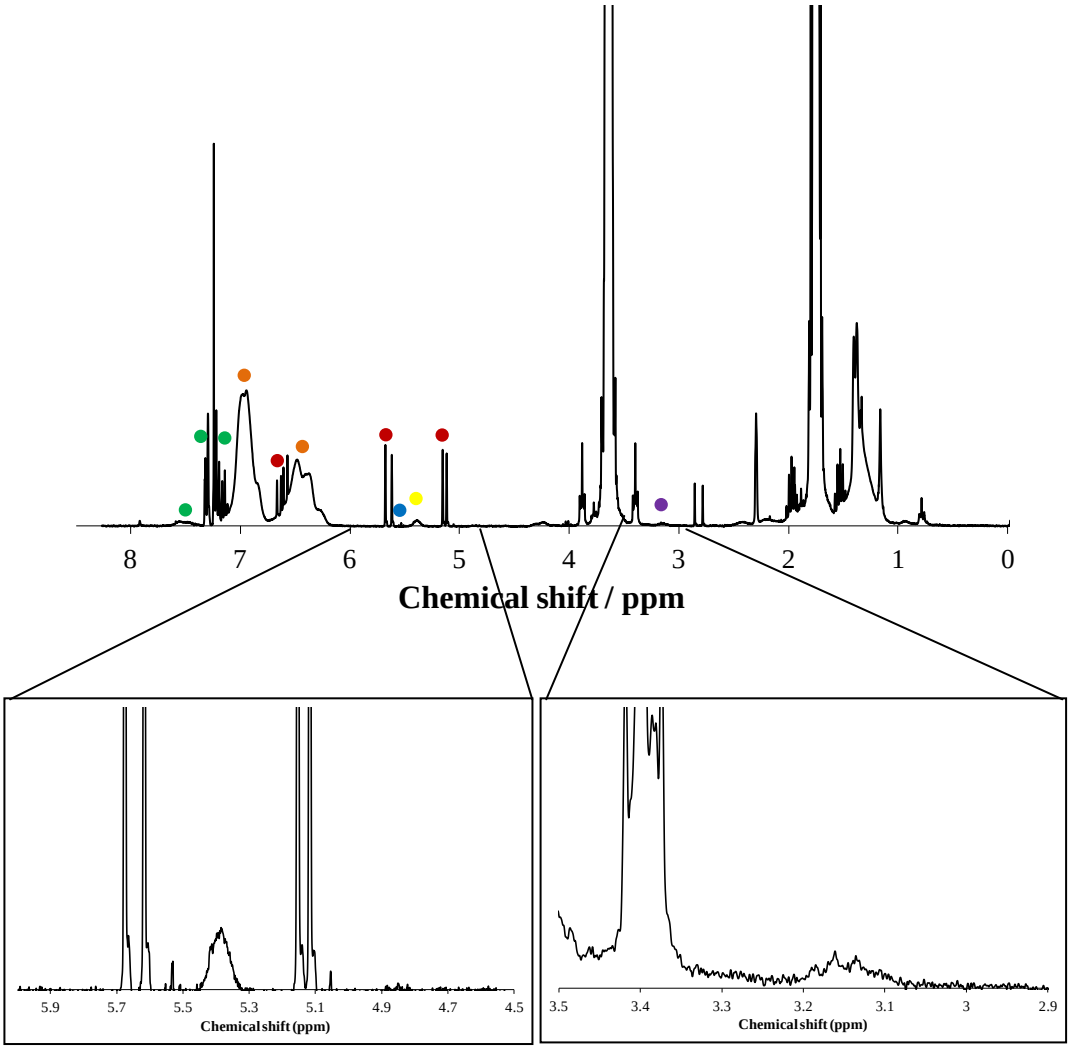

Figure 2.6. Example ^{1}H NMR spectrum (400 MHz, $CDCl_3$) during polymerization of 2.4, used to determine the conversion of the two monomers (see Scheme 2.5 for assignment), expansion of signals corresponding to the monomer (left) and CTA (right)

The polymerization conversion for each monomer was determined by ^{1}H NMR spectroscopy by comparing distinct signals of the monomer to the polymer in the ^{1}H NMR spectrum (Figure 2.6). The monomer signals used were δ 5.45 ppm (1H) for **2.3** and δ 5.13 ppm for styrene (1H); and polymer signals δ 5.30 ppm for poly-**2.3** (1H) and δ 6.20-7.30 ppm (5H) for PS. In each case where there are overlapping monomer and polymer signals, the integration achieved from a non-overlapping monomer signal was used and its contribution subtracted. The signal at δ 3.20 ppm for the CTA was used to

determine the DP of the two monomers in the final polymer, and thus the polymer molecular weight (Figure 2.7). However, the molecular weight estimated by ^{1}H NMR spectroscopy assumes 100% end group fidelity, i.e. each polymer chain has an end group. The ratio of the two monomers in the polymer was used to determine the percentage incorporation of the catalyst into the polymer, which was initially targeted to be approximately 5 mol%. However, as mentioned above, as monomer **2.3** was incorporated into the polymer at a faster rate (i.e. at the beginning of the polymerization) compared to the comonomer styrene, only the final DP of styrene could be controlled, which was monitored by ^{1}H NMR spectroscopy.

The copolymer was then analyzed by SEC with THF as the eluent and using PS calibration. The narrow polymer dispersity indices (< 1.1) achieved for the range of synthesized copolymers confirms that polymerization proceeded with good control (see below: Table 2.1). The comparable molecular weights achieved by ^{1}H NMR spectroscopy and SEC indicate that the end group was retained relatively well. The presence of CTA 1 in the polymer was also confirmed by examining the UV trace collected from SEC at 309 nm, the wavelength characteristic for the trithiocarbonate end group (Figure 2.8). A single trace overlapping with the RI trace was observed indicating high end group fidelity (the end group is attached to the polymer).

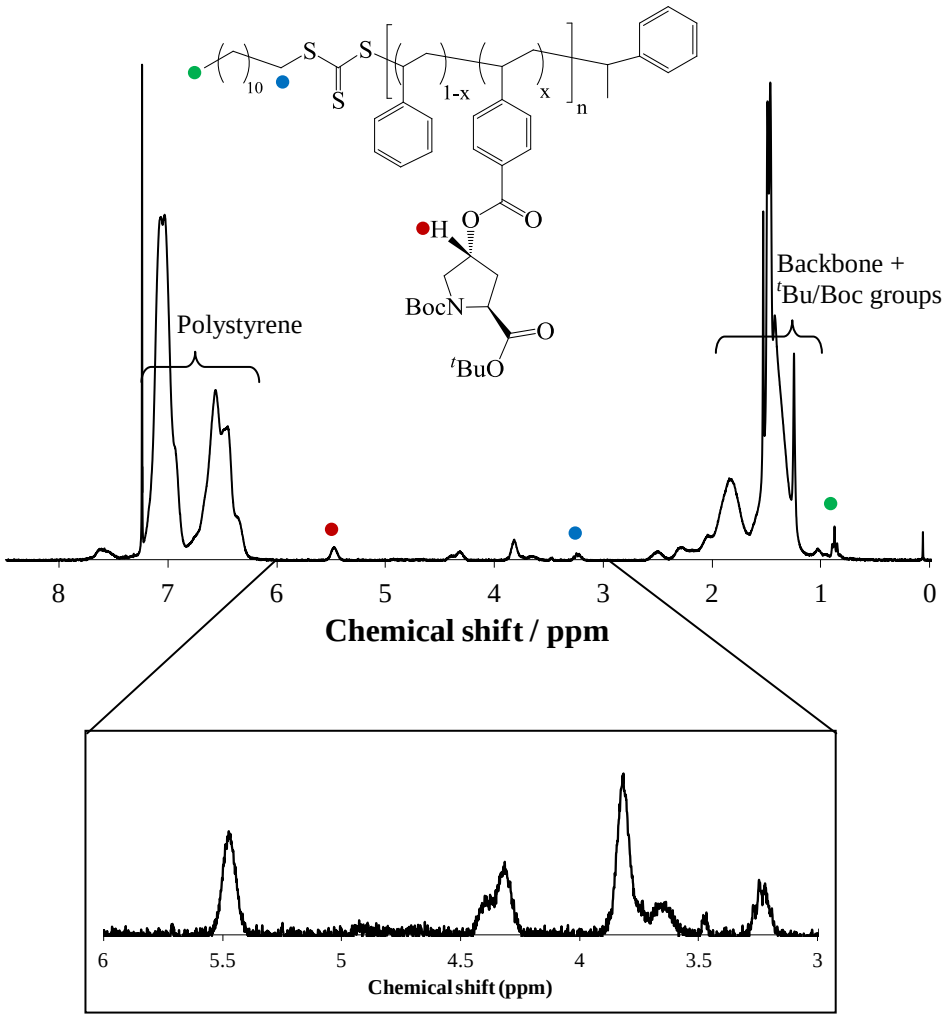

Figure 2.7. Representative ^{1}H NMR spectrum, with some signals expanded (400 MHz, $CDCl_3$) of final copolymer 2.4 after precipitation in cold methanol

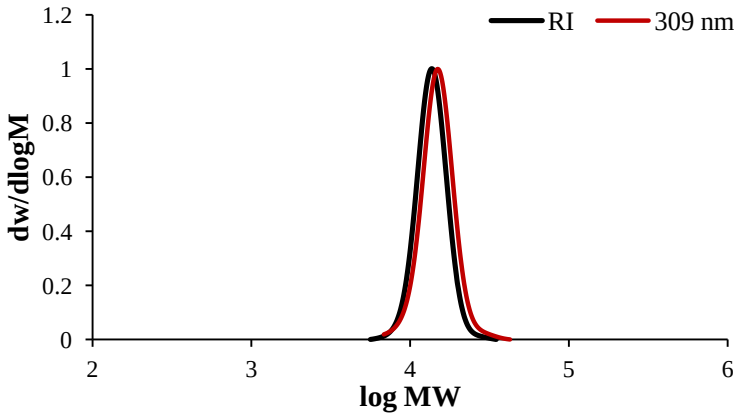

Figure 2.8. SEC trace of 2.4 in THF, showing the RI and the overlapping UV (309 nm) trace

As previously mentioned, a range of functional styrenic copolymers were synthesized, targeting different polymer lengths in order to investigate the influence of polymer

chain length on catalyst activity and selectivity. The range of functional copolymers synthesized (**2.4a-2.4g**) are detailed below in Table 2.1.

Table 2.1. Copolymerization data for 2.3 and styrene, carried out at a ratio of 95:5:1 for styrene:2.3:CTA1 under solvent free conditions at 110 °C where the reaction was quenched at different times (between 15-22 hours) to achieve polymers with different DPs

Polymer	Time / h	DP_{St}	$DP_{2.3}$	M_n[a] / kDa	M_n[b] / kDa	M_w/M_n[b]	Mol% incorp. of 2.3[a]	weight % 2.3[a]
2.4a	22	93	4	11.7	9.5	1.06	4	15
2.4b	15	34	3	5.2	5	1.07	8	26
2.4c	20	65	3	8.4	8.7	1.06	4	16
2.4d	20	64	3	8.3	8.5	1.13	4	16
2.4e	22	93	3	11.3	9.5	1.07	3	11
2.4f	22	83	4	10.7	12.3	1.07	5	16
2.4g	20	74	4	9.8	11.6	1.07	5	18

[a] Determined by ^{1}H NMR spectroscopy (400 MHz, $CDCl_3$)
[b] Determined by SEC, in THF, PS calibration

Considering the random coil structure of polymers in solution, we hypothesized that the copolymers with shorter chain lengths would have greater activity and selectivity. In theory, a longer polymer chain would cause a greater steric barrier resulting in reduced activity, whereas a shorter polymer chain would leave the catalyst functionalities more exposed to the surrounding solution. This may possibly increase substrate interactions with the catalytic sites or leave the catalyst more exposed to water present in the reaction. Nevertheless, it is also possible that a longer polymer chain may fold in solution in a way to allow for distinct catalytic pockets to be formed, increasing the activity of the reaction.

2.3.4.1. Monomer reactivity ratios

Previous studies in the group on the kinetics of copolymerization revealed that the functional monomer polymerized at a faster rate compared to the styrene comonomer.[36] This suggested that the polymerization was non-random in nature and proposed a more gradient-type or even block-like microstructure for copolymer **2.4**. Therefore, this prompted us to investigate the reactivity ratios[41, 42] of the two monomers under RAFT polymerization conditions. The reactivity ratios of styrene and **2.3** were determined by carrying out a series of copolymerization with different styrene:**2.3** ratios, including 95:5; 90:10; 80:20; 70:30; 60:40; 50:50. These copolymerization reactions were carried out under the same conditions as previously discussed, i.e. under solvent free conditions and at 110 °C. The molar fraction of the two monomers in the copolymer was obtained from ^{1}H NMR spectroscopy at low conversions (typically ≤ 10%), as the calculations make the assumption that monomer unit added to the growing polymer chain is only dependent on the monomer unit at the chain end. By determining f_1 (ratio of monomers in initial feed) and F_1 (ratio of monomers in copolymer), the reactivity ratios of the two monomers were estimated using Contour, software developed by van Herk (Figure 2.9), which applies a non-linear least squares (NLLS) method:[43] this calculates the best fitting curve which determines the reactivity ratios of the two monomers. The reactivity ratios, r_1 and r_2 were determined as 10.9 ± 1.8 and 0.03 ± 0.06 respectively, where **2.3** is M_1 and styrene is M_2. The large difference in r-values suggests that M_1 is preferentially added to the propagating species. The Contour software also provides 95% joint confidence intervals of the reactivity ratios (Figure 2.10) further confirming that r_1 is significantly larger than r_2.

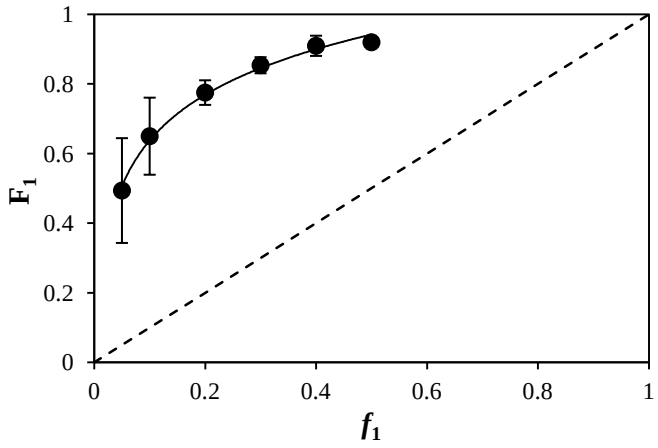

Figure 2.9. Plot of f_1 against F_1 for the copolymerization of 2.3 and styrene where the dashed line is the plot of f_1 against F_1 for an ideal polymerization where $r_1 = r_2 = 1$

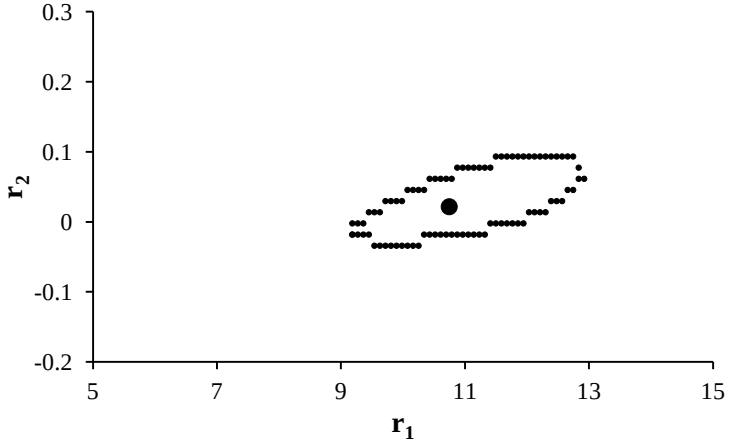

Figure 2.10. Plot of joint confidence intervals (95%) of the reactivity ratios for M_1 (2.3) and M_2 (St)

Furthermore, the reactivity ratios may be used to predict the composition of the two monomers in the resulting copolymer by determining the molar fraction of each monomer with conversion (Figure 2.11). The estimation was carried out on a copolymerization with an initial M_1 and M_2 feed ratio of 0.05 to 0.95. The plot confirms that M_1 is preferentially incorporated at the start of the copolymerization. Thus, as M_1 is preferentially added at the start of the polymerization and to the propagating species, the reactivity ratio experiments confirm that a block-type structure is formed and not the initially envisioned statistical copolymer.

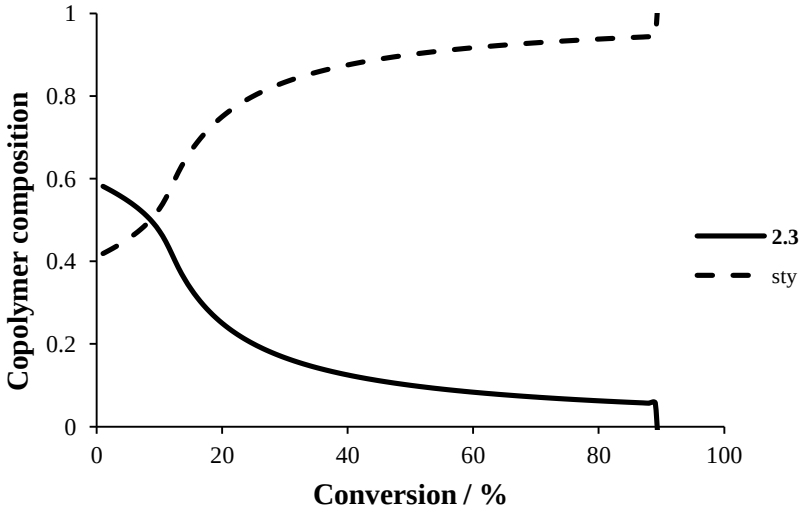

Figure 2.11. Predicted copolymer composition based on the estimated reactivity ratios of monomers 2.3 and styrene

The difference in reactivity is perhaps not entirely unexpected considering the presence of the electron-withdrawing ester linkage in the *para*-position of **2.3**, making it more activated towards polymerization. Thus, we propose that this block-like polymer microstructure (with non-random catalyst distribution) will result in an amphiphilic copolymer (after deprotection of **2.3**) which may have interesting solution self-assembly behaviours.

2.3.5. Polymer Deprotection

As previously mentioned, the two protecting groups Boc and ^{t}Bu for the amino and carboxylic acid functionalities respectively, were selected due to their straightforward and simultaneous deprotection chemistries.[37] Thus, copolymers **2.4a-g** were deprotected using TFA in CH_2Cl_2 to afford the catalytically active copolymers **2.5a-g**. The successful deprotection was confirmed by the disappearance of the ^{t}Bu signals in the ^{1}H NMR spectrum, causing simplification in the δ 1.1-2.6 ppm region (Figure 2.12). Additionally, a small shift was observed for signals characteristic of the catalytic L-

proline moiety, i.e. the proton on the stereocentre adjacent to the ester linkage, a change in shift was observed from δ 5.45 to 5.63 ppm.

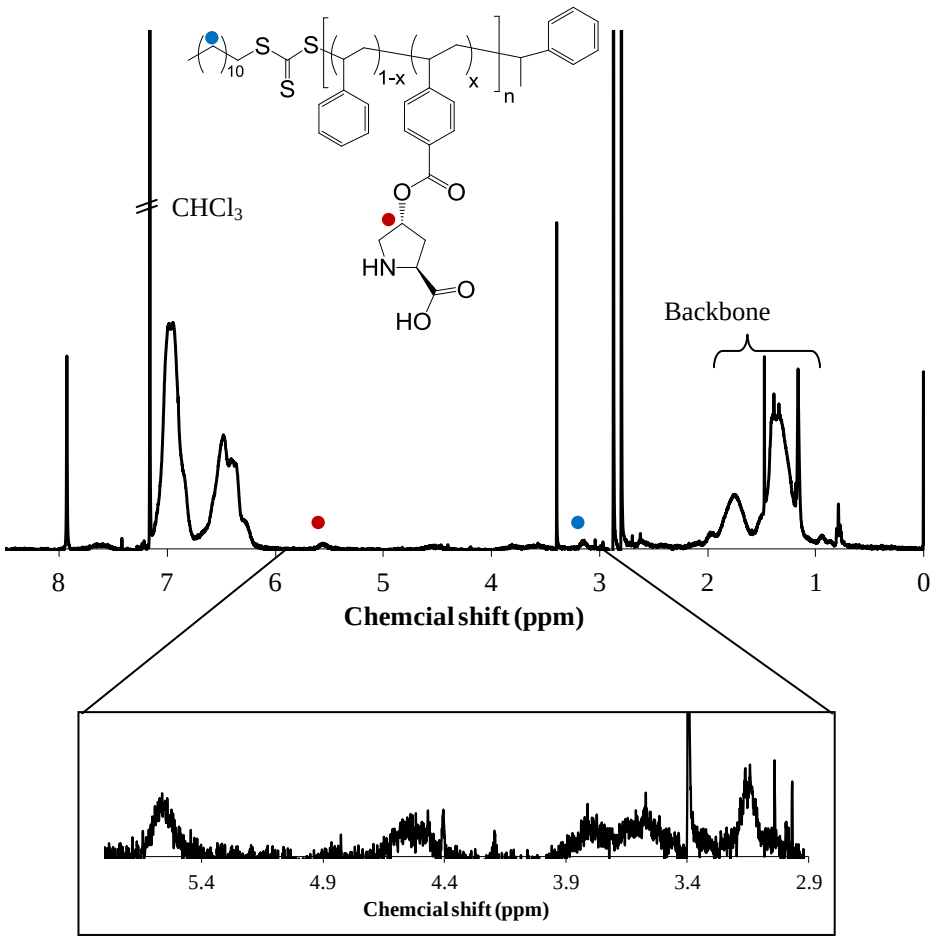

Figure 2.12. Representative ^{1}H NMR spectrum of copolymer 2.5 (400 MHz, $CDCl_3$) after deprotection of *tert*-butyl protecting groups, with some signals expanded

To further confirm that the ester linkage was not cleaved under the acidic conditions employed for deprotection, the monomer was stirred in a mixture of TFA and CH_2Cl_2 at room temperature for 24 hours. The reaction verified that the ester linkage was stable under these conditions and only deprotection of the ^{t}Bu and Boc groups occurred. Thus, the catalyst moieties were not cleaved from the polymer backbone under deprotection conditions.

2.3.6. Organocatalytic properties

To investigate the catalytic activity of the synthesized copolymers **2.5**, a representative aldol reaction between cyclohexanone and 4-nitrobenzaldehyde was employed (Scheme 2.6). This specific aldol reaction was selected as the model reaction as it has been shown to be the most active, due to the presence of the nitro-group and can therefore be readily used to evaluate the system. Moreover, it has previously been used to study the efficiency of a range of other supported systems and the catalytic activity can therefore be directly compared (mechanism discussed in Chapter 1).[16, 19, 44]

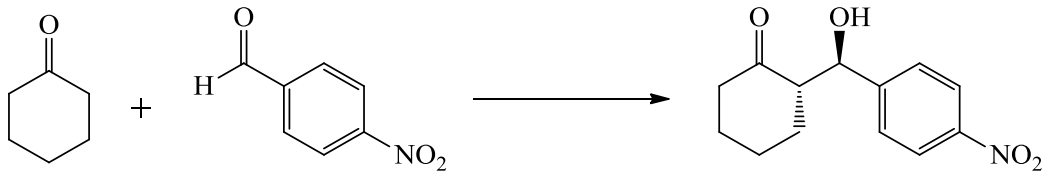

Scheme 2.6. Model aldol reaction used to evaluate the catalytic efficiency of the supported catalytic system, showing the major enantiomer formed in L-proline catalyzed reactions

Previous work in the group had shown good catalytic activity with copolymers synthesized by NMP. These copolymers were synthesized at a relatively high percentage incorporation and catalyzed the aldol reaction at high catalyst loading, i.e. 10 mol%.[36] Therefore, we wanted to further explore the potential of the supported catalytic system synthesized by RAFT polymerization, with lower percentage catalyst incorporation (*ca.* 5%). We proposed that by lowering catalyst incorporation, the solution properties of the copolymer may be altered which in turn may have an effect on the availability of the catalyst and thus its catalytic activity. Moreover, by changing the length of the polystyrene backbone, the recyclability of the polymer with respect to chain length might also be investigated.

2.3.6.1. Influence of water

Firstly, to confirm that the polymer-supported catalyst was still catalytically active it was used to catalyze the aldol reaction at relatively high loading, i.e. 20 mol%. The reaction was first catalyzed by copolymer **2.5c** (DP_{sty} = 65, DP_{pro} = 3), with a relatively short PS block length. Fortunately, the reaction was indeed catalyzed and higher conversions were observed after 24 hours in the presence of water compared with reactions catalyzed in the absence of water (Table 2.2, entries 1 to 4).

Table 2.2. Catalytic activity of copolymer 2.5c compared to unsupported L-proline, catalysis carried out at 20 mol% loading, room temperature and a range of DMF/water mixtures

Entry	Catalyst	vol% water in DMF	Conv.[a] / %	*anti/syn* ratio[a]	ee[b] / %
1	**2.5c**	0	49 ± 1	89/11	91
2	**2.5c**	5	98 ± 5	95/5	89
3	**2.5c**	7.5	90 ± 5	95/5	85
4	**2.5c**	12	90 ±3	91/9	94
5	L-proline	0	0	-	-
6	L-proline	5	99 ± 1	92/9	86
7	L-proline	7.5	99 ± 1	92/8	88
8	L-proline	12	98 ± 2	87/13	82

[a] Determined by ^{1}H NMR spectroscopy (400 MHz, $CDCl_3$) after 24 hours, reactions carried out in triplicate
[b] Determined by chiral HPLC, Chiralpak IA column 80:10:10 hexane:propan-2-ol:ethanol, 1 mL.min^{-1}

As previously reported in literature, the presence of water helps to drive the catalytic cycle towards formation of the product.[45-48] Moreover, it has also been suggested that water has an effect on the enantioselective outcome of the reaction as it forms a hydrogen bonding network with the catalyst and substrates in the transition states. Therefore, it was not unexpected to find that the activity was enhanced in the presence of water. Consequently, the amount of added water and its effect on the catalytic

activity and selectivity was investigated. A representative ^{1}H NMR spectrum of the aldol reaction mixture is presented in Figure 2.18 where signals from both the starting material and the product are shown and determination of reaction conversion is discussed.

The presence of 5 vol% water presented the best overall result, reaching 98% conversion, *anti/syn* ratio of 95/5 and 89% ee after 24 hours. In contrast, the presence of greater amounts of water, i.e. 7.5 and 12 vol% resulted in slightly lower conversions and comparable selectivities. The effect of greater amounts of water on the catalytic activity of copolymer **2.5c** was not investigated as the addition of more water caused the polymer to precipitate out of solution. This was a direct effect of the hydrophobic nature of the PS backbone.

For comparison, unsupported L-proline was also used to catalyze the reaction under the same conditions, i.e. at 20 mol% in a range of DMF/water solvent mixtures (Table 2.2, entries 5 to 8). The unsupported catalyst was found to catalyze the reaction to higher conversions at comparative reaction times whenever water was present in the solvent mixture (98-99%). The enantioselectivity on the other hand was slightly reduced in comparison. Interestingly, unsupported L-proline does not catalyze the reaction in 100% DMF, most likely due to the low solubility of the catalyst in pure DMF. This highlights how the scope of solvents used in organocatalytic reactions may be widened as a result of the use of a polymer scaffold. Nevertheless, in order to properly investigate the influence of the polymer scaffold on reaction progress, the kinetics of supported and unsupported catalysis were investigated.

2.3.6.2. Reaction kinetics at 20 mol%

The reaction was set up as previously described and reaction progress monitored by analyzing aliquots taken at regular intervals over 9 hours with a final sample taken after

24 hours, using HPLC. This allowed the start of the reaction to be monitored in more detail, as well as recording the final reaction conversion. For the unsupported system, it seems the reaction proceeded at a faster rate in the presence of 7.5 vol% water compared to 5 and 12 vol% (Figure 2.13). Nevertheless, after 24 hours the 5 and 7.5 vol% water reactions reached the same conversion (99% conversion). However, as previously reported, too much water can have a negative effect on the catalyst activity and even selectivity, which was also observed when catalysis was carried out with 12 vol% water. In this case the difference in activity was more significant than that in enantioselectivity upon the use of 12 vol% water in DMF.

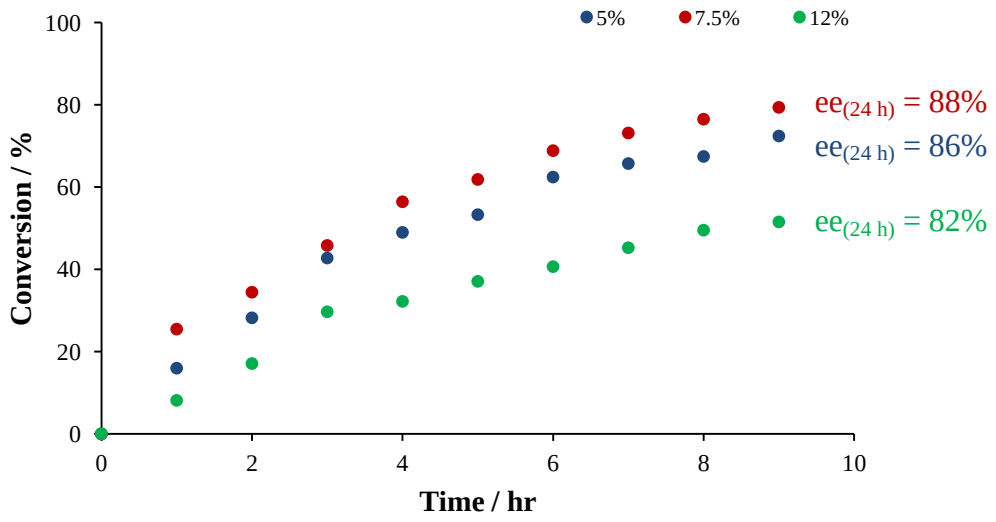

Figure 2.13. Progress of the aldol reaction catalyzed by unsupported L-proline at 20 mol% loading in a range of DMF/water mixtures

The increase in rate of reaction in the presence of water in the supported system is clearly shown in Figure 2.14. Even at high water contents, i.e. 12 vol% water in DMF, the reaction proceeds at a faster rate than in the absence of water. It is also clear that the presence of 5 vol% water was more beneficial than 7.5 and 12 vol%. We propose that this is directly related to the reduced solubility of copolymer in the solvent mixture with increasing water content, as the copolymer is highly hydrophobic. It is important to note

that the reaction reached similar conversions after 9 hours for both the unsupported and supported systems (90% conversion after 24 hours for both systems). Thus, catalyst activity and selectivity were retained after functionalization onto the polymeric scaffold.

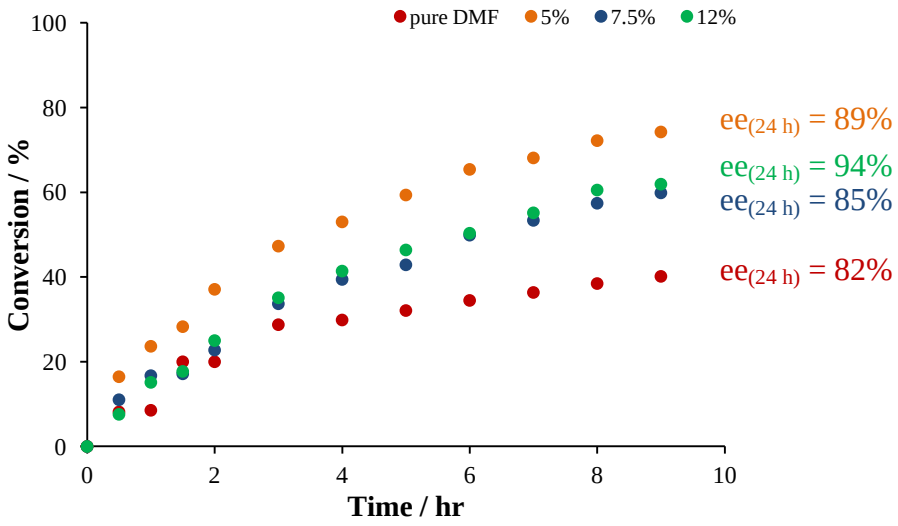

Figure 2.14. Progress of the aldol reaction catalyzed by copolymer 2.5c at 20 mol% loading and a range of DMF/water mixtures

2.3.6.3. Effect of catalyst loading on reaction efficiency

The catalytic efficiency of **2.5c** was further evaluated by carrying out catalysis at lower catalyst loadings. These reactions were carried out in 100% DMF and in DMF with 5 vol% water. Upon reducing the catalyst loading from 20 to 10 mol%, a drop in activity was observed in both solvent systems. Not surprisingly, after 9 hours, the 10 mol% reaction was only able to reach half the conversion of the 20 mol% reaction in pure DMF, though this difference was less significant after 24 hours. Interestingly, the selectivities were also found to be highly comparable at the end of the reaction (Table 2.3).

The addition of 5 vol% water to the reaction improved the activity of the supported catalyst, as previously observed in the 20 mol% reactions. Despite an improvement in

activity upon addition of water, only ~50% conversion was observed after 9 hours for 10 mol% compared to ~75% for 20 mol% (Figure 2.14, Figure 2.15). In the presence of 5 vol% water, both reactions (catalyzed at 10 and 20 mol%) reached comparable conversions after 24 hours despite the differences observed during initial stages of the reaction (Table 2.3). The selectivity (diastereo- and enantio-) were also found to be comparable at the two different loadings. This further highlights the importance of water in enhancing the catalytic activity of the catalyst and high conversions can be obtained at lower catalyst loadings.

Table 2.3. Catalytic activity of copolymer 2.5c at two different catalyst loadings and solvent mixtures

Entry	% water in DMF	catalyst loading / mol%	Conv.[a] / %	*anti/syn* ratio[a]	ee[b] / %
1	0	20	49	89/11	91
2	5	20	98	95/5	89
3	0	10	38	85/15	87
4	5	10	95	95/5	93

[a] Determined by ^{1}H NMR spectroscopy (400 MHz, $CDCl_3$) after 24 hours, reactions carried out in triplicate
[b] Determined by chiral HPLC, ChiralPak IA 80:10:10 hexane:propan-2-ol:ethanol, 1 mL.min^{-1}

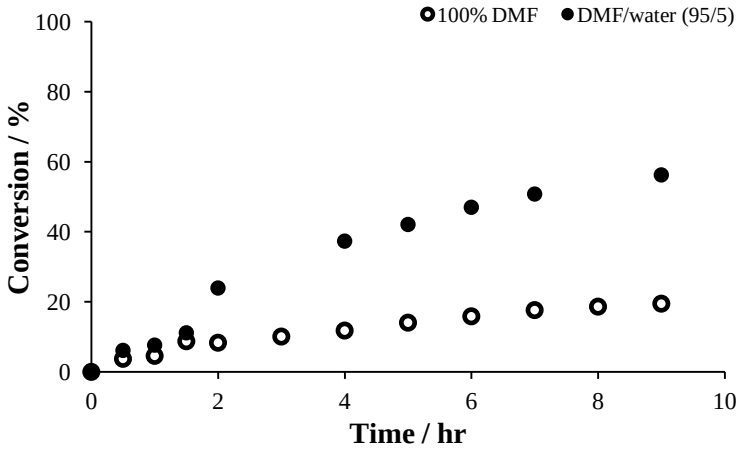

Figure 2.15. Copolymer 2.5c, at 10 mol% and different DMF/water solvent mixtures

The influence of the polymer support was further highlighted by reducing catalyst loading to 5 and 1 mol% and comparing the activity and selectivity to unsupported L-proline. The supported (copolymer **2.5c**) and unsupported catalytic reactions were carried out in a DMF:water (95:5) solvent mixture. As the same copolymer was used in each catalytic reaction, the catalyst loading was altered by changing the amount of polymer (in weight) used whilst keeping the amount of substrates constant.

As previously mentioned, the supported and unsupported systems are comparable in activity and selectivity at high catalyst loadings, i.e. 20 and 10 mol% (Table 2.4).

Table 2.4. Comparison of the activity and selectivity of copolymer 2.5c and unsupported L-proline in DMF:water (95:5) and at different catalyst loadings

Entry	Catalyst	Catalyst loading / mol%	Conv.[a] / %	*anti/syn* ratio[a]	ee[b] / %
1	**2.5c**	20	96	96/4	98
2	**2.5c**	10	95	95/5	93
3	**2.5c**	5	89	96/4	92
4	**2.5c**	1	57	95/5	91
5	L-proline	20	99	90/10	97
6	L-proline	10	99	92/8	94
7	L-proline	5	57	90/10	94
8	L-proline	1	12	92/8	77

[a] Determined by ^{1}H NMR spectroscopy (400 MHz, $CDCl_3$) after 24 hours, reactions carried out in triplicate
[b] Determined by chiral HPLC, ChiralPak IA, 80:10:10 hexane:propan-2-ol:ethanol, 1 mL.min^{-1}

At lower loadings, 5 and 1 mol%, a significant difference in the catalytic efficiency was observed, between the supported and unsupported systems. Polymer **2.5c** was considerably more active than unsupported L-proline at 5 mol%. This difference in activity was even more impressive at 1 mol% loading where only 12% conversion was observed for unsupported L-proline compared to 57% for **2.5c** after the same reaction

time. A significant difference in enantioselectivity was also observed, 91% for **2.5c** and as low as 77% for the unsupported system, which further highlighted the advantage of our polymer supported system.

2.3.6.4. Influence of polymer molecular weight on catalyst activity

The catalytic efficiency of two polymers with different molecular weights was compared to investigate the influence of polymer molecular weight. This was accomplished using copolymers **2.5c** and **2.5e**, with molecular weights ($M_{n,\ NMR}$ after deprotection) of 7.9 kDa (DP_{sty} = 65, DP_{pro} = 3) and 10.8 kDa (DP_{sty} = 93, DP_{pro} = 3) respectively. Catalysis was carried out at 10 mol% catalyst loading, in DMF:water (95:5) at room temperature for 24 hours. Thus, the reactions were carried out at the same catalyst and substrate concentration, but different total polymer concentration due to different polymer molecular weight. The reaction progress was followed by HPLC over the first 9 hours of the reaction (Figure 2.16) but ultimately, the difference in activity between the two polymers was finally found to be less significant than hypothesized (

Table 2.5).

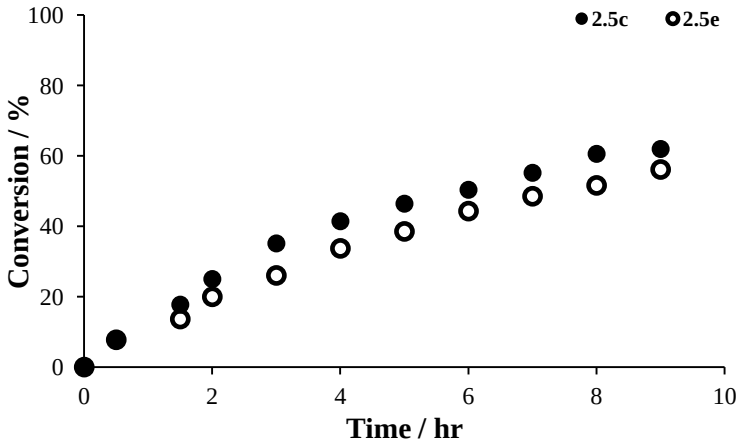

Figure 2.16. Reaction progress of aldol reaction catalyzed by 2.5c (7.9 kDa) and 2.5e (10.8 kDa) at 10 mol%

Table 2.5. The catalytic efficiency of 2.5c and 2.5e at 20 and 10 mol% loading

Entry	Catalyst	Catalyst MW / kDa	Catalyst loading / mol%	Conv.[a] / %	*anti/syn* ratio[a]	ee[b] / %
1	**2.5c**	7.9	20	98	95/5	89
2	**2.5c**	7.9	10	95	95/5	93
3	**2.5e**	10.8	20	96	96/4	98
4	**2.5e**	10.8	10	95	95/5	93

[a] Determined by ^{1}H NMR spectroscopy (400 MHz, $CDCl_3$) after 24 hours, reactions carried out in triplicate
[c] Determined by chiral HPLC, ChiralPak IA, 80:10:10 hexane:propan-2-ol:ethanol, 1 mL.min^{-1}

2.3.6.5. Background reactions

A number of background reactions were carried out to confirm the importance of having the catalyst functionalized on the polymer scaffold (Table 2.6). The reaction was first carried out on both small and larger scale in the absence of any catalyst, which verified that the reaction does not occur spontaneously in solution (Table 2.6, entries 1 and 2). Additionally, the reaction was carried out in the presence of a PS homopolymer but in the absence of L-proline (supported or unsupported) to confirm that reaction is not induced by the presence of a polymer scaffold (Table 2.6, entry 3) but no reaction was observed.

Table 2.6. Comparison of non-catalyzed and catalyzed aldol reaction in a DMF:water (95:5) solvent mixture

Entry	Catalyst	mol%	Conv.[a] / %	*anti/syn* ratio[a]	ee[b] / %
1	no catalyst	-	no reaction		
2	no catalyst[1]	-	no reaction		
3	PS	-	no reaction		

[a] Determined by ^{1}H NMR spectroscopy (400 MHz, $CDCl_3$) after 24 hours, reactions carried out in triplicate
[b] Determined by chiral HPLC, ChiralPak IA, 80:10:10 hexane:propan-2-ol:ethanol, 1 mL.min^{-1}
[1] Carried out under solvent free conditions

2.3.7. Characterization of aldol products

The model aldol reaction between 4-nitrobenzaldehyde and cyclohexanone used in this work to evaluate the efficiency of our polymer supported catalytic system can produce four stereoisomers: two diastereomers and their enantiomers (Figure 2.17). The ratio of the major and minor isomers catalyzed by L-proline was used to determine the diastereoselectivity (*anti/syn* ratio) of the catalyst. The anti-isomers (two top isomers) are the major isomers for D- and L-proline and were used to evaluate the enantioselectivity (or enantiomeric excess, ee).

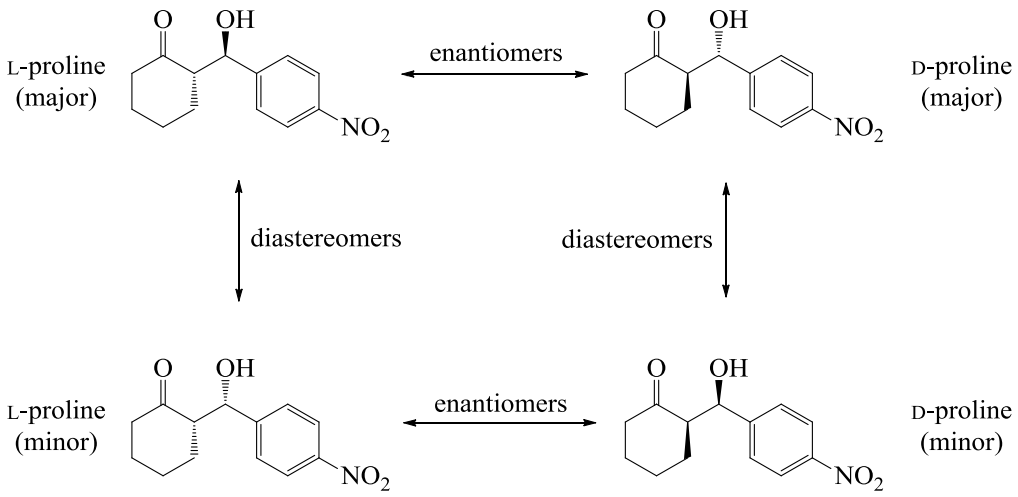

Figure 2.17. Stereoisomers produced in the aldol reaction between 4-nitrobenzaldehyde and cyclohexanone

Conversion was determined by ^{1}H NMR spectroscopy, comparing signals of the aromatic protons in the starting aldehyde substrate (c and d) to the same signals in the product (g and h) (δ 7.2-8.5 ppm) (Figure 2.18). This was accomplished by extracting both the substrate and product from the DMF/water reaction mixture with ethyl acetate and analyzing the dried crude product. The diastereomeric *anti/syn* ratio was determined by comparing the signal at 4.8 ppm (anti-H) to 5.4 ppm (syn-H), arising from the proton

adjacent to the alcohol functionality. The compound has already been well characterized in a number of reports.[49-52]

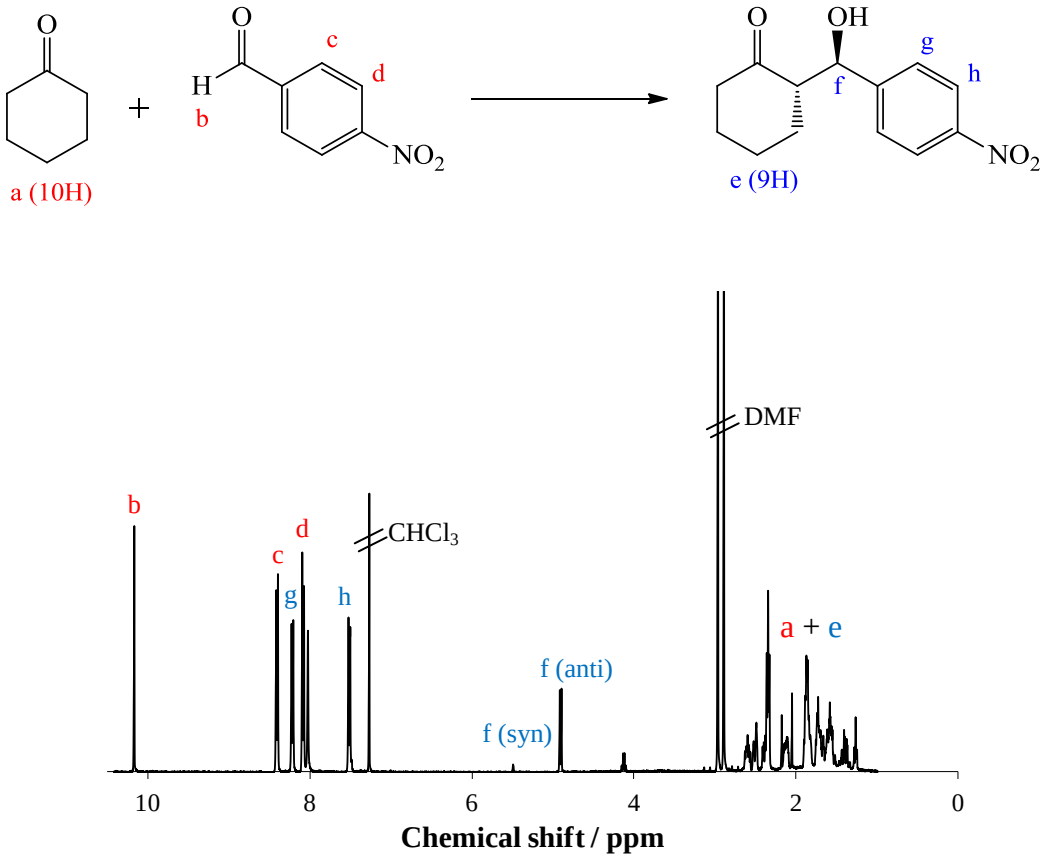

Figure 2.18. ^{1}H NMR spectrum of aldol reaction mixture with signals of both the starting reagents and product, used to determine reaction conversion and *anti*/*syn* ratio

The enantioselectivity of the reaction was determined by chiral HPLC, on a Chiralpak IA column. A mixture of isomers from the reaction was first run to provide a point of reference (Figure 2.19). The enantiomeric excess (ee) was determined using the equation represented in Equation 2.1, determining ee of the major anti-enantiomer.

$$ee = \frac{\left(anti_{L-pro} - anti_{D-pro}\right)}{\left(anti_{L-pro} + anti_{D-pro}\right)} \times 100$$

Equation 2.1. Equation used to determine ee of the reactions catalyzed by 2.5 and unsupported L-proline

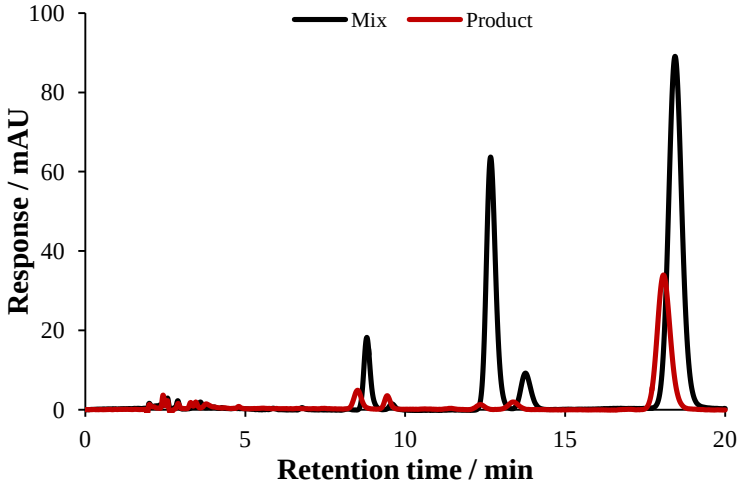

Figure 2.19. Representative HPLC traces of an isomeric aldol mixture and product from 2.5c catalyzed reaction

2.3.8. Self-assembly of copolymer in DMF:water mixture

It has been suggested that a polymer may influence the catalytic activity of a supported catalyst as a result of its arrangement in solution. Due to the gradient type microstructure of copolymer **2.5** (*vide supra*), aggregation in the DMF:water mixture was expected, and indeed upon addition of water to the polymer/DMF solution a change was observed, going from clear to slightly turbid with a minor bluish tint. We propose that upon addition of a non-selective solvent for PS, in this case water, the somewhat amphiphilic copolymer self-assembled into spherical aggregates. We rationalized that the observed differences in activity for **2.5** and unsupported L-proline, specifically at low catalyst loading was a direct result of the formation of these aggregates. Thus, the aggregates of copolymers **2.5c** and **2.5e** were thoroughly examined by dynamic light scattering (DLS) as well as TEM and SEM to investigate the influence of the polymer chain length on the assembly. The only difference was that it was necessary to change the polymer concentration to 10 mg.mL^{-1} for these analyses because it was not possible to perform them at the high polymer concentration used in the catalysis reactions (*ca.* 90

mg.mL^{-1}). We recognize this might not necessarily give the same size as but propose the morphology should be comparable.

DLS was used to determine the hydrodynamic diameter (D_h) of the self-assembled aggregates in solution. Firstly, copolymers **2.5c** and **2.5e** were fully dissolved in DMF and in both cases D_h of less than 5 nm (PDI ~ 0.20) were observed, which is indicative of free polymer chains in solution (Figure 2.20, Figure 2.21).

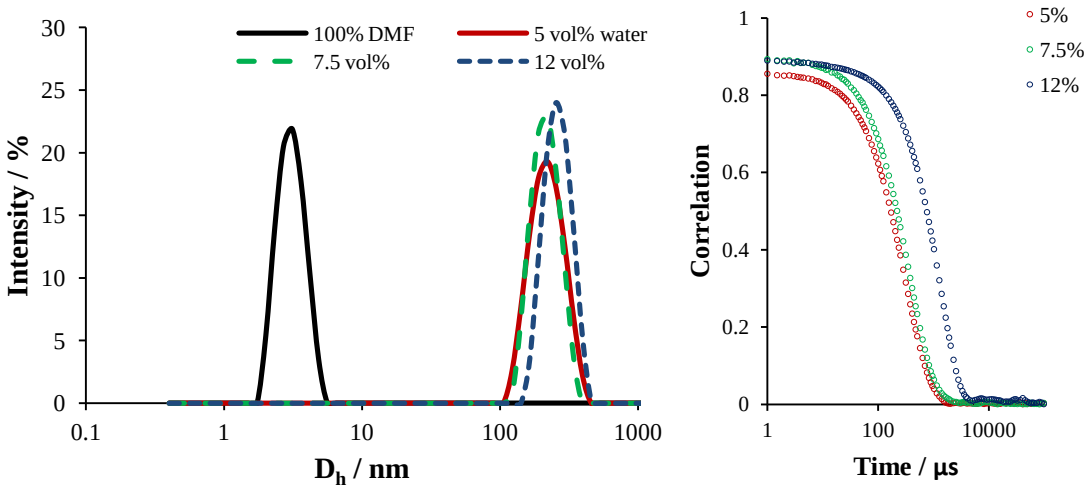

Figure 2.20. DLS traces of 2.5c in DMF and DMF:water mixtures at 0.2 mg.mL^{-1} and 25 °C and the corresponding correlation function

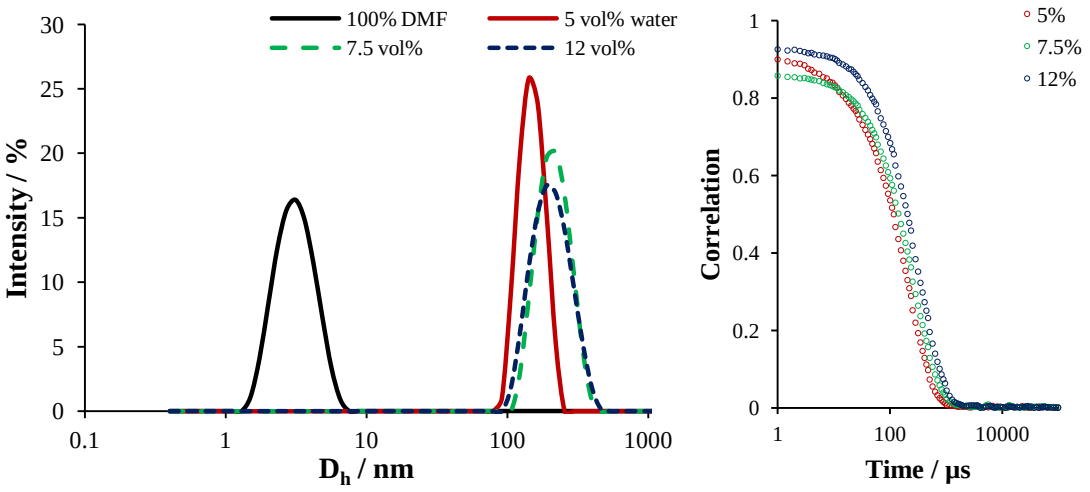

Figure 2.21. DLS traces of 2.5e in DMF and DMF:water mixtures at 0.2 mg.mL^{-1} and 25 °C and the corresponding correlation function

This confirmed that no self-assembled structures were formed in pure DMF, as the polymer chains were fully solubilized. However, upon addition of water (5 vol%) to the polymer (**2.5c** and **2.5e**)/DMF solutions, D_hs of about 160 nm (PDI = 0.17) were observed, confirming chain association to form aggregates (Figure 2.20, Figure 2.21). For polymer **2.5c**, particle D_h at 7.5 and 12 vol% water in DMF were then further investigated: D_h of 7.5 vol% water in DMF was found to be comparable to 5 vol% water in DMF, but further increasing the amount of water to 12 vol%, a significant increase in D_h to 220 nm (PDI = 0.33) was observed. It should also be noted that a broadening in the particle size dispersity was also observed with increasing water content. As the particle size of all aggregates formed was larger than expected for conventional micelles, we propose that **2.5** (both c and e) assemble into large aggregates, vesicles (polymersomes) or compound micelles.[53]

The self-assembled aggregates were further characterized by TEM. This was carried out by drop depositing a small sample of the assembled copolymer onto a grid previously treated with oxygen plasma and subsequently stained with either ammonium molybdate (AM) or uranyl acetate (UA). Copolymer **2.5c** assembled in DMF:water (95:5) at 10 $mg.mL^{-1}$ was first imaged with UA staining (Figure 2.22). Large structures and clusters of aggregates were observed, with a relatively large spread in particle size and an average diameter (D_{av}) of 215 ± 40 nm. The observed D_{av} was larger than observed by DLS at the same water content which is attributed to particle aggregation. It has been previously reported that UA staining may interact with the sample and cause aggregation. Thus, the particles were further characterized by TEM using a different stain, AM.

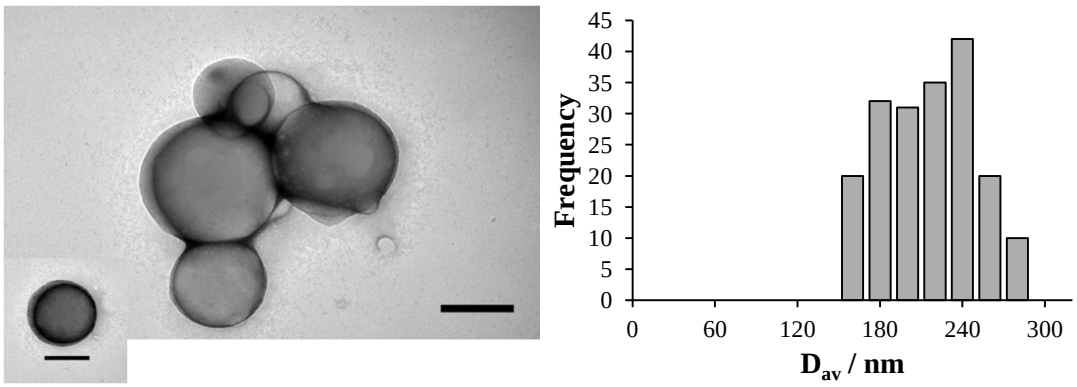

Figure 2.22. TEM image of 2.5c assembled in DMF:water (95:5) at 10 mg.mL^{-1}, stained with UA, D_{av} = 215 ± 40 nm, scale bar is 150 nm

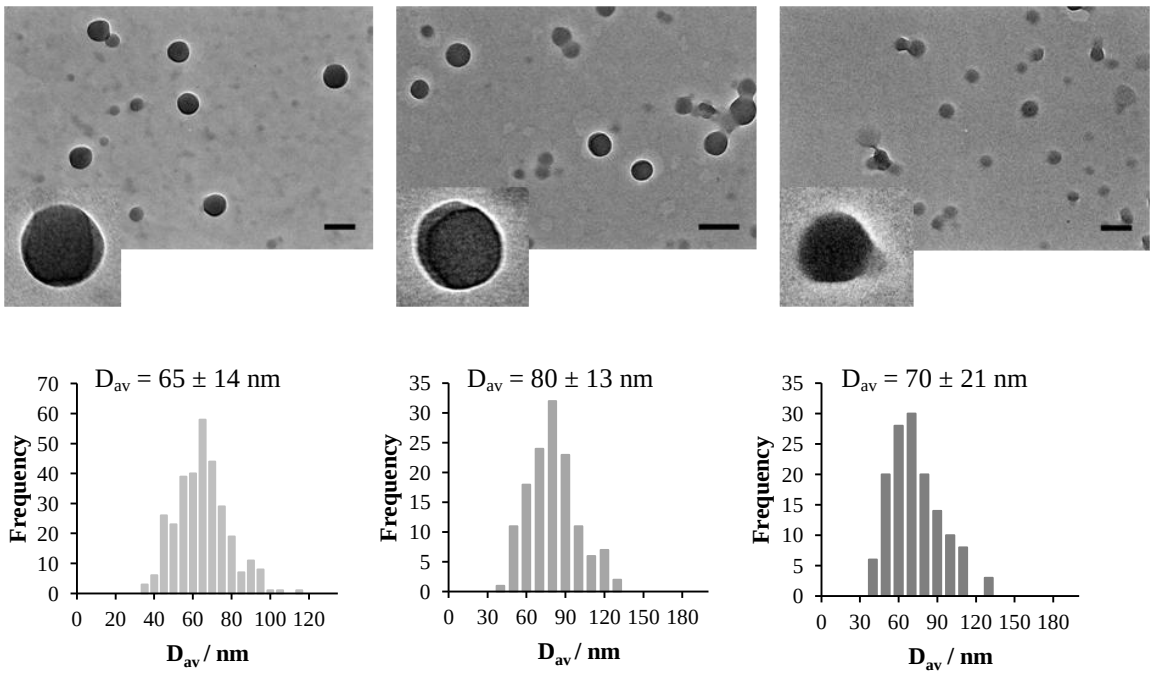

Figure 2.23. TEM images of 2.5c assembled in a range of DMF/water solvent mixtures at 10 mg.mL^{-1}, stained with AM, scale bar is 150 nm

Copolymer **2.5c** assembled in DMF:water (95:5) was first imaged at 10 mg.mL^{-1} with AM staining (Figure 2.23). Again spherical structures were observed but these were now found to be relatively well-defined with only a small amount of aggregation and with a D_{av} of 65 ± 14 nm. Particles assembled at 7.5 and 12 vol% water in DMF were then additionally imaged using the AM stain (Figure 2.23), providing similar spheres with D_{av} of 80 ± 13 and 70 ± 21 nm for 7.5 and 12 vol% water in DMF respectively. Furthermore, these particle sizes were found to be independent of polymer

concentration, as the particles assembled at 2 mg.mL^{-1} (Figure 2.24) showed similar sized structures by TEM to those imaged at 10 mg.mL^{-1}.

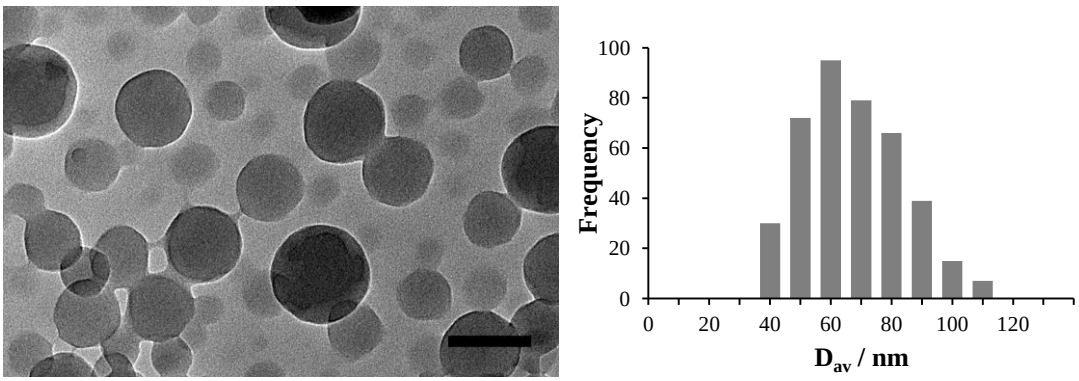

Figure 2.24. TEM image of 2.5c assembled in DMF:water (95:5) at 2 mg.mL^{-1}, stained with AM, D_{av} = 64 ± 14 nm, scale bar is 100 nm

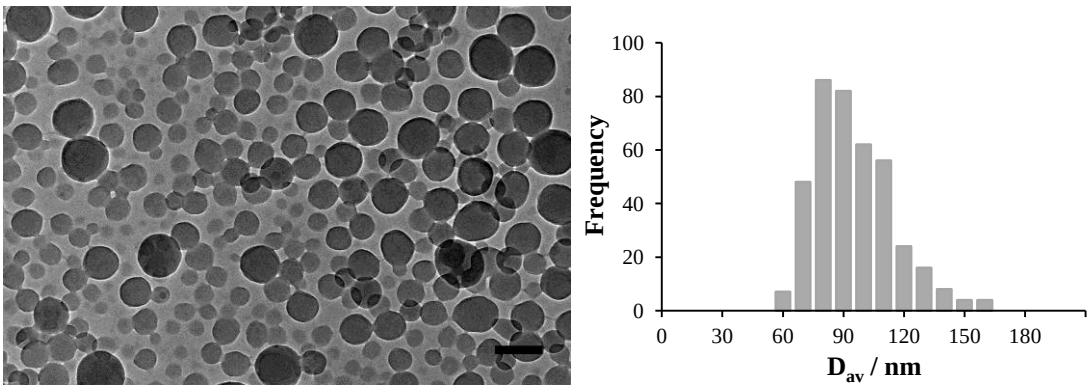

Figure 2.25. TEM image of 2.5e assembled in DMF:water (95:5), stained with AM, D_{av} = 90 ± 20 nm, scale bar is 150 nm

The effect of copolymer molecular weight on the size of the assembled particles was examined by additionally imaging copolymer **2.5e**, assembled in DMF/water (95/5) at 10 mg.mL^{-1}, with AM staining (Figure 2.25). The average particle size was determined to be 90 ± 20 nm, which is slightly larger than those obtained for **2.5c** (65 ± 14 nm) under the same solvent conditions. The small difference in particle size is most likely due to the longer PS chain in **2.5e** compared to **2.5c**. Nevertheless, this confirmed that

the assembly process is an effect of the polymer microstructure, where spherical aggregates are observed in the mixed DMF:water solvent system.

Large structures such as these are often indicative of vesicle-like assemblies or compound micelles but visually the aggregates do not present the bilayer type structure associated with vesicles, and minimal contrast variations inside the particles suggest a solid particle. The morphology of the particles was further explored by TEM imaging on graphene oxide (GO):[54] with recent developments in electron imaging, GO has emerged as an excellent support for TEM analysis of polymer samples, providing images with low contrast, due to the nearly electron transparent nature of GO, allowing polymer nanostructures to be readily imaged without staining. Therefore, aggregates of copolymer **2.5e** formed in DMF:water (95:5) were imaged using GO as the support. Relatively disperse structures were observed (D_{av} = 75 ± 25 nm) and the particles look reasonably solid. Both Figure 2.23 (AM stained) and Figure 2.26 (GO) show some overlaid particles and it was thought that the resulting contrast might indicate a disc-like or flattened morphology.

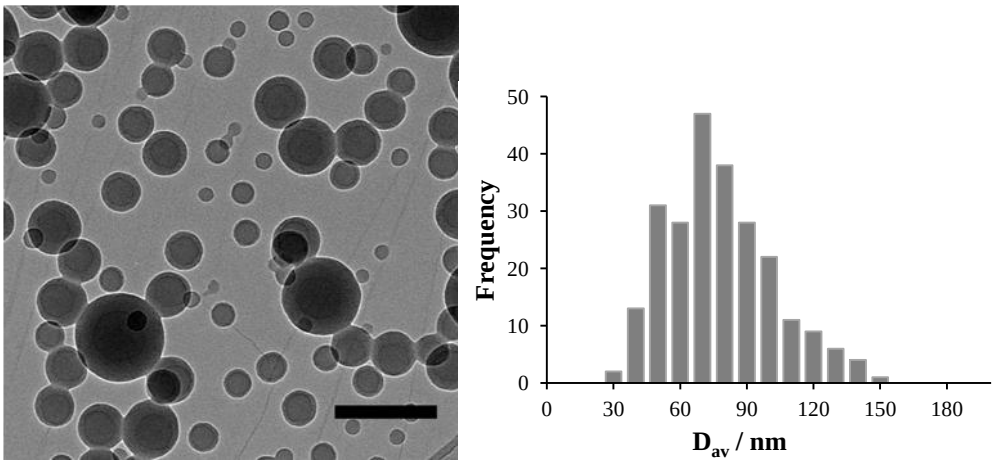

Figure 2.26. TEM images of 2.5e assembled in DMF:water (95:5), unstained and imaged on GO treated TEM grids, D_{av} = 75 ± 25 nm, scale bar is 200 nm

To further investigate the possible disc-like morphology, particles of **2.5e** assembled in DMF:water (95:5) were imaged by cryo-TEM at a range of tilt angles (-30° to +30°) (Figure 2.27). This was carried out under cryogenic conditions, as this allows the particles to be imaged in their hydrated state and eliminates flattening of the particles as a result of drying. The series of images confirmed the spherical nature of the particles, directly contradicting the earlier TEM data which suggested that there was a disc-like morphology.

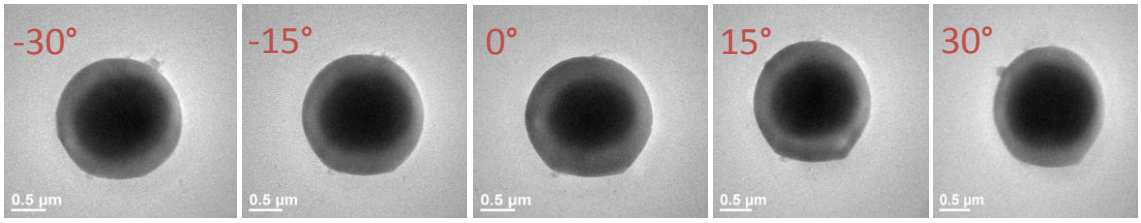

Figure 2.27. Representative cryo-TEM images of 2.5e assembled in DMF/water (95/5) and imaged at different tilt angles (with thanks to Dr Thomas Smart, University of Delaware)

Due to the large structures observed by TEM, the particles were further characterized by SEM: aggregates of **2.5e** assembled in DMF:water (95:5) were deposited onto a glass substrate, sputter coated with gold or platinum and imaged. Indeed, a large spread in particle size and clusters was observed, with a significant number of large particles present (D_{av} of 205 ± 45 nm, Figure 2.28). The broad range of sizes found is most likely an effect of the uncontrolled self-assembly process but nevertheless confirms that the copolymers do assemble into aggregates with a spherical morphology.

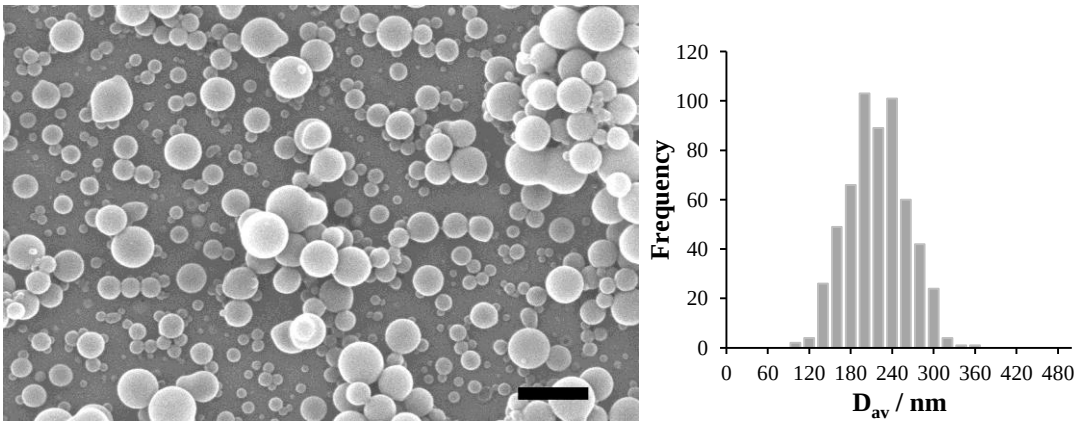

Figure 2.28. SEM image of 2.5e assembled in DMF:water (95:5), deposited onto a glass substrate and sputter coated with gold, D_{av} = 205 ± 45 nm, scale bar is 500 nm

The aggregates were subsequently imaged at a range of tilt angles to further verify the spherical morphology of the particles. A representative image at 30° is shown in Figure 2.29 confirming the solid nature of the particles as they did not flatten during sample preparation.

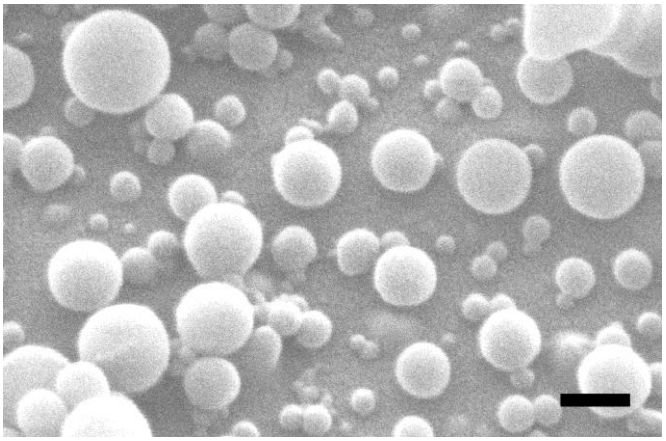

Figure 2.29. SEM image of 2.5e assembled in DMF:water (95:5), at a tilt angle of 30°, scale bar is 200 nm

2.3.9. Recycling

It was hypothesized that the hydrophobic nature of all the copolymers may allow recycling of the supported catalyst following reaction. Thus, the recycling potential of catalytic copolymer **2.5g** (9.1 kDa, DP_{sty} = 74, DP_{pro} = 4; D_h = 143 nm, PDI = 0.20) was

investigated, with the intention being to recover the polymer by precipitation, as a result of the insolubility of PS in water.

Thus copolymer 2.5g was fully dissolved in DMF and assembled *via* the addition of water (5 vol%), as previously described. The reagents were then added to the assembled aggregates and reaction allowed to proceed for 24 hours. After withdrawing an aliquot to determine the reaction conversion, water was added dropwise to the remaining solution causing the polymer to precipitate fully out of solution. This was then collected by filtration, washed with water and dried in the vacuum oven at 40 °C. The aldol product was extracted from the remaining DMF:water solution with ethyl acetate, dried and the product yield determined. Once the collected polymer was dried, it was re-dissolved in DMF, aggregates assembled *via* the addition of water and a second catalytic cycle then allowed to proceed. In order to maintain the same catalyst loading, in this case 10 mol%, throughout the recycling cycles, the amount of reactants added to a new catalytic cycle was adjusted according to the amount of polymer recovered from the previous cycle. The recycling efficiency of 2.5g is detailed in

Table 2.7 and shows high activity and selectivity over the three catalytic cycles. In each cycle, more than 85% of the polymer was recovered by precipitation. Additional recycling was carried out using copolymer, 2.5b (4.7 kDa, DP_{sty} = 34, DP_{pro} = 3, D_h = 120 nm, PDI = 0.23) to investigate the influence of polymer molecular weight on recyclability. Although the catalytic efficiency and selectivity of the first catalytic cycle was comparable to 2.5g, 2.5b showed significantly lower recoverability (

Table 2.7, compare entries 2 and 5). Surprisingly, high enantioselectivity was maintained throughout the catalytic cycles despite the observed drop in activity for **2.5b**.

Table 2.7. Recyclability of 2.5g and 2.5b over three catalytic cycles

Copolymer	Entry	Cycle	Conv.[a] / %	*anti/syn* ratio[a]	ee[b] / %	Polymer recovery[c] / %
2.5g (9.1 kDa)[d]	1	1	95	97/3	89	88
	2	2	99	95/5	90	85
	3	3	94	95/5	88	90
2.5b (4.7 kDa)[d]	4	1	97	95/5	93	76
	5	2	84	94/6	95	51
	6	3	48	93/7	92	57

[a] Determined by ^{1}H NMR spectroscopy (400 MHz, $CDCl_3$) after 24 hours
[b] Determined by chiral HPLC, Chiralpak IA, 80:10:10 hexane:propan-2-ol:ethanol, 1 mL.min^{-1}
[c] Based on polymer weight after recovery, compared to the previous cycle
[d] Determined by ^{1}H NMR spectroscopy (400 MHz, $CDCl_3$) after deprotection

The lower recyclability of **2.5b** (lower molecular weight polymer) may be linked to the microstructure of the polymers. As previously discussed in this chapter, the functional monomer **2.3** polymerized at a faster rate compared to the comonomer styrene and thus a block-like polymer was proposed. Due to this composition drift, the solubility of the polymers in the same batch may differ slightly causing the loss of polymer in each recycling step, which is more apparent at lower molecular weight. Thus, for this system it seems the molecular weight of the polymer support has an appreciable influence on the ease of recyclability.

2.4. Conclusion

RAFT polymerization was used to synthesize a range of well-defined L-proline containing polymers. The catalytic efficiency of the copolymers in a mixed solvent system (DMF:water) was assessed in a model aldol reaction. The copolymers showed comparable activity and selectivity to unsupported L-proline at high catalyst loadings, but significantly higher activity at as low as 1 mol%. The improved catalytic efficiency of the polymer-supported catalyst is proposed to be a direct result of the interesting

solution assembly behaviour exhibited by the copolymer in the reaction solvent system. We believe the assembled structures provide a unique microenvironment for catalysis which is accompanied by a high local substrate and catalyst concentration enhancing activity at very low loadings. Additionally, catalyst recovery and reuse were shown to be possible as a result of the polymer scaffold which was found to be dependent on the molecular weight of the scaffold. Nevertheless, the copolymer serves as the basis towards the design of a nanoreactor system able to efficiently catalyze organic reactions in water.

2.5. Experimental

2.5.1. Materials

Styrene was distilled over calcium hydride (CaH_2) and stored at 4 °C. AIBN was recrystallized from methanol and stored at 4 °C. Dodecyl-1-phenylethyl trithiocarbonate (CTA1) was prepared by modifying a previously reported procedure.[40] 4-Nitrobenzaldehyde was purchased from Sigma-Aldrich and filtered through silica prior to use. *Bis*-protected *trans*-4-hydroxy-L-proline was purchased from Fluka and used without further purification. All other reagents were purchased from Sigma-Aldrich and used without further purification.

2.5.2. Instrumentation

^{1}H and ^{13}C NMR spectra were recorded at 400 MHz on a Bruker DPX 400 FT-NMR spectrometer using deuterated solvents, $CDCl_3$ and d_6-DMSO. Chemical shifts are reported as δ in parts per million relative to $CHCl_3$ (7.26 ppm for ^{1}H and 77.0 ppm for ^{13}C) or DMSO (2.50 ppm for ^{1}H and 39.5 ppm for ^{13}C) as the internal standard. Size exclusion chromatography (SEC) data for all polymers was obtained in HPLC grade tetrahydrofuran (THF) containing 2% triethyl amine (TEA) with a flow rate of 1.0

$mL.min^{-1}$, on a set of two PLgel 5 µm Mixed-D columns, plus one guard column and analyzed using Cirrus GPC software based on PS standards. Dialysis tubing was purchased from Spectrumlabs with MW cut off of 3.5 kDa. Infrared spectroscopy was recorded on a Perkin-Elmer Spectrum 100 FT-IR ATR unit. Mass spectra were recorded on a Bruker Esquire 2000 ESI spectrometer. Elemental analysis was performed by Warwick Analytical Service. HPLC analysis was performed on a Varian 920-LC on an analytical column Discovery C18 (100 mm × 4.6 mm × 5 µm) purchased from Sigma-Aldrich, UK and a chiral column Chiralpak IA (150 mm × 4.6 mm × 5 µm) with guard cartridge (Chiralpak 5 µm) purchased from Chiral Technologies Europe. Hydrodynamic diameters (D_h) of the polymer aggregates were determined by dynamic light scattering (DLS) on a Malvern Zetasized Nano ZS instrument operating at 25 °C with a 4 mW He-Ne 633-nm laser module. Measurements were made at a detection angle of 173° (back scattering) and the data was analyzed using Malvern DTS 5.02. All determinations were made in triplicates (with 12 runs recorded for each measurement). TEM samples were prepared by drop deposition onto copper/carbon grids that had been treated with oxygen plasma to increase surface hydrophilicity, when staining was used. The particles were stained using a dilute 1% solution of UA or 2% solution of AM. Alternatively, the samples were drop deposited onto unstained but GO treated grids. The samples were subsequently examined with a transmission electron microscope (JEOL TEM-1200), operating at 80 or 200 kV. Micrographs were collected at magnifications varying from 30 K to 100 K and calibrated digitally. SEM samples were prepared by depositing the sample onto a silicon wafer or glass slide mounted onto an aluminium stub, or alternatively the copper/carbon TEM grid was directly mounted onto the aluminium stub. The sample was sputter coated with gold particles, (at 15 mA for 20 seconds) and examined with a ZEISS SUPRA55VP FEGSEM electron microscope at 3-10 eV and at magnifications varying from 30 K to 100K.

*2.5.3. Synthesis of triply protected Bn/^{t}Bu/Boc protected trans-4-hydroxy-L-proline **2.1***

Commercially available doubly protected *Boc-O*-benzyl-hydroxy-L-proline (Boc-Hyp(Bzl)-OH) (5.0 g, 15.6 mmol, 1.0 eq) was dissolved in dry dichloromethane (CH_2Cl_2) at 0 °C. A mixture of 1-(3-dimethylaminopropyl)-3-ethylcarbodiimide hydrochloride (EDCI.HCl) (3.3 g, 17.1 mmol, 1.1 eq), 4-dimethylaminopyridine (DMAP) (0.95 g, 7.8 mmol, 0.5 eq) and *tert*-butanol (^{t}BuOH) (4.6 g, 62.4 mmol, 4 eq) was then added to the solution at 0 °C. After 2 hours of stirring at 0 °C the reaction mixture was allowed to equilibrate to RT under constant stirring. Finally, the reaction was allowed to stir overnight at RT. The reaction was quenched by solvent evaporation. The residues were re-dissolved in ethyl acetate (EtOAc) and washed twice with water (2 × 20 mL) and twice with an aqueous solution of sodium hydrogen carbonate ($NaHCO_3$, 2 × 20 mL). The organic layer was collected, dried over magnesium sulfate ($MgSO_4$) and *in vacuo*. The crude product was then purified by flash column chromatography (1:1 petroleum ether:EtOAc). Yield: 5.1 g, 87%. ^{1}H NMR (400 MHz, $CDCl_3$): δ = 1.35 (18H, s, 6×C**H**$_3$), 1.92-2.34 (2H, m, C**H**$_2$), 3.39-3.62 (2H, m, C**H**$_2$), 4.00-4.11 (1H, m, C**H**), 4.13-4.24 (1H, m, C**H**), 4.41 (2H, q, C**H**$_2$), 7.20-7.29 (5H, m, Ar-**H**). The identity of proline signals were determined by 2D-COSY ^{1}H NMR spectroscopy. FTIR: ν_{max}/cm^{-1}: 2940-2970 alkyl C-H stretch, 1710 and 1770 C=O stretch, 1390 & 1410 aromatic C-C stretch.

*2.5.4. Synthesis of doubly protected ^{t}Bu/Boc protected trans-4-hydroxy-L-proline **2.2***

The Bn/^{t}Bu/Boc triply protected *trans*-hydroxy-L-proline (**2.1**) was deprotected by hydrogenation to yield the ^{t}Bu/Boc doubly protected *trans*-hydroxy-L-proline (**2.2**). Prior to deprotection, the 10% Pd/C catalyst (0.1 eq) was activated by heating at 140 °C

under vacuum overnight. **2.1** (5.1 g, 13.5 mmol) was dissolved in dry THF/CH_3OH (1:2) and added slowly to the activated Pd/C catalyst under nitrogen at room temperature. The reaction solution was then bubbled with hydrogen gas, *via* several balloons over approximately 20 hours. The reaction was quenched by exposing the solution to air. The Pd/C catalyst was removed from the solution *via* filtration through celite. The filtrate was dried *in vacuo* and the product purified by flash column chromatography (petroleum ether:EtOAc 3:1). Yield: 3.1 g, 82%. ^{1}H NMR (400 MHz, $CDCl_3$): δ = 1.40 (18H, 2×s, 6×C**H**$_3$), 1.93-2.25 (2H, m, C**H**$_2$), 3.30-3.61 (2H, m, C**H**$_2$), 4.03-4.28 (1H, m, C**H**), 4.39-4.45 (1H, m, C**H**). FTIR: ν_{max}/cm^{-1}: 2940-2970 alkyl C-H stretch, 1710 and 1770 C=O stretch.

*2.5.5. Synthesis of ^{t}Bu/Boc protected L-proline functionalized styrenic monomer **2.3***

Monomer precursor **2.2** was coupled with 4-vinylbenzoic acid to yield the polymerizable functional monomer (**2.3**). 4-Vinylbenzoic acid (2.5 g, 13.4 mmol, 1.25 eq), EDCI (3.0 g, 12.3 mmol, 1.15 eq) and DMAP (0.25 g, 1.6 mmol, 0.15 eq) were dissolved in dimethylformamide (DMF) and stirred at 0 °C for one hour. To this solution, a mixture **2.2** (3.1 g, 10.7 mmol, 1.0 eq) and *N*,*N*-diisopropylethylamine (DIEA) (1.8 g, 10.7 mmol, 1.0 eq) in DMF was added, at 0 °C. The resulting solution was allowed to warm to RT and was then stirred for 7 days. The reaction mixture was quenched *via* the addition of an aqueous ammonium chloride solution (NH_4Cl, 20 mL). EtOAc was then added to the solution and the resulting mixture washed twice with water (2 × 20 mL) and twice with a saturated $NaHCO_3$ solution (2 × 20 mL). The organic phase was dried over $MgSO_4$, and the solvent removed *in vacuo*. The crude product was purified by flash column chromatography in petroleum ether:EtOAc (3:1). Yield: 4.5 g, 98%. ^{1}H NMR (400 MHz, $CDCl_3$): δ = 1.35 (9H, s, C**H**$_3$), 1.45 (9H, s,

C**H**$_3$), 2.20-2.55 (2H, 2×m, C**H**$_2$), 3.55-3.80 (2H, 2×m, C**H**$_2$), 4.20-4.35 (1H, 2×t, J = 7.5 Hz, C**H**), 5.35 (1H, d, J = 10.9 Hz, vinyl C**H**), 5.45 (1H, m, C**H**), 5.80 (1H, d, J = 17.6 Hz, vinyl C**H**), 6.70 (1H, dd, J = 10.9 and 17.6 Hz, vinyl C**H**), 7.40 (2H, d, J = 8.3 Hz, Ar-**H**), 7.90 (2H, d, J = 8.3 Hz, Ar-**H**). ^{13}C NMR (400 MHz, $CDCl_3$): δ = 170.6, 164.7, 153.0, 141.3, 134.9, 129.0, 127.8, 125.1, 115.7, 80.4, 79.1, (71.5 & 72.3)*, 57.6, (51.0 & 51.4)*, (34.7 & 35.8)*, (27.0 & 27.3)*. *Denotes splitting from rotamers. $[\alpha]_D^{25} = -34°$ (c = 5.0, $CHCl_3$). FTIR: v_{max}/cm^{-1}: 1737 (C=O ester), 1407 & 1379 (C=C aromatic), 1157 & 1111 (C-O ester). ESI-MS found: 416.1 (M-H) $C_{23}H_{31}NO_6$; expected: 417.22. Elemental analysis found: C, 65.57; H, 7.57; N, 3.12 ($C_{23}H_{31}NO_6$); expected: C, 66.17; H, 7.48; N, 3.35.

2.5.6. Synthesis of dodecyl-1-phenylethyl trithiocarbonate, ***CTA1***[40]

Potassium phosphate (K_3PO_4) (1.36 g, 6.4 mmol) was added to acetone (40.0 mL) forming a suspension. To the stirred suspension, 1-dodecanethiol (1.18 g, 5.8 mmol) was added and stirred for 10 minutes. Subsequently, carbon disulfide (CS_2) (1.34 g, 17.5 mmol) was added to the reaction mixture and was stirred for one hour after which 1-bromoethyl benzene (1.07 g, 5.8 mmol) was added. After five hours of stirring at RT, K_3PO_4 was removed *via* filtration and the filtrate was dried *in vacuo*. The crude product was then purified by flash column chromatography (100% petroleum ether). Yield: 1.97 g, 89%. ^{1}H NMR (400 MHz, $CDCl_3$): δ = 0.87 (3H, t, J = 7.0 Hz, C**H**$_3$), 1.20-1.42 (18H, m, C**H**$_2$), 1.67 (2H, quin, J=7.6 Hz, C**H**$_2$), 1.74 (3H, d, J = 7.1 Hz, C**H**$_3$), 3.31 (2H, t, J = 7.5 Hz, C**H**$_2$), 5.32 (1H, q, J = 7.1 Hz, C**H**), 7.22-7.23 (5H, m, Ar-**H**). ^{13}C NMR (400 MHz, $CDCl_3$): δ = 13.3, 20.8, 22.1, 27.3, 28.3, 28.5, 28.7, 28.8, 28.9, 29.0, 31.3, 36.2, 49.4, 77.0, 76.4, 76.8, 127.1, 127.1, 128.0, 218.9. FTIR: v_{max}/cm^{-1}: 3050 aromatic C-H stretch, 2900 & 2950 alkyl C-H stretch, 1100 C=S stretch. ESI-MS found: 381.0 (M-H)

$C_{21}H_{34}S_3$, 283.2 $C_{14}H_{19}S_3$, 255.1 $C_{12}H_{14}S_3$; expected: 382.18. Elemental analysis found: C, 66.06; H, 9.01; S, 24.61 ($C_{21}H_{34}S_3$); expected: C, 65.91; H, 8.96; S, 25.14.

*2.5.7. General procedure for RAFT copolymerization of **2.3** and styrene to give copolymer **2.4***

Monomer **2.3** (0.20 g, 0.48 mmol, 5 eq), styrene (0.94 g, 9 mmol, 95 eq) and CTA1 (0.037 g, 0.096 mmol, 1.0 eq) were added to a dry ampoule with a small stirrer bar. The solution was degassed *via* three freeze-pump-thaw cycles. The ampoule was then backfilled with nitrogen gas, sealed and placed into a pre-heated oil bath at 110 °C and stirred for 22 hours. A small aliquot was withdrawn after 22 hours to determine the percentage conversion of both monomers by ^{1}H NMR spectroscopy. The polymerization was quenched *via* the addition of a small amount of THF and cooling in liquid nitrogen. The polymer solution was precipitated in rapidly stirring cold CH_3OH, filtered and dried in the vacuum oven at 40 °C overnight. Polymer molecular weight and distributions were measured by SEC in THF and compared to polystyrene (PS) standards. ^{1}H NMR spectroscopy was used to determine ratio of the two monomers in the final copolymer. Molecular weight by ^{1}H NMR spectroscopy was determined by comparing characteristic signals of the two monomers in the polymer relative to characteristic end group signals.

*Representative characterization data for RAFT copolymerization of **2.3** and styrene, [where H_{ps} = proton from polystyrene; H_{ppr} = proton from **2** in polymer; H_{eg} = proton from end group]*

^{1}H NMR (400 MHz, $CDCl_3$): δ = 0.85 ($3H_{eg}$, t, J=7.1 Hz, C**H**$_3$), 1.15-2.60 ($3H_{ps}$ backbone, $3H_{ppr}$ backbone, $9H_{ppr}$+$9H_{ppr}$, *tert*-butyl groups, $20H_{eg}$, alkyl chain), 3.20

($2H_{eg}$, C**H**$_2$), 3.75 ($2H_{ppr}$, C**H**$_2$), 4.40 ($1H_{ppr}$, C**H**) 5.45 ($1H_{ppr}$, C**H**), 6.25-7.20 ($5H_{ps,}$ Ar-**H**, $4H_{ppr}$, Ar-**H**).

*2.5.8. General procedure for deprotection of copolymer **2.4** to give deprotected copolymer **2.5***

Copolymer **2.4** (0.64 g, 0.063 mmol) was dissolved in dry CH_2Cl_2. TFA (0.56 mL, 15 eq wrt to each *tert*-butyl group) was slowly added to the stirred polymer solution and the resulting solution was stirred for 24 hours at RT. The reaction was quenched *via* the removal of excess acid under a flow of N_2 (g). The resulting polymer residues were dissolved in a DMF:water (1:1) solution and dialyzed exhaustively against nanopure water (18.2 Ω) (MWCO = 3.5 kDa) and lyophilized (freeze-dried) to give deprotected copolymers **2.5**, or alternatively the copolymer was dissolved in THF and precipitated into CH_3OH. The polymer was then collected by filtration, further washed with water and dried in the vacuum oven at 40 °C overnight.

*2.5.9. General procedure for the organocatalytic application of RAFT copolymer **2.5** in the model aldol reaction*

Copolymer **2.5** (20, 10, 5 or 1 mol% loading) was fully dissolved in DMF (950, 925, 880 μL) and water (50, 75, 120 μL) was added dropwise to the stirring polymer solution. Cyclohexanone (104 μL, 1.0 mmol, 4.0 eq) was added to the solution and the reaction mixture stirred for 30 minutes. 4-Nitrobenzaldehyde (38 mg, 0.25 mmol, 1.0 eq) was then added and the resulting solution was stirred for 24 hours at RT. The reaction was quenched *via* dilution with an aqueous solution of lithium bromide (LiBr) (10.0 mL, 4 wt%). The product was extracted into EtOAc and the combined organic layers were dried over $MgSO_4$ and the solvent removed *in vacuo*. The product was purified by column chromatography (petroleum ether:EtOAc 1:1). The diastereomeric

anti/syn ratio was determined by ^{1}H NMR spectroscopy and the enantiomeric excess (ee) determined by chiral HPLC, Daicel Chiralpak IA (80:10:10 hexane:propan-2-ol:ethanol), at a flow rate of 1.0 mL.min^{-1}. The aliquots withdrawn during the kinetic studies were analyzed on a reversed-phase Discovery C18 HPLC column, using a gradient solvent method in H_2O:CH_3OH going from 95:5 to 5:95 over a 12 minute time period at a flow rate of 2.0 mL.min^{-1}.

Aldol product: (S)-2-((R)-hydroxyl-(4-nitrophenyl)methyl)-cyclohexan-1-one

^{1}H NMR (400 MHz, $CDCl_3$): δ = 1.19-2.57 (8H, m, C**H**$_2$), 4.00 (1H, s, O**H**), 4.82 (1-xH, d, J=4.5 Hz, C**H**, anti), 5.41 (xH, C**H**, syn), 7.44 (2H, d, J=8.6 Hz, Ar-**H**), 8.15 (2H, d, J=8.6 Hz, Ar-**H**). ^{13}C NMR (400 MHz, $CDCl_3$): δ = 24.9, 27.0, 36.5, 42.0, 57.0, 74.0, 123.7, 127.9, 147.3, 148.5, 213.3. ESI-MS found: 272.1 ($M+Na^+$) $C_{13}H_{15}NO_4$; expected 249.10. Chiral HPLC: minor enantiomer t_R = 12.4 min, major enantiomer t_R = 18.3 min This compound has been fully characterized by others.[7, 15, 44, 51]

2.6. References

1. M. Movassaghi and E. N. Jacobsen, *Science*, 2002, **298**, 1904.

2. W. Notz, F. Tanaka and C. F. Barbas, *Acc. Chem. Res.*, 2004, **37**, 580.

3. N. Mase, Y. Nakai, N. Ohara, H. Yoda, K. Takabe, F. Tanaka and C. F. Barbas, *J. Am. Chem. Soc.*, 2006, **128**, 734.

4. Y. Hayashi, T. Sumiya, J. Takahashi, H. Gotoh, T. Urushima and M. Shoji, *Angew. Chem. Int. Ed.*, 2006, **45**, 958.

5. A. J. A. Cobb, D. M. Shaw, D. A. Longbottom, J. B. Gold and S. V. Ley, *Org. Biomol. Chem.*, 2005, **3**, 84.

6. E. Veverková, J. Strasserová, R. Sebesta and S. Toma, *Tetrahedron: Asymmetry*, 2010, **21**, 58.

7. F. Giacalone, M. Gruttadauria, P. L. Meo, S. Riela and R. Noto, *Adv. Synth. Catal.*, 2008, **350**, 2747.

8. E. Bellis and G. Kokotos, *Tetrahedron*, 2005, **61**, 8669.

9. Z. Tang, F. Jiang, X. Cui, L.-Z. Gong, A.-Q. Mi, Y.-Z. Jiang and Y.-D. Wu, *Proc. Natl. Acad. Sci. U.S.A*, 2004, **101**, 5755.

10. Z. Tang, Z.-H. Yang, X.-H. Chen, L.-F. Cun, A.-Q. Mi, Y.-Z. Jiang and L.-Z. Gong, *J. Am. Chem. Soc.*, 2005, **127**, 9285.

11. Y. Hayashi, S. Aratake, T. Okano, J. Takahashi, T. Sumiya and M. Shoji, *Angew. Chem. Int. Ed.*, 2006, **45**, 5527.

12. M. Benaglia, G. Celentano and F. Cozzi, *Adv. Syn. Cat.*, 2001, **343**, 171.

13. M. Benaglia, M. Cinquini, F. Cozzi, A. Puglisi and G. Celentano, *Adv. Syn. Cat.*, 2002, **344**, 533.

14. M. Benaglia, M. Cinquini, F. Cozzi, A. Puglisi and G. Celentano, *J. Mol. Catal.A: Chem.*, 2003, **204**, 157.

15. D. Font, C. Jimeno and M. A. Pericas, *Org. Lett.*, 2006, **8**, 4653.

16. M. Gruttadauria, F. Giacalone, A. M. Marculescu, P. Lo Meo, S. Riela and R. Noto, *Eur. J. Org. Chem.*, 2007, **28**, 4688.

17. M. Gruttadauria, A. M. P. Salvo, F. Giacalone, P. Agrigento and R. Noto, *Eur. J. Org. Chem.*, 2009, **31**, 5437.

18. Y. X. Liu, Y. N. Sun, H. H. Tan, W. Liu and J. C. Tao, *Tetrahedron: Asymmetry*, 2007, **18**, 2649.

19. D. Font, A. Bastero, S. Sayalero, C. Jimeno and M. A. Pericàs, *Org. Lett.*, 2007, **9**, 1943.

20. W. S. Miao and T. H. Chan, *Adv. Synth. Catal.*, 2006, **348**, 1711.

21. C. Aprile, F. Giacalone, M. Gruttadauria, A. M. Marculescu, R. Noto, J. D. Revell and H. Wennemers, *Green Chem.*, 2007, **9**, 1328.

22. E. Bellis and G. Kokotos, *J. Mol. Cat. A. Chem.*, 2005, **241**, 166.

23. F. Sanda and T. Endo, *Macromol. Chem. Phys.*, 1999, **200**, 2651.

24. B. S. Lokitz, J. E. Stempka, A. W. York, Y. Li, H. K. Goel, G. R. Bishop and C. L. McCormick, *Aust. J. Chem.*, 2006, **59**, 749.

25. J. Skey, C. F. Hansell and R. K. O'Reilly, *Macromolecules*, 2010, **43**, 1309.

26. J. Skey and R. K. O'Reilly, *J. Polym. Sci., Part A: Polym. Chem.*, 2008, **46**, 3690.

27. M. Casolaro, S. Bottari, A. Cappelli, R. Mendichi and Y. Ito, *Biomacromol.*, 2004, **5**, 1325.

28. B. L. Moore and R. K. O'Reilly, *J. Polym. Sci., Part A: Polym. Chem.*, 2012, **50**, 3567.

29. T. E. Kristensen and T. Hansen, *Eur. J. Org. Chem.*, 2010, **17**, 3179.

30. T. E. Kristensen, K. Vestli, K. A. Fredriksen, F. K. Hansen and T. Hansen, *Org. Lett.*, 2009, **11**, 2968.

31. T. E. Kristensen, K. Vestli, M. G. Jakobsen, F. K. Hansen and T. Hansen, *J. Org. Chem.*, 2010, **75**, 1620.

32. B. S. Lokitz, J. E. Stempka, A. W. York, Y. Li, H. K. Goel, G. R. Bishop and C. L. McCormick, *Aust. J. Chem.*, 2006, **59**, 749.

33. H. Mori, I. Kato, M. Matsuyama and T. Endo, *Macromolecules*, 2008, **41**, 5604.

34. M. K. Dhaon, R. K. Olsen and K. Ramasamy, *J. Org. Chem.*, 1982, **47**, 1962.

35. B. Neises and W. Steglich, *Angew. Chem. Int. Ed.*, 1978, **17**, 522.

36. A. C. Evans, A. Lu, C. Ondeck, D. A. Longbottom and R. K. O'Reilly, *Macromolecules*, 2010, **43**, 6374.

37. Q. Ma and K. L. Wooley, *J. Polym. Sci., Part A: Polym. Chem.*, 2000, **38**, 4805.

38. M. Benaglia, M. Chen, Y. K. Chong, G. Moad, E. Rizzardo and S. H. Thang, *Macromolecules*, 2009, **42**, 9384.

39. M. Benaglia, J. Chiefari, Y. K. Chong, G. Moad, E. Rizzardo and S. H. Thang, *J. Am. Chem. Soc.*, 2009, **131**, 6914.

40. J. Skey and R. K. O'Reilly, *Chem. Commun.*, 2008, **46**, 4183.

41. D. M. Haddleton, M. C. Crossman, K. H. Hunt, C. Topping, C. Waterson and K. G. Suddaby, *Macromolecules*, 1997, **30**, 3992.

42. Y. Kang, A. Lu, A. Ellington, M. C. Jewett and R. K. O'Reilly, *ACS Macro Lett.*, 2013, **2**, 581.

43. A. M. van Herk, *J. Chem. Educ.*, 1995, **72**, 138.

44. D. Font, S. Sayalero, A. Bastero, C. Jimeno and M. A. Pericas, *Org. Lett.*, 2007, **10**, 337.

45. D. Blackmond, A. Armstrong, V. Coombe and A. Wells, *Angew. Chem. Int. Ed.*, 2007, **46**, 3798.

46. A. P. Brogan, T. J. Dickerson and K. D. Janda, *Angew. Chem. Int. Ed.*, 2006, **45**, 8100.

47. N. Zotova, A. Franzke, A. Armstrong and D. G. Blackmond, *J. Am. Chem. Soc.*, 2007, **129**, 15100.

48. M. Gruttadauria, F. Giacalone and R. Noto, *Adv. Synth. Catal.*, 2009, **351**, 33.

49. J. Paradowska, M. Pasternak, B. Gut, B. Gryzło and J. Mlynarski, *J. Org. Chem.*, 2011, **77**, 173.

50. B. H. Lipshutz and S. Ghorai, *Org. Lett.*, 2011, **14**, 422.

51. M. Gruttadauria, F. Giacalone, A. Mossuto Marculescu, P. Lo Meo, S. Riela and R. Noto, *Eur. J. Org. Chem.*, 2007, **28**, 4688.

52. H. Yang and R. G. Carter, *Org. Lett.*, 2008, **10**, 4649.

53. L. Zhang and A. Eisenberg, *J. Am. Chem. Soc.*, 1996, **118**, 3168.

54. J. P. Patterson, A. M. Sanchez, N. Petzetakis, T. P. Smart, III. T. H. Epps, I. Portman, N. R. Wilson and R. K. O'Reilly, *Soft Matter*, 2012, **8**, 3322.

3. Aldol Reactions Catalyzed by L-Proline Functionalized Polymeric Nanoreactors in Water

3.1. Abstract

This chapter explores the application of L-proline functionalized core-shell micelles as nanoreactors for organic reactions in water using spherical micelles based on two well-defined diblock copolymers, poly(styrene-*stat*-proline-St)-*block*-poly(acrylic acid) (P(St-*stat*-ProSt)-*b*-PAA) and poly(methylmethacrylate-*stat*-proline-MA)-*block*-poly(methacrylic acid) (P(MMA-*stat*-ProMA)-*b*-PMAA), synthesized by reversible addition-fragmentation chain transfer (RAFT) polymerization. The catalytic efficiency of the two systems was evaluated in a model asymmetric aldol reaction. Both micelle systems showed excellent catalytic properties, achieving high activity and selectivity in water and relatively short reaction times. The activity was also found to be superior to unsupported L-proline in water and organic solvents at comparable loadings which was attributed to the hydrophobic concentrator effect. The placement of the catalytic motifs within the nanoreactor core were found to influence the catalyst enantioselectivity where for the PMMA based micelle system higher selectivity was observed when the catalyst was buried deeper within the core. The importance of the local hydrophobic catalytic environment was further highlighted when a shell-functionalized micelle system showed high activity by significantly reduced enantioselectivity which was attributed to the high water content around the catalytic site.

3.2. Introduction

Core-shell type supramolecular structures formed by the assembly of amphiphilic diblock copolymers are attractive systems due to their high stability and durability compared to small molecule assemblies. Spherical micelles in water have been extensively studied as a hydrophobic micelle core is presented upon assembly which may act as a protective compartment for the encapsulation of lipophilic molecules.[1-3]

Thayumanavan and co-workers[4-7] elegantly utilized this environment as a nanocarrier for drug molecules in biomedical applications. Helms *et al.*[8] reported the efficient uptake of small molecules from the surrounding solvent based on polarity. The substrates were efficiently concentrated by the dendrimer and brought into close proximity of the catalyst moieties. This is now known as the concentrator effect as the hydrophobic pockets of the dendrimers were able to efficiently concentrate organic substrates. The ability and preferential uptake of hydrophobic molecules from the surrounding aqueous environment by hydrophobic micelle cores has also been demonstrated by Nagarajan *et al.*[9] and Cotanda and O'Reilly[10] Micelles with a catalytic motif contained within its core have successfully catalyzed reactions with enhanced activity in water,[11-15] which is attributed to the unique compartmentalized nature of the protected hydrophobic core, increasing the local concentration of both the substrates and catalyst.

By carefully tuning the hydrophobicity of the core-forming block, the unique core environment can be readily tailored.[16] Rossbach *et al.*[17] and Liu *et al.*[13] both designed polymer nanoreactors for hydrolytic kinetic resolution of epoxides in water and highlighted the importance of the hydrophobic core environment in order to achieve high activity and enantioselectivity. It was found that the penetration of a small amount of water into the hydrophobic core was crucial in achieving the observed activity.

The importance of water in L-proline catalyzed reactions has been investigated since it re-introduction by List and co-workers in the year 2000.[18-20] A small amount of water has resulted in enhanced activity and enantioselectivity in both polymer supported and non-supported systems.[19-23] We observed the same effect with our PS-supported L-proline system[24, 25] and wanted to further explore this effect by placing the L-proline moiety in the core environment of two micelles with different hydrophobicities and

investigate its effect on the activity and enantioselectivity of L-proline. Thus, two block copolymers, P(St-*stat*-ProSt)-*b*-PAA and P(MMA-*stat*-ProMA)-*b*-PMAA were synthesized by RAFT polymerization[26] and their catalytic efficiency in water evaluated. The study was further extended by tailoring the location of the catalytic motif within the hydrophobic core and thus altering its proximity to the surrounding water. Lastly, the surface of the micelle, i.e. the shell was decorated with the catalytic motif, placing it in a contrasting hydrophilic environment. In this work we aim to synthesize L-proline functionalized polymer micelles for organic reactions in water and investigate the importance of the local catalyst environment on its catalytic efficiency by careful design of the micelle scaffold.

3.3. Results and Discussion

3.3.1. Synthesis and characterization of P(St-stat-ProSt)-b-PAA micelles, ***3.3***

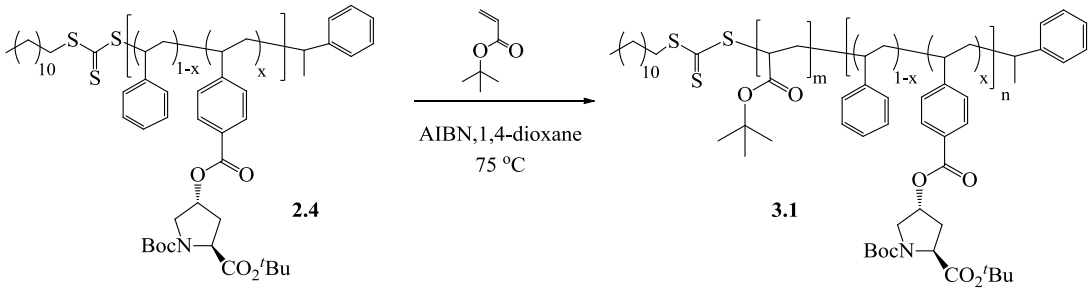

Scheme 3.1. Chain extension of 2.4 with *tert*-butyl acrylate *via* RAFT to yield diblock copolymer 3.1

The synthesis and characterization of the doubly protected styrenic monomer **2.3** and RAFT copolymerization of **2.3** with styrene to afford copolymer **2.4** were discussed in Chapter 2 and will not be further discussed here. Copolymer **2.4** was used as MacroCTA in the chain extension polymerization of *tert*-butyl acrylate (^{t}BuA) using RAFT polymerization (93% conversion) (Scheme 3.1). The catalytic functionalities on **2.4** remained protected, as this allows for efficient characterization of the resulting

polymer by size exclusion chromatography (SEC) (Figure 3.2). The degree of polymerization (DP) of ^{t}BuA in **3.1** was determined by ^{1}H NMR spectroscopy by comparing signals of the catalytic functionality (δ 5.5 ppm) and PS (δ 6.2-7.2 ppm) to signals of P^{t}BuA (δ 1.0-2.5 ppm) (Figure 3.1). As the DP of the first block was known, its contribution to the backbone signals in the ^{1}H NMR spectrum could be accounted for, making it possible to determine DP of the P^{t}BuA block. M_n (^{1}H NMR) = 20.0 kDa, DP_{St} = 52, $DP_{\mathbf{2.3}}$ = 3, DP_{tBuA} = 93; M_n (SEC, THF, PS calibration) = 20.3 kDa, M_w (SEC) = 23.7 kDa, Đ = 1.17. A small high molecular weight shoulder was observed in the SEC spectrum which was attributed to polymer-polymer coupling.

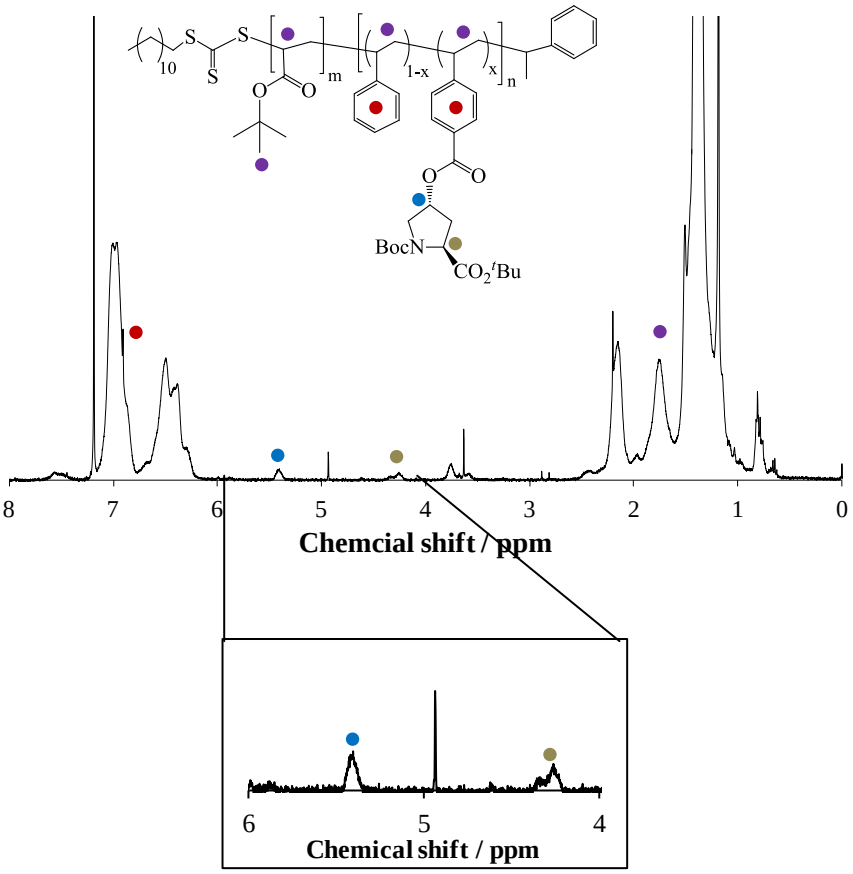

Figure 3.1. Representative ^{1}H NMR spectrum (400 MHz, $CDCl_3$) of block copolymer 3.1, highlighted are signals of the catalytic moiety

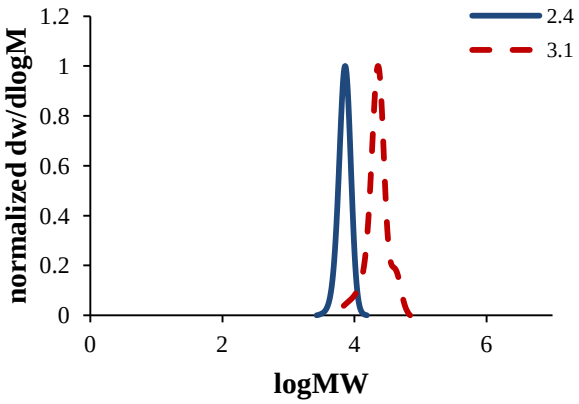

Figure 3.2. SEC RI trace of the starting copolymer 2.4 and final diblock copolymer 3.1 in THF using PS standards

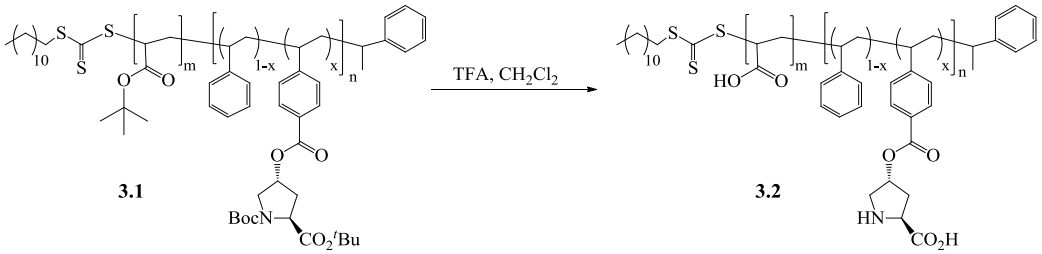

Scheme 3.2. Deprotection of P^{t}BuA and L-proline protecting groups to yield amphiphile 3.2

The diblock copolymer **3.1** was stirred in CH_2Cl_2/TFA to reveal the desired hydrophilic poly(acrylic acid) block and active amino and carboxylic acid functionalities of the catalyst.[27] The final catalyst concentration was determined to be 0.224 mmol.g^{-1}. The deprotected amphiphile **3.2** was subsequently self-assembled into micelles *via* solvent switch from DMF to water, at 1 mg.mL^{-1}. This method involved complete dissolution of **3.2** in DMF, a good solvent for both blocks and slow addition of a non-solvent for the core forming block, which in this case is water.[28-32] DMF was then removed *via* exhaustive dialysis against nanopure water. Thus, micelles with a hydrophobic PS core stabilized by the water soluble PAA shell were formed.

Moreover, as the catalytic moieties are functionalized on the PS block, they are embedded within the micelle core, i.e. in a confined hydrophobic environment. This was an important feature as majority of aldol substrates are insoluble in water and will therefore allow the hydrophobic core to efficiently sequester hydrophobic substrates from the surrounding water. A representation of the self-assembly process is show below in Figure 3.3.

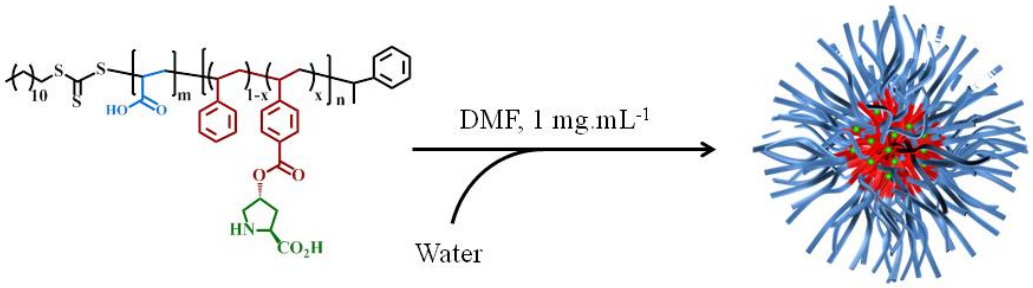

Figure 3.3. The self-assembly of 3.2, from DMF to water to yield micelles 3.3

The hydrodynamic diameter (D_h) of micelles **3.3** was determined to be 23 nm (PDI = 0.148) by dynamic light scattering (DLS), at a concentration of 0.5 mg.mL^{-1} (Figure 3.4). Micelle **3.3** was subsequently characterized by transmission electron microscopy (TEM), **3.3** in water (0.5 mg.mL^{-1}) was drop casted onto a graphene oxide (GO) treated lacey carbon grid. The use of stains to achieve good contrast was not necessary as GO treated grids alone was able to provide the desired contrast.[33] The average diameter (D_{av}) of **3.3** in the dry state was determined to be 17 nm ± 3 nm from the analysis of approximately 320 particles (Figure 3.5).

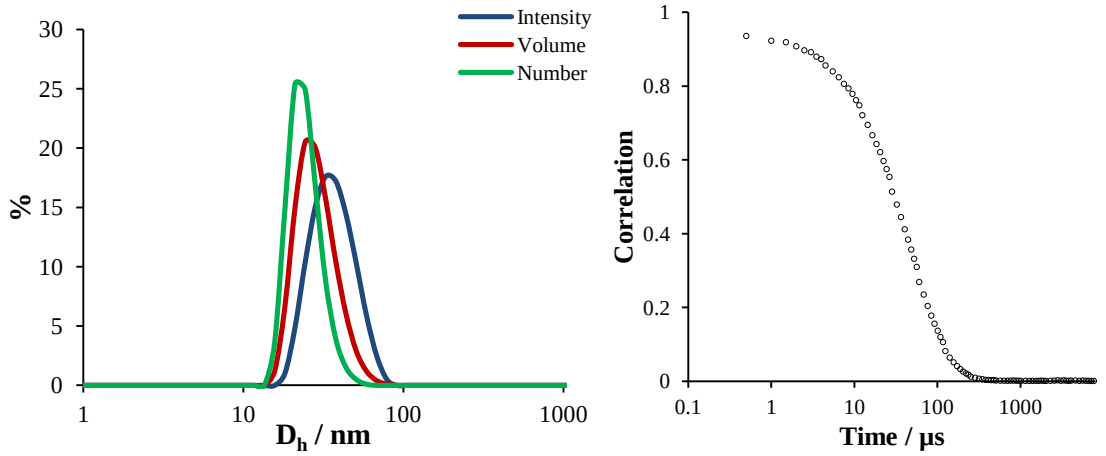

Figure 3.4. DLS trace of micelles 3.3 in water, at 25 °C and 0.5 mg.mL^{-1} and the corresponding correlation function, D_h = 23 nm (PDI = 0.148)

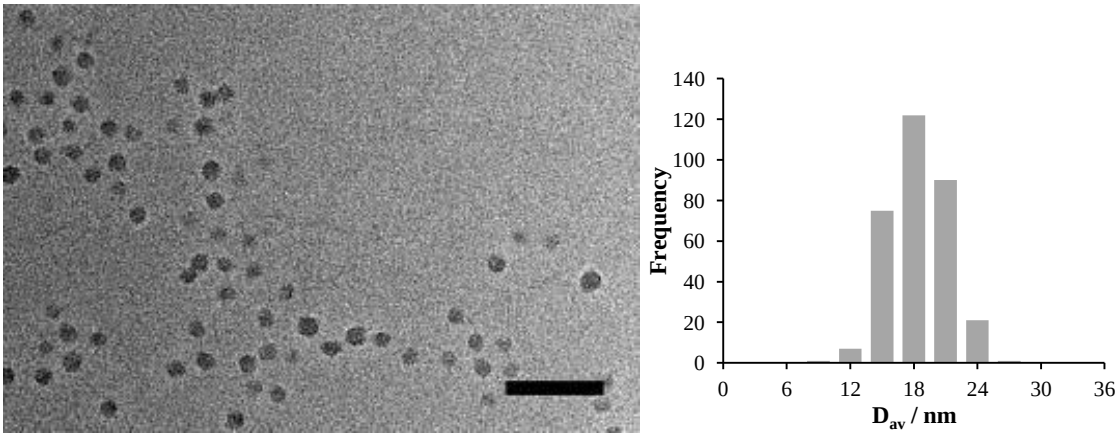

Figure 3.5. TEM image of micelles 3.3 on GO grid, D_{av} = 17 ± 3 nm, scale bar is 100 nm

*3.3.1. Synthesis and characterization of P(MMA-co-ProMA)-b-PMAA micelles, **3.8***

3.3.1.1. Monomer synthesis

To further understand the importance of the confined core environment on the catalytic activity of the embedded catalyst, a second micelle system was designed. For this purpose, a methacrylate type polymer was synthesized, providing a different, but still

hydrophobic environment for catalysis. The main aim was to examine the influence of the core hydrophobicity on the catalytic activity of L-proline.

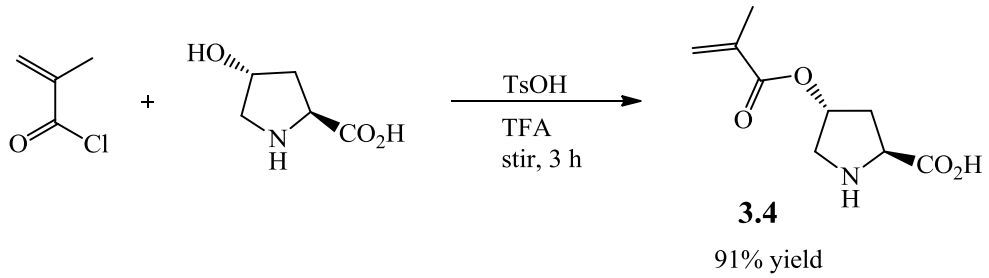

Scheme 3.3. Coupling reaction to yield the desired monomer 3.4

For RAFT copolymerization compatibility, a functional methacrylate type monomer was first synthesized following a literature procedure reported by Kristensen *et al.*[34] The commercially available unprotected 4-hydroxy-L-proline was coupled with methacryloyl chloride in a one-step reaction to yield the desired monomer **3.4** (7.7 g, 91%), according to Scheme 3.3.

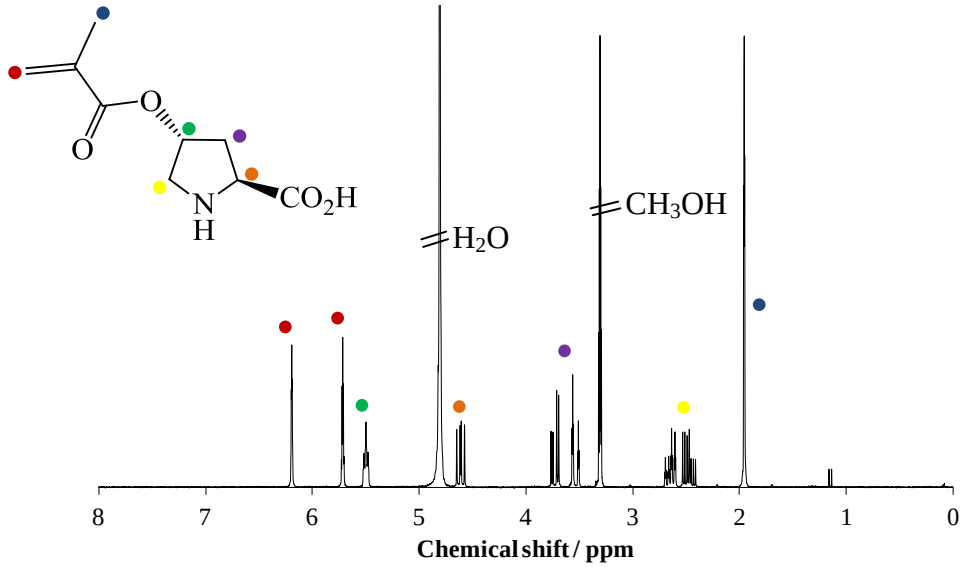

Figure 3.6. ^{1}H NMR spectrum (400 MHz, CD_3OD) of 3.4, after recrystallization

^{1}H NMR analysis of **3.4** after recrystallization suggests the coupling reaction was successful (Figure 3.6) as the expected chemical shifts and integrations match those reported by Kristensen *et al.*[34]

3.3.1.2. Polymer synthesis

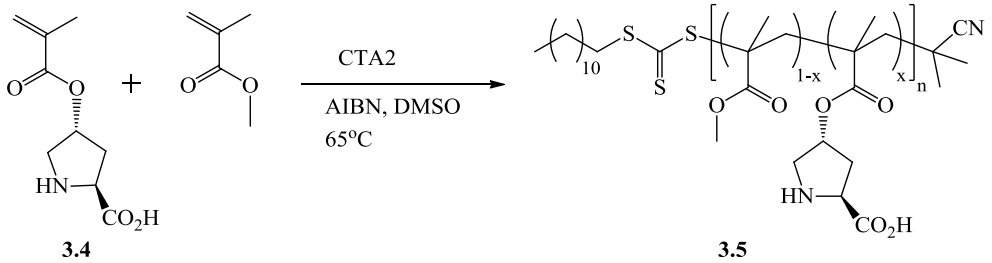

3.4 **3.5**

Scheme 3.4. RAFT copolymerization of 3.4 and MMA in DMSO to yield copolymer 3.5

Copolymerization of **3.4** and methyl methacrylate (MMA) was carried out using the commercially available 2-cyano-2-propyl dodecyl trithiocarbonate (CTA2) as the CTA (Scheme 3.4). CTA2 has been shown to be suitable for a range of monomers, including methacrylate type monomers.[35] A similar degree of catalyst incorporation was targeted (~13 mol% catalyst) as achieved for the PS system. The DP of PMMA and **3.4** were determined by ^{1}H NMR spectroscopy by comparing signals of the monomers to the polymer as previously described. Despite achieving a relatively short functional PMMA polymer ($PMMA_{27}$-*co*-$ProMA_2$) we decided to carry on with the polymer as the molar percentage of catalyst matched that of the functional PS polymer (PSt_{52}-*stat*-$ProSt_3$). The carboxylic acid functionalities on copolymer **3.5** were further protected with a *tert*-butyl group prior to SEC analysis to avoid interactions with the column (Figure 3.7). M_n (^{1}H NMR) = 3.3 kDa, DP_{MMA} = 27, $DP_{\mathbf{3.4}}$ = 2; M_n (SEC, THF, PMMA calibration) = 4.4 kDa, M_w (SEC) = 4.7 kDa, Đ = 1.07.

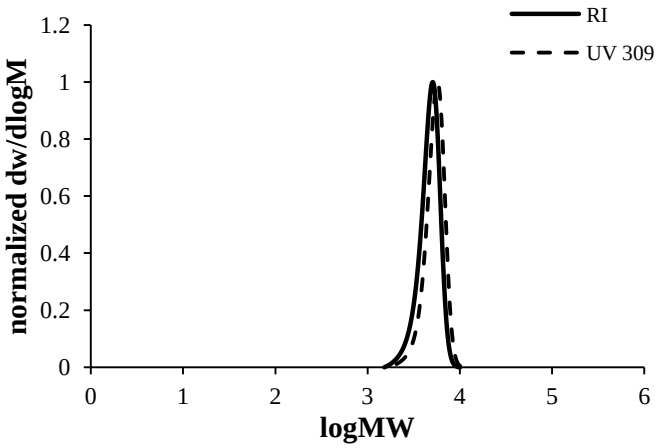

Figure 3.7. SEC traces (RI and UV) of 3.5 in THF, after protection of carboxylic acid functionalities on L-proline moieties

The monomer ratios were unfortunately not investigated in detail, instead the incorporation of **3.4** into copolymer **3.5** was investigated by following the RAFT copolymerization progress of **3.4** and MMA at a 50:50 molar ratio. This was determined by following the conversion of the two monomers with time by ^{1}H NMR spectroscopy (Figure 3.8). Monomer **3.4** appears to be incorporated into the copolymer throughout the copolymerization process, we therefore propose that the catalytic motifs should be well distributed along the copolymer backbone of the resulting copolymer, as opposed to the PS 'copolymerization' (discussed in Chapter 2).

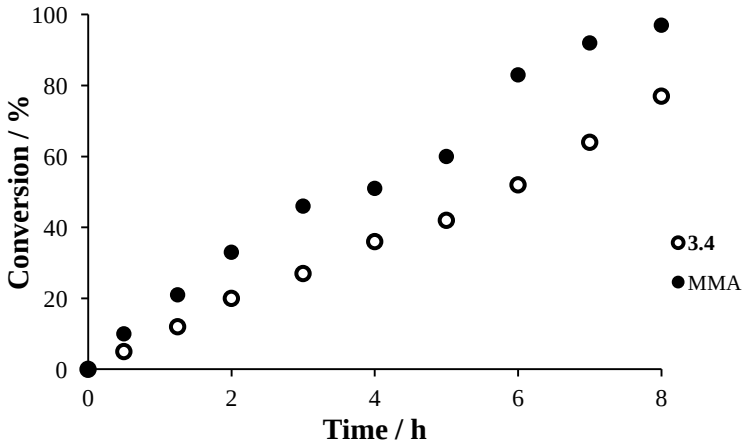

Figure 3.8. RAFT copolymerization of 3.4 and MMA with CTA2, followed by ^{1}H NMR spectroscopy

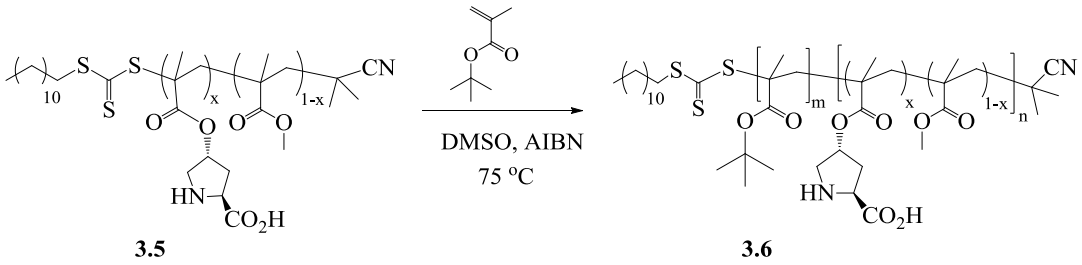

Scheme 3.5. Chain extension of 3.5 with ^{t}BuMA in DMSO to yield diblock copolymer 3.6

Copolymer **3.5** was subsequently chain extended with *tert*-butyl methacrylate (^{t}BuMA) *via* a RAFT polymerization process. By comparing ^{1}H NMR signals of P^{t}BuMA (δ 0.8-2.8 ppm) to those of the hydrophobic block (δ 5.3 ppm for poly-**3.4** and δ 3.6 ppm for PMMA), the final DP of P^{t}BuMA block was determined, P(MMA$_{27}$-*co*-Pro$_2$)-*b*-P^{t}BuMA$_{54}$ (Figure 3.9).

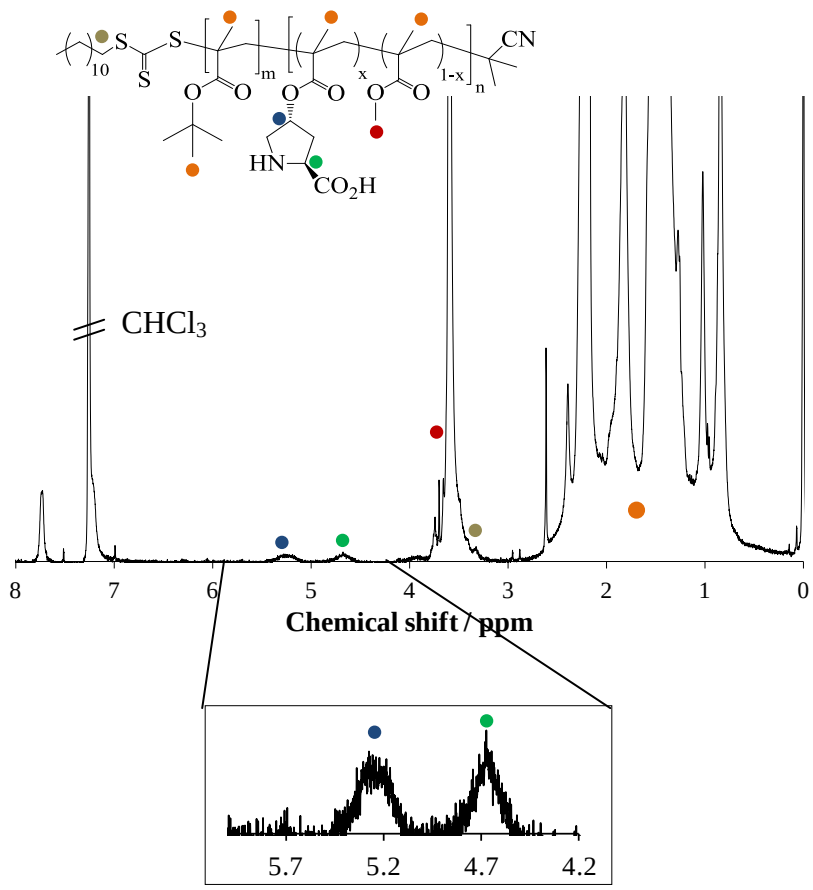

Figure 3.9. ^{1}H NMR (400 MHz, $CDCl_3$) spectrum of block copolymer 3.6 where key signals for the catalyst functionalities are highlighted

As the DP of the initial block was previously known, this could be accounted for in the backbone signals (δ 0.8-2.8 ppm), making it possible to determine DP of the second P^{t}BuMA block (52% conversion). The molecular weight of diblock **3.6** was confirmed by SEC prior to deprotection of P^{t}BuMA but following protection of the carboxylic acid functionalities of L-proline (Figure 3.10). M_n (^{1}H NMR) = 11.2 kDa, DP_{MMA} = 27, $DP_{\mathbf{3.4}}$ = 2, $DP_{t\text{BuMA}}$ = 54; M_n (SEC, THF, PMMA calibration) = 11.3 kDa, M_w (SEC) = 12.4 kDa, Đ = 1.09.

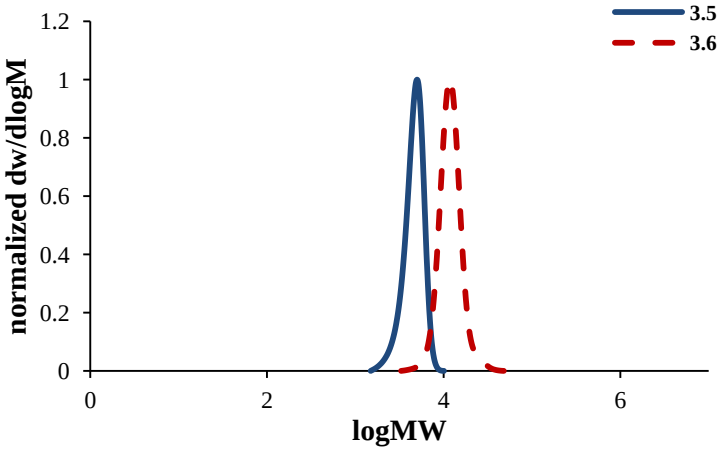

Figure 3.10. SEC RI trace of 3.5 and 3.6 in THF following protection of carboxylic acid functionalities of L-proline

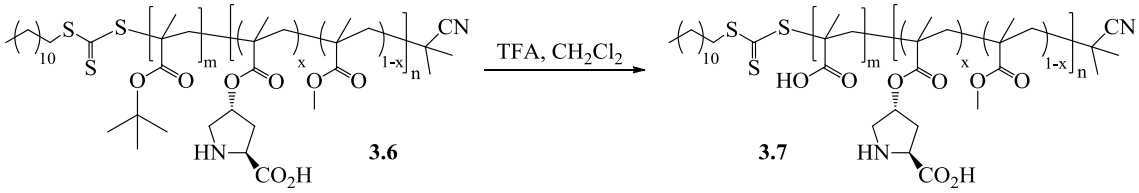

Scheme 3.6. Deprotection of 3.6 to yield amphiphile 3.7

The poly(methacrylic acid) (PMAA) block was revealed using deprotection chemistries with TFA.[27] The final catalyst concentration was determined to be 0.282 mmol.g^{-1}, comparable to the concentration achieved for **3.3** (pH *ca.* 7). Amphiphile **3.7** was self-assembled as described above in Figure 3.3 *via* a solvent switch method from DMF to

water at 1 mg.mL^{-1} to yield micelles **3.8**. In this case, the catalyst containing hydrophobic PMMA core is stabilized by the PMAA shell in water.

Micelles **3.8** were first characterized by DLS at 25 °C where a D_h of 21 nm was determined (PDI = 0.120) (Figure 3.11). The particle D_h achieved is comparable to those observed for micelles **3.3** at the same concentration. **3.8** was then characterized by dry-state TEM, using the same sample previously used for DLS analysis. Again good contrast was achieved by using GO treated TEM grids[33] and spherical micelles were observed with D_{av} = 19 ± 4 nm, from the analysis of approximately 200 particles (Figure 3.12).

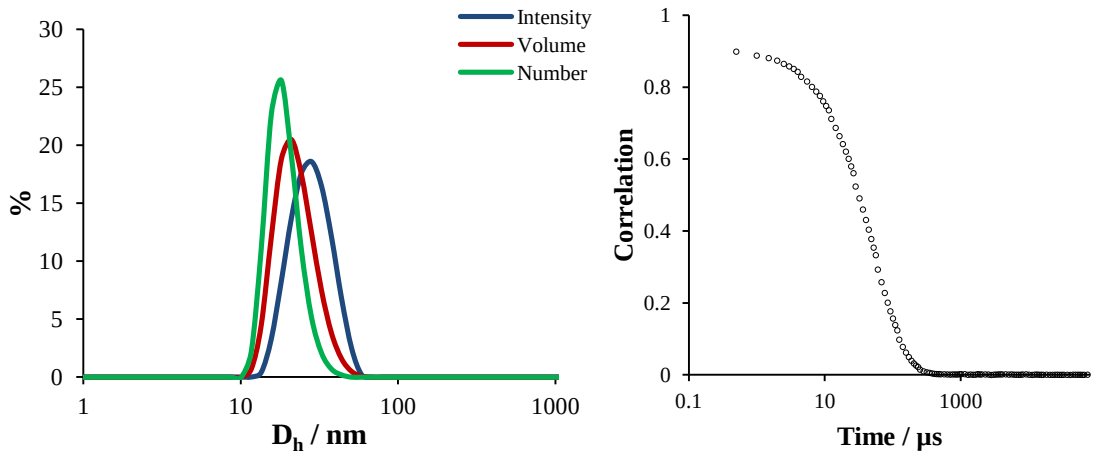

Figure 3.11. DLS trace of 3.8 in water at 0.5 mg.mL^{-1}, and its corresponding correlation function, D_h = 21 nm (PDI = 0.120)

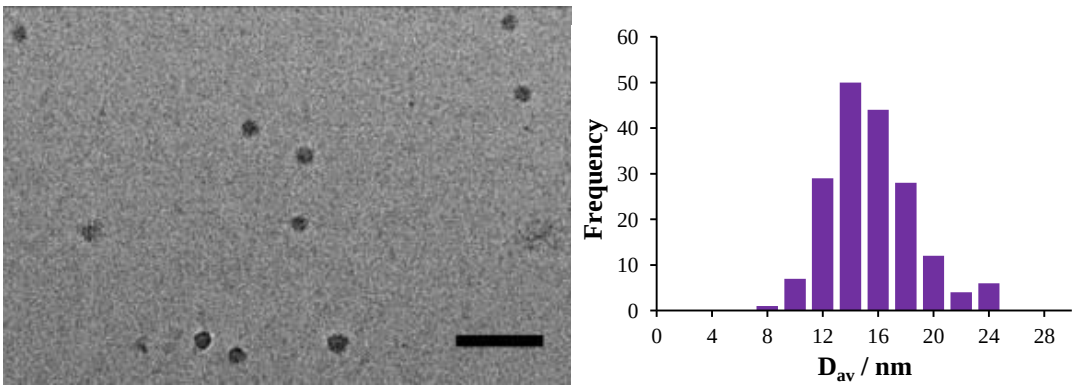

Figure 3.12. Representative TEM image of 3.8 in water imaged on GO treated grids, D_{av} = 19 ± 4 nm, scale bar is 100 nm

*3.3.2. Catalytic efficiency of polymer micelles **3.3** and **3.8***

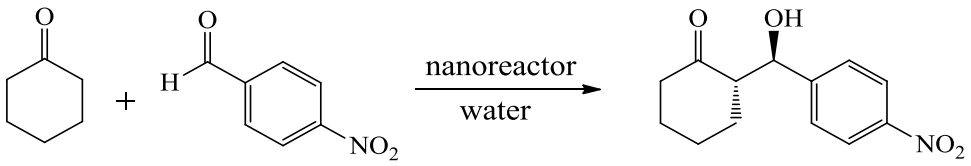

Scheme 3.7. Model aldol reaction between 4-nitrobenzaldehyde and cyclohexanone

The aldol reaction between 4-nitrobenzaldehyde and cyclohexanone was used as a model reaction as it has previously been used to assess the catalytic activity of our catalytic RAFT copolymers in Chapter 2. In contrast to the reactions carried out in Chapter 2, where copolymer **2.5** catalyzed the reaction in a mixed solvent system (DMF:water), the reactions catalyzed by the micelles are carried out in 100% water. We propose that the concentrator effect[8, 12] will have a positive effect on the catalytic activity of the core-functionalized catalysts.

3.3.2.1. Concentrator effect

Initial catalytic experiments were carried out using micelles **3.3** (pH *ca*. 6), for direct comparison with the results obtained for copolymers **2.5** in the mixed solvent system. Initial experiments were carried out to attain an efficient protocol for micelle catalyzed reactions in water. Features such as micelle and substrate concentration and use of a co-solvent were first investigated. However, the change in particle size with addition of co-solvents was not investigated.

Initial catalysis experiments using **3.3** were carried out at 1 $mg.mL^{-1}$, the concentration at which the micelles were assembled. As a result of the low concentration (*ca*. 1 $mg.mL^{-1}$), a large volume of micelles was required to achieve the desired catalyst loading (mol%). Thus, for a 1 mol% loading reaction, 11 mL micelles (catalyst

concentration 0.08 mg.mL^{-1}) was required. The reaction substrates were first added to the stirring micelle solution without a co-solvent; however, some precipitation was observed and no product was detected after 24 hours. It has previously been shown that a co-solvent can enhance substrate uptake by the hydrophobic micelle core.[36] Thus, a range of co-solvents were used in an attempt to promote micelle activity. Solvents including chloroform, DMF, DMSO, THF and ethyl acetate (EtOAc) were used due to their reported compatibility with L-proline catalyzed aldol reactions.[24, 37] The selected solvents are of further interest due to their miscibility/immiscibility with water and compatibility/incompatibility with the styrenic core. Unfortunately, micelle catalysis was not promoted by the addition of the selected co-solvents (Table 3.1).

Table 3.1. Aldol reaction catalyzed by 3.3 with and without a co-solvent, at RT

Volume micelle / mL	Co-solvent	Volume co-solvent / mL	Catalyst loading[a] / mol%	Conv.[b] / %	Precipitation?
11	-	-	1	-	Yes
2	-	-	0.18	-	Yes
11	$CHCl_3$	0.5	1	-	No
11	DMF	0.5	1	-	No
11	DMSO	0.5	1	-	Yes
11	THF	0.5	1	-	No
11	EtOAc	0.5	1	-	No

[a] Catalysis carried out at the same substrate concentration
[b] Determined by ^{1}H NMR spectroscopy (400 MHz, $CDCl_3$) after 24 hours, reactions carried out in triplicate

To further enhance the concentrator effect, the micelle solution was concentrated to a concentration of 6.25 mg.mL^{-1} *via* ultrafiltration. Thus, only 2 mL micelle solution was required for a 1 mol% reaction, with respect to the same amount of substrates, dramatically increasing both micelle and substrate concentrations. Incredibly, a small

amount of product was observed after 24 hours in the absence of a co-solvent (Table 3.2, entry 2), suggesting micelle/substrate concentration should be taken into account into the design of nanoreactor systems.

A mini-work-up using EtOAc was carried out to extract the product and unreacted substrates from the micelle core. The reaction was carried out at a range of catalyst loadings which was achieved by altering the amount of substrates in each reaction, keeping the micelle concentration constant. Thus, 10 times less substrates are present in a 10 mol% reaction compared to 1 mol% (Figure 3.13).

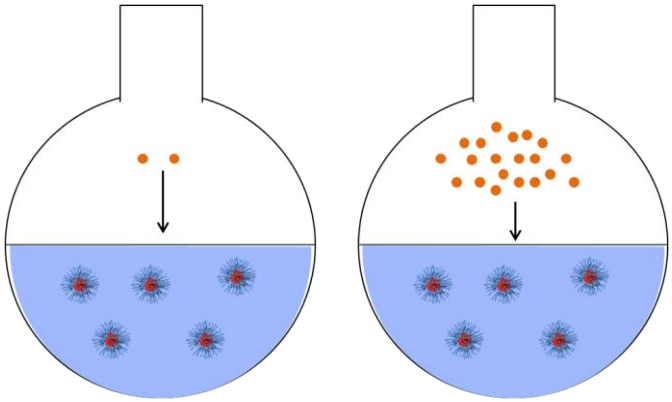

Figure 3.13. Representation of a reaction carried out at 10 mol% (left) and 1 mol% loading (right) by changing substrate (●) concentration (number of micelles and substrates are comparative and not actual)

Disappointingly low conversions (< 15%) were observed when catalyzed by **3.3** at relatively low loadings (Table 3.2). Despite achieving higher conversions at 5 and 10 mol% loading, these were still lower than desired (compared to copolymer **2.5**) considering the long reaction time (24 hours).

Table 3.2. The catalytic activity and selectivity of micelles 3.3 (concentration = 6.25 mg.mL^{-1}) in water at different catalyst loading

Entry	Catalyst loading / mol%	Conv.[a] / %	*anti/syn* ratio[a]	ee[b] / %	TON[c]
1	0.5	6	-	-	12
2	1	13	-	96	13
3	2	2	-	-	1
4	5	30	98/2	95	6
5	10	67	98/2	96	6.7

[a] Determined by ^{1}H NMR spectroscopy, (400 MHz, $CDCl_3$) after 24 hours, reactions carried out in triplicate
[b] Determined by chiral HPLC, ChiralPak IA, 80:10:10 hexane:propan-2-ol:ethanol, 1 mL.min^{-1}
[c] Catalyst turnover number used to determine catalyst efficiency, calculated as the moles of substrates converted by one mole of catalyst in a given time (in this case was 24 hours), used here as a ratio to easily determine the difference in catalytic activity when reactions at different catalyst loadings are directly compared

The reaction progress of micelle catalyzed reactions at 1, 5 and 10 mol% loading was followed by ^{1}H NMR spectroscopy, by comparing signals of the starting aldehyde to the product. A 5 hour induction period was observed at all three catalyst loadings, possibly due to slow diffusion of substrates into the micelle core. The reaction was found to be most efficient at 10 mol% catalyst loading i.e. where the least amount of substrates was used (Figure 3.14). We hypothesized that this was the result of less substrates having to diffuse into the core and thus more being successfully converted to product.

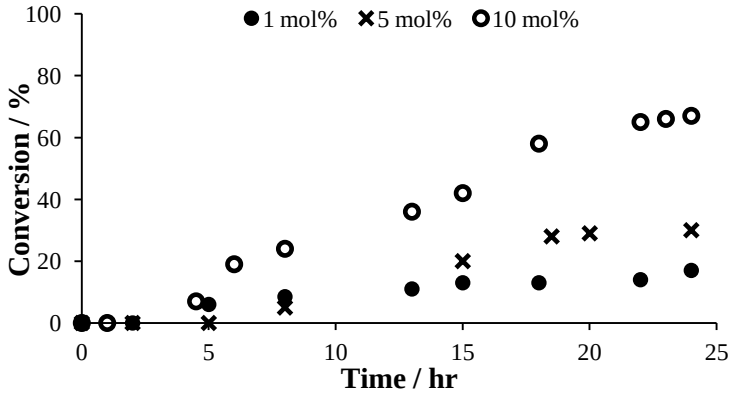

Figure 3.14. Conversion plot of micelle 3.3 catalyzed aldol reactions in water

To enhance substrate uptake and increase rate of diffusion, the aldol substrates were added together with a co-solvent, chloroform, DMSO or DMF. Again the choice of co-solvent was based on their compatibility or incompatibility with the micelle core and surrounding water. Both DMF and $CHCl_3$ are good solvents for the PS core block where DMF is miscible but chloroform immiscible with the surrounding water phase. DMSO on the other hand, is a poor solvent for the PS core but is miscible with water. The co-solvents seem to have a negligible effect on the catalytic activity of the core-functionalized catalyst (Table 3.3). Interestingly, the reaction did not proceed at all with chloroform which we propose is an effect of its water immiscibility as some phase separation was observed. Thus, the substrates were most likely contained in the chloroform phase and hence not in close proximity to the catalytic sites in the micelle core. The low activity observed with DMF may be attributed to the high solubility of the substrates in DMF which may be stabilizing the substrates in the water phase rather than guiding them into the hydrophobic core.

Table 3.3. The catalytic activity and selectivity of 3.3 at 1 mol% loading in the presence of a co-solvent

Co-solvent	% Co-solvent / vol%	Conv.[a] / %	*anti/syn* ratio[a]	ee[b] / %
DMSO	5	9	-	-
$CHCl_3$	5	0	-	-
DMF	5	5	-	-

[a] Determined by ^{1}H NMR spectroscopy (400 MHz, $CDCl_3$) after 24 hours, reactions carried out in triplicate
[b] Determined by chiral HPLC, ChiralPak IA, 80:10:10 hexane:propan-2-ol:ethanol, 1 mL.min^{-1}

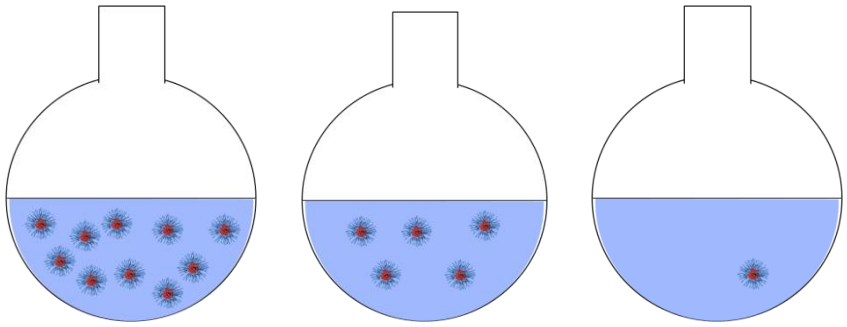

Figure 3.15. Representation of the different concentration of micelles used to catalyze the aldol reaction, from left to right 10, 5 and 1 mol% loading at constant substrate concentration (number of micelles are relative and not actual)

Previously, reaction loadings were altered by changing the substrate concentration, maintaining a constant micelle concentration. We wanted to further explore the micelle system by carrying out reactions at a constant substrate concentration and changing the micelle concentration. This was carried out by diluting the required amount of micelles, for each loading 10, 5, and 1 mol%, with water to the same total volume (Figure 3.15). These reactions were found to proceed at a considerably slower rate, only resulting in trace amounts of products after 24 hours. If the reactions were allowed to proceed for an additional 3 days, 23 and 28% conversions were achieved for 5 and 1 mol% loading respectively. Thus, micelle concentration has a more significant effect on catalysis than substrate concentration (in terms of achieving the aldol product after 24 hours) as less substrates may be successfully sequestered into the micelles at the lower loadings. This supports the observations previously made when catalysis was carried out at much lower polymer concentration (i.e. high dilution), which was discussed above.

In order to ensure all the product was extracted from the core, a second work-up procedure was designed. Previously, the product and any unreacted reagents were extracted from the micelle core using EtOAc and the conversion determined by ^{1}H NMR spectroscopy by comparing the signals from the starting aldehyde to the product.

In the second work-up procedure, DMF was added to the reaction mixture resulting in disassembly of the polymer micelles, ensuring complete release of substrates from the micelle core. The organic product/unreacted reagents were then extracted into EtOAc and the conversion determined by ^{1}H NMR spectroscopy following the procedure detailed above. The block copolymer appeared to remain in the DMF:water phase, as no polymer signals were observed in the ^{1}H NMR spectrum of the organic phase. The success of this work-up protocol was confirmed by the high conversions achieved. The work up procedure was carried out as quickly as possible to reduce the chance of catalysis taking place in the DMF:water phase. However, any reaction taking place in this phase cannot be completely ruled out as further reactions at this DMF:water ratio was not investigated. The catalytic efficiency and selectivity of **3.3** are further detailed in the next section.

3.3.2.2. Effect of micelle core hydrophobicity on catalytic activity of supported catalyst

The extent of the hydrophobic concentrator effect was investigated by comparing the activity and selectivity of **3.3** to the second P(MMA-*stat*-ProMA)-*b*-PMAA micelles **3.8**. **3.8** was similarly self-assembled at low concentration and subsequently concentrated *via* ultrafiltration to a concentration of 6.79 mg.mL^{-1} (compare concentration of **3.3** 6.25 mg.mL^{-1}). Both micelles appeared stable at this concentration as no precipitation was observed. Reactions were carried out at 1, 5 and 10 mol% loading which was altered by changing the concentration of substrates maintaining a constant micelle concentration (Figure 3.13). In other words, for reactions at 1 and 10 mol% loading, the latter reaction consisted of 10 times less substrates. The new work-up protocol was able to accurately determine the catalytic efficiency of **3.3** and **3.8** (Table 3.4).

Table 3.4. The catalytic efficiency of 3.3 and 3.8 at different catalyst loadings

Catalyst	Catalyst loading[a] / mol%	Conv.[b] / %	*anti/syn* ratio[b]	ee[c] / %	TON[d]
	10	90	97/3	98	9
3.3	5	80	95/5	94	16
	1	96	99/1	93	96
	10	65	99/1	92	6.5
3.8	5	90	95/5	82	18
	1	96	89/11	85	96

[a] Catalyst loading altered by changing substrate concentration maintaining a constant micelle concentration
[b] Determined by ^{1}H NMR spectroscopy (400 MHz, $CDCl_3$) after 24 hours, reactions carried out in triplicate
[c] Determined by chiral HPLC, ChiralPak IA, 80:10:10 hexane:propan-2-ol:ethanol, 1 mL.min^{-1}
[d] TON refers to the moles of substrates converted by a mole of catalyst at a given time (in this case 24 hours)

High conversions were observed for both micelle systems at all three catalyst loadings, with high diastereo- and enantioselectivities, indicative of two highly efficient nanoreactor systems. To easily compare the catalyst efficiency between reactions at different loadings, turnover numbers (TON) was used (TON refers to the moles of substrates converted by a mole of catalyst at a given time, which in all these reactions were 24 hours). Interestingly, both micelle systems (**3.3** and **3.8**) showed high efficiency at as low as 1 mol% loading, i.e. when the greatest amount of substrates were used, reaching 96% conversion after 24 hours. In other words, in the presence of a higher concentration of substrates, at the same micelles concentration, the functionalized catalyst was working more efficiently which was attributed to the higher local substrate concentration (within the micelle core). No precipitation of substrate or product was observed upon increasing the amount of substrate in the reaction, suggesting good solubility within the micelle. However, the difference in solubility of the substrates and products within the two micelle systems was not examined

The selectivity on the other hand was found to be significantly different with high enantioselectivity at 10 mol% which we propose is due to a lower substrate concentration, resulting in less saturated micelle cores. **3.3** showed both high *anti/syn* ratio and ee at all loadings. **3.8** on the other hand showed comparatively lower selectivity with an *anti/syn* ratio of 89/11 and only 85% ee. We believe this may be influenced by the difference in hydrophobicity of the two micelle cores.

We further examined the two micelle systems by following the rate of conversion with time. Interestingly, when catalyzed at 1 mol% by **3.3** approximately 90% conversion was observed in just 6 hours. A comparable conversion was observed after 10 hours at 10 mol%. Strangely, the reaction proceeded the slowest at 5 mol%, also reaching the lowest conversion after 24 hours (Figure 3.16). Nevertheless, these results confirm that a highly efficient catalytic system has been successfully designed and synthesized.

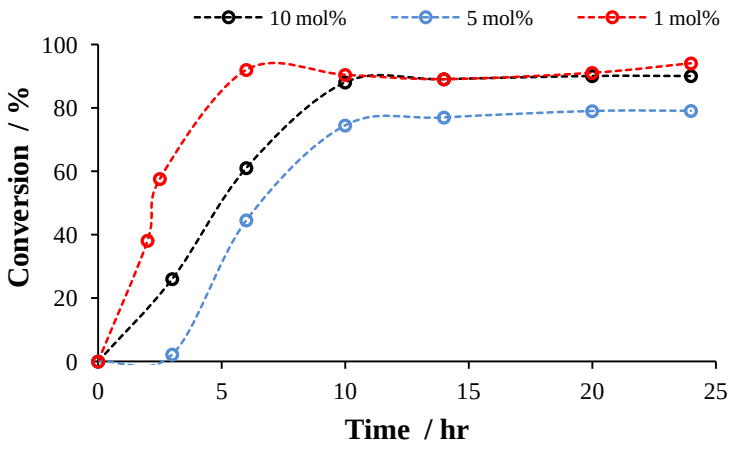

Figure 3.16. Aldol reaction catalyzed by micelles 3.3 at three different catalyst loadings

Micelles **3.8** showed a similar catalytic trend where the reaction at 1 mol% loading was the most efficient reaching approximately 90% conversion after 6 hours, where the greatest amount of substrates were catalyzed. However, unlike **3.3**, the reaction was more efficient at 5 mol% than 10 mol%. Both reactions seem to proceed for about 10-12

hours after which they both reach a plateau (Figure 3.17). The low conversion at 10 mol% loading is most likely a combined effect of the low substrate concentration and less efficient concentrator effect as a result of the lower micelle core hydrophobicity (**3.8**: 65% conversion *vs* **3.3**: 90% conversion, at 10 mol% catalyst loading after 24 hours). Hence, both micelle systems achieve comparable final conversions after 24 hours of reaction at 1 and 5 mol% catalyst loading, with some differences in enantioselectivity. Micelles **3.3** showed greater enantioselectivity overall, which we propose is related to the hydrophobicity of the micelle core.

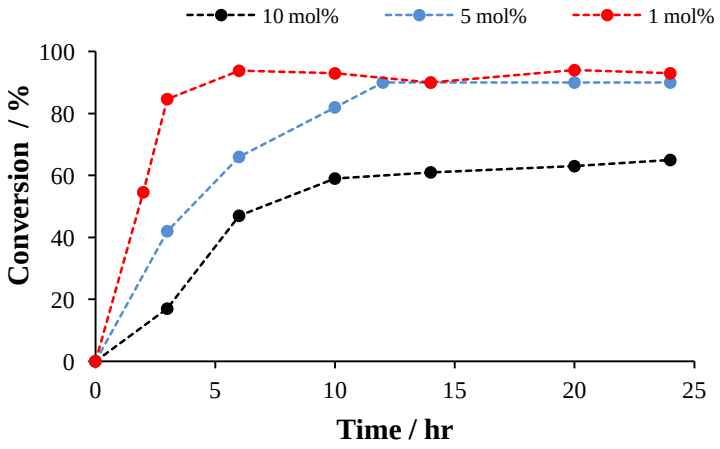

Figure 3.17. Aldol reaction catalyzed micelles 3.8 at three different catalyst loadings

The efficiency of our micelle systems at 1 mol% loading was further highlighted when the activity was compared to unsupported L-proline in water at the same loading. L-Proline has not shown great activity in water due to the low solubility of the organic substrates in water.[24, 38] Thus, it was not surprising that the reaction did not proceed at all in water at 1 mol% (Figure 3.18). Further increasing the catalyst loading to 10 mol% did not result in any product. Moreover, in both cases precipitation of the starting reagents were observed. This highlights how important the hydrophobic cavity is in reactions with water incompatible substrates.

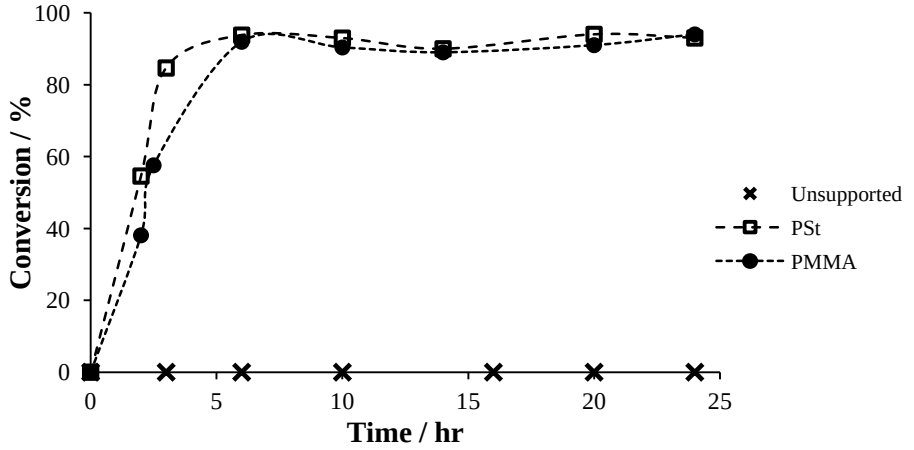

Figure 3.18. Aldol reaction catalyzed by 3.3, 3.8 and unsupported L-proline in water, at 1 mol% loading

3.3.3. Effect of catalyst location within micelle

3.3.3.1. Synthesis and characterization of PMMA-*b*-P(MMA-*co*-ProMA)-*b*-PMAA, 3.10

The copolymerization of **2.3** and styrene under RAFT conditions was investigated in Chapter 2. The determined reactivity ratios suggested a gradient type copolymer was synthesized as polymerization of **2.3** was preferred over styrene. The reactivity ratios of monomer **3.4** and MMA were not fully explored; however, as both monomers were consumed at comparable rates in a copolymerization at 50:50 molar ratio of MMA:**3.4**, we previously hypothesized that the catalytic moieties would be more evenly distributed along the polymer backbone, compared to the PS copolymerization. However, it can be imagined that due to the low incorporation of monomer **3.4** in polymer **3.7**, the difference in architecture between the two polymers is small, which is also reflected in their comparable catalytic activity. Nevertheless, to ensure any differences between micelles **3.3** and **3.8** was not associated with the proposed polymer microstructure, a triblock-like PMMA polymer (**3.9**) was synthesized. This was accomplished by first

synthesizing a short block containing MMA and **3.4**, ensuring the placement of **3.4** at the end of the polymer chain. This was followed by the polymerization of a second MMA block and finally the deprotectable ^{t}BuMA block (Figure 3.19). M_n (^{1}H NMR) = 19.8 kDa, DP_{MMA} = 47, $DP_{\mathbf{3.4}}$ = 3, DP_{tBuMA} = 100: P(MMA_{10}-*stat*-$ProMA_3$)-*b*-$PMMA_{37}$-*b*-P^{t}$BuMA_{100}$; M_n (SEC, THF, PMMA calibration) = 17.5 kDa, M_w (SEC) = 23.2 kDa, Đ = 1.33.

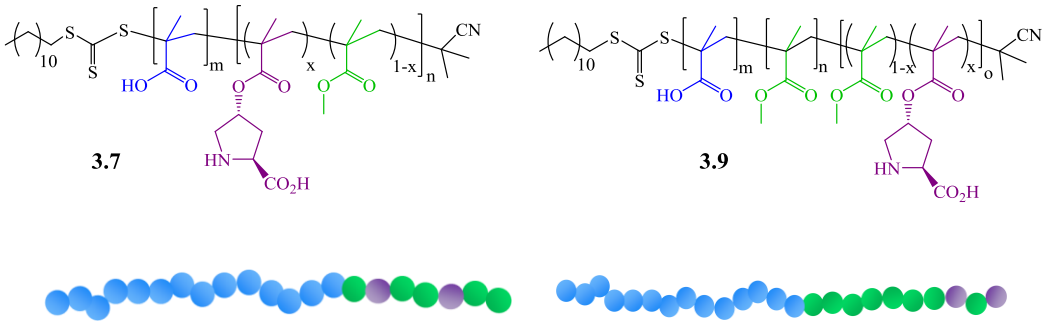

Figure 3.19. The proposed placement of the catalytic moieties in 3.7 and 3.9

After deprotection of P^{t}BuMA, **3.9** was self-assembled *via* solvent switch from DMF to water, yielding micelles **3.10** at 1 mg.mL^{-1}. **3.10** was subsequently concentrated *via* ultrafiltration to yield a final concentration of 7.56 mg.mL^{-1}. D_h by DLS was determined at 0.5 mg.mL^{-1} and 25 °C to be 23 nm (PDI = 0.111) (Figure 3.20). The micelles were then imaged by dry-state TEM, on unstained GO grids where spherical structures were observed. A D_{av} of 17 ± 2 nm was determined by TEM and were found to be comparable to those determined by DLS (Figure 3.21).

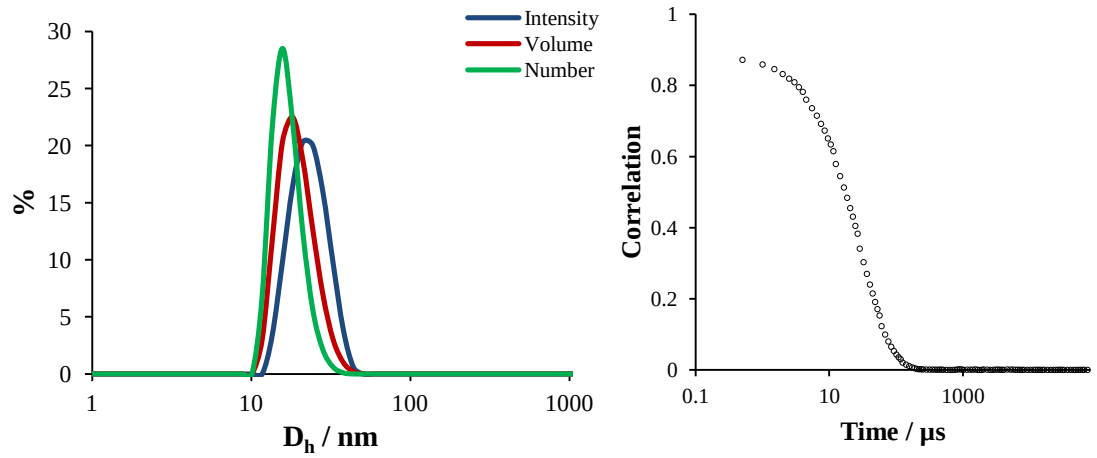

Figure 3.20. Self-assembled triblock micelles 3.10 in water after dialysis and its corresponding correlation function, D_h = 23 nm (PDI = 0.111)

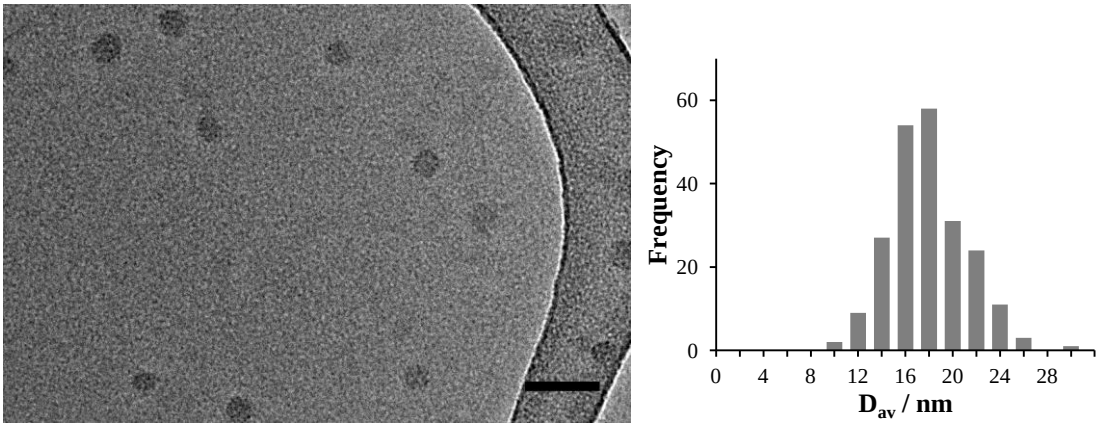

Figure 3.21. Representative TEM image of micelles 3.10 in water, imaged at 0.5 mg.mL^{-1} on GO, D_{av} = 17 ± 3 nm, scale bar is 50 nm

3.3.3.2. Catalytic efficiency of 3.10

The catalytic efficiency of **3.10** (triblock-like) was then compared to **3.8** (evenly distributed catalytic moieties). The reaction progress was monitored by ^{1}H NMR spectroscopy and appears to be highly comparable to **3.8** (Figure 3.22). However, a somewhat longer induction period was observed for **3.10**, of about 1 hour after which the reaction surges to approximately 70%. A less dramatic increase in activity was observed for micelles **3.8**. It is possible the induction period observed for **3.10** was a result of the catalytic moieties being buried deeper within the micelle core resulting in a

somewhat longer diffusion time. Nevertheless, both systems reach 80-90% conversion in 3 hours reinforcing the fact that the micelles are highly efficient regardless of the placement of catalyst functionalities along the polymer backbone. Interestingly, **3.10** showed slightly higher enantioselectivity reaching 92% ee (compare **3.8** 85% ee, Table 3.4) which we propose is an effect of the more hydrophobic local environment in **3.10**.

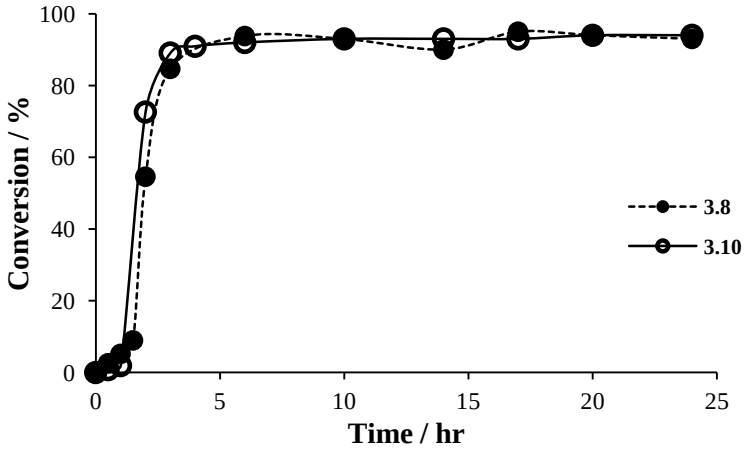

Figure 3.22. Reaction progress of aldol reaction catalyzed by 3.8 (random catalyst distribution) and 3.10 (triblock-like)

3.3.4. Control experiments

A number of background reactions were carried out to verify the reactions did indeed take place because the substrates were driven into a confined space and into close proximity to the catalyst. Thus, two non-functional block copolymer, PS-*b*-PAA (**3.11**) and PMMA-*b*-PMAA (**3.12**) were synthesized *via* RAFT (Figure 3.23). Both polymers were self-assembled *via* solvent switch from DMF to water, at 1 $mg.mL^{-1}$ to yield micelles **3.13** and **3.14**. The micelles were characterized by DLS and D_hs were determined as 38 and 47 nm for micelles **3.13** and **3.14** respectively (Figure 3.24). The micelles were then concentrated *via* ultrafiltration to achieve polymer concentrations similar to those of the functional micelles.

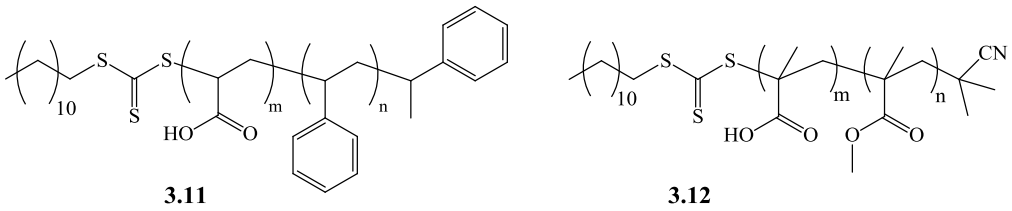

3.11 3.12

Figure 3.23. Non-functional diblock copolymers 3.11 (left) and 3.12 (right)

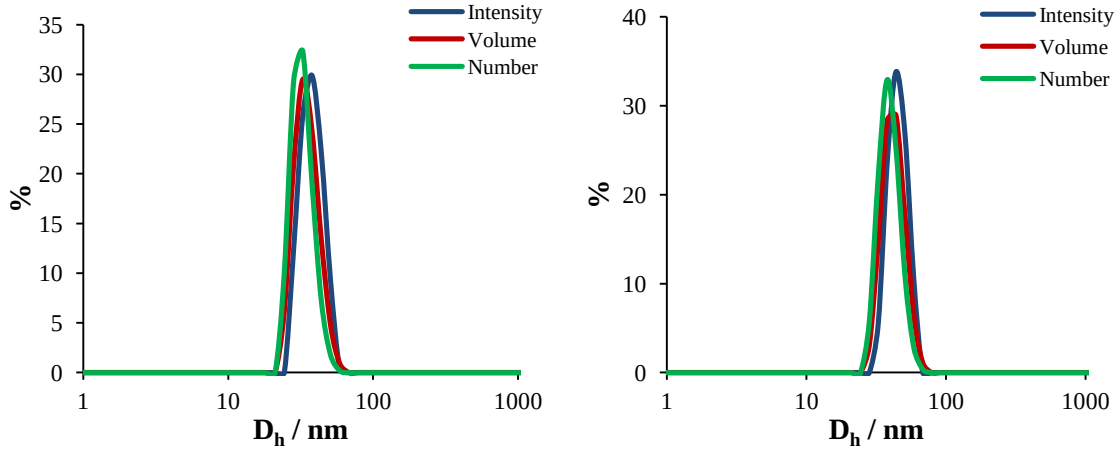

Figure 3.24. DLS traces of non-functional micelles PS-*b*-PAA, D_h(3.13) = 38 nm, PDI = 0.38 (left) and PMMA-*b*-PMAA, D_h(3.14) = 47 nm, PDI = 0.40 (right)

The reaction was carried out under both 1 and 10 mol% loading conditions and no reaction was observed in either of the non-functional micelle systems (Table 3.5). This verifies the two substrates do not react by simply concentrating them together in a confined hydrophobic environment within a micelle core.

Table 3.5. Background reactions carried out in the presence of 3.13 and 3.14

Micelle	Catalyst loading / mol%	Conv.[a] / %	*anti/syn* ratio[a]	ee[b] / %
3.13	1[i]	0	-	-
	10[ii]	0	-	-
	1 + L-proline[iii]	0	-	-
3.14	1[i]	0	-	-
	10[ii]	0	-	-
	1 + L-proline[iii]	0	-	-

[a] Determined by ^{1}H NMR spectroscopy (400 MHz, $CDCl_3$) after 24 hours
[b] Determined by chiral HPLC, ChiralPak IA, 80:10:10 hexane:propan-2-ol:ethanol, 1 mL.min^{-1}
[i/ii] The equivalent of a reaction at 1 mol% and 10 mol% by altering the amount of substrates in each reaction
[iii] Amount of micelles equivalent to a micelle reaction carried out at 1 mol%, with additional unsupported L-proline at 10 mol% loading

Next, unsupported L-proline (10 mol%) was added to the micelle solution together with the reagents but again no reaction was observed. The catalytic inefficiency was attributed to the segregation of substrates and catalyst as a result of the catalyst's high water solubility. This further highlights the design of the micelle systems as catalysts and substrates with different solubilities are uniquely brought together in a confined environment.

Additional reactions were carried out to investigate the activity of unsupported L-proline in a range of solvents, mimicking the environment within the micelle core. As previously discussed, the reaction does not proceed in 100% water (Table 3.6, entry 1). Thus, the addition of a co-solvent to aid substrate solubilization was investigated with 5 vol% DMF and DMSO in water. However, despite the presence of a small volume of co-solvent, precipitation was still observed and again no reaction was detected.

Table 3.6. The catalytic activity of unsupported L-proline at 10 and 1 mol% in a range of solvents

Entry	Catalyst loading / mol%	Solvent	Conv.[a] / %	*anti/syn* ratio[a]	ee[b] / %
1	10	water	0	-	-
2	10	5% DMF in water	0	-	-
3	10	5% DMSO in water	0	-	-
4	10	toluene	0	-	-
5	10	benzene	5	-	-
6	10	solvent free (1 eq water)*	10	-	-
7	1	MMA	0	-	-
8	1	MA	0	-	-

*6 eq of cyclohexanone was used instead of 4 for complete solubilization
[a] Determined by ^{1}H NMR spectroscopy (400 MHz, $CDCl_3$) after 24 hours
[b] Determined by chiral HPLC, ChiralPak IA, 80:10:10 hexane:propan-2-ol:ethanol, 1 mL.min^{-1}

Toluene and benzene were used to mimic the PS core environment, but with no or ≤ 5% conversion observed. MMA and methyl acrylate (MA) were used to mimic the PMMA core environment, but equally, no reaction was observed. The most efficient reaction was observed under solvent free conditions in the presence of 10 vol% water, reaching 10% conversion after 24 hours. The inefficiency of unsupported L-proline in a range of solvents including those which mimic the environment within the micelle core highlights the importance of the unique environment presented by the micelles.

3.3.5. Shell-functionalized micelles

The high catalytic activity exhibited by the synthesized micelles is directly attributed to the hydrophobic concentrator effect as the reagents are concentrated in a confined environment in close proximity to the catalyst functionalities. Polymer micelles with the catalyst functionalized in the shell have also been reported, one example being the thermo-responsive poly(*N*-isopropylacrylamide)-*block*-poly(vinylimidazole) (PNIPAM-*block*-Vim) micelle system reported by Ge *et al.* (Figure 3.25).[39]

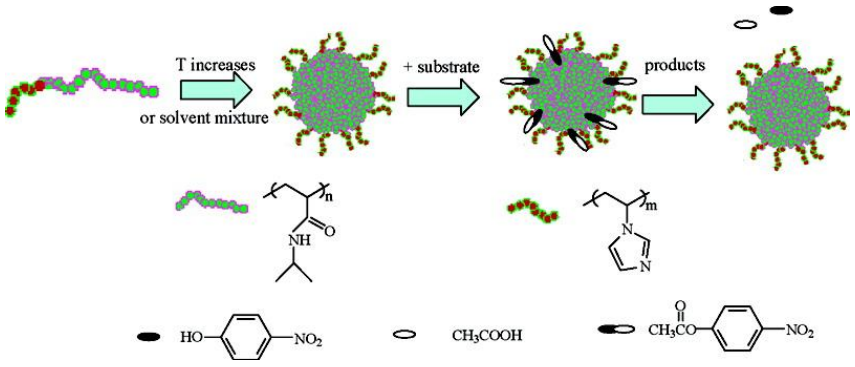

Figure 3.25. The thermo-responsive micelle systems reported by Liu and co-workers where the catalyst moieties were functionalized in the micelle shell[39]

Micellar aggregates were formed at temperatures above the lower critical solution temperature (LCST) of the PNIPAM block with the catalyst decorating the surface of

the micelle. The catalyst, imidazole was used to catalyze the hydrolysis of *p*-nitrophenyl acetate. As the substrates are hydrophobic, the micelle core is able to sequester the substrates from the surrounding aqueous environment allowing the reaction to take place as the substrates diffuse into the core.

Our aim was to design a similar system and investigate what effect the local catalyst environment may have on the catalyst activity and selectivity, i.e. catalyst contained within the hydrophobic core or facing the surrounding aqueous environment. This is of interest as the catalyst has been reported to exhibit different activity and selectivity in the presence of different amounts of water.[20, 21, 40, 41] Thus, micelles with a non-functional core and catalyst functionalized shell was designed, synthesized and its activity in water examined. The aim was to highlight the importance of the careful design of the polymer support and micelle for efficient micelle supported catalysis.

3.3.5.1. Synthesis and characterization of PS-*b*-P(AA-*co*-ProA) micelles, 3.19

A more hydrophilic L-proline functional monomer, **3.15** was synthesized following a previously described procedure (Scheme 3.8).[34] Monomer **3.15** was characterized by ^{1}H NMR spectroscopy (Figure 3.26), and identity of the proline signals was further confirmed by 2D COSY NMR spectroscopy. Monomer **3.15** was found to have similar solubilites to its corresponding methacryloyl monomer **3.4**, being highly soluble in methanol and water.

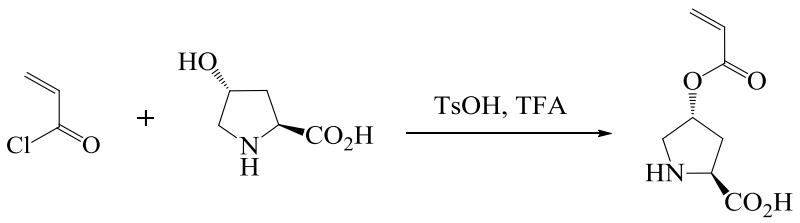

Scheme 3.8. Coupling reaction to yield the desired functional acrylate monomer 3.15

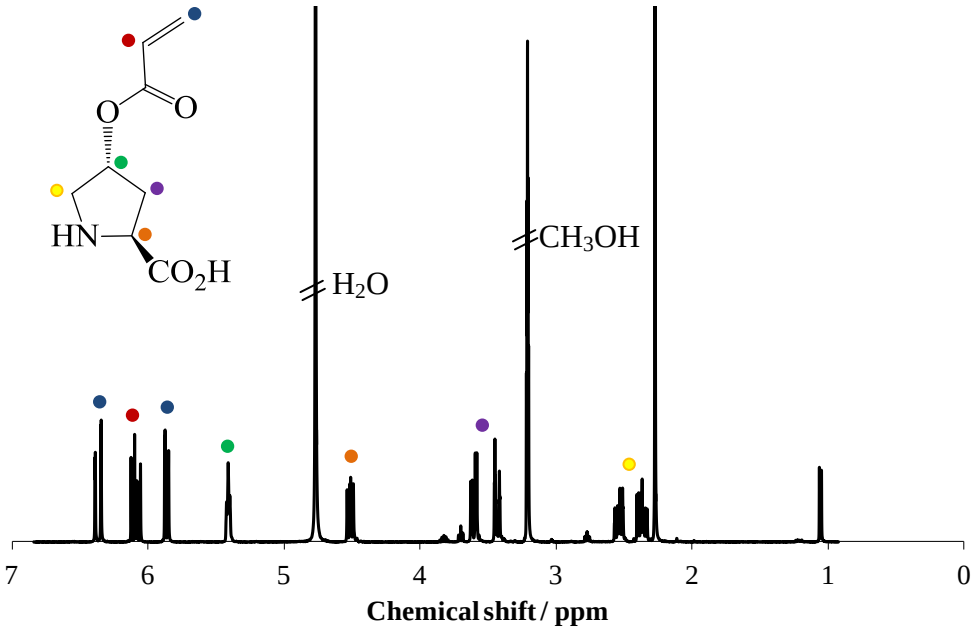

Figure 3.26. ^{1}H NMR spectrum of 3.15 (400 MHz, CD_3OD), with residual solvent signals of methanol, water, acetone and propan-2-ol

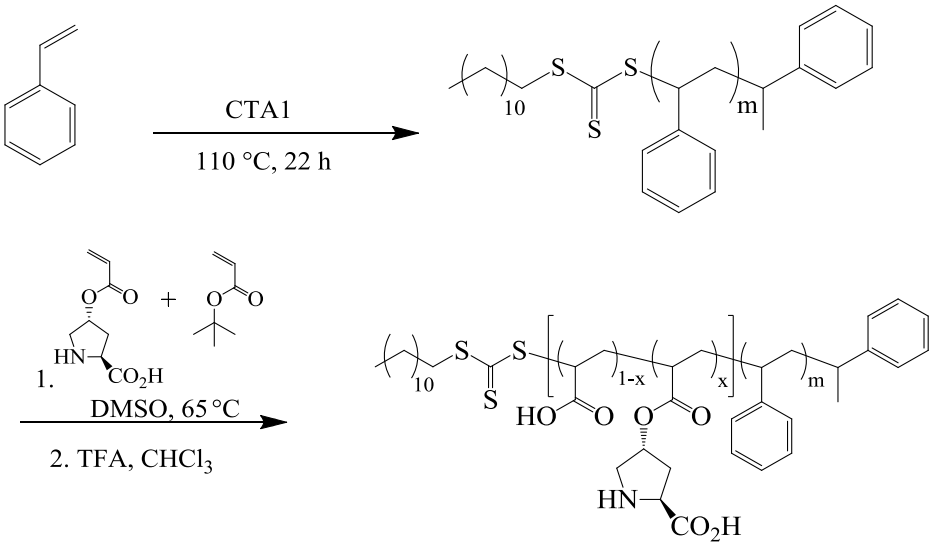

Scheme 3.9. Three step synthesis to yield diblock copolymer, 3.18

The functional diblock copolymer **3.18** was synthesized in a three step reaction starting with homopolymerization of styrene followed by chain extension with ^{t}BuA and **3.15** and finally deprotection of ^{t}BuA protecting groups to reveal the PAA block (Scheme 3.9). M_n (^{1}H NMR) 11.8 kDa, DP_{PS} = 24; $DP_{\mathbf{3.15}}$ = 2; DP_{tBuA} = 70; M_n (SEC, THF, PS

calibration) = 12.4 kDa; M_w (SEC) = 14.5 kDa; Đ = 1.17.The micelles (**3.19**) were self-assembled at 1 mg.mL^{-1} *via* a solvent switch method from DMF to water. **3.19** was then concentrated *via* ultrafiltration, resulting in a concentration of 4.77 mg.mL^{-1}.

The micelles were characterized by DLS and dry-state TEM at 0.5 mg.mL^{-1}. The D_h (30 nm, PDI = 0.108) was found to be comparable to the corresponding core-functionalized micelles (**3.3**) (Figure 3.27). The D_{av} (18 ± 3 nm) determined by TEM was found to be somewhat smaller than the D_h at the same concentration which was attributed to the hydrated *vs* non-hydrated nature of the two techniques (Figure 3.28).

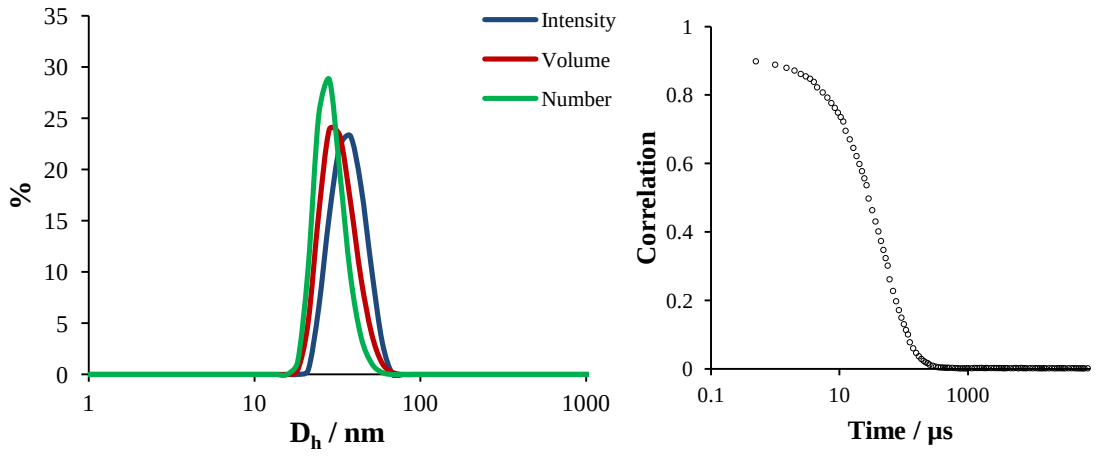

Figure 3.27. DLS trace of 3.19 in water, at 0.5 mg.mL^{-1}, D_h = 30 nm (PDI = 0.108)

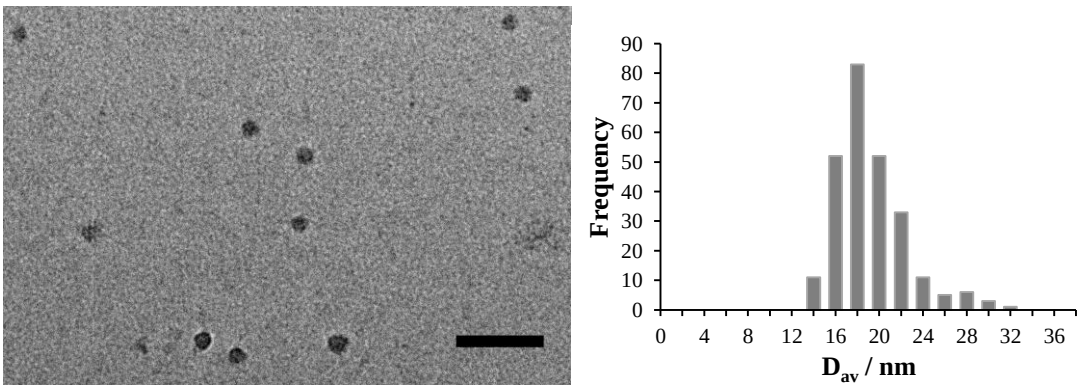

Figure 3.28. Representative TEM image of 3.19, D_{av} = 18 ± 3 nm, scale bar is 100 nm

3.3.5.2. Catalytic efficiency of 3.19

The catalytic activity and selectivity of **3.19** was compared to **3.3** due to the matching PS core as both will be equally influenced by the concentrator effect (Figure 3.29). The micelle concentration of **3.19** was tailored to allow for the reactions to be carried out under conditions similar to **3.3**. The reaction progress, catalyzed by **3.19** at 1 mol% was followed by ^{1}H NMR spectroscopy and compared to results previously achieved for **3.3** (Figure 3.30).

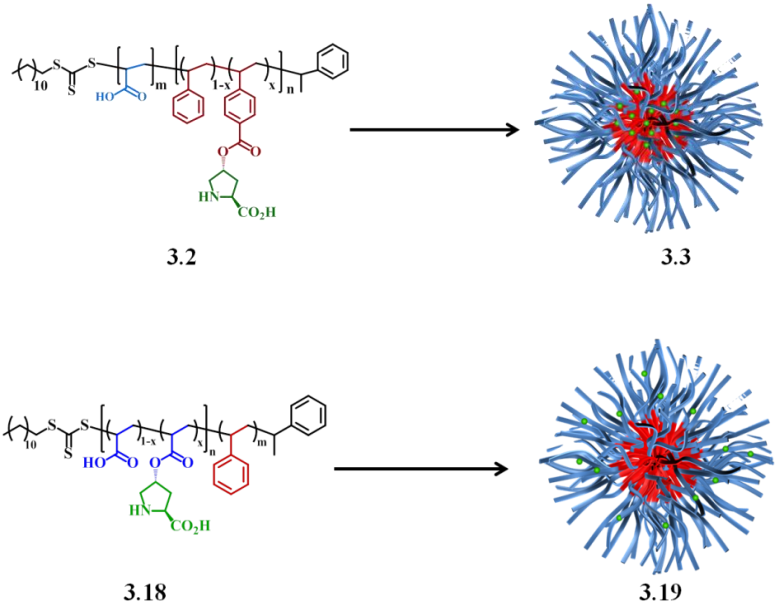

Figure 3.29. Comparison of core-functionalized micelle 3.3 and shell-functionalized micelle 3.19

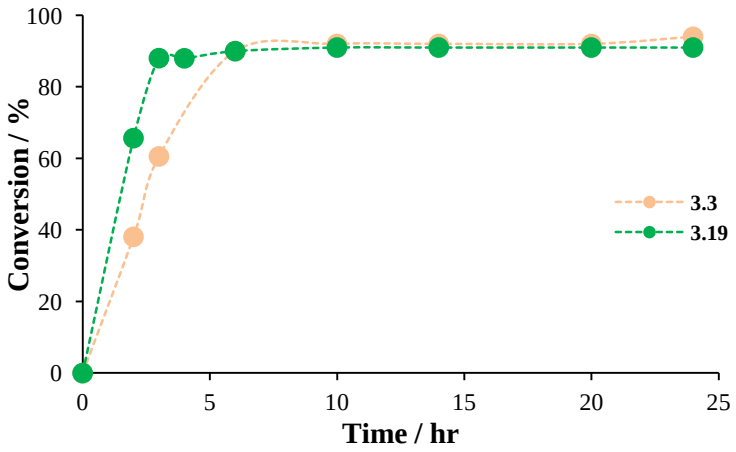

Figure 3.30. The reaction progress of 3.3 and 3.19, carried out at 1 mol% loading

Comparable conversions were found for both systems after 24 hours, confirming the efficiency of the concentrator effect in our micelle systems. The results suggest diffusion of substrates into the micelle core is a slower process than the catalysis reaction, as substrates are successfully catalyzed during diffusion. Interestingly, approximately 80% conversion was reached in only 3 hours for **3.19** whereas comparable conversions were achieved after 6 hours for **3.3** (reactions carried out in triplicate). For **3.3**, substrate diffusion must occur prior to catalysis whereas for **3.19**, the reaction takes place during diffusion which explains the difference in reaction progress observed in the first 5-6 hours (Figure 3.30). The enantioselectivity of **3.19** was found to be low (54% ee), considerably lower than **3.3** (93% ee). We propose that more water will be involved in the reaction catalyzed by **3.19** as the catalytic moieties are facing the surrounding aqueous environment resulting in the surprisingly low enantioselectivity. This truly highlights the importance of the local catalyst environment, its hydrophobic nature and its effect on the catalyst activity and selectivity. Further studies are ongoing to fully investigate the influence of catalyst placement on its catalytic activity.

3.4. Conclusion

Two well-defined L-proline functionalized diblock copolymers, P(St-*stat*-ProSt)-*b*-PAA and P(MMA-*stat*-ProMA)-*b*-PMAA, were successfully synthesized by RAFT polymerization. Both were self-assembled into spherical nanostructures, confirmed by TEM. The potential of these micelles as nanoreactors were assessed in a model asymmetric aldol reaction. Both micelle systems showed excellent catalytic properties, achieving high activity and selectivity in water and relatively short reaction times. The activity was also found to be superior to unsupported L-proline in water and organic solvents at comparable loadings which was attributed to the hydrophobic concentrator

effect. Interestingly, the placement of the catalytic motifs within the nanoreactor influences the enantioselectivity of the catalyst where higher selectivity was observed when the catalyst was buried deeper within the micelle core. The importance of the local hydrophobic catalytic environment was further highlighted when the catalyst was functionalized in the micelle core. Although high catalytic activity was observed, suggesting the reaction occurs during diffusion into the non-functional hydrophobic core, significantly lower enantioselectivity was observed. This was attributed to the high water content around the catalytic site.

3.5. Experimental

3.5.1. Materials

Styrene was distilled over CaH_2, MMA, ^{t}BuA and ^{t}BuMA were filtered through an aluminium oxide column and stored at 4 °C prior to use. CTA1 was prepared as previously detailed in Chapter 2.[42] 2-Cyano-2-propyldodecyl trithiocarbonate (CTA2) was purchased from Sigma-Aldrich and used without further purification. 4-Nitrobenzaldehyde was purchased from Sigma-Aldrich and filtered through a silica column in ethyl acetate previous to use. All other reagents were purchased from Sigma-Aldrich and used without further purification.

3.5.2. Instrumentation

Both ^{1}H and ^{13}C NMR spectra were recorded at 400 MHz on a Bruker DPX 400 FT-NMR spectrometer using deuterated solvents. Chemical shifts are reported as δ in parts per million relative to $CHCl_3$ (7.26 ppm for ^{1}H and 77.2 ppm for ^{13}C) or d_6-DMSO (2.50 ppm for ^{1}H and 39.5 ppm for ^{13}C) or CD_3OD (3.31 ppm for ^{1}H and 49 ppm for ^{13}C) as the internal standard. Size exclusion chromatography (SEC) data for all polymers was obtained in HPLC grade tetrahydrofuran (THF) containing 2% TEA with

a flow rate of 1.0 mL per minute, on a set of two PLgel 5µm Mixed-D columns, plus one guard column. SEC data was analyzed using Cirrus SEC software based on PS standards. Dialysis tubing was purchased from Spectrum labs with molecular weight cut off of 3.5 and 6-8.0 kDa. Mass spectra were recorded on a Bruker Esquire 2000 ESI spectrometer. High performance liquid chromatography (HPLC) analysis was performed on a Varian 920-LC using an analytical column (reverse phase) Discovery C18 (100 mm × 4.6 mm × 5 µm) purchased from Sigma-Aldrich, UK and a chiral column Chiralpak IA (150 mm × 4.6 mm × 5 µm) with guard cartridge (Chiralpak 5 µm) purchased from Chiral Technologies Europe. Hydrodynamic diameters (D_h) and size distributions of micelles were determined by dynamic light scattering (DLS) on a Malvern Zetasized Nano ZS instrument operating at 25 °C with a 4 mW He-Ne 633-nm laser module. Measurements were made at a detection angle of 173° (back scattering) and the data was analyzed using Malvern DTS 6.20 software. All determinations were made in triplicate (with 12 runs recorded for each measurement). TEM samples were prepared by drop deposition onto copper/carbon grids that had been treated with GO and examined with a transmission electron microscope (JEOL TEM-1200), operating at 80 or 200 kV. Micrographs were collected at magnifications varying from 30 K to 100 K and calibrated digitally.

*3.5.3. Chain extension of P(St_{52}-stat-ProSt_3) (**2.4**) to give diblock copolymer **3.1** and subsequent deprotection to yield amphiphile **3.2***

MacroCTA, copolymer **2.4** (1.0 eq), AIBN (0.2 eq) and deprotectable hydrophilic monomer ^{t}BuA (100-150 eq, depending on desired DP of hydrophilic block) were dissolved in 1,4-dioxane and put into a dry polymerization ampoule under nitrogen. The polymerization mixture was then degassed *via* three freeze-pump-thaw cycles, back-filled with nitrogen and put into a pre-heated oil bath at 75 °C. After 2 hours an aliquot

was taken to determine the polymerization conversion by ^{1}H NMR spectroscopy. The polymerization was quenched *via* the addition of THF and cooling in liquid nitrogen. The block copolymer was then precipitated into cold CH_3OH, filtered under vacuum and dried overnight in the vacuum oven at 40 °C. Block copolymer molecular weight was determined by ^{1}H NMR spectroscopy and SEC prior to deprotection of the *tert*-butyl protecting groups. M_n (^{1}H NMR) = 20.0 kDa, DP_{St} = 52, $DP_{\mathbf{2.3}}$ = 3, $DP_{t\text{BuA}}$ = 93; M_n (SEC, THF, PS calibration) = 20.3 kDa, M_w (SEC) = 23.7 kDa, Đ = 1.17.

The *tert*-butyl protecting groups were then removed using trifluoroacetic acid (TFA) (5 eq wrt each protecting group) in CH_2Cl_2 by stirring the solution overnight. The amphiphilic block copolymer (**3.2**) was recovered either *via* precipitation or by dialysis against nanopure water**:** $P(St_{52}\text{-stat-}ProSt_3)\text{-}PAA_{93}$.

*3.5.4. Synthesis of O-methylacryloyl-trans-4-hydroxy-L-proline hydrochloride, **3.4**[34]*

Trans-hydroxy-L-proline (5.0 g, 38 mmol, 1.0 eq) was added in small portions to vigorously stirring TFA (21.8 g, 191 mmol, 5.0 eq) at 0 °C. To the viscous solution, *para*-toluenesulfonic acid (TsOH) (1.31 g, 7.6 mmol, 0.2 eq) was added and stirred for 5 min. Methacryloyl chloride (7.9 g, 76 mmol, 2.0 eq) was then added, resulting in a clear solution. The reaction was stirred for 3 hours at RT and subsequently cooled in an ice bath. Diethyl ether (Et_2O) was added dropwise to the reaction. The resulting precipitate was filtered off using vacuum filtration, further washed with additional cold Et_2O twice and dried. The monomer was recrystallized in propan-2-ol/water (95/5), yielding white crystals (7.7 g, 91%). ^{1}H NMR (400 MHz, CH_3OD): δ = 1.86 (3H, t, C**H**$_3$, J = 1.3 Hz), 2.30-2.60 (2H, m, C**H**$_2$), 3.41 & 3.46 (2H, m, C**H**$_2$), 4.51 (1H, dd, C**H**, J = 10.5 & 7.8 Hz), 5.40 (1H, m, C**H**), 5.63 (1H, quin, C**H** vinyl, J = 1.5 Hz), 6.10

(1H, m, C**H** vinyl, J = 1.1 Hz). $[\alpha]_D^{25} = -20°$ (c = 1.0, CH_3OH). This compound has previously been fully characterized elsewhere.[34]

*3.5.5. RAFT copolymerization: MMA and **3.4** to give copolymer **3.5***

Monomer **3.4** (5.0 eq), MMA (60 eq), CTA2 (1.0 eq) and AIBN (0.2 eq) were dissolved in DMSO and put into a dry polymerization ampoule under nitrogen. The polymerization mixture was degassed *via* three freeze-pump-thaw cycles, back-filled with nitrogen and put into a pre-heated oil bath at 65 °C for 5 hours. Small aliquots were taken to determine degree of conversion by ^{1}H NMR spectroscopy. The polymerization was quenched *via* the addition of a small amount of THF and cooling in liquid nitrogen. The polymer was then precipitated into cold Et_2O, filtered under vacuum and dried overnight in the vacuum oven at 40 °C. Molecular weights were determined by ^{1}H NMR spectroscopy and size exclusion chromatography (SEC). Polymer polydispersities were also determined by SEC analysis. M_n (^{1}H NMR) = 3.3 kDa, DP_{MMA} = 27, $DP_{\mathbf{3.4}}$ = 2; M_n (SEC, THF, PMMA calibration) = 4.4 kDa, M_w (SEC) = 4.7 kDa, Đ = 1.07.

*3.5.6. Chain extension of $PMMA_{27}$-co-$ProMA_2$ (**3.5**) to give diblock copolymer **3.6***

MacroCTA, copolymer **3.5** (1.0 eq), AIBN (0.2 eq) and deprotectable hydrophilic monomer *tert*-butyl methacrylate (100-150 eq, depending on desired DP of hydrophobic block) were dissolved in DMSO and put into a dry polymerization ampoule under nitrogen. The polymerization mixture was then degassed *via* three freeze-pump-thaw cycles, back-filled with nitrogen and put into a pre-heated oil bath at 75 °C. After 2-3 hours an aliquot was taken to determine the polymerization conversion by ^{1}H NMR spectroscopy. The polymerization was quenched *via* the addition of THF and cooling in

liquid nitrogen. The block copolymer was then precipitated into cold CH_3OH/H_2O mixture, filtered under vacuum and dried overnight in the vacuum at 40 °C. Molecular weight was determined by ^{1}H NMR spectroscopy and SEC after protection of the L-proline acid functionalities with a *tert*-butyl group prior to analysis. M_n (^{1}H NMR) = 11.2 kDa, DP_{MMA} = 27, $DP_{\mathbf{3.4}}$ = 2, $DP_{t\text{BuMA}}$ = 54; M_n (SEC, THF, PMMA calibration) = 11.3 kDa, M_w (SEC) = 12.4 kDa, Đ = 1.09.

*3.5.7. Deprotection of block copolymer **3.6** to yield amphiphile **3.7***

Block copolymer **3.6** was dissolved in CH_2Cl_2 and stirred at RT. TFA (5 eq wrt each protecting group) was added dropwise to the polymer solution. The reaction was allowed to stir overnight and was quenched *via* the removal of excess acid by a flow of air. The amphiphile **3.7** was recovered either by precipitation or by dialysis against nanopure water.

*3.5.8. Micellization of L-proline functionalized diblock copolymers (**3.2** and **3.7**) to give styrenic micelles 3.3 and methacrylic micelles **3.8***

The two amphiphilic diblock copolymers **3.2** and **3.7** (20 mg each) were each dissolved in DMF (10 mL) and stirred at room temperature. Nanopure water (20 mL) was added dropwise, at a slow rate (1.7 $mL.min^{-1}$) to the stirring polymer solution *via* a peristaltic pump. After complete addition of water, the solution was exhaustively dialyzed against nanopure water (MWCO = 6-8.0 kDa) removing residual DMF from the micelles. Aqueous micelle solutions with concentrations of *ca.* 1.0 $mg.mL^{-1}$ were obtained. The pH of the resulting micelles **3.3** and **3.8** were determined to be *ca.* 5 and *ca.* 6 respectively. The micelles were then concentrated *via* ultrafiltration techniques to yield micelles of 6.25 and 6.79 $mg.mL^{-1}$.

3.5.9. Aldol reaction catalyzed by functionalized polymer micelles

A representative procedure is as follows: the required volume of micelles was pipetted into a small glass vial and additional nanopure water was added to make up a total micelle volume of 2.0 mL (see below for further details). 4-Nitrobenzaldehyde (0.038 g, 0.25 mmol, 1.0 eq) was dissolved in cyclohexanone (0.104 mL, 1.0 mmol, 4.0 eq) and slowly added to the stirring micelle solution. The micelle solution was then shaken and vortexed until a homogeneous solution was achieved. In the cases when precipitation was observed it was left in the reaction and was found to homogenize after additional stirring of approximately 10 min. After 24 hours an aliquot was taken for ^{1}H NMR analysis to determine the percentage conversion. To effectively remove the product and remaining starting materials from the core of the micelles at the end of the reaction, DMF was added to completely break up the micelle. The H_2O/DMF micelle solution was then sonicated for 5 min to ensure breakup of the micelle structure. EtOAc was added to move the product/starting materials from the aqueous phase into the organic phase. The organic phase was then collected and analyzed by ^{1}H NMR spectroscopy. The aqueous phase was dried and the recovered polymer re-assembled for additional catalysis reactions.

The catalyst loading in the reactions (i.e. mol% catalyst) were determined by calculating the amount of functionalized catalyst on each polymer chain and thus in the micelle solution based on polymer concentration in the micelle solution (concentration of micelle solution **3.3** = 6.25 mg.mL^{-1} and **3.8** = 6.79 mg.mL^{-1}).

Aldol product: (S)-2-((R)-hydroxyl-(4-nitrophenyl)methyl)-cyclohexan-1-one

^{1}H NMR (400 MHz, $CDCl_3$): δ = 1.19-2.57 (8H, m, C**H**$_2$), 4.00 (1H, s, O**H**), 4.82 (1-xH, d, J=4.5 Hz, C**H**, anti), 5.41 (xH, C**H**, syn), 7.44 (2H, d, J=8.6 Hz, Ar-**H**), 8.15 (2H,

d, J=8.6 Hz, Ar-**H**). ^{13}C NMR (400 MHz, $CDCl_3$): δ = 24.9, 27.0, 36.5, 42.0, 57.0, 74.0, 123.7, 127.9, 147.3, 148.5, 213.3. ESI-MS found: 272.1 ($M+Na^+$) $C_{13}H_{15}NO_4$; expected 249.10. Chiral HPLC: minor enantiomer t_R = 12.4 min, major enantiomer t_R = 18.3 min This compound has been fully characterized by others.[19, 43-45]

*3.5.10. Triblock like PMMA block copolymer (**3.9**) and its self-assembly to yield micelles **3.10***

Monomer **3.4** (5.0 eq), MMA (10 eq), CTA 2 (1.0 eq) and AIBN (0.1 eq) were dissolved in DMSO and put into a dry polymerization ampoule under nitrogen. The polymerization mixture was degassed *via* three freeze-pump-thaw cycles, back-filled with nitrogen and put into a pre-heated oil bath at 65 °C for 5 hours. A small aliquot was withdrawn to determine degree of conversion by ^{1}H NMR spectroscopy. The polymerization was quenched *via* cooling in liquid nitrogen. A second monomer solution containing MMA (40 eq) and AIBN (0.1 eq) in DMSO was added to the quenched polymerization mixture. The combined mixture degassed *via* three freeze-pump-thaw cycles, back-filled with nitrogen and put into a pre-heated oil bath at 65 °C. The polymerization was allowed to proceed for 5 hours after which another aliquot was withdrawn to determine the total degree of polymerization. The polymerization was quenched *via* addition of THF and cooling in liquid nitrogen. The functional PMMA copolymer was precipitated into cold Et_2O, filtered under vacuum and dried overnight in the vacuum oven at 40 °C. M_n (^{1}H NMR) = 19.8 kDa, DP_{MMA} = 47, $DP_{\mathbf{3.4}}$ = 3, $DP_{t\text{BuMA}}$ = 100: $P(MMA_{10}\text{-}co\text{-}ProMA_3)\text{-}b\text{-}PMMA_{37}\text{-}b\text{-}P^tBuMA_{100}$; M_n (SEC, THF, PMMA calibration) = 17.5 kDa, M_w (SEC) = 23.2 kDa, Đ = 1.33.

The block copolymer **3.9** was deprotected to yield an amphiphilic block copolymer which was subsequently self-assembled into micelles **3.10** by solvent switch from DMF to water. The amphiphilic block copolymer was first fully dissolved in DMF and water

was then added dropwise *via* a peristaltic pump at a rate of 1.7 mL.min^{-1}. After complete addition of water, the micelles were exhaustively dialyzed against nanopure water (MWCO = 6-8 kDa). Micelles **3.10** were concentrated *via* ultrafiltration to yield a concentration of 7.56 mg.mL^{-1}.

*3.5.11. Synthesis of non-functional PS-b-PAA (**3.11**) and PMMA-b-PMAA (**3.13**) block copolymers*

Styrene (100 eq) was mixed with CTA1 (1 eq) and polymerized in bulk at 110 °C for 20 hours. Alternatively, MMA (100 eq), CTA2 (1 eq) and AIBN (0.1 eq) was dissolved in 1,4-dioxane and polymerized at 65 °C for 23 hours. The degree of conversion was determined by ^{1}H NMR spectroscopy and the reaction quenched via the addition of THF and cooling in liquid nitrogen. The PS polymer was precipitated into cold methanol and the PMMA polymer into cold water:methanol (90:10). Both polymers were collected by filtration and dried in the vacuum oven at 40 °C overnight.

PS and PMMA homopolymers were then used as MacroCTAs in the chain extension polymerization of *tert*-butyl acrylate (^{t}BuA) and *tert*-butyl methacrylate (^{t}BuMA) respectively. PS (DP 75, 1 eq), ^{t}BuA (200 eq) and AIBN (0.1 eq) were dissolved in 1,4-dioxane. PMMA (DP 78, 1 eq), ^{t}BuMA (200 eq) and AIBN (0.1 eq) were dissolved in DMSO. The polymerization mixtures were both degassed *via* three freeze-pump-thaw cycles, back-filled with nitrogen, submerged into a pre-heated oil bath at 65 °C and allowed to proceed for 1.5 hours (PS) or 3 hours (PMMA). The polymerizations were quenched *via* the addition of THF and cooling in liquid nitrogen. The non-functional block copolymers were both precipitated into cold hexane and dried in the vacuum oven at 40 °C overnight. $M_{n\mathbf{3.11}}$ (^{1}H NMR) = 26.1 kDa, DP_{St} = 75, $DP_{t\text{BuA}}$ = 140; M_n (SEC, THF, PS calibration) = 18.3 kDa, M_w (SEC) = 22.9 kDa, Đ = 1.26. $M_{n\mathbf{3.12}}$ (^{1}H NMR) = 36.5 kDa, DP_{MMA} = 78, $DP_{t\text{BuMA}}$ = 200; M_n (SEC, THF, PS calibration) = 28.7 kDa, M_w

(SEC) = 37.6 kDa, Đ = 1.31.

The *tert*-butyl protecting groups were deprotected using TFA in CH_2Cl_2 to reveal the acid functionalities. TFA (15 eq wrt each protecting group) was added to a solution of the block copolymer (1 eq) in CH_2Cl_2. The polymer solution was allowed to stir overnight. The solvent was removed by flow of nitrogen and the polymer residues re-dissolved in THF and precipitated into cold hexane or dialyzed against nanopure water.

*3.5.12. Self-assembly of non-functional **2.11** and **3.12** to yield micelles **3.13** and **3.14***

The final polymer amphiphiles were self-assembled *via* solvent switch from DMF to water. This was carried out by first dissolving the polymer in DMF and slow addition of water, dropwise at a rate of 1.7 $mL.min^{-1}$. After complete addition of water, the micelles were exhaustively dialyzed against nanopure water (MWCO 6-8 kDa) to yield PS-*b*-PAA **3.13** and PMMA-*b*-PMAA **3.14** micelles.

*3.5.13. L-Proline functionalized acrylate type monomer, **3.15***

Trans-hydroxy-L-proline (5.0 g, 38 mmol, 1.0 eq) was added in small portions to vigorously stirring TFA (21.8 g, 191 mmol, 5.0 eq) at 0 °C. To the viscous solution, *para*-toluenesulfonic acid (1.31 g, 7.6 mmol, 0.2 eq) was added and stirred for 5 min. Acryloyl chloride (3.8 g, 42 mmol, 1.1 eq) was then added, resulting in a clear solution. The reaction was stirred for 3 hours at RT and subsequently cooled in an ice bath. Diethyl ether (Et_2O) was added dropwise to the reaction. The resulting precipitate was filtered off using vacuum filtration, further washed with additional cold Et_2O twice and dried. The monomer was recrystallized in propan-2-ol:water (95:5), yielding white crystals (7.7 g, 91%). ^{1}H NMR (400 MHz, CH_3OD): δ = 2.43-2.67 (2H, m, C**H**$_2$), 3.52-3.73 (2H, m, C**H**$_2$), 4.61 (1H, dd, C**H**, J = 9.64 & 4.82 Hz), 5.51 (1H, m, C**H**), 5.96 (1H,

dd, C**H** vinyl, J = 1.25 Hz), 6.20 (1H, m, C**H** vinyl, J = 10.5 Hz), 6.47 (1H, dd, C**H** vinyl, J = 1.25 Hz). $[\alpha]_D^{25} = -25°$

*3.5.14. Homopolymerization of styrene, **3.16***

Styrene (50 eq) and CTA1 (1 eq) were added into a dry polymerization ampoule under nitrogen. The polymerization mixture was degassed *via* three freeze-pump-thaw cycles after which the ampoule was back-filled with nitrogen and submerged into a pre-heated oil bath at 110 °C. The reaction was carried out in bulk and 24 hours. The degree of conversion was determined by ^{1}H NMR spectroscopy and the reaction quenched *via* the addition of THF and cooling in liquid nitrogen. The polymer was precipitate into cold CH_3OH, collected by filtration and dried in the vacuum oven at 40 °C overnight. M_n (^{1}H NMR) = 2.9 kDa, DP = 24; M_n (SEC, THF calibration) = 2.9 kDa; M_w (SEC) = 3.1 kDa; Đ = 1.08.

*3.5.15. Chain extension of **3.16** with **3.15** and ^{t}BuA, to yield block copolymer **3.17** (deprotected **3.18**)*

MacroCTA (PS **3.16**, DP 24), monomer **3.15** (5 eq), ^{t}BuA (70 eq) and AIBN (0.1 eq) were dissolved in a mixture of 1,4-dioxane and DMF (80:20). The polymerization mixture was degassed *via* three freeze-pump-thaw cycles, back-filled with nitrogen and submerged into a pre-heated oil bath at 65 °C. The polymerization was allowed to proceed for 5 hours after which an aliquot was withdrawn to determine the degree of conversion by ^{1}H NMR spectroscopy. The polymerization was then quenched *via* addition of THF and cooling in liquid nitrogen. The block copolymer was then precipitated into cold hexane, collected by filtration and dried in the vacuum oven at 40 °C overnight. The DP of the two monomers in the final copolymer was determined by ^{1}H NMR spectroscopy by comparison to signals of the RAFT end group.

Due to the presence of acid functionalities on the catalyst moieties, a small polymer sample was protected with a *tert*-butyl group prior to SEC analysis. This was carried out by dissolving the block copolymer **3.17** (1 eq) in $CHCl_3$ with DMAP (1 eq), EDCI (2 eq) and *tert*-butanol (40 eq) where the equivalences are with respect to each acid group. The reaction was allowed to stir for 24 hours after which the reaction was quenched *via* addition of aqueous ammonium chloride. The coupling agents were removed by washing reaction mixture with water and aqueous sodium bicarbonate. The remaining $CHCl_3$ solution was dried *in vacuo* and the polymer residues re-dissolved in THF and precipitated into cold hexane or re-dissolved in THF/water, dialyzed against nanopure water and freeze-dried. M_n (^{1}H NMR) 11.8 kDa, DP_{PS} = 24; $DP_{\mathbf{3.15}}$ = 2; $DP_{t\text{BuA}}$ = 70; M_n (SEC, THF, PS calibration) = 12.4 kDa; M_w (SEC) = 14.5 kDa; Đ = 1.17.

Copolymer **3.17** was deprotected to yield the amphiphile **3.18** by first dissolving **3.17** in CH_2Cl_2. TFA (5 eq wrt each protecting group) was then added dropwise to the stirring polymer solution. The reaction was quenched *via* the removal of excess acid and solvent by a flow of air. The polymer residues were re-dissolved in THF and precipitated into cold hexane or dialyzed against nanopure water.

*3.5.16. Solution self-assembly of shell-functionalized micelles, **3.19***

The block copolymer was self-assembled *via* solvent switch from DMF to water. The copolymer was first fully dissolved in DMF and water was added dropwise to the stirring solution *via* a peristaltic pump at a rate of 1.7 $mL.min^{-1}$. After complete addition of water, the resulting micelles were dialyzed against nanopure water (MWCO 7-8 kDa) to remove residual DMF. Final polymer concentration after ultrafiltration was determined to be 4.77 $mg.mL^{-1}$.

3.6. References

1. M. J. Joralemon, R. K. O'Reilly, C. J. Hawker and K. L. Wooley, *J. Am. Chem. Soc.*, 2005, **127**, 16892.

2. C. F. Hansell and R. K. O'Reilly, *ACS Macro Lett.*, 2012, **1**, 896.

3. R. K. O'Reilly, M. J. Joralemon, C. J. Hawker and K. L. Wooley, *Chem. Eur. J.*, 2006, **12**, 6776.

4. J.-H. Ryu, R. T. Chacko, S. Jiwpanich, S. Bickerton, R. P. Babu and S. Thayumanavan, *J. Am. Chem. Soc.*, 2010, **132**, 17227.

5. R. T. Chacko, J. Ventura, J. Zhuang and S. Thayumanavan, *Adv. Drug Deliv. Rev.*, 2012, **64**, 836.

6. J.-H. Ryu, S. Bickerton, J. Zhuang and S. Thayumanavan, *Biomacromolecules*, 2012, **13**, 1515.

7. S. Bickerton, S. Jiwpanich and S. Thayumanavan, *Mol. Pharm.*, 2012, **9**, 3569.

8. B. Helms, C. O. Liang, C. J. Hawker and J. M. J. Fréchet, *Macromolecules*, 2005, **38**, 5411.

9. R. Nagarajan, M. Barry and E. Ruckenstein, *Langmuir*, 1986, **2**, 210.

10. P. Cotanda and R. K. O'Reilly, *Chem. Commun.*, 2012, 48, 10280.

11. B. Helms, S. J. Guillaudeu, Y. Xie, M. McMurdo, C. J. Hawker and J. M. J. Fréchet, *Angew. Chem. Int. Ed.*, 2005, **44**, 6384.

12. P. Cotanda, A. Lu, J. P. Patterson, N. Petzetakis and R. K. O'Reilly, *Macromolecules*, 2012, **45**, 2377.

13. Y. Liu, Y. Wang, Y. Wang, J. Lu, V. Piñón and M. Weck, *J. Am. Chem. Soc.*, 2011, **133**, 14260.

14. H. A. Zayas, A. Lu, D. Valade, F. Amir, Z. Jia, R. K. O'Reilly and M. J. Monteiro, *ACS Macro Lett.*, 2013, **2**, 327.

15. E. Huerta, P. J. M. Stals, E. W. Meijer and A. R. A. Palmans, *Angew. Chem. Int. Ed.*, 2013, **52**, 2906.

16. E. Lejeune, M. Drechsler, J. Jestin, A. H. E. Müller, C. Chassenieux and O. Colombani, *Macromolecules*, 2010, **43**, 2667.

17. B. M. Rossbach, K. Leopold and R. Weberskirch, *Angew. Chem. Int. Ed.*, 2006, **45**, 1309.

18. B. List, R. A. Lerner and C. F. Barbas III, *J. Am. Chem. Soc.*, 2000, **122**, 2395.

19. M. Gruttadauria, F. Giacalone, A. Mossuto Marculescu, P. Lo Meo, S. Riela and R. Noto, *Eur. J. Org. Chem.*, 2007, **28**, 4688.

20. P. M. Pihko, K. M. Laurikainen, A. Usano, A. I. Nyberg and J. A. Kaavi, *Tetrahedron*, 2006, **62**, 317.

21. I. Ibrahem and A. Córdova, *Tetrahedron Lett.*, 2005, **46**, 3363.

22. H. Torii, M. Nakadai, K. Ishihara, S. Saito and H. Yamamoto, *Angew. Chem. Int. Ed.*, 2004, **43**, 1983.

23. S. Aratake, T. Itoh, T. Okano, N. Nagae, T. Sumiya, M. Shoji and Y. Hayashi, *Chem. Eur. J.*, 2007, **13**, 10246.

24. A. C. Evans, A. Lu, C. Ondeck, D. A. Longbottom and R. K. O'Reilly, *Macromolecules*, 2010, **43**, 6374.

25. A. Lu, T. P. Smart, T. H. Epps, D. A. Longbottom and R. K. O'Reilly, *Macromolecules*, 2011, **44**, 7233.

26. G. Moad, E. Rizzardo and S. H. Thang, *Aust. J. Chem.*, 2006, **59**, 669.

27. Q. Ma and K. L. Wooley, *J. Polym. Sci., Part A: Polym. Chem.*, 2000, **38**, 4805.

28. Y. Mai and A. Eisenberg, *Chem. Soc. Rev.*, 2012, **41**, 5969.

29. R. C. Hayward and D. J. Pochan, *Macromolecules*, 2010, **43**, 3577.

30. T. Nicolai, O. Colombani and C. Chassenieux, *Soft Matter*, 2010, **6**, 3111.

31. L. Zhang and A. Eisenberg, *J. Am. Chem. Soc.*, 1996, **118**, 3168.

32. Y. Yu and A. Eisenberg, *J. Am. Chem. Soc.*, 1997, **119**, 8383.

33. J. P. Patterson, A. M. Sanchez, N. Petzetakis, T. P. Smart, I. I. I. T. H. Epps, I. Portman, N. R. Wilson and R. K. O'Reilly, *Soft Matter*, 2012, **8**, 3322.

34. T. E. Kristensen, K. Vestli, K. A. Fredriksen, F. K. Hansen and T. Hansen, *Org. Lett.*, 2009, **11**, 2968.

35. Y. Kang, A. Lu, A. Ellington, M. C. Jewett and R. K. O'Reilly, *ACS Macro Lett.*, 2013, **2**, 581.

36. R. K. O'Reilly, M. J. Joralemon, K. L. Wooley and C. J. Hawker, *Chem. Mater.*, 2005, **17**, 5976.

37. A. C. Evans, J. Skey, M. Wright, W. Qu, C. Ondeck, D. A. Longbottom and R. K. O'Reilly, *J. Polym. Sci., Part A: Polym. Chem.*, 2009, **47**, 6814.

38. A. Cordova, W. Notz and C. F. Barbas Iii, *Chem. Commun.*, 2002, 3024.

39. Z. Ge, D. Xie, D. Chen, X. Jiang, Y. Zhang, H. Liu and S. Liu, *Macromolecules*, 2007, **40**, 3538.

40. S. S. Chimni, D. Mahajan and V. V. Suresh Babu, *Tetrahedron Lett.*, 2005, **46**, 5617.

41. K. Sakthivel, W. Notz, T. Bui and C. F. Barbas, *J. Am. Chem. Soc.*, 2001, **123**, 5260.

42. J. Skey and R. K. O'Reilly, *Chem. Commun.*, 2008, **46**, 4183.

43. D. Font, C. Jimeno and M. A. Pericas, *Org. Lett.*, 2006, **8**, 4653.

44. D. Font, S. Sayalero, A. Bastero, C. Jimeno and M. A. Pericas, *Org. Lett.*, 2007, **10**, 337.

45. F. Giacalone, M. Gruttadauria, P. L. Meo, S. Riela and R. Noto, *Adv. Synth. Catal.*, 2008, **350**, 2747.

4. Tuning the Catalytic Activity of L-Proline Functionalized Hydrophobic Nanogel Particles in Water

4.1. Abstract

L-Proline functionalized cross-linked nanogels have been synthesized *via* a one-pot emulsion polymerization process. The influence of cross-linking density (CLD) and degree of catalyst functionalization (DoF) on catalyst efficiency in a model aldol reaction was thoroughly investigated. Interestingly, the catalytic dependency on CLD was negligible but found to be of considerable importance to maintain high enantioselectivity. At low CLD, an increase in DoF was accompanied by a decrease in enantioselectivity. We propose this is an effect of a change in hydrophobic-to-hydrophilic balance within the nanogel as the same trend was not observed at higher CLD which is most likely related to the more compact structure of the nanogel. The importance of nanogel hydrophobicity was further confirmed when enhancements in catalytic activity were observed for more hydrophobic nanogels, based on for example ethyl methacrylate or butyl methacrylate.

4.2. Introduction

Amphiphilic diblock copolymers with active catalytic functionalities have been successfully synthesized and self-assembled into polymer micelles in water. A range of organocatalysts including 4-dimethylaminopyridine (DMAP),[1] L-proline[2, 3] and imidazole[4] have been successfully incorporated into the hydrophobic compartment of assembled micelles. In each case, enhanced catalytic efficiency was observed, often in a significantly shorter reaction time compared to the native catalyst in organic solvents. This was a result of the successful formation of a favourable micro-environment able to sequester and concentrate organic substrates in its hydrophobic cavity, known as the concentrator effect.[5] However, to achieve the desired amphiphilic diblock copolymer

and its corresponding micelles, a multi-step synthetic process is required. Related to these systems are cross-linked microgels and nanogels, unimolecular nanostructures that are readily synthesized in a one-pot emulsion polymerization process with controllable particle sizes in the nanometer to millimeter range. As a result of their cross-linked nature, the particles are able to retain their shape in a range of conditions including changes to temperature, solvent and concentration. Their application as nanoreactors has already been well demonstrated, successfully immobilizing a selection of metal NPs such as Au, Pt, Ag and Pd and enzymes to catalyze a range of reactions including reductions,[6, 7] hydrolysis,[8] carbon-carbon bond forming reactions[9, 10] and polymerization reactions.[11, 12] Other applications of these cross-linked particles can be found in fields such as membranes,[13] magnetic resonance imaging,[14] drug delivery,[15, 16] biotechnology,[17] biomedical diagnostics (theranostics)[18] and cosmetics.[19]

More relevant to our work is the work of Kristensen *et al.*[20, 21] who synthesized micron-sized cross-linked beads (~100 μm) with L-proline functionality incorporated within. Both methacrylic and methacrylic/styrenic beads were synthesized and showed high activity, selectivity and more importantly recyclability.

Nevertheless, the influence of key parameters such as degree of catalyst functionalization (DoF) and cross-linking density (CLD) on the catalytic efficiency of the incorporated catalyst has not yet been investigated in detail. The influence of CLD on the rate of substrate diffusion and hence catalytic efficiency of nanoreactor efficiency has previously been investigated by Rodionov *et al.*[22] PS nanogels were synthesized with a range of CLDs and access by a range of alkyne molecules into the azide-decorated core was examined. They found that access of the larger molecules into the core was significantly retarded with increasing CLD but the access by the smaller alkynes remained unrestricted regardless of CLD.

In the first part of this chapter we aim to synthesize a range of PMMA nanogels with different DoFs and CLDs to investigate their effect on the catalytic activity of the incorporated catalyst. In the second part, the catalytic efficiency of more hydrophobic nanogels will be evaluated, further exploring the importance of tailoring the local catalyst environment for efficient catalysis.

4.3. Results and Discussion

4.3.1. Synthesis and characterization of PMMA nanogels

The L-proline functionalized methacrylate monomer[20] (**3.4**) (synthesis and characterization discussed in Chapter 3), was used in the synthesis of a range of cross-linked nanogels. Monomer **3.4** was first copolymerized with a comonomer, methyl methacrylate (MMA) and a cross-linker, ethylene glycol dimethacrylate (EDGMA) in an emulsion polymerization (Scheme 4.1).[23, 24] The functional monomer, comonomer and cross-linker were copolymerized in water containing the surfactant sodium dodecyl sulfate (SDS). SDS was used to stabilize the system by forming surfactant micelles able to stabilize both the water insoluble monomer droplet and the resulting hydrophobic nanogels in water.[25] A high concentration of SDS (25 wt%) was used to ensure a small particle size was achieved:[25-27] smaller sized particles were targeted to increase the surface area of the nanogel and active sites, hopefully resulting in greater substrate uptake and thus high catalytic activity/efficiency. It was pleasing to find that particles in the size range of 20-50 nm were readily synthesized with low particle size distribution. All 16 synthesized nanogels (differing in DoF and CLD) were purified by dialysis removing excess SDS to ensure no competitive sequestration of the substrates would take place. Monomer conversions were not determined due to the cross-linked nature of the resulting particles which is further discussed below. DoF was altered by changing the amount of **3.4** in the polymerization, keeping amount of comonomer constant.

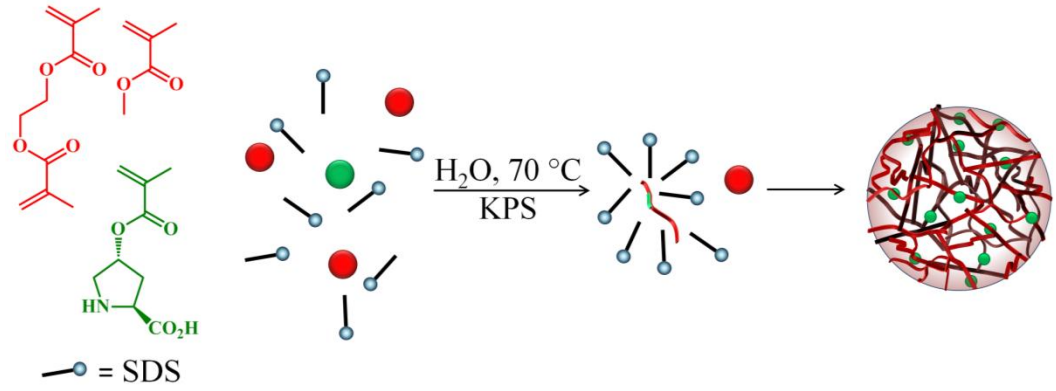

Scheme 4.1. Representation of hydrophobic nanogel synthesis *via* an emulsion polymerization process

The nanogel copolymer is structurally represented in Figure 4.1 where x represents the weight% of co-monomer (in this case MMA), y the DoF in weight% (2, 5, 9 or 15 wt%) and z the CLD in weight% (0.5, 2, 5 or 10 wt%). From this point, the functional nanogels will be named as presented in Table 4.1: the first number represents the DoF and the second the CLD.

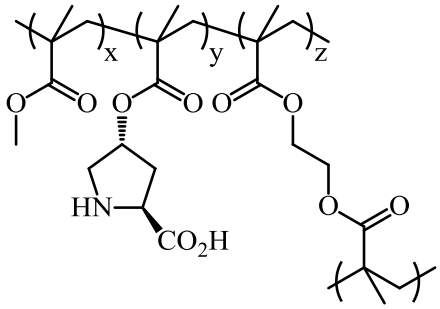

Figure 4.1. Representation of L-proline functionalized PMMA cross-linked nanogel, where x represents weight% of co-monomer, z the CLD and y the DoF (also in weight%) of the synthesized nanogels

Table 4.1. Naming of the 16 functional nanogels based on DoF and CLD

CLD \ DoF	2	5	9	15
0.5	M2.05	M5.05	M9.05	M15.05
2	M2.2	M5.2	M9.2	M15.2
5	M2.5	M5.5	M9.5	M15.5
10	M2.10	M5.10	M9.10	M15.10

The particle size of the hydrophobic nanogels was determined by dynamic light scattering (DLS) and transmission electron microscopy (TEM). The particle sizes obtained from both techniques were comparable and suggest spherical particles were synthesized. The particle size determined by TEM was slightly smaller than those determined by DLS which was attributed to the nature of the two techniques.

A representative DLS trace for the functional hydrophobic nanogels stabilized by SDS is shown in Figure 4.2. The nanogel particles were found to have relatively low size dispersity indicated by the presence of a single scattering population. As a result of the use of SDS to stabilize the hydrophobic particles in water, the particles were also found to be stable towards aggregation.

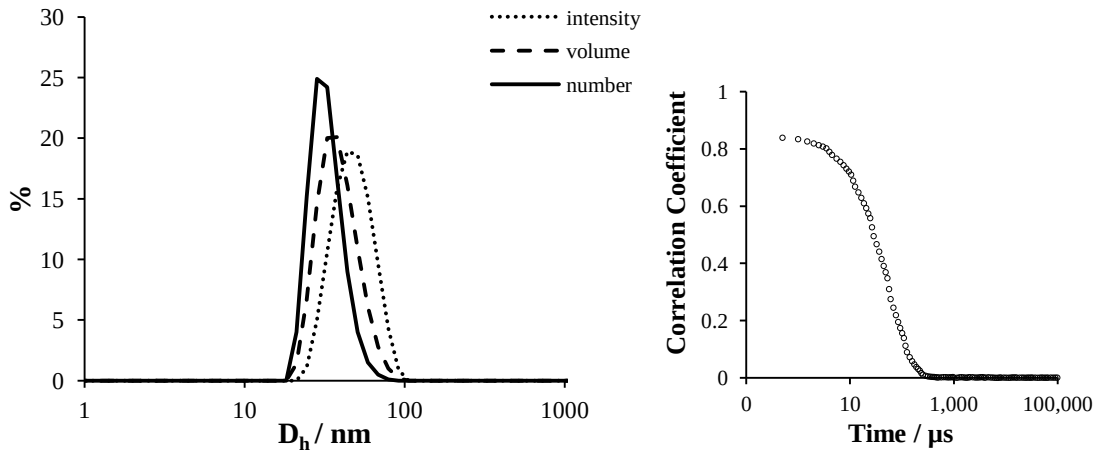

Figure 4.2. Representative DLS trace for the functional hydrophobic nanogel particles (M2.10, 27 nm, PDI = 0.095) and the intensity correlation function

The particle size of the 16 nanogels (DoF = 2, 5, 9, 15 wt%, CLD = 0.5, 2, 5, 10 wt%) determined by DLS is detailed in Table 4.2 and were found to be in the size range of 20-50 nm. This is indicative of a dependable synthetic route for the synthesis of these hydrophobic nanogel particles, where the particle size is readily controlled by the concentration of surfactant in the polymerization process.[25-27] A representative nanogel

(M2.10) was characterized by TEM. A representative TEM image (Figure 4.3). The particles were found to be somewhat spherical with a D_{av} of 25 ± 5 nm which is agreement with the D_h (27 nm, PDI = 0.095) determined by DLS.

Table 4.2. D_h (dispersity, PDI) of the hydrophobic nanogels determined by DLS.

DoF (%) \ CLD (%)	0.5	2	5	10
2	23 (0.192)	32 (0.080)	38 (0.093)	27 (0.095)
5	28 (0.232)	35 (0.142)	36 (0.162)	21 (0.111)
9	42 (0.128)	36 (0.109)	33 (0.148)	41 (0.081)
15	49 (0.252)	48 (0.101)	42 (0.167)	38 (0.250)

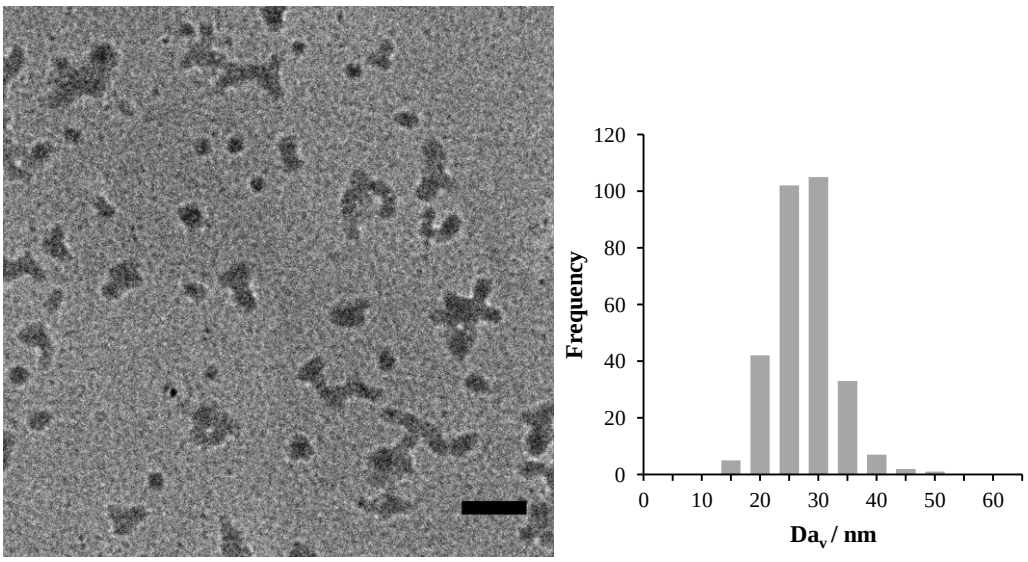

Figure 4.3. Representative unstained TEM images of M2.10 (D_{av} = 25 ± 5 nm)

4.3.1.1. Monomer reactivity

As the reactivity of the two monomers with respect to each other is unknown under radical polymerization conditions, it was important to determine the possible arrangement of the two monomers in the nanogel. It can be imagined that the two

monomers might undergo different types of polymerizations under these conditions in the presence of a water soluble radical initiator. It was already known that MMA is water insoluble whereas monomer **3.4** is water soluble; thus, resulting in emulsion and precipitation polymerization processes respectively (poly-**3.4** is water insoluble).[28] Therefore, the reaction of the two monomers under polymerization conditions in the absence of the cross-linker was studied. The polymerization was carried out with 15 wt% of **3.4**, allowing for easy identification of both monomer and polymer signals by ^{1}H NMR spectroscopy. Following an induction period, both monomers start to polymerize at the same time (Figure 4.4), with **3.4** showing a slightly faster rate of polymerization. Nevertheless, the fact that both monomers started to polymerize at the same time indicates that copolymerization is likely to occur. However, as a result of the fraction of the two monomers used, gradient type polymers, with more catalytic functionality at one end of the polymer, were most likely to be the product. Thus, is its unlikely that core-shell type structures were prepared with the more hydrophilic **3.4** decorating the surface of the nanogel.

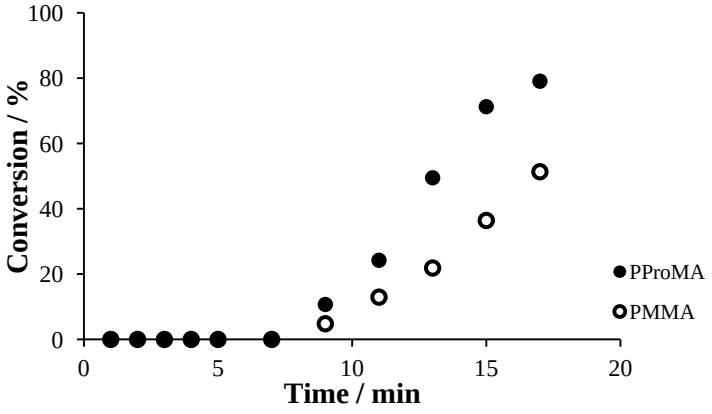

Figure 4.4. The copolymerization progress of 3.4 (15 wt%) and MMA, followed by ^{1}H NMR spectroscopy (400 MHz, $CDCl_3$)

4.3.1.2. Particle swelling experiments

The ability of the nanogels to swell in an organic solvent was investigated to confirm the presence of cross-links within the nanogels. As the hydrophobic nanogels are stabilized in water by surfactants, this stabilization is interrupted upon the addition of organic solvent. Thus, cross-linked particles will swell and linear chains will be soluble, resulting in the absence of cross-links being observed, a change which can be characterized by DLS. In addition, we hypothesized that the lightly cross-linked systems should be able to swell to greater extents than the highly cross-linked systems[29] and thus, the experiments were carried out using nanogels with 0.5 and 10 wt% CLD.

The addition of THF (approx. 1 mL THF to a few drops aqueous nanogels, <20% water in volume) confirmed that the particles were indeed cross-linked demonstrated by the larger D_h observed in both cases, indicative of particle swelling. Certainly, a difference in swelling abilities for nanogels with 0.5 and 10 wt% CLD, where a change in D_h of 45 and 13 nm respectively was observed (Figure 4.5), confirming that particles with high CLD are held together more tightly.[30]

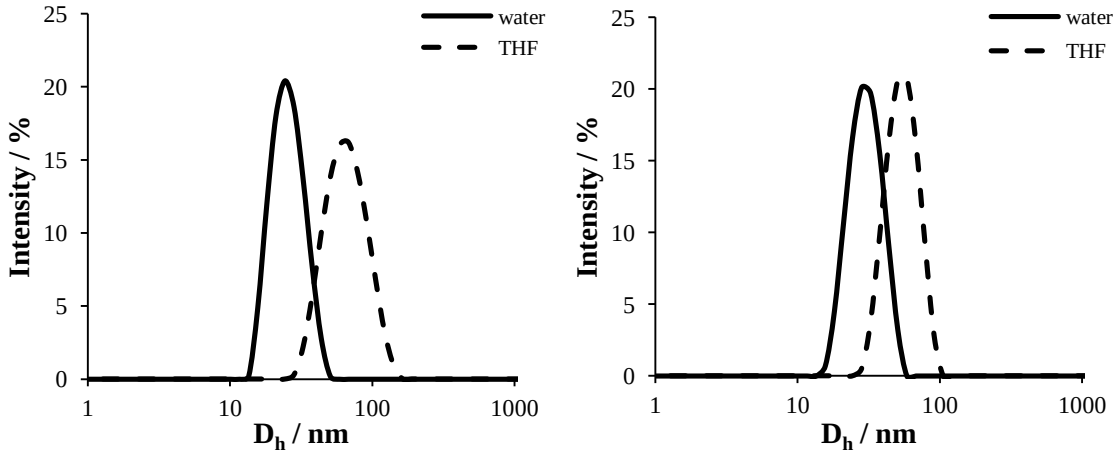

Figure 4.5. DLS traces of cross-linked PMMA nanogels in water and THF (with <20% water content), left: 0.5 wt% CLD, 23 nm to 68 nm, (Δ size = 45 nm) and right: 10 wt% CLD, 27 nm to 40 nm, (Δ size = 13 nm)

A similar experiment was carried out using cyclohexanone and confirmed that the nanogels have high affinity for the substrate as a similar increase in D_h was observed as with THF, 43 and 18 nm for 0.5 wt% and 10 wt% CLD respectively (Figure 4.6). We hypothesized that this difference would be reflected in the catalytic activity: nanogels with low CLD should be able to contain greater amounts of organic substrates, potentially leading to better catalytic function than those with high CLD. In both cases the viscosity and refractive index were altered for the solvent in the DLS.

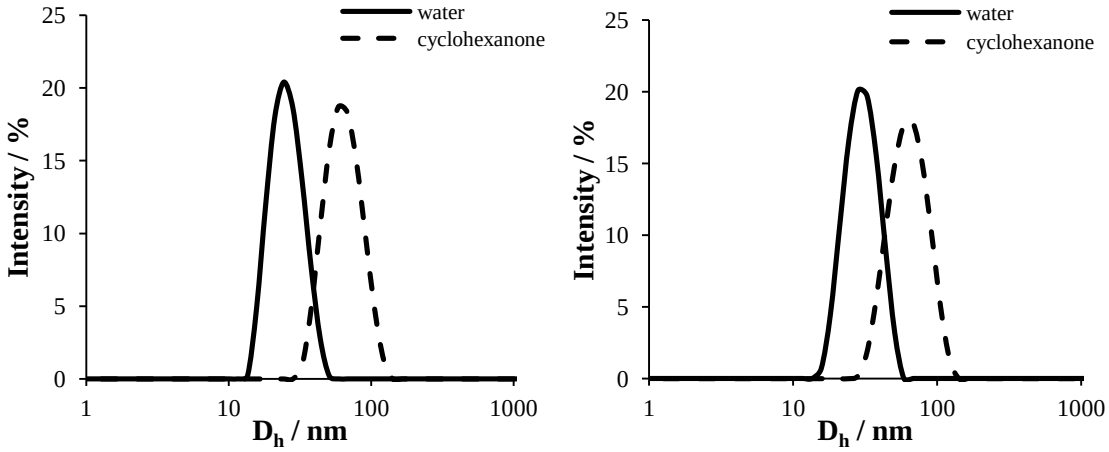

Figure 4.6. DLS traces of cross-linked PMMA nanogels in water and cyclohexanone (with <20% water content), left: 0.5 wt% CLD, 23 nm to 66 nm, (Δ size = 43 nm) and right: 10 wt% CLD, 27 nm to 45 nm, (Δ size = 18 nm)

Additionally, the equivalent DLS experiment was carried out on the non-cross-linked nanogels. In this case, a decrease in D_h to < 10 nm was observed upon addition of THF, which is indicative of unimers (free polymer chains in solution) (Figure 4.7). This is an important feature to take into account, as the addition of organic substrates may break up the hydrophobic pockets formed by the stabilizing surfactant micelles and have dramatic effects on the catalytic activity of the polymer system. The catalytic activity of the non-cross-linked nanogels is discussed at a later stage in this chapter.

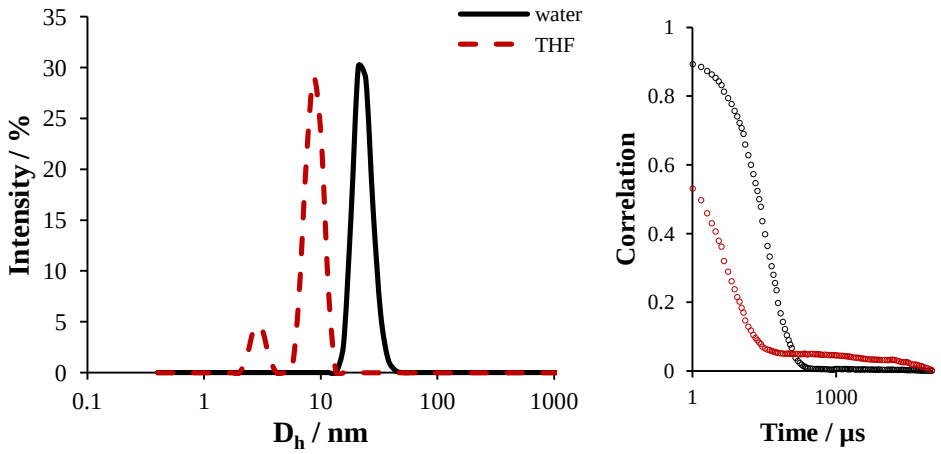

Figure 4.7. DLS traces of PMMA nanogels with 0 wt% CLD in water and THF, 24 nm to <10 nm

4.3.2. Catalysis

The aldol reaction between 4-nitrobenzaldehyde and cyclohexanone has been used to assess the catalytic efficiency of a range of polymer- and micelle-supported L-proline systems and was therefore chosen as a reliable model with which to evaluate our nanogels (Scheme 4.2).[31-34]

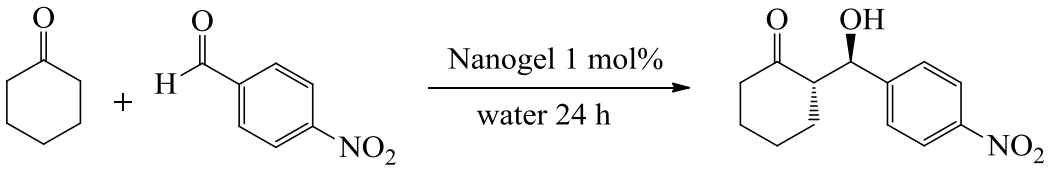

Scheme 4.2. Model aldol reaction between 4-nitrobenzaldehyde and cyclohexanone

The reaction was firstly catalyzed by the nanogels at 1 mol% catalyst loading. As the nanogels were functionalized with the catalyst to different degrees (2-15 wt% DoF), different concentrations of nanogels (or number of nanoreactors) were required to achieve 1 mol% loading (Figure 4.8). In each reaction, the concentration of reagents was kept constant by maintaining the same overall reaction volume.

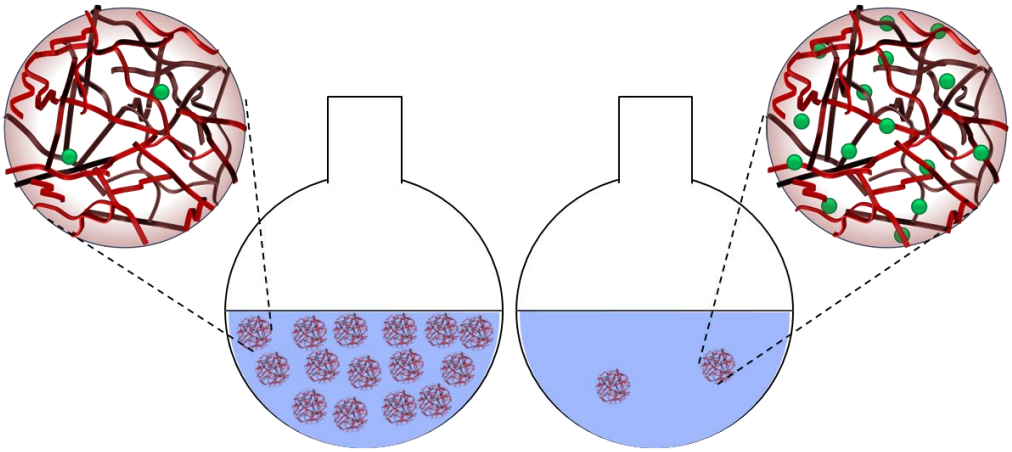

Figure 4.8. Different concentrations of nanogels were required to provide 1 mol% catalyst loading, represented by nanogels with DoF = 2 wt% (left) and 15 wt% (right)

4.3.2.1. Effect of DoF on particle size and catalytic activity

Nanogels with different DoFs (2-15 wt%) were used to investigate the importance of local catalyst environment for efficient catalysis. The effect of DoF on the final particle D_h is shown below in Figure 4.6. A small trend was observed for particles with 0.5 and 2 wt% CLD, showing an increase in particle size with increasing DoF. The effect was attributed to the use of greater amounts of monomer **3.4** in the polymerization to account for the higher DoF. No significant difference was observed at the higher CLDs, which is not unexpected as the particle size is perhaps easiest influenced at the lower CLDs.

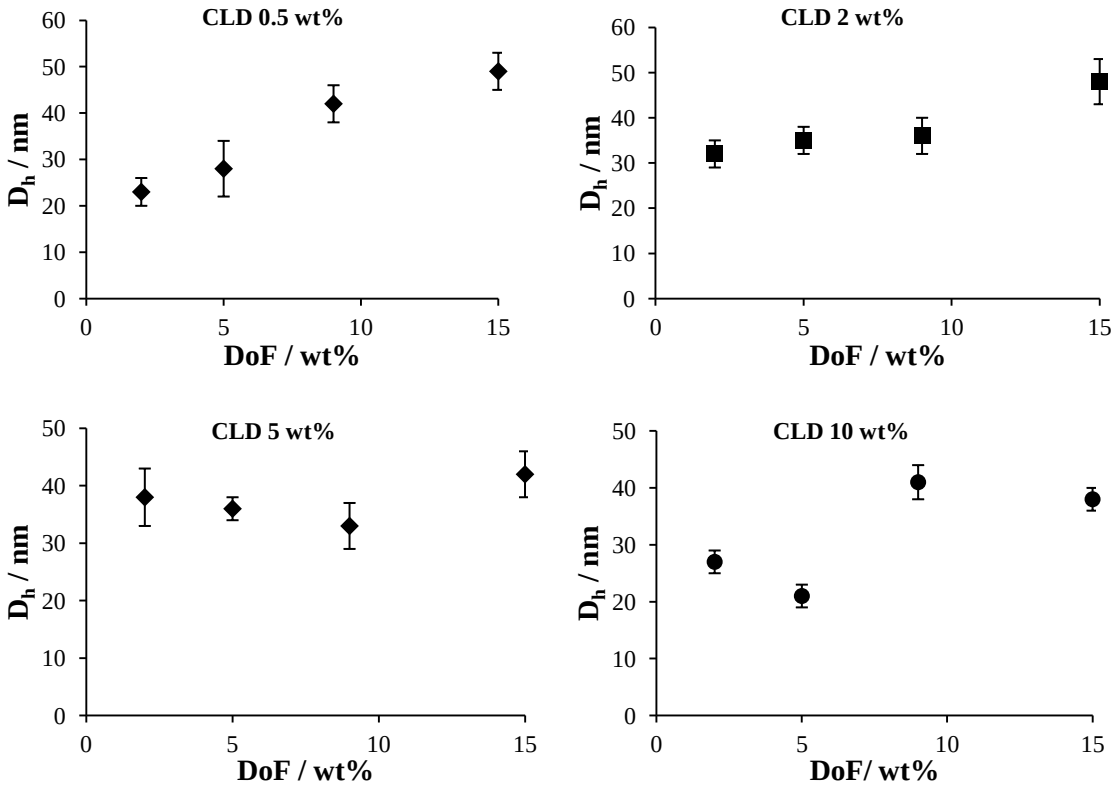

Figure 4.9. Effect of DoF on particles size, comparing particles with the same CLD

The catalytic reactions were all carried out at 1 mol% catalyst loading, for 24 hours. Thus, a significantly lower concentration of nanogels with 15 wt% DoF was used to catalyze the reaction compared to nanogels with 2 wt% DoF (Figure 4.8) which seems to be somewhat reflected in the catalytic activity. Nanogels with low DoF (i.e. 2 wt%) were found to be more efficient than nanogels with comparatively higher DoF (Figure 4.10). M2.05 showed 80% higher conversions than M15.05 over the same reaction time; however, this difference in activity was less pronounced at higher CLD (Figure 4.10). This suggests the catalytic activity of particles with high CLD is less affected by change in DoF supporting the idea that these particles are held together more effectively. Interestingly, the catalytic activity of the nanogels in water at 1 mol% loading is comparable to the activity of the unsupported catalyst in organic solvents at higher loading (Table 4.3).[35, 36] This highlights the ability of the nanogels to efficiently

sequester reagents from the surrounding aqueous environment. Moreover, all reactions go to completion if left to react for an additional 24-48 hours, on top of the original 24 hours. We attribute this effect to slow diffusion of substrates into the nanogels, simply due to them not coming into contact with nanogels at high loading, as then only very small amounts of nanogels were added to achieve the correct concentration. However, it is also worth mentioning that once formed, the product does not leave the nanoreactor core as it is also hydrophobic in nature, so one can imagine there is a limit to how much starting substrate/product the nanoreactor can contain. Thus, there will also be a limit to how low the catalyst concentration in a reaction may be reduced to. In addition, due to the high amount of water present in the reaction, the retro-aldol reaction is a possible side-reaction. However, this was not investigated.

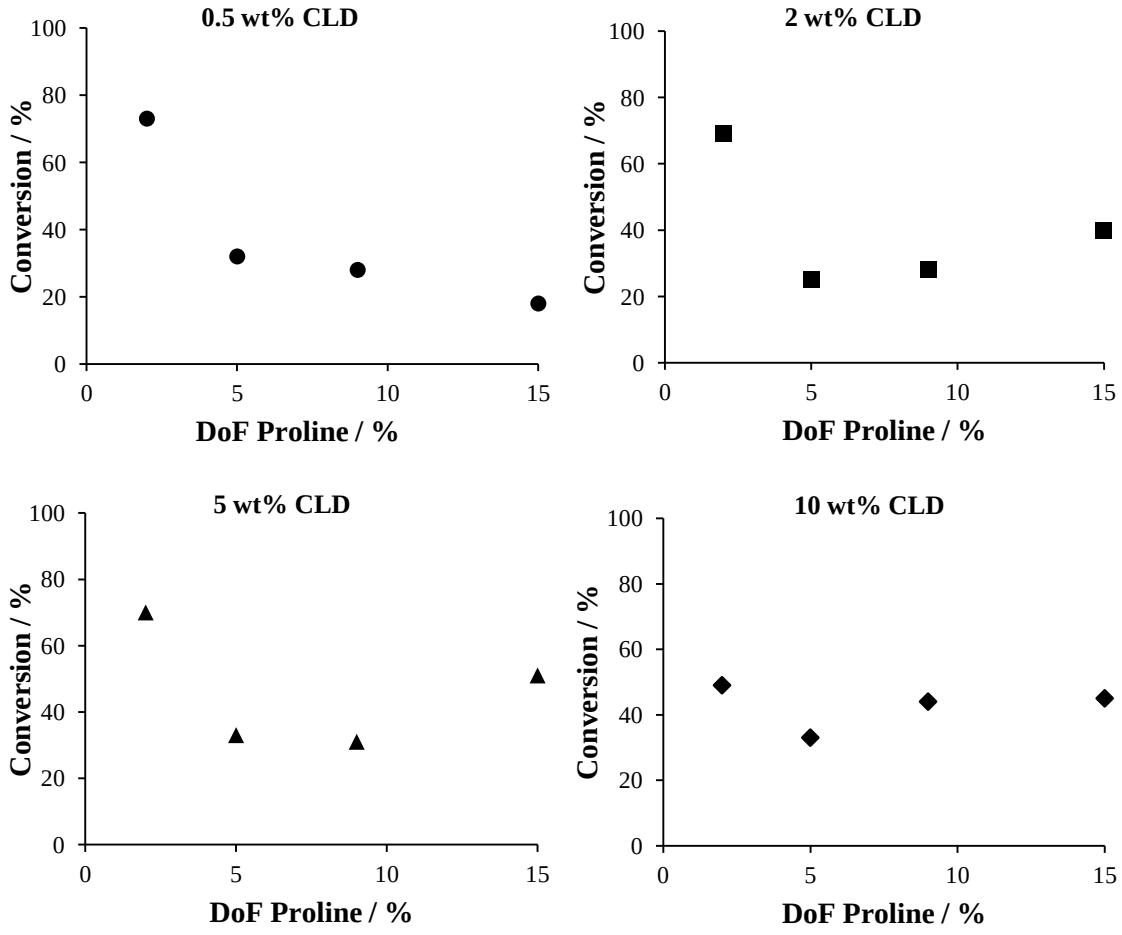

Figure 4.10. Effect of DoF on catalytic activity of nanogels at 1 mol% catalyst loading and a range of CLD

Table 4.3. The effect of nanogel DoF on activity and selectivity catalyzed at 1 mol% loading

CLD = 0.5%				CLD = 2%			
DoF	**Conv.[a] / %**	***anti/syn* ratio[a]**	**ee[b] / %**	**DoF**	**Conv.[a] / %**	***anti/syn* ratio[a]**	**ee[b] / %**
2	73	97/3	99	2	69	95/5	98
5	32	98/2	89	5	25	96/4	97
9	28	99/1	86	9	28	96/4	96
15	18	95/5	81	15	40	97/3	94

CLD = 5%				CLD = 10%			
DoF	**Conv.[a] / %**	***anti/syn* ratio[a]**	**ee[b] / %**	**DoF**	**Conv.[a] / %**	***anti/syn* ratio[a]**	**ee[b] / %**
2	75	93/7	95	2	49	96/4	95
5	33	97/3	97	5	33	95/5	98
9	31	95/5	95	9	44	96/4	95
15	51	95/5	98	15	37	95/5	96

[a] Determined by ^{1}H NMR spectroscopy (400 MHz, $CDCl_3$), after 24 hours, reactions carried out in triplicate
[b] Determined by chiral HPLC, ChiralPak IA, 80:10:10 hexane:propan-2-ol:ethanol, 1 mL.min^{-1}

Further lowering the catalyst DoF to 0.5 wt% (0.5 wt% CLD) required the use of a higher concentration of nanogels. Surprisingly, this did not result in the expected increase in activity. Instead, less than 5% conversion was achieved after 24 hours. We propose this was an effect of the greater total volume of nanogels required to achieve 1 mol% loading, resulting in a lower substrate concentration within each nanosphere, making sequestration of substrates less efficient (Figure 4.11, compare reactions left and middle).

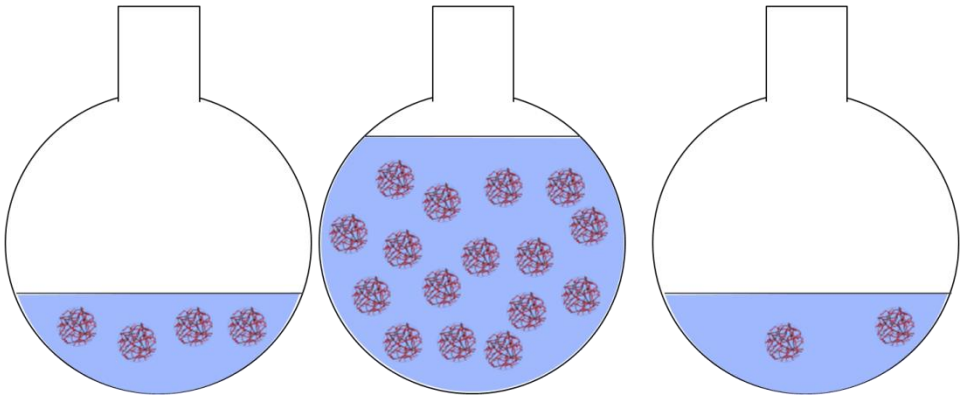

Figure 4.11. Reaction at 1 mol% catalyzed by M2.05 (left), M05.05 (middle) and at 0.125 mol% catalyzed by M05.05

When the reaction was instead carried out at the same nanogel concentration as previous reactions, (i.e. same ratio of reagents to nanogels, thus lowering catalyst loading to 0.125 mol%) 28% conversion was observed (*anti/syn* 98/2, 97% ee) (Figure 4.10). Although this brings the turnover number (TON) up to 224, it highlights the importance of nanoreactor design and how catalytic activity may be easily tailored by making alterations to the DoF. (TON refers to the number of moles of substrates that one mole of catalyst can convert into product in a given time, which in this case was 24 hours.)

Interestingly, a slight but steady decrease in enantioselectivity was observed with increasing DoF for nanogels with 0.5 wt% CLD (Table 4.3). The same trend was not observed for nanogels with higher CLD. We propose that the observed decrease in enantioselectivity may be associated with a change in the hydrophobic-to-hydrophilic balance within the nanogel core upon increasing DoF: due to the more hydrophilic nature of the catalyst functionality, more water may then be present within the nanoreactors at higher DoF and low CLD, interfering with the reaction process. This is further discussed at a later point.

4.3.2.2. Effect of CLD on particle size and catalytic activity

The effect of CLD on particle size was next studied: in line with previous findings in this area,[29, 37] we hypothesized that particles with greater CLD should be held together more closely, resulting in a smaller particle size. However, no significant difference in particle size was observed by TEM in the CLD range studied, an observation which was further supported by DLS analysis (Figure 4.12).

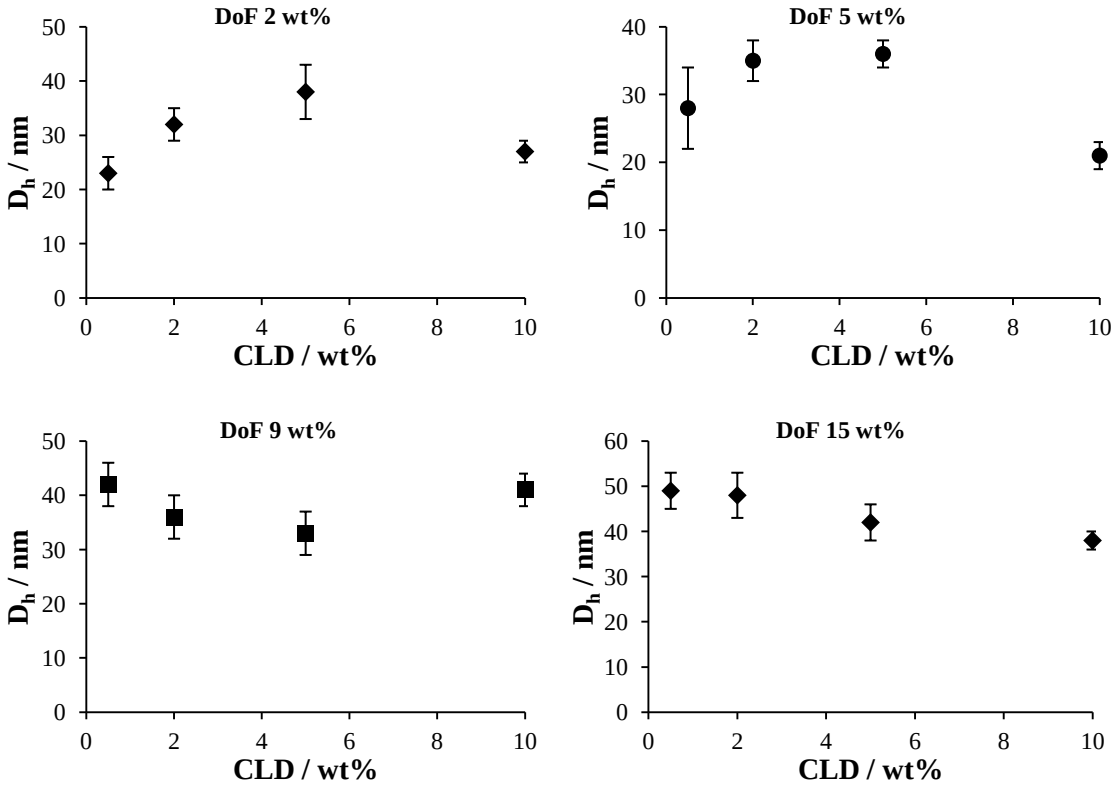

Figure 4.12. The effect of CLD on particle size for a range of DoF

Taking into account the swelling behaviour exhibited by the nanogels, we hypothesized that the more compact nanogels (i.e. high CLD) would be catalytically less efficient, due to the diffusion of substrates being able to occur less readily. Moreover, it was also reasoned that particles with low CLD should be able to hold greater amounts of substrates and consequently show greater catalytic activity.

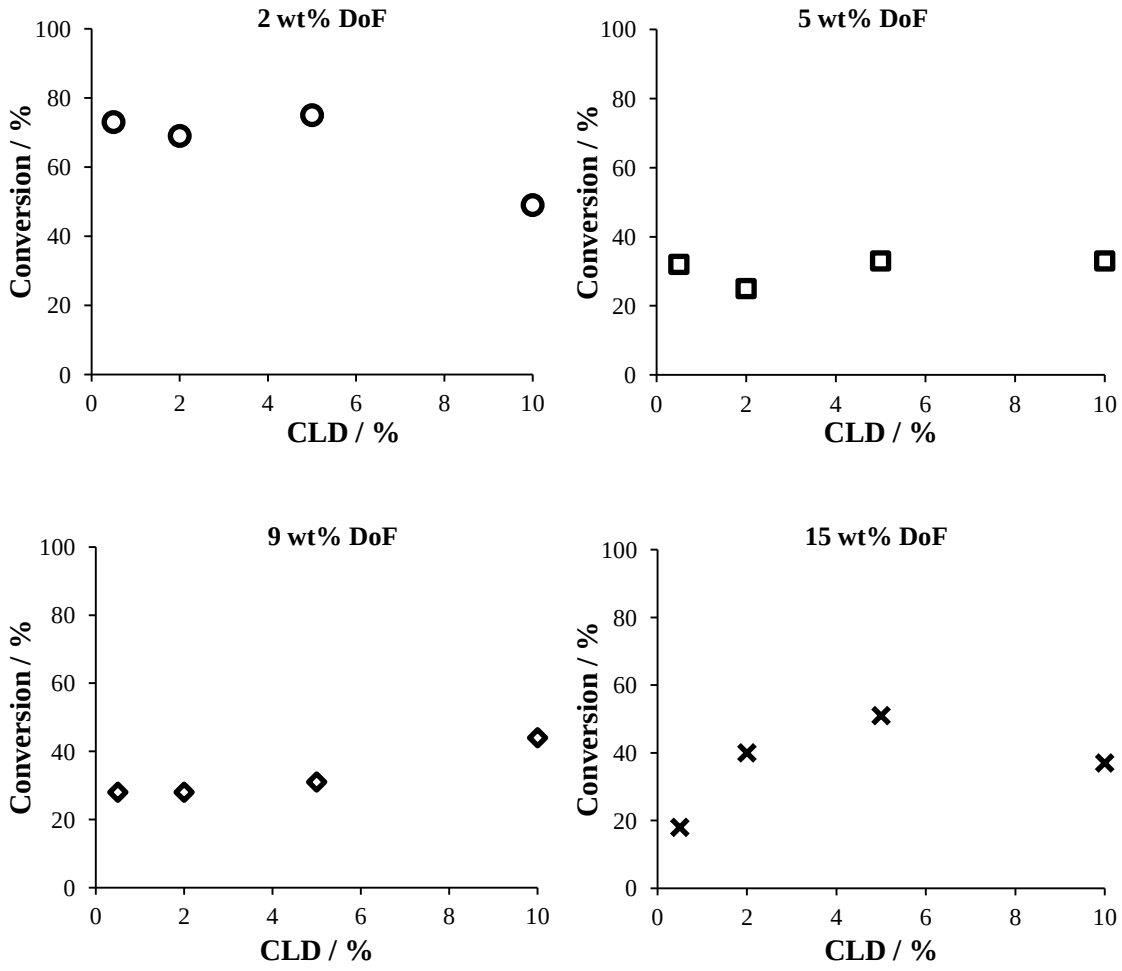

Figure 4.13. Effect of CLD on the nanogel catalytic efficiency at 1 mol% catalyst loading and room temperature after 24 hours

However, the effect of CLD was not ultimately so clear cut: whilst it had a significant effect on the catalytic activity of nanogels with low DoF, i.e. 2 wt%, at higher DoFs, CLD was found to have negligible effect on nanogel activity (Figure 4.13, Table 4.4). This is an interesting difference and we propose that the influence of CLD was successfully observed for the 2 wt% DoF nanogels due to their high catalytic efficiency compared with nanogels of higher DoF.

Table 4.4. The effect of DoF on activity and selectivity catalyzed at 1 mol% loading and room temperature

DoF = 2 wt%				DoF = 5 wt%			
CLD	**Conv.[a] / %**	***anti/syn* ratio[a]**	**ee[b] / %**	**CLD**	**Conv.[a] / %**	***anti/syn* ratio[a]**	**ee[b] / %**
0.5	73	97/3	99	0.5	32	98/2	89
2	69	95/5	98	2	25	96/4	98
5	75	93/7	95	5	33	97/3	95
10	49	96/4	95	10	33	95/5	95

DoF = 9 wt%				DoF = 15 wt%			
CLD	**Conv.[a] / %**	***anti/syn* ratio[a]**	**ee[b] / %**	**CLD**	**Conv.[a] / %**	***anti/syn* ratio[a]**	**ee[b] / %**
0.5	28	99/1	86	0.5	18	95/5	81
2	28	96/4	96	2	40	97/3	94
5	31	95/5	95	5	51	95/5	98
10	44	96/4	95	10	37	95/5	96

[a] Determined by ^{1}H NMR spectroscopy (400 MHz, $CDCl_3$), after 24 hours, reactions carried out in triplicate
[b] Determined by chiral HPLC, ChiralPak IA, 80:10:10 hexane:propan-2-ol:ethanol, 1 mL.min^{-1}

The enantioselectivity of the aldol reaction was not found to be significantly affected by the change in DoF, if we consider each series of nanogels with the same DoF. However, when we examined across the series of DoFs, comparing all those with CLD 0.5, 2, 5 and 10, an interesting observation could be made: although differences were minimal for CLDs of 2, 5 and 10 wt% (ee remained constant at 94-98%), for nanogels with 0.5 wt% CLD a decrease in enantioselectivity was observed with increasing DoF (for clarity, 0.5 and 10 wt% CLD are compared directly with one another in Figure 4.14). We propose that the decrease in enantioselectivity of nanogels with low CLD is related to a change in the hydrophobic-to-hydrophilic character of the core with increasing

catalyst content: the hydrophilic nature of the L-proline moiety will then render the core more hydrophilic and potentially allow more water inside, which can disrupt the transition state for the reaction. The same effect was not observed at higher CLD, which we propose is due to the more compact structure of the nanogels' core, maintaining a hydrophobic local environment for selective catalysis. Furthermore, this may suggest that less water is able to penetrate into the nanogel core, maintaining high enantioselectivity even with increasing DoF.

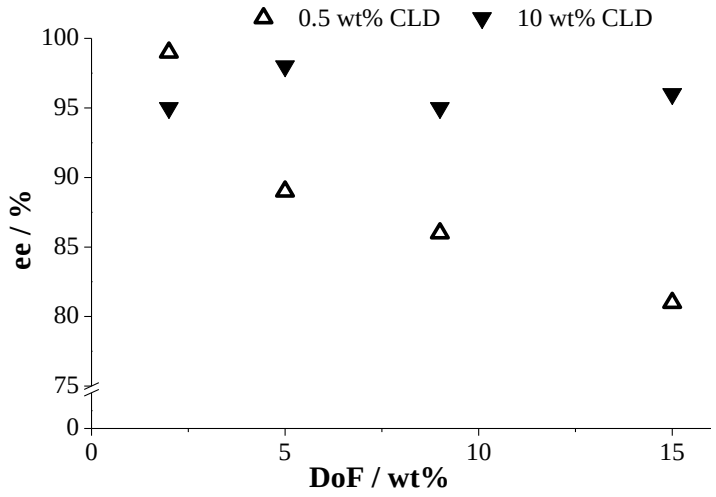

Figure 4.14. The observed difference in enantioselectivity as a result of different CLDs, 0.5 and 10 wt% for catalysis carried out at 1 mol% loading

The importance of having a cross-linked network to maintain the integrity of the hydrophobic system, was emphasized when nanogels without any cross-linking were used to catalyze the asymmetric reaction. Nanogels with 2 wt% DoF were synthesized and determined to have an average diameter of 24 nm (PDI = 0.152) by DLS. The catalysis reaction was then carried out at 1 mol% loading, providing just 41% conversion (*anti/syn* 98/2, 94% ee) was achieved after 24 hours compared with 0.5 wt% CLD, 2 wt% DoF which gave 73% conversion (*anti/syn* 97/3, 99% ee). As the system lacks cross-linking, the hydrophobic polymers functionalized with the catalytic moieties

are held together by the SDS, as micelles in the aqueous environment. Potentially, one consequence of this could be that catalytic sites become submerged in a polymer tangle in the absence of a cross-linker to hold the polymer chains open and reveal the catalyst to the reagents effectively. Additionally, it is possible that the SDS micelles break up upon addition of the organic substrates, removing entirely the hydrophobic pockets represented in the first place by the micelles, thus further highlighting the importance of carefully designing the polymeric support to achieve an efficient catalytic system.

4.3.2.3. Catalyst shut down

To investigate if there is a possible CLD limit, above which no catalyst activity is observed (i.e. no or extremely little substrate diffusion into the nanogel core is observed as a result of the high CLD), two additional nanogels were synthesized. Both nanogels were synthesized with 2 wt% DoF and considerably higher CLDs, 25 and 50 wt%. The nanogels were found to be in a similar size range as those previously synthesized, by both DLS and TEM: 25 wt% CLD 22 nm (PDI = 0.234) and 50 wt% CLD 20 nm (PDI = 0.108) (Figure 4.15).

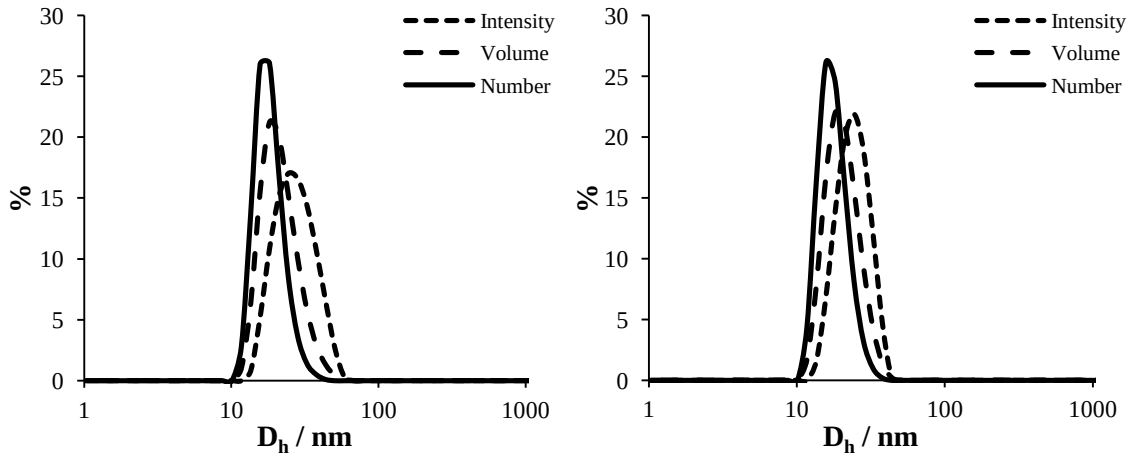

Figure 4.15. DLS traces of nanogels with 2 wt% DoF and two different CLDs, 25 wt% CLD (left), 50 wt% CLD (right)

However, although they did have reduced reactivity even 50% CLD did not entirely shut it down: nanogels with 25 wt% CLD (at 1 mol% loading) gave 31% conversion after 24 hours (*anti/syn* 97/3, 95% ee) whereas nanogels with 50 wt% CLD provided just 14% conversion by ^{1}H NMR (*anti/syn* 95/5, 95% ee). Unfortunately, the swelling of these particles in organic solvent or cyclohexanone was not investigated.

We hypothesized that the particles can remain reactive even at high CLD for one (or both) of two reasons: firstly, the presence of L-proline moieties close to the water interface of the nanogels means that however much cross-linking there is to block diffusion of reagents, they can still react with those catalyst sites which reside close enough to the surface of the micelle core. Secondly, as the core remains hydrophobic, reagents could, even at 50% cross-linking, be sequestered by the nanogel, the lower activity over 24 hours than simply due to slower diffusion of substrates as a result of the higher CLD. The difference in activity of the 2 wt% DoF nanogels with a variety of CLDs is represented below in Figure 4.16, illustrating very convincingly the effect of changes in CLD across the series.

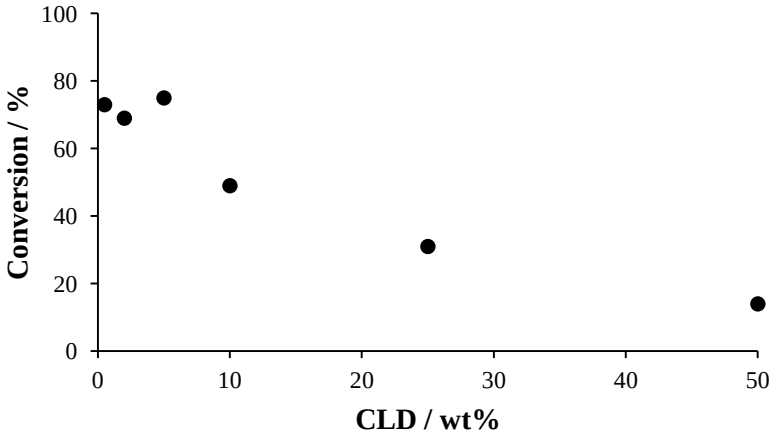

Figure 4.16. Catalytic activity of nanogels with 2 wt% DoF and a range of CLDs, all carried out at 1 mol% loading

In order to eliminate possible surface activity caused by the presence of catalytic functionalities at the water interface, core-shell (CS) type nanogels[29, 38, 39] were synthesized in a bid to force catalyst shut down. This was done by introducing an additional and non-functional hydrophobic shell around the original nanogel particle and was achieved in practice *via* a seeded emulsion polymerization process, where a cross-linked poly(*tert*-butyl methacrylate) (P^{t}BuMA) shell (50 wt% CLD) was grown around the original M2.50 nanogels (seeds). We proposed that the hydrophobic shell would eliminate any surface activity associated with the original nanogel by preventing access of substrate to the catalytic sites.

As expected, a small increase in particle size upon addition of the shell was observed by DLS: the double-hydrophobic CS nanogels were determined to be 25 nm (PDI = 0.119), compared with the original M2.50 (Figure 4.17). Again, the particles were not characterized by ^{1}H NMR spectroscopy due to their corss-linked nature, only a small change in turbidity was observed upon addition of the hydrophobic shell.

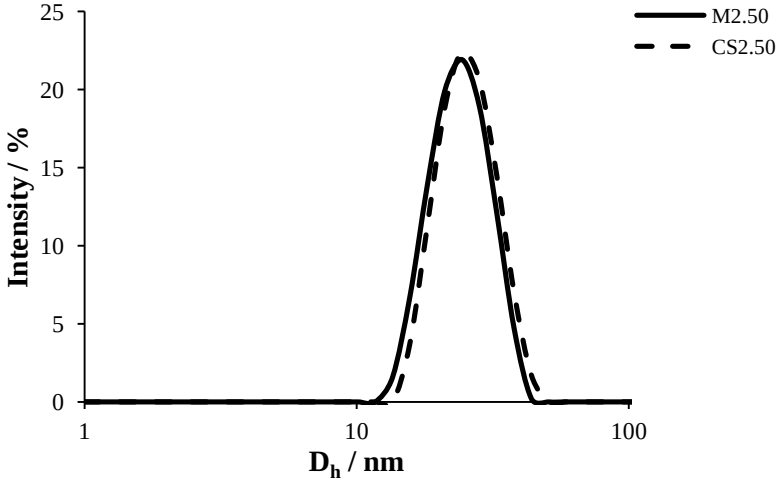

Figure 4.17. DLS traces of M2.50 (seed) and the corresponding double hydrophobic CS nanogel, 20 nm (PDI = 0.108) to 25 nm (PDI = 0.119)

The highly cross-linked double hydrophobic core-shell nanogels showed low activity as predicted, reaching less than 5% conversion after 24 hours and allowing the reaction to stir for an additional week resulted in just 30% conversion. The catalytic activity and selectivity of nanogels with 2 wt% DoF across the entire range of CLDs investigated are summarized in Table 4.5 and show clearly the detrimental effect of cross-linking on reactivity at higher wt% .

Table 4.5. Activity and selectivity of nanogels with 2 wt% DoF at 1 mol% loading

CLD / wt%	Conv.[a] / %	*anti/syn* ratio[a]	ee[b] / %
0.5	73	97/3	99
2	69	95/5	98
5	75	93/7	95
10	49	96/4	95
25	31	97/3	95
50	14	95/5	95
50[c]	< 5[d]	-	-

[a] Determined by ^{1}H NMR spectroscopy (400 MHz, $CDCl_3$) after 24 hours, reactions carried out in triplicate
[b] Determined by chiral HPLC, Chiralpak IA, hexane:propan-2-ol:ethanol 80:10:10, 1 mL.min^{-1}
[c] PMMA nanogel with P^{t}BuMA shell
[d] Conversion reached 30 % when reaction was left for 8 days

4.3.2.4. Effect of catalyst concentration

The catalytic reactions discussed up until this point were carried out at 1 mol% catalyst loading, i.e. using different concentrations of nanogels (Figure 4.8). To eliminate the effects of having different amounts of polymeric material in each reaction, further reactions were carried out using the same concentration of nanogels, altering catalyst loading but maintaining substrate concentration (Figure 4.18).

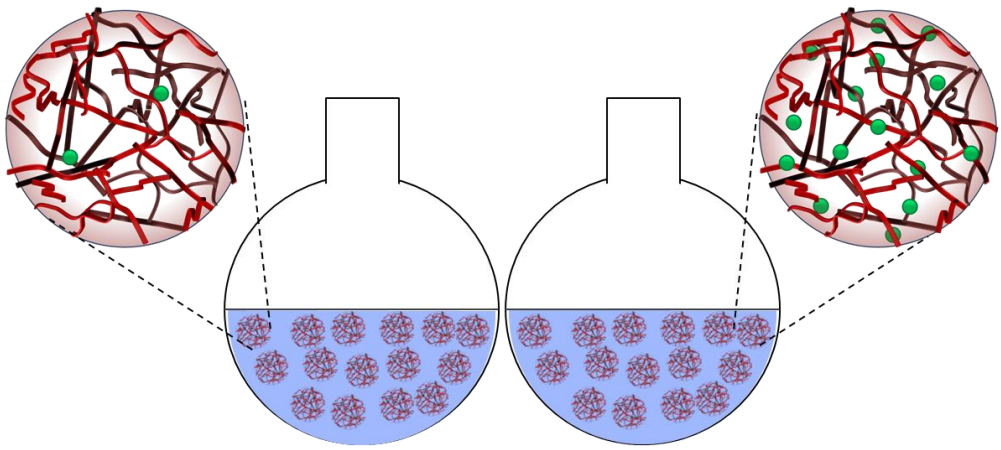

Figure 4.18. Catalysis carried out using the same nanogel concentration, left: 2 wt% DoF, 1 mol% loading, right: 15 wt% DoF, 8.5 mol% loading

Thus, the reactions were designed to investigate the effect of having more polymeric materials in the reaction rather than the efficiency of the catalyst at a specific loading. Nevertheless, because different mol% catalyst were used, the catalytic efficiency of the nanogels will be represented by TON. For this specific study, nanogels with 0.5 wt% CLD were tested and, as an example, reactions carried out at the same concentration of polymeric material resulted in a loading of 1 and 8.5 mol% for nanogels M2.05 and M15.05 respectively. We predicted that M15.05 would show the greatest catalytic activity, simply due to the higher over catalyst loading as well as greater number of catalytic sites within each nanogel. Hence, each nanoreactor should theoretically be able to produce more products compared to nanoreactors containing fewer catalytic sites (i.e. M2.05).

However, this was not observed and once again, the results suggest that particles with low DoF are more efficient: M2.05 was found to be approximately 4 times more efficient than M5.05. Apart from M2.05, the other three nanogels showed comparable catalytic activity, reaching 51, 57 and 53% conversion for 5, 9 and 15 wt% DoF

respectively. Disregarding the result achieved by the 2 wt% DoF nanogel system, the results suggest that regardless of the average number of catalytic sites within each nanogel, the efficiency of each nanoreactor is comparable (Table 4.6).

Table 4.6. The catalytic efficiency of PMMA nanogels with 0.5 wt% CLD, catalysis carried out at the same concentration of nanogels

DoF / %	Catalyst loading / mol%	Conv.[a] / %	*anti/syn* ratio[a]	ee[b] / %	TON[c]
2	1	73	97/3	99	73
5	3	51	97/3	88	17
9	5	57	97/3	81	11
15	8.5	53	98/2	67	6

[a] Determined by ^{1}H NMR spectroscopy (400 MHz, $CDCl_3$) after 24 hours, reactions carried out in triplicate
[b] Determined by chiral HPLC, ChiralPak IA, hexane:propan-2-ol:ethanol 80:10:10, 1 mL.min^{-1}
[c] Defined as the moles of substrates converted into product by one mole of catalyst at a given time (in this case 24 hours)

Further lowering the catalyst DoF to 0.5 wt% (CLD 0.5 wt%, 25 nm, PDI = 0.091), but maintaining the same number of nanoreactors in the reaction then showed some interesting results: catalysis (now at just 0.125 mol%) produced a dramatic increase in TON from 73 (at DoF 2 mol%, catalyst loading 1%) to 192. Excellent selectivity was also maintained (*anti/syn* ratio 98/2, 97% ee), highlighting the potential for effectively reducing the catalyst loading and maximizing product output in these nanogel systems.

In terms of explaining these interesting results, we hypothesized that the comparable conversions achieved for the nanogel systems with > 5 mol% catalyst loading was the result of one of the following two effects: increasing steric hindrance around the catalytic sites with increasing DoF or a diffusion limitation created by the same higher concentration of catalytic sites. When considering the former, the importance of a confined space where the reagents are able to efficiently interact with the catalyst in a chiral space has been studied by Dzierzak *et al*[40] using inorganic supports. We

rationalize that in our case, having fewer, more isolated catalytic sites within the particles allows for efficient formation of the transition states responsible for the high activity and enantioselectivity observed in L-proline catalyzed reactions.[41, 42] In the case of M2.05, this is seen through the significantly greater activity and selectivity compared to the other nanogels. The results suggest that an increase in DoF from 2 to 5 wt% is enough to affect the chiral space and reduce interactions between substrate and catalyst, and further increases to the DoF had little effect on the catalyst activity (as the damage is already done). This was further supported by the trend observed in enantioselectivity where a decrease in enantioselectivity with increasing DoF, (99% at 2 wt% DoF, down to 67% at 15 wt% DoF, Table 4.6) was observed. The same effect was previously seen for nanogels with 0.5 wt% CLD when carried out at 1 mol% loading (24 hour reaction): a decrease in enantioselectivity from 99% *ee* (DoF 2 wt%) to 81% *ee* (DoF 15 wt%.) was observed and we then attributed this effect to gradual changes in the hydrophobic-to-hydrophilic balance within the nanogel, where more catalytic moieties increased the degree of hydrophilicity in the core and as a result the water content. An increase in water content may also increase the occurrence of the retro-aldol reaction which may account for the lower conversion and *ee* observed. These results support our hypothesis but suggest the environment around the catalytic motif is indeed of great importance.

To further investigate this effect, the same reactions were carried out using a series of nanogels with 10 wt% CLD. These nanogels will exhibit the same change in hydrophobic-to-hydrophilic properties but because of the higher CLD, we proposed that the nanogels would be better able to repel water from the nanogel core and thus maintain high enantioselectivity. Indeed, the same significant decrease in enantioselectivity was not observed and was instead maintained in the 90s (Table 4.7, Figure 4.19). We propose this was a direct result of the higher CLD as it was able to protect the core from allowing too much water to penetrate the core.

Table 4.7. The catalytic activity and selectivity of nanogels with 10 wt% CLD, catalysis carried out at the same concentration of nanogels

DoF / %	Catalyst loading / mol%	Conv.[a] / %	*anti/syn* ratio[a]	ee[b] / %	TON[c]
2	1	49	96/4	95	49
5	3	62	97/3	91	21
9	5	79	97/3	96	16
15	8.5	71	96/4	92	8

[a] Determined by ^{1}H NMR spectroscopy (400 MHz, $CDCl_3$) after 24 hours, reactions carried out in triplicate
[b] Determined by chiral HPLC, Chiralpak IA, hexane:propan-2-ol:ethanol 80:10:10, 1 mL.min^{-1}
[c] Defined as the moles of substrates converted into product by one mole of catalyst at a given time (in this case 24 hours)

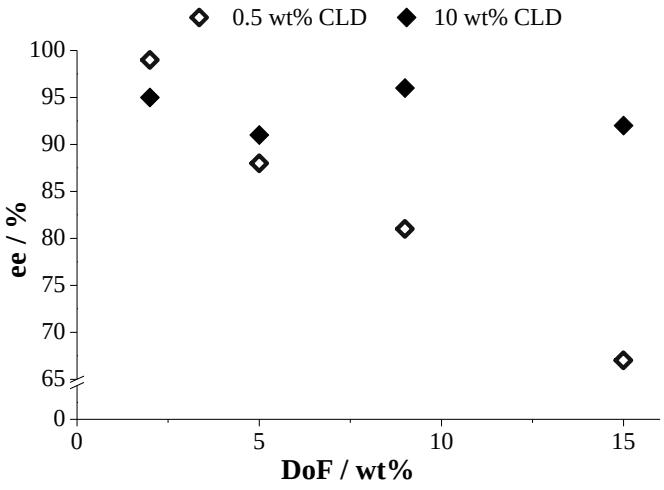

Figure 4.19. Comparing the enantioselectivity of reactions catalyzed by nanogels with two different CLDs, 0.5 and 10 wt% where catalysis was carried out at the same concentration of nanogels

What is not explained however is that M2.10 was actually found to be the least efficient system when compared to nanogels with the same CLD, providing now increased conversions at higher DoF, the inverse of M2.05's pattern (*c.f.* Table 4.7, Figure 4.20). This contradictory result is out of line with all previous investigations and introduces a

new level of complexity, suggesting that steric hindrance or diffusion cannot fully explain the differences observed in catalytic activity.

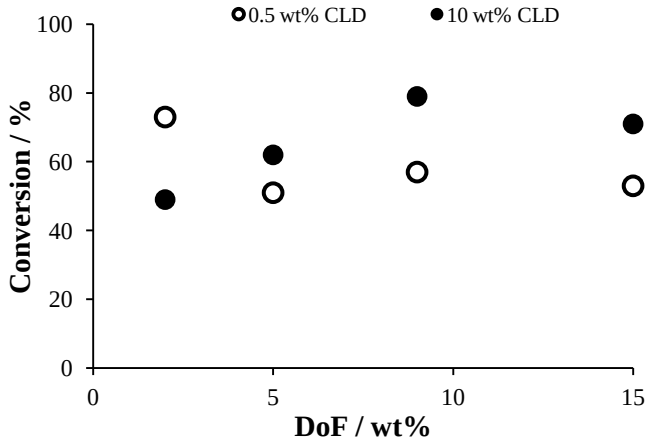

Figure 4.20. Comparing the catalytic activity of reactions catalyzed by nanogels with two different CLDs, 0.5 and 10 wt%, carried out at the same concentration of nanogels

4.3.2.5. Control experiments

Control reactions were carried out to further support the results generated by the nanogels. Non-functionalized PMMA nanogels were synthesized at 0.5 wt% CLD and were determined to be 24 nm (PDI = 0.120) by DLS. In the absence of the tethered catalyst, no reaction was observed after 24 hours, confirming that substrates do not react in the absence of a catalyst; no reaction occurs by simply concentrating the substrates in a confined environment. Unsupported L-proline was then added to the non-functionalized nanogels and again no reaction was observed after 24 hours: as unsupported L-proline is highly soluble in water, it was expected to remain in the surrounding aqueous environment and not diffuse into the hydrophobic nanogel. The aldol substrates, on the other hand, are insoluble in water and will readily diffuse into the nanogel as a result of hydrophobic effects. This essentially segregates the catalyst and reagents resulting in the observed lack of reaction and emphasizes the importance

of having the catalyst tethered within the nanogel particles in order to bring reaction components with different solubilities together within the same reaction sphere. This effect was further highlighted as no reaction was observed when carried out in the presence of SDS micelles (in the absence of our hydrophobic nanogel) with or without additional unsupported L-proline catalyst.

4.3.3. Synthesis and characterization of nanogels with increased hydrophobicity

The results presented so far are very interesting, as they show a counterintuitive and dramatic decrease in enantioselectivity with increasing L-proline content, which warranted further investigation. In order to understand more concerning the role of nanogel hydrophobicity and its influence on catalytic activity and selectivity, four additional nanogel systems were synthesized. We believed that an increase in both activity and selectivity should result from the use of slightly more (though not entirely) hydrophobic monomers, due to a potential increase in substrate and decrease in water uptake.

The presence of a small amount of water is known to improve both the activity and selectivity of L-proline;[43,44-46] thus, we hypothesized that a peak in activity and selectivity should appear when a perfect hydrophobic-to-hydrophilic balance is achieved. However, for the range of nanogels planned, it was realised that increasing hydrophobicity would also result in an increase in steric hindrance within the core. Hence, the two isomeric versions of butyl methacrylate (^{n}butyl and ^{t}butyl) were used to investigate the influence of sterics within the core without altering the hydrophobicity of the nanogel.

Four additional nanogel systems were synthesized with 0.5 wt% CLD, in order to compare the enantioselectivity with that observed for the PMMA nanogels. The same range of DoFs were used, i.e. 2, 5, 9 and 15 wt% to provide a direct comparison. The four comonomers used were ethyl methacrylate (EMA), *n*-butyl methacrylate (^{n}BuMA), *tert*-butyl methacrylate (^{t}BuMA) and lauryl methacrylate (LMA) (Figure 4.21). The nanogels were successfully synthesized *via* the emulsion polymerization procedure previously discussed, resulting in 16 new nanogels, with a range of increased hydrophobicities.

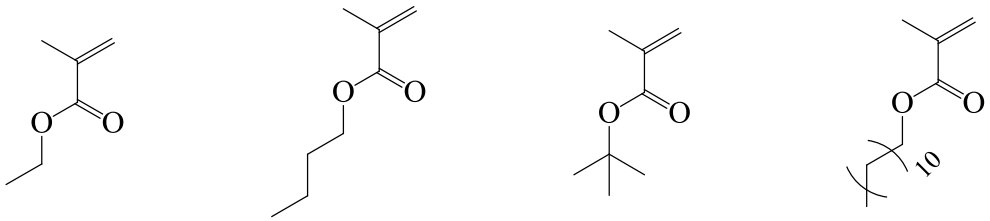

EMA ^{n}BuMA ^{t}BuMA LMA

Figure 4.21. Representation of the more hydrophobic comonomers

The more hydrophobic nanogels were also characterized by DLS and TEM. By DLS, the particle sizes were found to be in a similar range to those reported for the PMMA nanogels (Figure 4.22, Figure 4.23) and the sizes determined by dry-state TEM were found to correspond quite well to those observed by DLS (Figure 4.24), taking into account the differences usually observed between these techniques. Two of the most hydrophobic LMA particles were found to be bimodal by DLS; thus, the correlation function was extracted and used to determine the decay time and size of both populations. The contribution of the larger population was determined to be small and hence only the size of the smaller population is reported here.

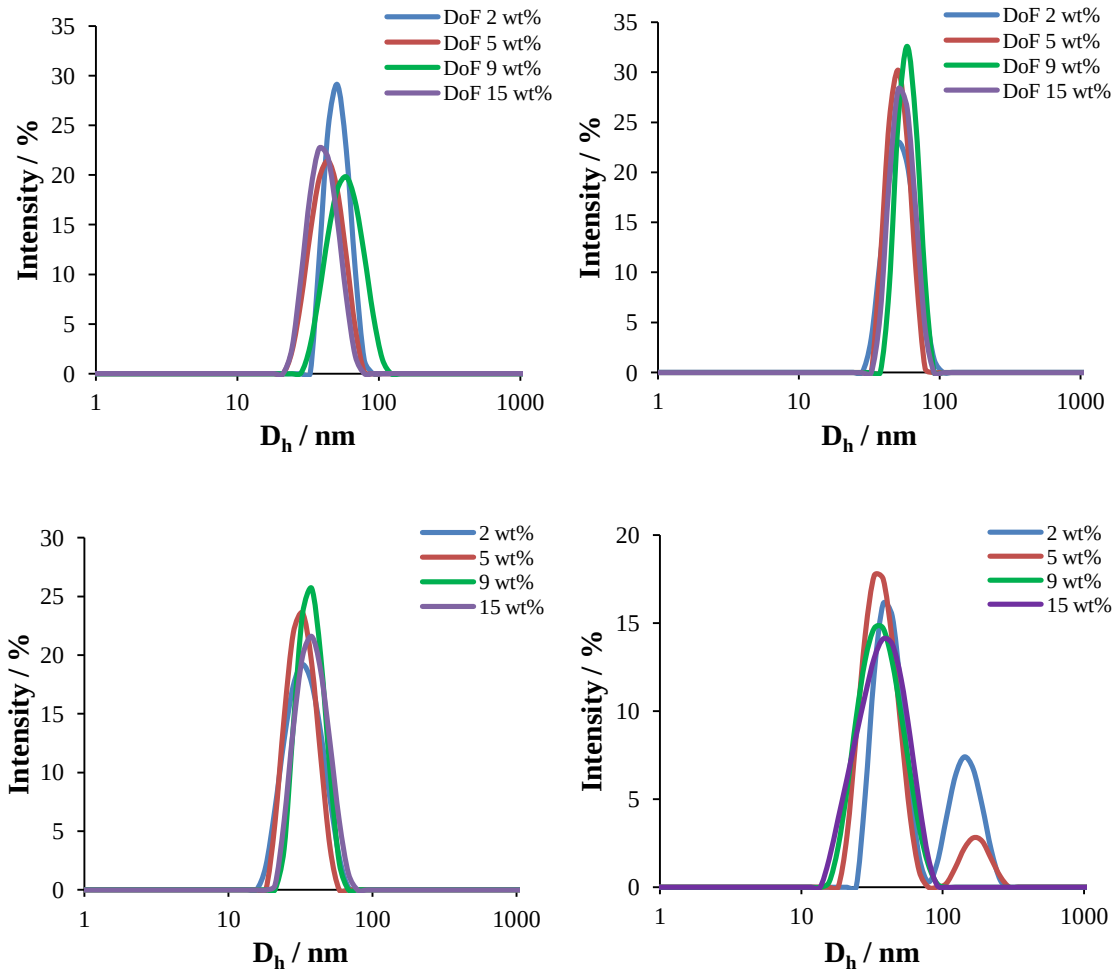

Figure 4.22. DLS traces of PEMA, P^{n}BuMA, P^{t}BuMA and PLMA nanogels with 0.5 wt% CLD and a range of DoFs

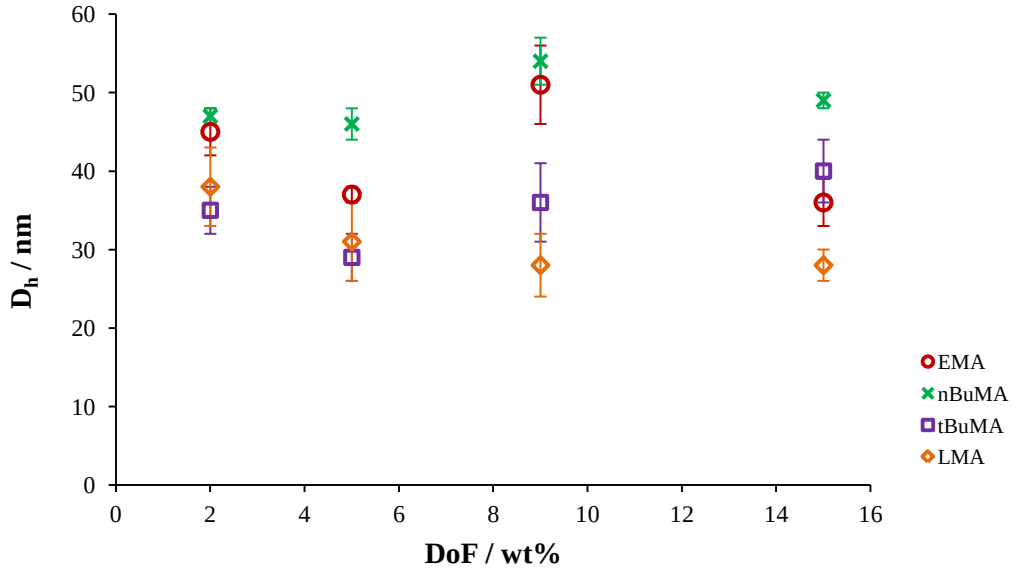

Figure 4.23. Size of more hydrophobic nanogels with 0.5 wt% CLD and catalyst DoF in the range 2-15 wt%, determined by DLS

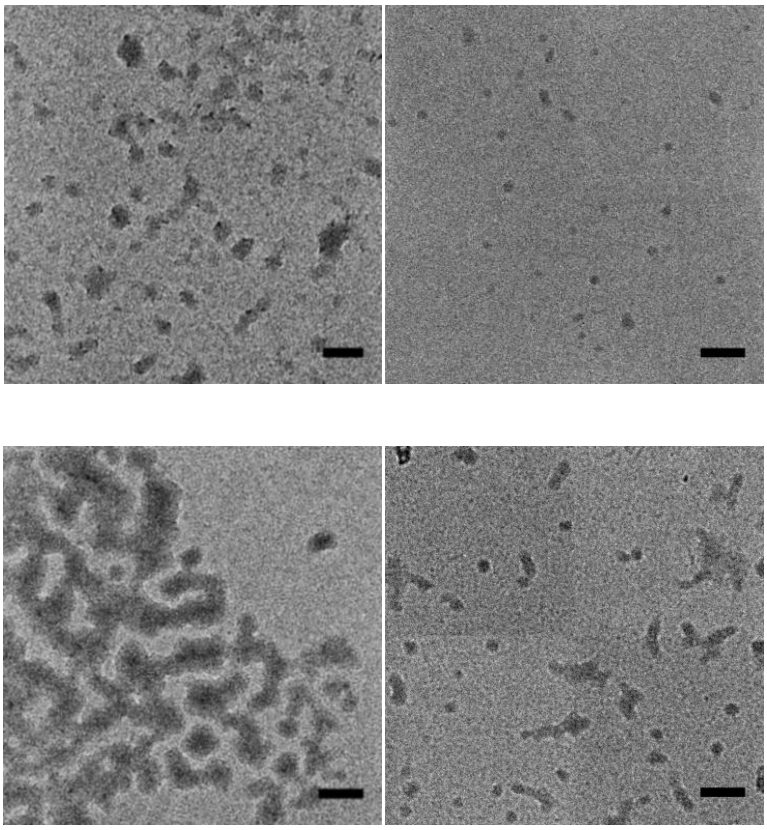

Figure 4.24. Unstained TEM images of PEMA (D_{av} = 35 ± 5 nm), P^{t}BuMA (D_{av} = 20 ± 4 nm), P^{n}BuMA (D_{av} = 42 ± 6 nm) and PLMA (D_{av} = 22 ± 5 nm) nanogels, 0.5 wt% CLD, 2 wt% DoF, scale bar = 100 nm

Swelling experiments, similar to those previously discussed for the PMMA nanogels, were also carried out for the more hydrophobic nanogels, with 2 wt% DoF and 0.5 wt% CLD (Figure 4.25). The greatest change in D_h was observed for the PEMA and P^{n}BuMA nanogels, with a 40 and 38 nm difference respectively, with slightly smaller ones for P^{t}BuMA and PLMA, 25 and 16 nm respectively, which may be reflected in the catalytic activity of the four nanogel systems.

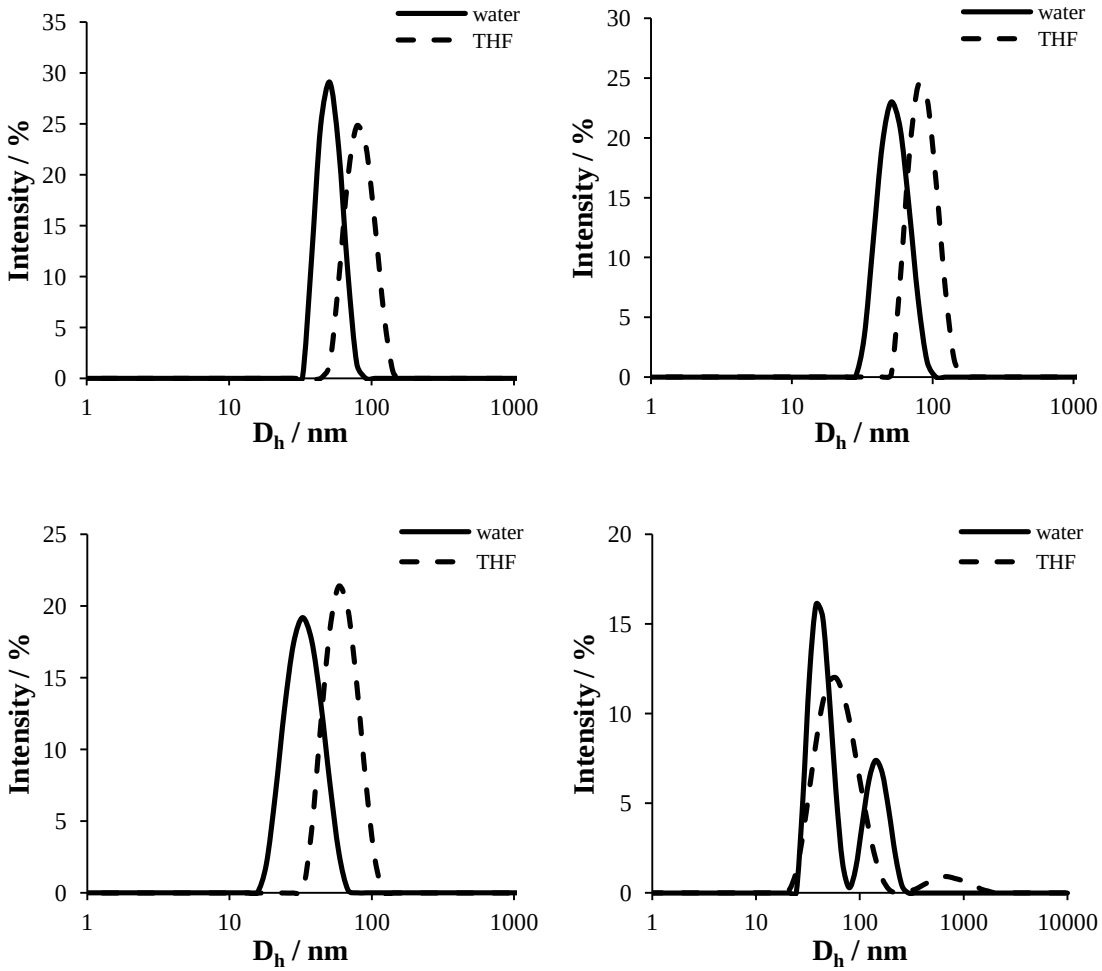

Figure 4.25. DLS traces of E2.05 (45 to 85 nm), ^{n}B2.05 (47 to 85 nm), ^{t}B2.05 (35 to 60 nm) and L2.05 (38 to 54 nm) in water and THF

4.3.4. Catalytic efficiency of nanogels with increased hydrophobicity

Catalysis with the new hydrophobic nanogels was initially carried out with the same concentration of nanogels (i.e. same amount of polymeric material), resulting in different catalyst loadings. This was done to provide a direct comparison to the PMMA nanogel catalyzed reactions, where a dramatic drop in enantioselectivity was observed with increasing DoF. In all cases, however, apart from the lauryl example where there was a reduction in *ee* with increasing DoF (Table 4.8), *ee*s remained generally high. This suggests that the effect of steric hindrance or reduced chiral space with increasing DoF we originally suggested for the PMMA nanogels does not explain the trend in

enantioselectivity. Additionally, we expected the bulkier comonomers to interfere with the catalyst chiral space. The effects of sterics with respect to comonomer will be further discussed in the next section. Thus, we propose the decrease in enantioselectivity with increasing DoF for the PMMA nanogel systems is a result of the more significant change in the hydrophobic-to-hydrophilic balance within the core compared to the more hydrophobic ones.

Table 4.8. The catalytic efficiency of nanogels with 0.5 wt% CLD, a range of DoF and different cores, catalysis carried out at the same concentration of nanoreactors

Core	DoF / %	Catalyst loading / mol%	Conv.[a] / %	*anti/syn* ratio[a]	ee[b] / %	TON[c]
EMA	2	1	99	99/1	99	99
	5	3	97	98/2	99	32
	9	5	95	98/2	99	19
	15	8.5	95	98/2	97	11
^{n}BuMA	2	1	78	99/1	99	78
	5	3	63	99/1	99	21
	9	5	79	97/3	99	16
	15	8.5	78	98/2	99	9
^{t}BuMA	2	1	79	97/3	93	79
	5	3	48	99/1	94	16
	9	5	44	99/1	95	9
	15	8.5	53	99/1	92	6
LMA	2	1	16	95/5	99	16
	5	3	19	96/4	98	6
	9	5	13	95/5	97	3
	15	8.5	14	98/2	89	2

[a] Determined by ^{1}H NMR spectroscopy (400 MHz,$CDCl_3$) after 24 hours, reactions carried out in triplicate, determined conversion is an average
[b] Determined by HPLC, ChiralPak IA, hexane:propan-2-ol:ethanol 80:10:10, 1 mL.min^{-1}
[c] Defined as the moles of substrates converted into product by one mole of catalyst at a given time (in this case 24 hours)

In terms of overall catalytic activity, this seems to broadly decrease with increasing steric hindrance (ethyl > ^{n}butyl > ^{t}butyl), though with PLMA nanogels demonstrating a dramatically lower catalytic activity with a small drop in *ee* with increasing DoF (Figure 4.26, Table 4.8). Although the weight percentage of functional monomer to comonomer was kept constant, taking into account the molecular weight of LMA (254.41 g.mol^{-1}) compared to EMA (114.14 g.mol^{-1}), the final molar concentration of catalyst is different. In other words, the LMA nanogels will contain a higher concentration of catalyst compared to EMA nanogels and can account for the difference in activity observed. The difference in T_g of the polymer may also have a significant effect on the overall catalytic activity, which in these cases decreases with increasing hydrophobicity.

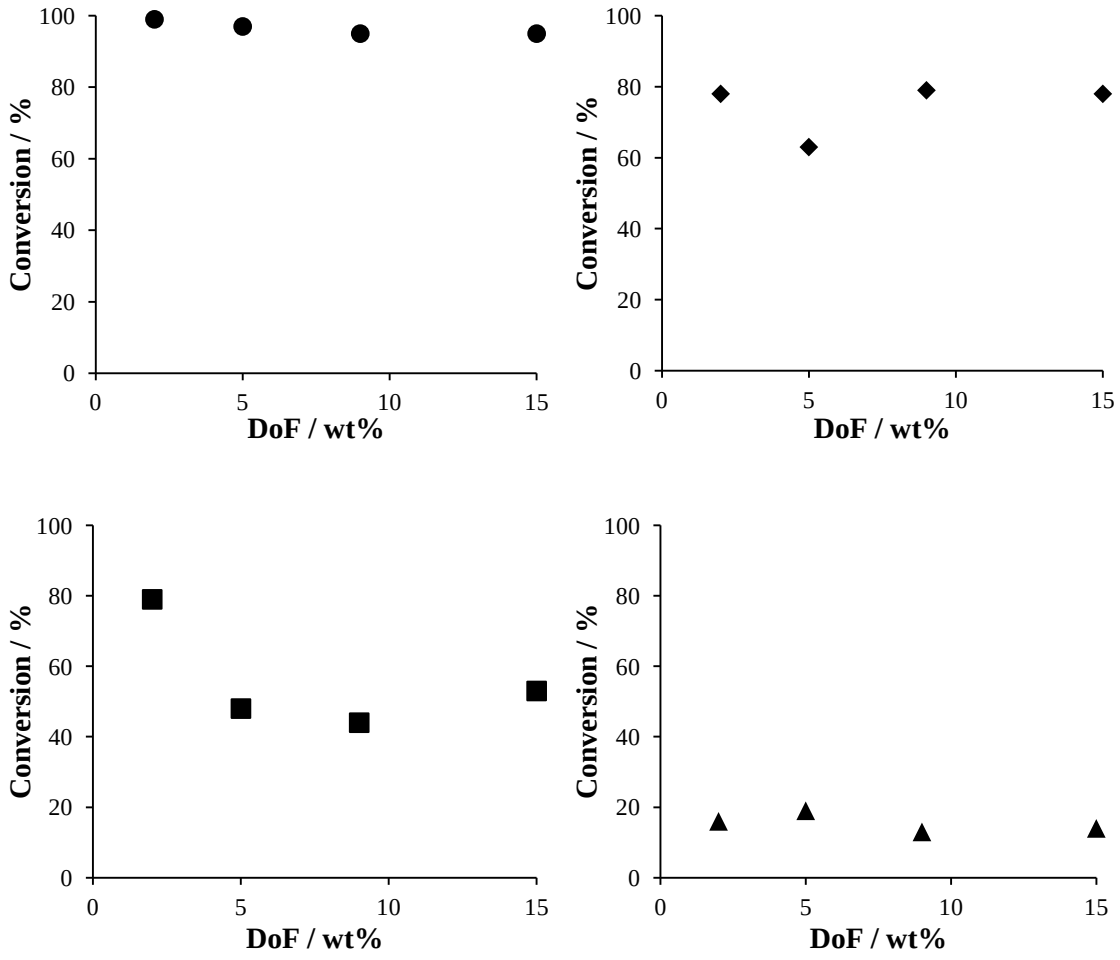

Figure 4.26. Catalytic efficiency of PEMA, P^{n}BuMA, P^{t}BuMA and PLMA, carried out at the same concentration of nanoreactors

By this point, it was clear that the PEMA systems were the most exciting ones yet, as reactions catalyzed by the entire range of nanogels reached near completion after 24 hours and with excellent enantioselectivities across the board. Therefore, reaction progress was followed by ^{1}H NMR spectroscopy to determine the rate and interestingly, E15.05 nanogels were found to catalyze the reaction slightly more efficiently than E2.05 when carried out at the same concentration of nanoreactors (Figure 4.27). Nevertheless, comparable conversions were achieved after 24 hours and in terms of absolute TON, the E2.05 functionalized polymer is working more efficiently.

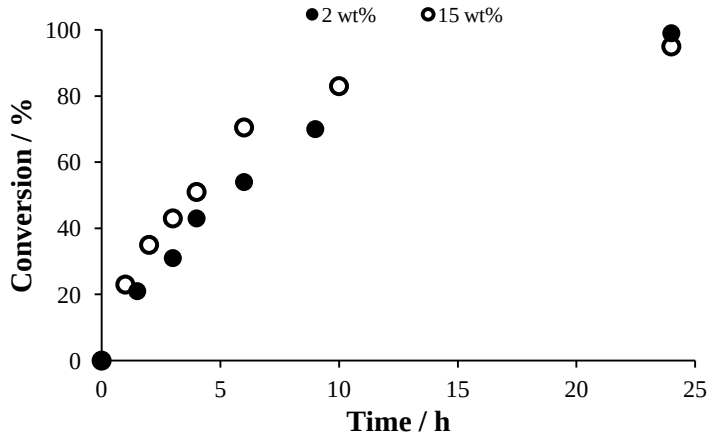

Figure 4.27. Reaction progress catalyzed by E2.05 and E15.05 carried out at the same concentration of nanoreactors

4.3.4.1. Effect of steric hindrance

The influence of steric bulk contributed by the comonomer will be further discussed, using the two BuMA nanogels as comparitors. Given the difference in sterics of *n*butyl and *t*butyl we had previously rationalized that this might result in different hydrophobic environments for catalysis, which might then be reflected in their activity and selectivity. The catalytic results suggest that P*n*BuMA nanogels are much more efficient (higher conversions) and provide a slight advantage in enantioselectivity compared with

P^{t}BuMA nanogels at DoF ≤ 5 wt%, indicating that steric crowding may play a role in the both activity and selectivity of the tethered catalyst (Figure 4.28). The P^{n}BuMA nanogels at 2 through to 15 wt% DoF showed similar activities and excellent enantioselectivities, indicative of a great system, closest in comparison to the PEMA nanogel systems. This shows that adding one extra CH_2 to the comonomer (from PMMA to PEMA) did not significantly decrease the efficiency of the nanogels. The ^{t}butyl version on the other hand, is a bulkier monomer, which is reflected in the activity (at DoF > 5 wt%) and selectivity in all cases to a small extent. Interestingly, the activity at low DoF, i.e. 2 wt%, was comparable to the P^{n}BuMA nanogel, again illustrating the greater efficiency of nanogels with low DoF whereas at higher DoF, the activity dropped significantly compared with P^{n}BuMA. We propose this is a direct reflection of the increased steric bulk around the catalytic sites of ^{t}BuMA compared to ^{n}BuMA, a hypothesis which is further supported by the considerably lower catalytic activity reported for the PLMA nanogels, which are bulkier again than the ^{t}BuMA congener. Unfortunately, the T_gs of the two systems were not determined and thus its effect on the activity, as an alternative explanation to only sterics cannot be elucidated.

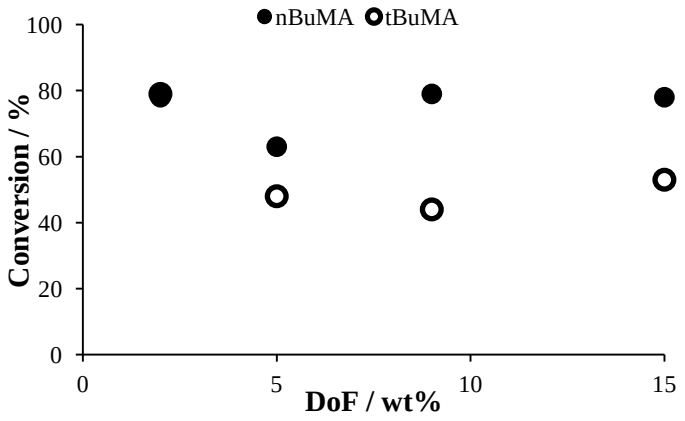

Figure 4.28. Comparing the catalytic efficiency of the P^{n}BuMA and P^{t}BuMA nanogels at different DoF

4.3.5. Synthesis and characterization of double hydrophobic core-shell nanogels

As previously discussed, the exact effect of water in aldol reactions catalyzed by L-proline is still not completely known, though most report suggests that a small amount of water is beneficial for both the catalyst activity and selectivity.[44, 46, 49] In terms of this project, the difference in catalyst selectivity when tethered to a PMMA scaffold *versus* a more hydrophobic scaffold such as PEMA is more prominent at higher DoFs. We hypothesize that this is an effect of changes in core hydrophobicity with the introduction of more catalyst functionality, which is hydrophilic in nature. This was evidenced through the selectivity dropping off with increasing DoF and we therefore sought to introduce a hydrophobic shell around the PMMA nanogel core, with the highest DoF, i.e. 15 wt%, where we saw the greatest drop in selectivity.

We proposed that by introducing a hydrophobic shell around the core, water should be more efficiently excluded from the core and catalytic functionalities thus shielded from the surrounding aqueous environment. This should in theory enhance the enantioselectivity of the catalyst by changing the absolute volume of water that is absorbed. Nevertheless, a drop in activity was expected with the introduction of a hydrophobic shell, as the concentrator effect is no longer an effect of just the core, but for the entire nanoreactor system. Two different types of shells, PEMA and P^{t}BuMA, which are both more hydrophobic than PMMA core, were introduced and some retention of the substrates in the shell was expected. The PMMA nanogels with a PEMA shell will be referred to as CS.M/E and P^{t}BuMA shell as CS.M/B.

The double hydrophobic CS nanogels were synthesized as detailed above and DLS was used to confirm the successful addition of the hydrophobic shell (0.5 wt% CLD), as a small increase in D_h was expected (Figure 4.29). The following increase in particle D_h

was observed: M2.05 23 to 27 nm, M5.05 28 to 30 nm, M9.05 42 to 44 nm and M15.05 49 to 50 nm. Small increases in D_h was expected as both the core and shell are hydrophobic and thus in a collapsed state. Similarly to previous core-shell nanogels, ^{1}H NMR spectroscopy was not used to confirm the addition of the shell due to the cross-linked nature of the particles.

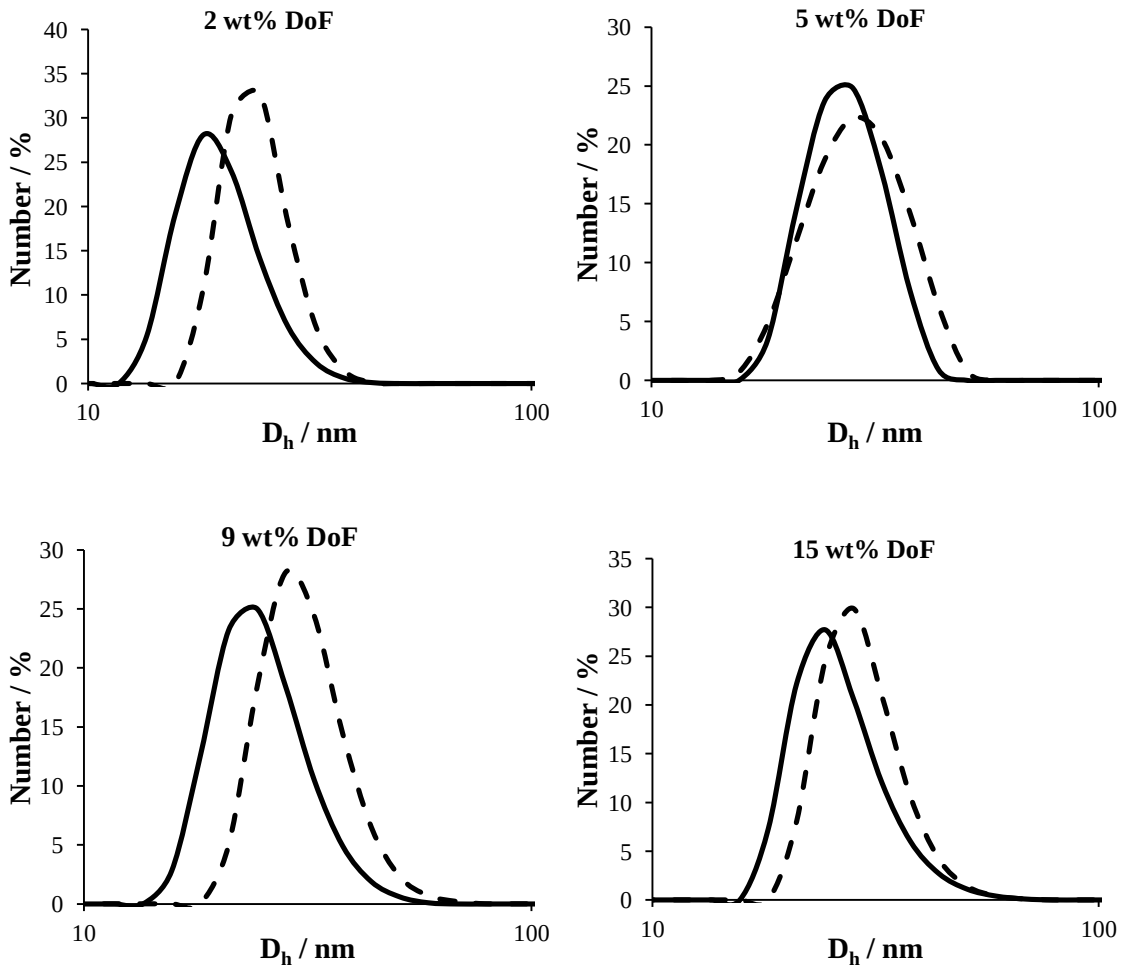

Figure 4.29. DLS traces of original PMMA nanogels and the corresponding double hydrophobic CS.M/E

CS.M/B double hydrophobic nanogels were similarly characterized by DLS and confirmed the successful addition of the P^{t}BuMA shell to the original functional PMMA nanogel. The D_h of the original nanogels and their corresponding core-shell nanogels

were determined as follows: M2.05 23 to 27 nm, M5.05 28 to 32 nm, M9.05 42 to 45 nm and M15.05 49 to 52 (Figure 4.30).

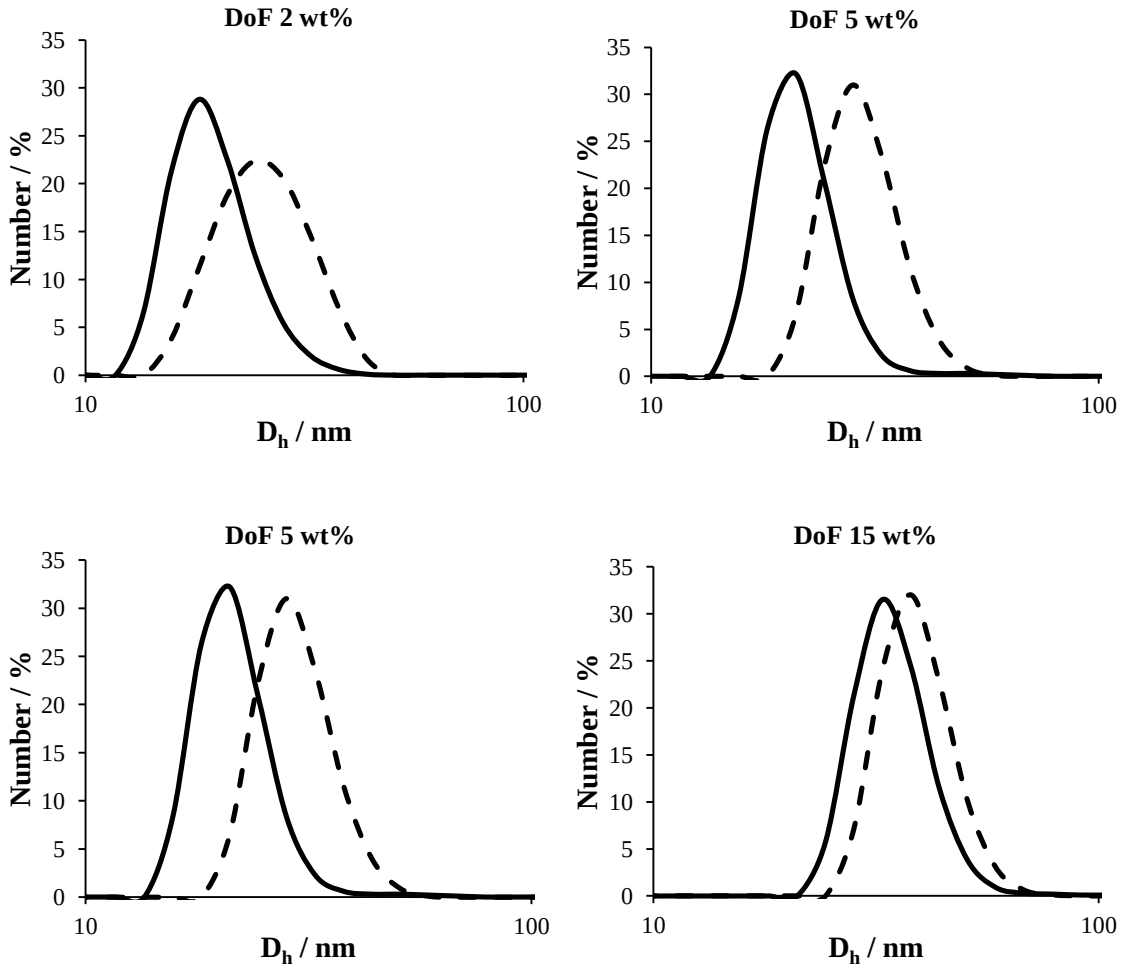

Figure 4.30. DLS traces of original PMMA nanogels and the corresponding double hydrophobic CS.M/B

4.3.6. Catalytic efficiency of double hydrophobic core-shell nanogels

4.3.6.1. CS.M/E

The double hydrophobic CS nanogels were then used to catalyze the aldol reaction between 4-nitrobenzaldehyde and cyclohexanone. In order to keep substrate concentration the same as previous reactions, the catalyst loading of CS reactions had to be halved because the presence of the additional shell effectively halves the amount of

catalytic moieties in same volume of nanogels. Therefore, TON will be used to represent the efficiency of the CS nanogels when compared to the original PMMA nanogels. As we had predicted, the turn over numbers were reduced in all cased but more importantly, we were delighted to see that a great improvement in enantioselectivity was observed, with all ees now up in the high 90s (Table 4.9). This confirms the importance of the hydrophobic-hydrophilic balance around the catalytic site. We propose therefore, that our original hypothesis has been supported and the additional hydrophobic EMA shell does indeed effectively shield the core from the surrounding aqueous environment, thus blocking too much water from entering the catalytic core.

Table 4.9. Catalytic activity of double hydrophobic CS.M/E nanogels at different catalyst loadings

Catalyst loading / mol%	Conv.[a] / %	*anti/syn* ratio[a]	ee[b] / %	TON[c]
0.5	30	98/2	98	59
1.5	55	98/2	96	37
2.5	28	97/3	98	11
4.25	44	93/7	99	10

[a] Determined by ^{1}H NMR spectroscopy (400 MHz, $CDCl_3$) after 24 hours, reactions carried out in triplicate
[b] Determined by chiral HPLC, ChiralPak IA, hexane:propan-2-ol:ethanol 80:10:10, 1 mL.min^{-1}
[c] Defined as the moles of substrates converted into product by one mole of catalyst at a given time (in this case 24 hours)

4.3.6.2. CS.M/B

Similarly, the reaction was catalyzed by the second set of double hydrophobic CS.M/B nanogels, at a variety catalyst loadings. The concentration of nanoreactors is comparable to the reactions catalyzed by CS.M/E nanogels, but again not comparable to the reactions catalyzed by the original core. The activity of these CS nanogels is highly comparable to that observed for CS.M/E and pleasingly, high enantioselectivity was

observed, all in the 90s, further supporting the importance of the hydrophobic environment around the catalytic sites (Table 4.10).

Table 4.10. Catalytic activity of double hydrophobic CS.M/B nanogels at different catalyst loading

Catalyst loading / mol%	Conv.[a] / %	*anti/syn* ratio[a]	ee[b] / %	TON[c]
0.5	31	99/1	92	62
1.5	33	99/1	94	22
2.5	33	99/1	92	13
4.25	34	98/2	96	8

[a] Determined by ^{1}H NMR spectroscopy (400 MHz, $CDCl_3$) after 24 hours, reactions carried out in triplicate
[b] Determined by chiral HPLC, ChiralPak IA, hexane:propan-2-ol:ethanol 80:10:10, 1 mL.min^{-1}
[c] Defined as the moles of substrates converted into product by one mole of catalyst at a given time (in this case 24 hours)

4.4. Conclusion

A selection of L-proline containing hydrophobic nanogels has been successfully synthesized using emulsion polymerization. The effect of CLD and DoF on the catalytic efficiency of L-proline functionalized PMMA nanogels in a model aldol reaction was carefully investigated. An increase in DoF was found to have a significant effect on the enantioselectivity of the catalyst at low CLD which was attributed to the increasing hydrophilic nature of the nanogels with increasing percentage of catalytic moieties. The same trend was not observed for nanogels with higher CLD which we propose it due to the more compact nature of the nanogel, hence providing a more protective hydrophobic environment. The enantioselectivity was also maintained when the catalyst was functionalized within more hydrophobic nanogels, supporting our previous observations. Interestingly, the PEMA nanogels showed the highest activity and

selectivity and further increasing the hydrophobic nature of the nanogel did not result in higher activity which was attributed to increasing steric hindrance.

4.5. Experimental

4.5.1. Materials

Para-toluenesulfonic acid monohydrate was purchased from Alfa Aesar. All other chemicals used were purchased from Sigma-Aldrich. MMA, EMA, ^{n}BuMA, ^{t}BuMA and LMA were filtered through a basic aluminium oxide column prior to use. 4-Nitrobenzaldehyde was filtered through a silica column prior to use. All other reagents were used without further purification.

4.5.2. Instrumentation

^{1}H NMR spectra were recorded at 400 MHz on a Bruker DPX 400 FT-NMR spectrometer using deuterated solvents. Chemical shifts are reported as δ in parts per million relative to $CHCl_3$ (7.26 ppm) or CD_3OD (3.31 ppm) as the internal standard. Dialysis tubing was purchased from Spectrum labs with MW cut off of 6-8 and 12-14 kDa. HPLC analysis was performed on a Varian 920-LC on a chiral column, Chiralpak IA (150 mm × 4.6 mm × 5 µm) with guard cartridge (Chiralpak 5 µm) purchased from Chiral Technologies Europe. Hydrodynamic diameters (D_h) and size distributions of nanogels were determined by DLS on a Malvern Zetasized Nano ZS instrument operating at 25 °C with a 4 mW He-Ne 633-nm laser module. Measurements were made at a detection angle of 173° (back scattering) and the data was analyzed using Malvern DTS 6.20. All determinations were made in triplicate (with 12 runs recorded for each measurement). TEM samples were prepared by drop deposition onto copper/carbon grids that had been treated with oxygen plasma to increase surface hydrophilicity and examined with a transmission electron microscope (JEOL TEM-2100), operating at 200

kV. Micrographs were collected at magnifications varying from 30 K to 100 K and calibrated digitally.

4.5.1. Synthesis of L-proline functionalized methacrylate monomer

A representative procedure for the synthesis of the L-proline functionalized methacrylate monomer[28] (**3.4**) is given in Chapter 3.

4.5.2. Synthesis of hydrophobic functional nanogels

A representative synthetic procedure is as follows for a functional nanogel with 0.5 wt% CLD and 2 wt% DoF: the surfactant SDS (0.125 g) was dissolved in nanopure water (50 mL) and purged with nitrogen. The cross-linker, ethylene glycol dimethacrylate (EGDMA) (0.0023 mL) was added to the SDS/water solution under nitrogen. The functional monomer **3.4** (0.01 g) and the comonomer MMA (0.5 mL) were added to the solution under constant stirring. The polymerization mixture was allowed to stir under nitrogen for 10 minutes. Finally, the initiator potassium persulfate (KPS, 0.005 g) was added and the reaction flask was immersed into a pre-heated oil bath set to 70 °C. The reaction was allowed to stir for 12 hours under continuous stirring at 800 rpm. The polymerization was quenched by cooling in room temperature and exposure to oxygen. The hydrophobic nanogels were purified by dialysis against nanopure water, removing excess SDS.

4.5.3. Synthesis of double hydrophobic core-shell nanogels

A representative procedure for the core-shell nanogel synthesis is as follows (shell 0.5 wt% CLD): the previously synthesized hydrophobic nanogels (25 mL) was stirred and heated at 70 °C under nitrogen. SDS (0.063 g) was dissolved in nanopure water (25 mL) and purged with nitrogen. EGDMA (0.0013 mL), hydrophobic monomer (EMA or ^{t}BuMA, 0.266 mL) and the initiator KPS (2.5 mg) was added to the SDS/water solution

under nitrogen. The degassed reaction mixture was added to the heated polymerization seeds using an automated syringe pump, at a rate of 25 $mL.h^{-1}$. The polymerization was allowed to proceed for 12 hours at 70 °C. The polymerization was terminated by exposure to oxygen and cooling to room temperature. The final core-shell nanogels were purified by dialysis against nanopure water to remove excess SDS.

4.5.4. Aldol reactions: a representative procedure

4-Nitrobenzaldehyde (0.038 g, 0.25 mmol, 1 eq) was dissolved in cyclohexanone (0.104 mL, 1 mmol, 4 eq) and added to a solution of the functionalized nanogel (0.0025 mmol, 1 mol%, 2.5 mL). The reaction mixture was sonicated for 5 min and then stirred at RT for 24 hours. The reaction was quenched *via* the addition of THF/acetone (1:5) to induce swelling of the nanogels and thus allowing extraction of the products from the nanogel core into the organic phase. The crude product was characterized by ^{1}H NMR spectroscopy determining the reaction conversion and product diastereomeric *anti/syn* ratio. The crude product was then filtered through a short silica column before the enantiomeric excess (ee) was determined by HPLC (ChiralPak IA, 80:10:10 hexane:propan-2-ol:ethanol, 1.0 $mL.min^{-1}$.

(S)-2-((R)-hydroxyl-(4-nitrophenyl)methyl)-cyclohexan-1-one: ^{1}H NMR (400 MHz, $CDCl_3$): δ = 1.19-2.57 (8H, m, C**H**$_2$), 4.00 (1H, s, O**H**), 4.82 (1-xH, d, J = 4.5 Hz, C**H**, anti), 5.41 (xH, C**H**, syn), 7.44 (2H, d, J = 8.6 Hz, Ar-**H**), 8.15 (2H, d, J = 8.6 Hz, Ar-**H**). ^{13}C NMR (400 MHz, $CDCl_3$): δ = 24.9, 27.0, 36.5, 42.0, 57.0, 74.0, 123.7, 127.9, 147.3, 148.5, 213.3. ESI-MS found: 272.1 ($M+Na^+$) $C_{13}H_{15}NO_4$; expected 249.10. Chiral HPLC: minor enantiomer t_R = 12.4 min, major enantiomer t_R = 18.3 min. This compound has been fully characterized by others.[32, 50-53]

4.6. References

1. P. Cotanda, A. Lu, J. P. Patterson, N. Petzetakis and R. K. O'Reilly, Macromolecules, 2012, 45, 2377.

2. H. A. Zayas, A. Lu, D. Valade, F. Amir, Z. Jia, R. K. O'Reilly and M. J. Monteiro, *ACS Macro Lett.*, 2013, **2**, 327.

3. A. Lu, P. Cotanda, J. P. Patterson, D. A. Longbottom and R. K. O'Reilly, *Chem. Commun.*, 2012, **48**, 9699.

4. Z. Ge, D. Xie, D. Chen, X. Jiang, Y. Zhang, H. Liu and S. Liu, *Macromolecules*, 2007, **40**, 3538.

5. B. Helms, C. O. Liang, C. J. Hawker and J. M. J. Fréchet, *Macromolecules*, 2005, **38**, 5411.

6. Y. Lu, Y. Mei, M. Drechsler and M. Ballauff, *Angew. Chem. Int. Ed.*, 2006, **45**, 813.

7. Y. Wang, G. Wei, F. Wen, X. Zhang, W. Zhang and L. Shi, *J. Mol. Catal. A: Chem.*, 2008, **280**, 1.

8. G. Wang, K. Kuroda, T. Enoki, A. Grosberg, S. Masamune, T. Oya, Y. Takeoka and T. Tanaka, *Proc. Natl. Acad. Sci. U.S.A*, 2000, **97**, 9861.

9. Y. Wang, J. Zhang, W. Zhang and M. Zhang, *J. Org. Chem.*, 2009, **74**, 1923.

10. G. Wei, W. Zhang, F. Wen, Y. Wang and M. Zhang, *J. Phys. Chem. C*, 2008, **112**, 10827.

11. T. Terashima, A. Nomura, M. Ito, M. Ouchi and M. Sawamoto, *Angew. Chem. Int. Ed.*, 2011, **50**, 7892.

12. T. Terashima, A. Nomura, M. Ouchi and M. Sawamoto, *Macromol. Rapid Commun.*, 2012, **33**, 833.

13. H. Siddique, L. G. Peeva, K. Stoikos, G. Pasparakis, M. Vamvakaki and A. G. Livingston, *Ind. Eng. Chem. Res.*, 2012, **52**, 1109.

14. K. Y. Cho, J.-W. Choi, S.-H. Lee, S. S. Hwang and K.-Y. Baek, *Polym. Chem.*, 2013, **4**, 2400.

15. G. M. Eichenbaum, P. F. Kiser, A. V. Dobrynin, S. A. Simon and D. Needham, *Macromolecules*, 1999, **32**, 4867.

16. X. Qiu, S. Leporatti, E. Donath and H. Möhwald, *Langmuir*, 2001, **17**, 5375.

17. K. Ogawa, B. Wang and E. Kokufuta, *Langmuir*, 2001, **17**, 4704.

18. D. C. González-Toro, J.-H. Ryu, R. T. Chacko, J. Zhuang and S. Thayumanavan, *J. Am. Chem. Soc.*, 2012, **134**, 6964.

19. J.-Y. Kim, J.-Y. Song, E.-J. Lee and S.-K. Park, *Colloid Polym. Sci.*, 2003, **281**, 614.

20. T. E. Kristensen, K. Vestli, K. A. Fredriksen, F. K. Hansen and T. Hansen, *Org. Lett.*, 2009, **11**, 2968.

21. T. E. Kristensen and T. Hansen, *Eur. J. Org. Chem.*, 2010, **17**, 3179.

22. V. Rodionov, H. Gao, S. Scroggins, D. A. Unruh, A.-J. Avestro and J. M. J. Fréchet, *J. Am. Chem. Soc.*, 2010, **132**, 2570.

23. N. Dingenouts, C. Norhausen and M. Ballauff, *Macromolecules*, 1998, **31**, 8912.

24. J. H. Kim and M. Ballauff, *Colloid. Polym. Sci.*, 1999, **277**, 1210.

25. W. McPhee, K. C. Tam and R. Pelton, *J. Colloid Interface Sci.*, 1993, **156**, 24.

26. C. S. Chern, *Prog. Polym. Sci.*, 2006, **31**, 443.

27. R. Arshady, *Colloid. Polym. Sci.*, 1992, **270**, 717.

28. T. E. Kristensen, K. Vestli, M. G. Jakobsen, F. K. Hansen and T. Hansen, *J. Org. Chem.*, 2010, **75**, 1620.

29. C. D. Jones and L. A. Lyon, *Macromolecules*, 2003, **36**, 1988.

30. P. Hazot, J. P. Chapel, C. Pichot, A. Elaissari and T. Delair, *J. Polym. Sci., Part A: Polym. Chem.*, 2002, **40**, 1808.

31. A. Lu, T. P. Smart, T. H. Epps, D. A. Longbottom and R. K. O'Reilly, *Macromolecules*, 2011, **44**, 7233.

32. M. Gruttadauria, F. Giacalone, A. Mossuto Marculescu, P. Lo Meo, S. Riela and R. Noto, *Eur. J. Org. Chem.*, 2007, **2007**, 4688.

33. D. Font, C. Jimeno and M. A. Pericàs, *Org. Lett.*, 2006, **8**, 4653.

34. M. Benaglia, G. Celentano and F. Cozzi, *Adv. Synth. Catal.*, 2001, **343**, 171.

35. B. List, *Tetrahedron*, 2002, **58**, 5573.

36. A. C. Evans, A. Lu, C. Ondeck, D. A. Longbottom and R. K. O'Reilly, *Macromolecules*, 2010, **43**, 6374.

37. I. Varga, T. Gilányi, R. Mészáros, G. Filipcsei and M. Zrínyi, *J. Phys. Chem. B*, 2001, **105**, 9071.

38. E. Pavlopoulou, G. Portale, K. E. Christodoulakis, M. Vamvakaki, W. Bras and S. H. Anastasiadis, *Macromolecules*, 2010, **43**, 9828.

39. C. D. Jones and L. A. Lyon, *Macromolecules*, 2000, **33**, 8301.

40. J. Dzierzak, E. Bottinelli, G. Berlier, E. Gianotti, E. Stulz, R. M. Kowalczyk and R. Raja, *Chem. Commun.*, 2010, **46**, 2805.

41. E. R. Jarvo and S. J. Miller, *Tetrahedron*, 2002, **58**, 2481.

42. B. List, L. Hoang and H. J. Martin, *Proc. Natl. Acad. Sci. USA*, 2004, **101**, 5839.

43. M. Gruttadauria, A. M. P. Salvo, F. Giacalone, P. Agrigento and R. Noto, *Eur. J. Org. Chem.*, 2009, **31**, 5437.

44. K. Sakthivel, W. Notz, T. Bui and C. F. Barbas, *J. Am. Chem. Soc.*, 2001, **123**, 5260.

45. N. Mase and I. I. I. C. F. Barbas, *Org. Biomol. Chem.*, 2010, **8**, 4043.

46. P. M. Pihko, K. M. Laurikainen, A. Usano, A. I. Nyberg and J. A. Kaavi, *Tetrahedron*, 2006, **62**, 317.

47. Y. Kim, M. H. Pourgholami, D. L. Morris and M. H. Stenzel, *Biomacromolecules*, 2012, **13**, 814.

48. D. Kim, J. M. Caruthers and N. A. Peppas, *Macromolecules*, 1993, **26**, 1841.

49. S. S. Chimni, D. Mahajan and V. V. Suresh Babu, *Tetrahedron Lett.*, 2005, **46**, 5617.

50. F. Giacalone, M. Gruttadauria, P. L. Meo, S. Riela and R. Noto, *Adv. Synth. Catal.*, 2008, **350**, 2747.

51. D. Font, C. Jimeno and M. A. Pericas, *Org. Lett.*, 2006, **8**, 4653.

52. D. Font, S. Sayalero, A. Bastero, C. Jimeno and M. A. Pericas, *Org. Lett.*, 2007, **10**, 337.

53. A. J. A. Cobb, D. M. Shaw, D. A. Longbottom, J. B. Gold and S. V. Ley, *Org. Biomol. Chem.*, 2005, **3**, 84.

5. Recyclable Catalytic Core-Shell and Core-Shell-Corona Cross-linked Nanogels

5.2. Abstract

Core-shell (CS) type cross-linked nanogels with a thermo-responsive PNIPAM shell were synthesized *via* a seeded precipitation polymerization process. Dynamic light scattering (DLS) was used to determine the successful addition of the shell, confirmed by a change in particle size and the thermo-responsive nature of the resulting CS nanogel particle. The catalytic activity of the thermo-sensitive CS nanogels was assessed in a model asymmetric aldol reaction. An enhancement in catalytic activity was observed with increasing temperature which was attributed to the hydrophobic nature of the PNIPAM shell. For comparison, a second type of nanostructures was synthesized with a core-shell-corona (CSC) morphology. Interestingly, the collapse of the linear corona at elevated temperatures blocked access to the catalytic core and a dramatic drop in activity was observed. The effect of degree of catalyst functionalization (DoF) and thus concentration of CS nanogels on the catalytic activity was further explored.

5.3. Introduction

The hydrophobic cavity of core-shell nanostructures in water has been used to accommodate a range of lipophilic molecules such as dyes and drugs.[1-4] The introduction of a catalytic functionality within this cavity, such as a transition metal or organocatalyst has yielded highly efficient nanoreactors.[5-9] The polymer scaffold is able to protect the catalyst from the surrounding aqueous environment and enhanced catalytic activity has been observed as a result of hydrophobic and concentrator effects.[10, 11] Although, catalyst loading has been significantly lowered in majority of these systems, it is still highly desirable to design a readily recyclable nanoreactor

system. PNIPAM is a well-studied thermo-responsive polymer with a lower critical solution temperature (LCST) of approximately 32 °C,[12-14] a property which has been utilized in a number of recyclable catalytic systems where recovery is usually achieved by precipitation at elevated temperatures.[15, 16] In contrast, Urbani and Monteiro[17] utilized the solubility of PNIPAM in water at low temperatures for the recovery of their nanoreactors. Their system was based on the responsive PNIPAM and the permanently hydrophilic poly(dimethylacrylamide) (PDMA). Core-shell nanostructures were formed at elevated temperatures with a hydrophobic cavity able to sequester lipophilic molecules and fully soluble polymers were once again obtained by cooling the system below the LCST, releasing the lipophilic molecules. This design has been used to successfully mediate the polymerization of styrene in aqueous media.

Cross-linked PNIPAM microgels have also been used as intelligent microreactors where the reversible hydrophobic nature of PNIPAM as a response to temperature has been used to control access of substrates into the catalytic core. In some cases, enhanced catalytic activity was observed at elevated temperatures as substrate uptake was increased as a result of the hydrophobic nature of PNIPAM.[18-24] Nevertheless, the opposite has also been reported where the collapse of PNIPAM at elevated temperatures instead blocked the catalytic sites and thus nanoreactor activity.[25-32] Several groups have successfully taken advantage of both the hydrophilic and hydrophobic property of PNIPAM, allowing catalysis of hydrophilic and hydrophobic substrates by simply tuning the temperature of the system.[33-35]

We wanted to expand on this by synthesizing thermo-responsive core-shell (CS) nanogels and investigate the catalytic activity and selectivity dependency on temperature. This was achieved by synthesizing a thermo-responsive PNIPAM shell on our hydrophobic nanogel, following a well-established seeded precipitation

polymerization procedure.[36-39] Two PNIPAM shells with different morphologies were synthesized to investigate the effect of their collapse on the activity of the core-functionalized catalyst. The first system consisted of a cross-linked PNIPAM shell and the other of a small cross-linked shell and linear PNIPAM polymer chains making up the corona. We hypothesize that the linear PNIPAM chains will collapse in a different manner to the cross-linked PNIPAM network at elevated temperatures and imagine that this will yield two nanoreactor systems with unique and tuneable catalytic efficiencies. The effect of increasing the nanogel concentration by reducing the DoF will also be investigated as this effectively increasing the concentration of hydrophobic material in the reaction.

5.4. Results and Discussion

5.4.1. Synthesis of CS nanogels

The hydrophobic L-proline functionalized PEMA nanogels synthesized in Chapter 4 *via* an emulsion polymerization process was used as the seed in the precipitation polymerization of NIPAM to yield the desired CS nanogels (Scheme 5.1).[36-39] This was first investigated using E15.05 (EMA, 15 wt% DoF, 0.5 wt% CLD) as the hydrophobic core. From this point, CS nanogel with a E15.05 core will be referred to as CS(15) with the number indicating core DoF. CS nanogels were synthesized to double the mass of the original core, making the mass of the shell equal to that of the core.

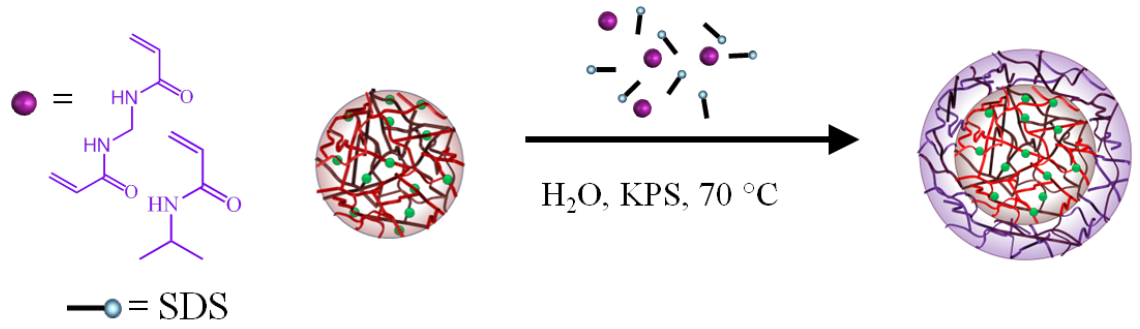

Scheme 5.1. Schematic representation of CS nanogel synthesis *via* a seeded precipitation polymerization process

5.4.2. Synthesis of core-shell-corona (CSC) nanogels

The attempted synthesis of core-shell-corona (CSC) nanogels was carried out in a one-pot-two-step reaction where the first step involved formation of a cross-linked PNIPAM shell (to form a core-shell nanogel) and the second step, growth of linear PNIPAM polymer chains from the cross-linked PNIPAM shell (Scheme 5.2).

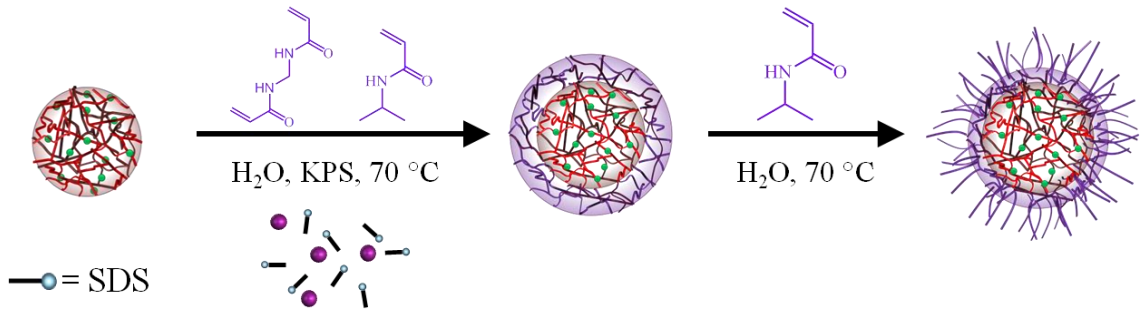

Scheme 5.2. Schematic representation of the proposed one-pot-two-step synthesis of CSC nanogels

The *N,N*'-methylenebisacrylamide (*bis)* cross-linker has been reported to polymerize at a faster rate than NIPAM which results in an uneven distribution of the cross-linker: with higher cross-linking density (CLD) towards the centre of the particle and some dangling 'linear' polymer chains towards the particle periphery.[40] In this case, half the

amount of the desired shell monomer (NIPAM) and all of the cross-linker were added in the first step of the synthesis, after which we believe the cross-linker will be completely consumed. The second batch of monomer was then added and we propose the monomer will continue to polymerize from the already formed PNIPAM shell, yielding the desired CSC morphology in the absence of additional cross-linker, with longer 'linear' polymer chains.

5.4.2.1. Monitoring growth of shell and corona

The growth of the shell and corona during the seeded precipitation polymerization process was monitored by DLS. Due to the temperature-responsive nature of PNIPAM, DLS analysis was carried out at low temperature to ensure PNIPAM is in a swollen state to more readily observed addition of shell/corona. To begin with, D_h of the seed nanogel (E15.05) was determined at 5 °C (57 nm, PDI = 0.084) which changed after 35 minutes in the presence of NIPAM and *bis* to 74 nm (PDI = 0.092) (Figure 5.1), as well as displaying an increase in turbidity. When a change in D_h was no longer observed, indicating complete formation of the cross-linked shell, the second step of the polymerization was initiated. A change in solution turbidity was immediately observed, accompanied by an additional increase in D_h to 128 nm (PDI = 0.178) and subsequently to 161 nm (PDI = 0.232) at 5 °C (Figure 5.1). A final D_h of 175 nm (PDI = 0.236) was observed after dialysis. The successive increase in D_h with time clearly highlights a two step change occurring in the polymerization. We propose that the desired shell/corona morphology is formed; however, it is possible that the second batch of NIPAM monomer simply diffused into the existing shell and continued to polymerize within forming a more densely cross-linked shell.

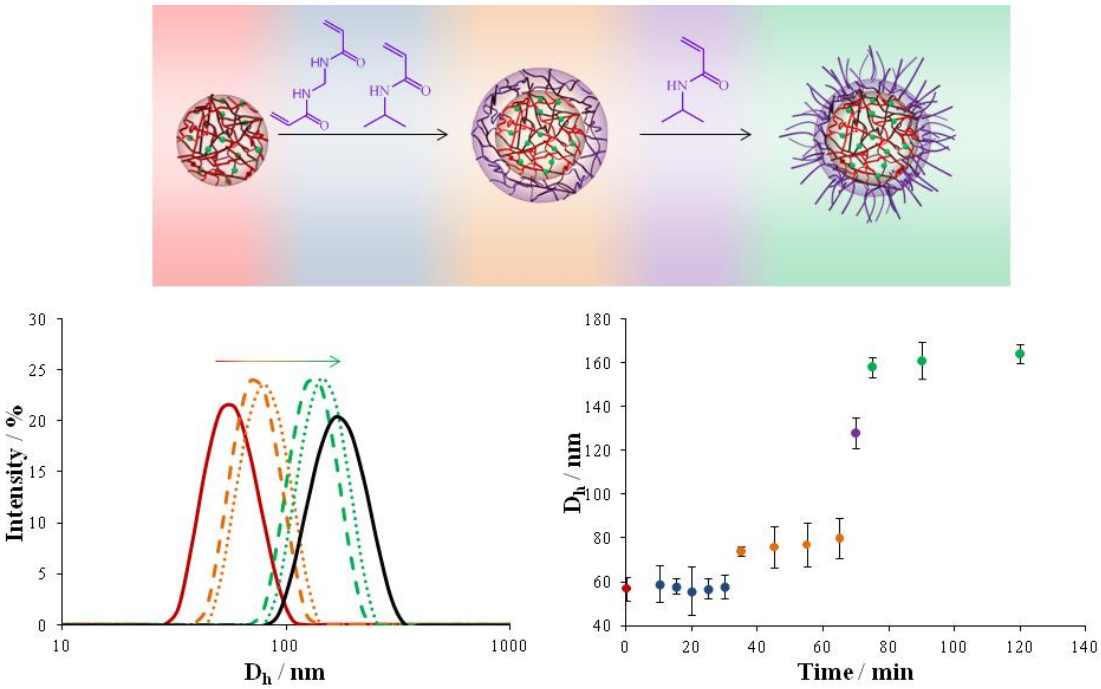

Figure 5.1. Schematic representation of the shell and corona growth (top), representative DLS traces before and after shell/corona addition (bottom left) and change in D_h with time of polymerization (bottom right), both determined at 5 °C

5.4.3. Characterization of CS and CSC nanogels

The change in D_h of nanogels during polymerization of PNIPAM confirmed successful addition of the shell/corona (Figure 5.2). For CS(15) a change in D_h from 35 to 70 nm was observed at 25 °C with CSC(15) showing a similar change from 35 to 88 nm. The PNIPAM shell is expected to be somewhat hydrophilic at this temperature, as it is below the reported LCST for PNIPAM in aqueous media (about 32 °C).[13, 41-43] The temperature-responsive property of the synthesized nanogels was studied and is discussed below.

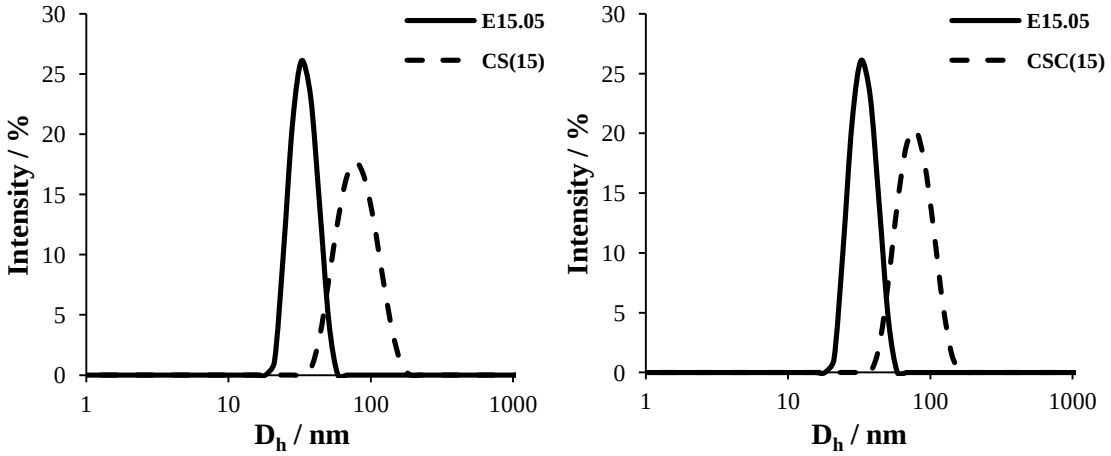

Figure 5.2. DLS traces of core E15.05 nanogel and the corresponding CS(15) (left) and CSC(15) (right) nanogels at 25 °C

The CS and CSC systems were both characterized by dry-state TEM on GO treated grids (Figure 5.3, Figure 5.4).[44] Unfortunately, average diameter (D_{av}) found by TEM for both systems (D_{av} = 39 ± 7 nm and 38 ± 7 nm) was found to be similar in size to the original hydrophobic core (D_{av} = 35 ± 9 nm) than the larger size expected from the CS/CSC structures. However, this is most likely an effect of sample preparation where removal of water from the grid and thus PNIPAM shell will cause it to shrink. The addition of a cross-linked shell has successfully been characterized using cryo-TEM;[45] unfortunately, this has not been possible to carry out on our CS and CSC nanogels at this point due to instrument downtime.

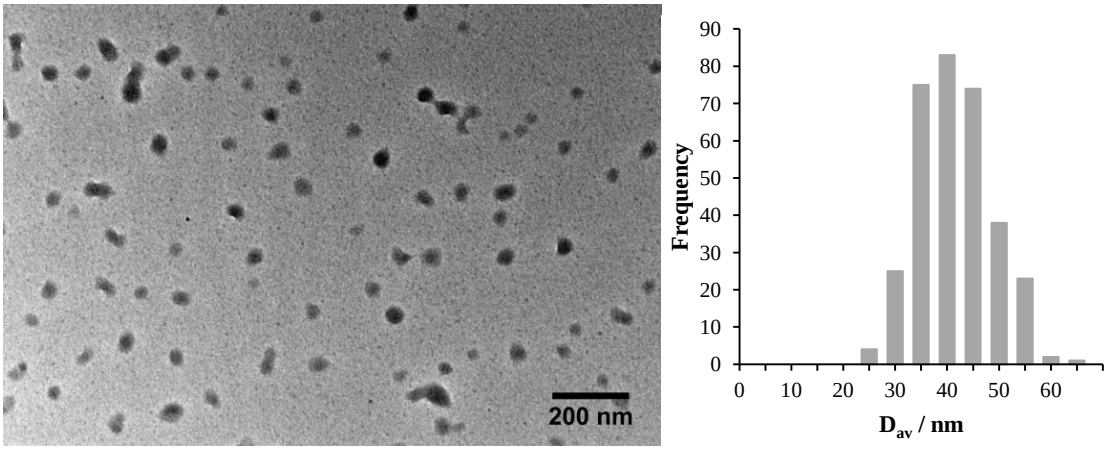

Figure 5.3. GO-TEM image of CS(15), D_{av} = 39 ± 7 nm

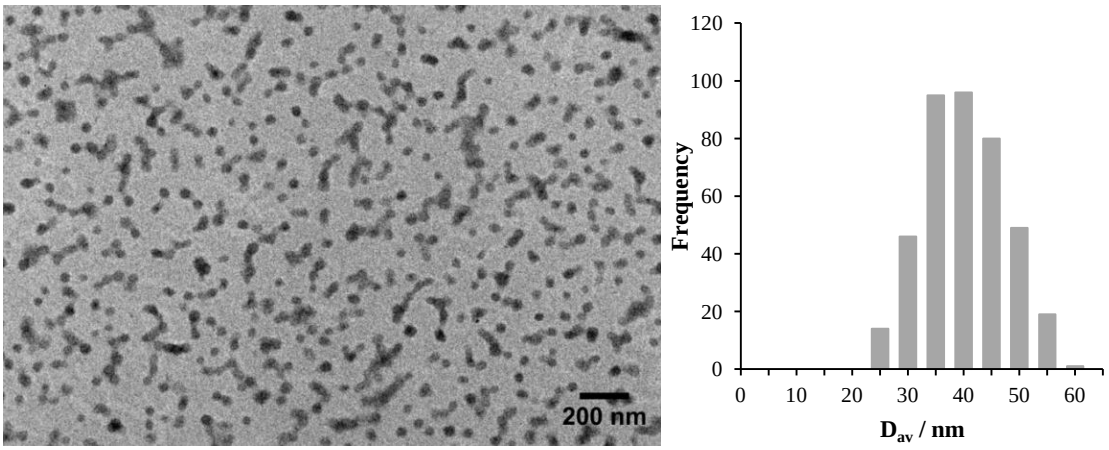

Figure 5.4. GO-TEM image of CSC(15), D_{av} = 38 ± 7 nm

Turbidimetry is often used to determine the cloud point of polymer systems;[46, 47] however, this is highly dependent on polymer molecular weight and concentration. Alternatively, DLS has been successfully used to study the thermo-responsive property of a range of PNIPAM nanostructures.[38, 45, 48-51] By investigating the change in D_h with temperature, the hydrophilic to hydrophobic transition of the PNIPAM can be monitored. At low temperatures, PNIPAM will be fully solvated in the surrounding water and will therefore be in a swollen state with large D_h. However, as the temperature is increased, the solubility of PNIPAM in water decreases and inter-chain association is favoured.[41, 42] As a result, water is expelled from the PNIPAM network resulting in a smaller D_h (Scheme 5.3, Scheme 5.4). We hypothesized that the collapse of linear PNIPAM chains and cross-linked PNIPAM will differ, resulting in two separate temperature transitions. Thus, by using the thermo-responsive property of PNIPAM it may be possible to differentiate between the two PNIPAM morphologies.

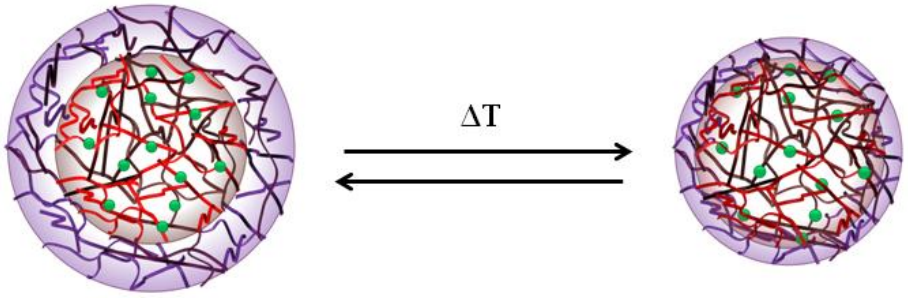

Scheme 5.3.Schematic representation of change in D_h of CS nanogels with temperature

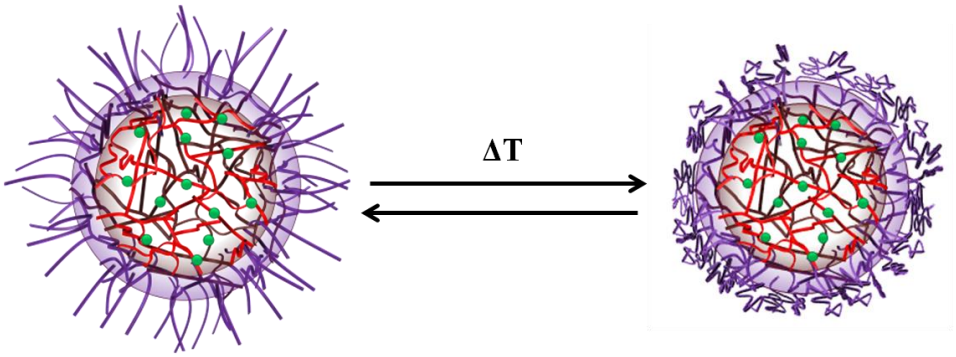

Scheme 5.4. Schematic representation of the proposed collapse of linear PNIPAM corona onto the hydrophobic nanogel core

A change in D_h with temperature was observed for both CS(15) and CSC(15) clearly demonstrating their thermo-responsive property (Figure 5.5). As expected, decreasing D_h was observed with increasing temperature as a result of the collapsed PNIPAM shell and corona.

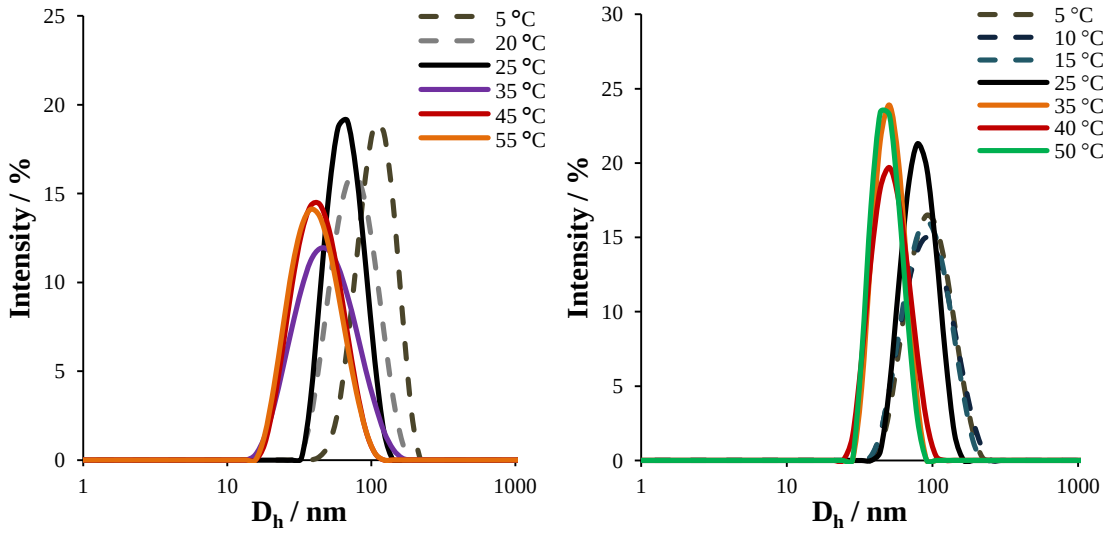

Figure 5.5. Demonstration of change in D_h with temperature of CS(15) (left) and CSC(15) (right) nanogels

By plotting the change in D_h with respect to temperature it is possible to determine the transition temperature of the PNIPAM shell/corona. The change in D_h with temperature is detailed in Figure 5.6 and Table 5.1 and seem to be very similar in nature.

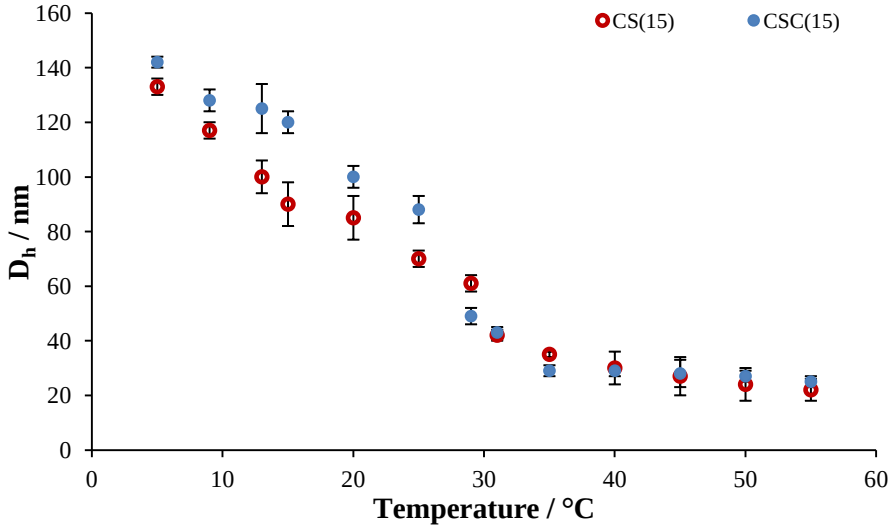

Figure 5.6. Change in D_h with temperature of CS(15) and CSC(15) nanogels, measured in triplicate

Relatively comparable D_hs for both nanogels at 25 °C (70 and 88 nm) and 40 °C (30 and 29 nm) were determined (Table 5.1). Although a significant change in D_h was observed between 20 and 30 °C, the transitions are not as sharp as those previously observed for PNIPAM based systems.[14] Small changes in particle size were observed after 30 °C for both systems, suggesting PNIPAM continues to shrink even up to 55 °C. Comparable transition temperatures have previously been reported for a range of PNIPAM based microgel or nanogel systems.[38, 45, 48-50] However, no significant difference in thermo-responsive property was observed between the two nanogels that would suggest the CS and CSC are different.

Table 5.1. The determined D_h of CS(15) and CSC(15) nanogels at a range of temperatures

CS(15)		CSC(15)	
T / °C	**D_h / nm**	**T / °C**	**D_h / nm**
5	133	5	142
9	117	9	128
13	100	13	125
15	90	15	120
20	85	20	100
25	70	25	88
29	61	29	49
31	42	31	43
35	35	35	29
40	30	40	29
45	27	45	28
50	24	50	27
55	22	55	25

To more accurately determine the transition temperature, the first derivative of the change in D_h was plotted against temperature.[50] The minimum of the graph indicates that the transition temperature determined for CS and CSC nanogels was 30 and 27 °C

respectively (Figure 5.7). In both cases, the transition temperature was lower than the LCST reported for PNIPAM (about 32 °C).[13, 41-43] This may perhaps be attributed to its cross-linked nature.

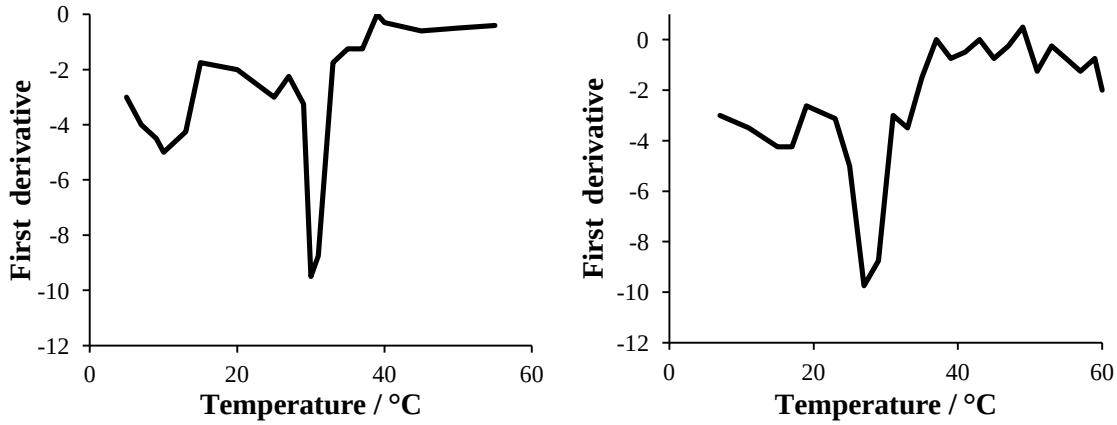

Figure 5.7. The first derivative of change in D_h with temperature to determine the transition temperature of CS(15) (left), CSC(15) (right) nanogels, 30 °C and 27 °C respectively

The reversible swelling and shrinking of the nanogels in response to temperature was investigated by exposing the nanostructures to repeated heating and cooling cycles. For this purpose, three different temperatures were used, 5, 25 and 40 °C. With only a 2 minute equilibrium time at each temperature, relatively comparable particle sizes were achieved throughout two heating and cooling cycles (Figure 5.8), clearly highlighting the stability of the nanostructures in the studied temperature range.

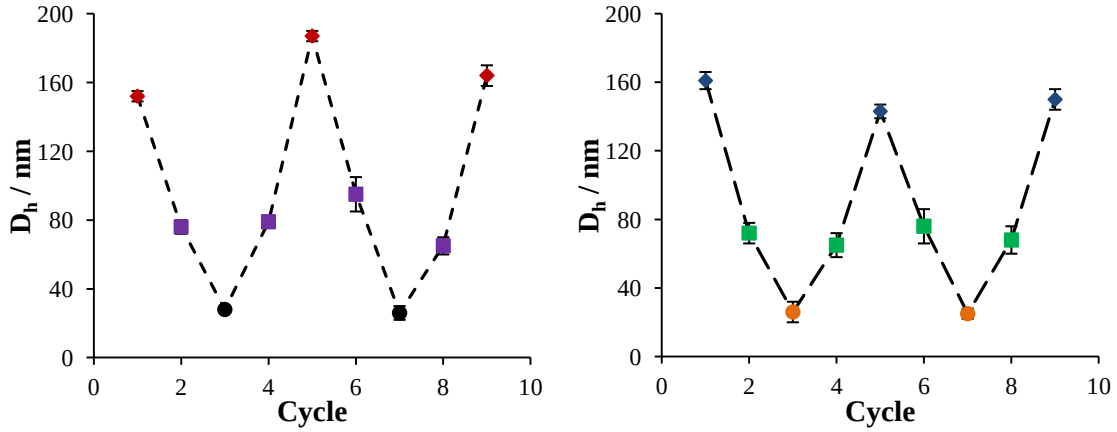

Figure 5.8. Repeated heating and cooling cycles for CS(15) (left) and CSC(15) (right) nanogels at three different temperatures (◊ = 4 °C, □ = 25 °C, ○ = 40 °C)

5.4.4. Catalytic efficiency of CS(15) and CSC(15) nanogels

We next investigated the catalytic activity of the two nanogels in a model asymmetric aldol reaction at three different temperatures, at 4 °C where PNIPAM is hydrophilic and in a solvated (swollen) state, at 25 °C where the transition towards hydrophobic PNIPAM starts to take place and then finally at 40 °C where NIPAM is hydrophobic and in a non-solvated (shrunken) state. We hypothesized that the collapse of cross-linked PNIPAM and linear PNIPAM chains would differ, resulting in different catalytic efficiencies at elevated temperatures (Scheme 5.3, Scheme 5.4).

The reaction between 4-nitrobenzaldehyde and cyclohexanone was once again used as the model reaction, as it has successfully determined the catalytic efficiency of hydrophobic nanogels synthesized in Chapter 4 (Scheme 5.5). Even though this specific reaction has been used to determine the efficiency of a range of supported systems in both organic solvent and water, catalysis at different temperatures is not often investigated.[51-54] This is most likely related to the reduced stability of key transition states at elevated temperatures often resulting in lower selectivities.[55-57]

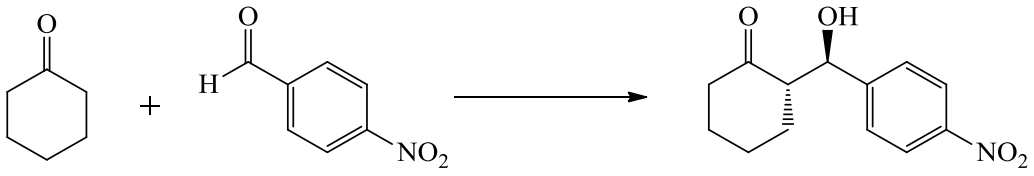

Scheme 5.5. Model aldol reaction where the major (anti-isomer) product for L-proline is shown

5.4.4.1. The effect of temperature on catalytic activity and selectivity

The aldol reactions catalyzed by CS(15) and CSC(15) nanogels were first carried out at 1 mol% catalyst loading at a range of temperatures, where it was revealed that the two nanogels did indeed exhibit a temperature dependent catalytic activity. At low

temperatures (swollen PNIPAM), CSC(15) nanogels showed appreciably greater catalytic activity than the corresponding CS(15) nanogel crossing over at 25 °C to then display the converse behavior, with CS(15) now displaying greater activity than their CSC(15) counterparts. Regarding enantioselectivity, comparable selectivities were found throughout for CSC(15) but reducing with increasing temperature for CS(15) (Table 5.2, Figure 5.9). We attribute the difference in conversion at low temperature to slower diffusion of substrates into CS(15), as a result of the thicker cross-linked shell. The cross-linked PNIPAM network in the CSC system on the other hand is thinner and the linear polymer corona may restrict access comparatively less when totally swollen. Interestingly, catalytic activity were found to be comparable at 25 °C, which is often reported to be the best temperature for L-proline catalyzed reactions, reaching 95% ee in both cases (Table 5.2, entries 2 and 7, Figure 5.9).

The most striking difference in activity is observed above the transition temperature where PNIPAM is hydrophobic and in a shrunken state in both systems. CS(15) followed the expected Arrhenius type dependence on temperature, where an increase in catalytic activity is observed with increasing temperature.[18, 21, 22, 24] We propose this is due to an increase in substrate uptake as a result of the hydrophobic nature of CS(15). A similar increase in activity at elevated temperatures has also been observed for other systems containing PNIPAM.[26, 27, 29] CSC(15) on the other hand did not show the same trend; instead a significant drop in activity at elevated temperatures was observed (Figure 5.9). A decrease in conversion from 50% at 25 °C to 17% at 40 °C was observed. This is consistent with our hypothesis that the linear polymer chains collapse differently to the cross-linked PNIPAM network. The collapse of the linear chains seems to block access to the core rather than help sequester substrates. This effect was further supported by the low activity observed at 50 °C for CSC(15) (Table 5.2). Nevertheless, if a more densely cross-linked shell was formed for CSC(15) rather than

the suggested longer linear chains, it is possible the same decrease in activity would be observed at elevated temperatures. Additional experiments are ongoing to determine the possibility of the second hypothesis.

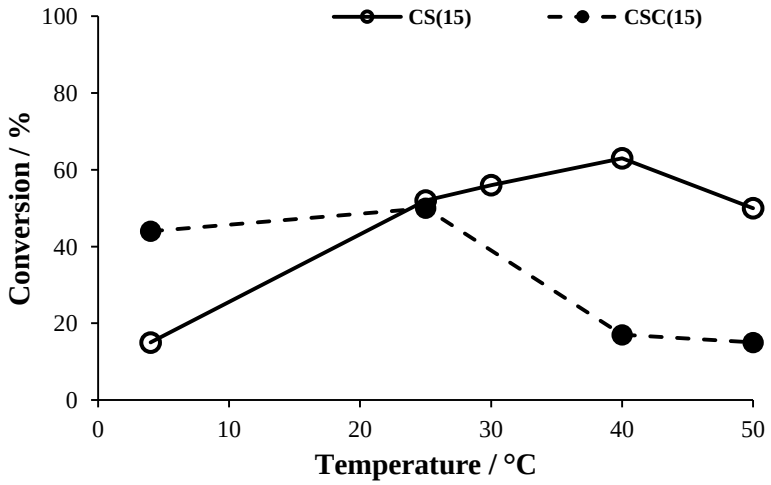

Figure 5.9. The catalytic activity of CS(15) and CSC(15) at 1 mol% catalyst loading and different temperatures

Table 5.2. The catalytic activity and selectivity of CS(15) and CSC(15) at a range of temperatures

Catalyst	Entry	T / °C	D_h[a] / nm	Catalyst loading / mol%	Conv.[b] / %	*anti/syn* ratio[b]	ee[c] / %
CS(15)	1	4	133	1	15	98/2	90
	2	25	70	1	52	97/3	95
	3	30	56	1	56	94/6	96
	4	40	30	1	63	95/5	93
	5	50	24	1	50	90/10	74
CSC(15)	6	4	142	1	44	97/3	92
	7	25	88	1	50	95/5	95
	8	40	28	1	17	-	92
	9	50	26	1	15	-	95

[a] Determined by DLS
[b] Determined by ^{1}H NMR spectroscopy (400 MHz, $CDCl_3$) after 24 hours, reactions carried out in triplicate
[c] Determined by chiral HPLC, ChiralPak IA, 80:10:10 hexane:propan-2-ol:ethanol, 1 mL.min^{-1}

To further confirm the temperature dependent activity of both nanogels, catalysis was carried out at 2 and 3 mol% catalyst loading, i.e. higher concentration of nanogels and catalyst. The reactions were carried out using the same total reaction volume, i.e. keeping substrate concentration constant and at three temperatures, 4, 25 and 40 °C. We proposed that having a greater number of thermo-responsive entities present in the reaction should confirm the differences observed between the two systems (Figure 5.10). Both nanogels seemed stable at all three temperatures with no precipitation of the polymers observed. However, some substrate precipitation was observed at the lower reaction temperature (5 °C).

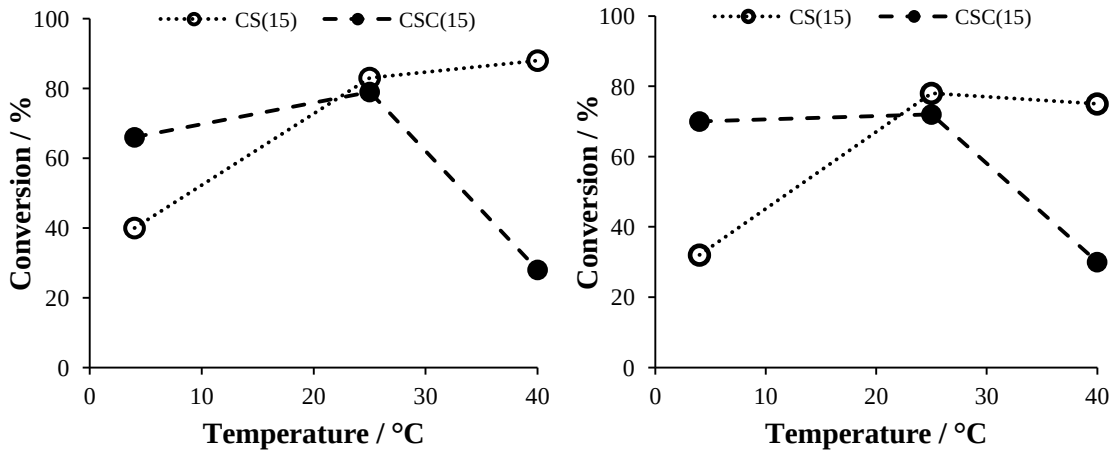

Figure 5.10. The catalytic activity of CS(15) and CSC(15) 2 mol% (left) and 3 mol% (right) at different temperatures

As anticipated, the same temperature dependence was indeed observed at both 2 and 3 mol% loading. A general increase in activity with temperature was once again observed for CS(15) nanogels and a significant drop in activity was observed for CSC(15) system at 40 °C. This further highlights our previous observations and strengthens our hypothesis regarding the difference between the two nanogels (Figure 5.10 and Table

5.3). Except for a slightly lower ee for CS(15) nanogels at 4 °C, both nanogels showed high ee's at 2 and 3 mol% loading, highlighting the successful design of our nanogel-supported systems (Table 5.3).

Table 5.3. The catalytic activity and selectivity of CS(15) and CSC(15) at 2 and 3 mol% loading, compared at three different temperatures

Catalyst	T / °C	D_h[a] / nm	Catalyst loading / mol%	Conv.[b] / %	*anti/syn* ratio[b]	ee[c] / %	TON[d]
CS(15)	4	133	2	40	98/2	86	20
	25	70	2	83	97/3	93	41
	40	30	2	88	96/4	96	44
CSC(15)	4	142	2	66	96/4	95	33
	25	88	2	79	97/3	95	39
	40	28	2	28	95/5	97	14
CS(15)	4	133	3	32	98/2	88	10
	25	70	3	78	98/2	95	39
	40	30	3	75	95/5	95	25
CSC(15)	4	142	3	70	98/2	96	23
	25	88	3	72	98/2	99	24
	40	28	3	30	98/2	97	10

[a] Determined by DLS
[b] Determined by ^{1}H NMR spectroscopy (400 MHz, $CDCl_3$) after 24 hours, reactions carried out in triplicate
[c] Determined by chiral HPLC, ChiralPak IA, 80:10:10 hexane:propan-2-ol:ethanol, 1 mL.min^{-1}
[d] Defined as the moles of substrates converted into product by one mole of catalyst at a given time (in this case 24 hours)

Although the reaction reaches higher conversions at 2 mol% loading, the catalyst is more efficient at 1 mol% (higher TONs). Interestingly, the catalytic efficiency of the nanogels was not improved at all by increasing catalyst loading from 2 to 3 mol% for either nanogels (Figure 5.11), even dropping for CS(15). We propose this is most likely due to a decrease in the local substrate concentration as a result of the increasing concentration of nanogels.

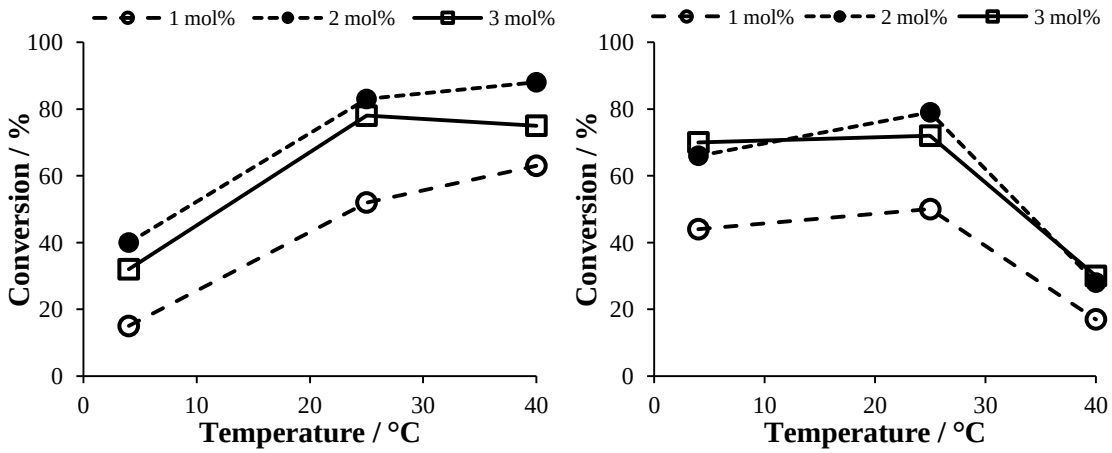

Figure 5.11. Comparison of the catalytic activity at 1, 2 and 3 mol% catalyst loading at different temperatures for the CS(15) (left) and CSC(15) (right) nanogel systems

5.4.5. Recycling

One of the main motivations behind the design and synthesis of these CS type nanoreactors was their potential recyclability, an important feature to take into account as high catalyst loadings (~30 mol%) are often required in conventional organocatalytic reactions. PNIPAM has been incorporated in number of recyclable systems where recovery has been achieved by precipitation at elevated temperatures or by complete dissolution at low temperatures.[17, 51] Our aim is to develop a recovery and reuse protocol which requires a limited number of steps for recovery but where high catalytic activity is maintained throughout the cycles, demonstrating potential not only here but for other more expensive catalytic species in future years.

5.4.5.1. Development of recycling protocol

The recyclability of the nanogels was evaluated using CS nanogels with a E2.05 core, CS(2). The first catalytic cycle was carried out as previously described for 24 hours, after which diethyl ether (Et_2O) was added to both quench the reaction and for extraction of products from the nanoreactor core. PNIPAM is insoluble in Et_2O,

allowing the nanogels to remain in the aqueous phase and the aldol products to be extracted into the Et_2O phase. After complete extraction of products, Et_2O was simply removed with a flow of air prior to addition of a second batch of reagents. However, the recycling efficiency of CS(2) was found to be unpredictable with this protocol, most likely due to presence of residual organic solvents and required further investigation (Figure 5.12).

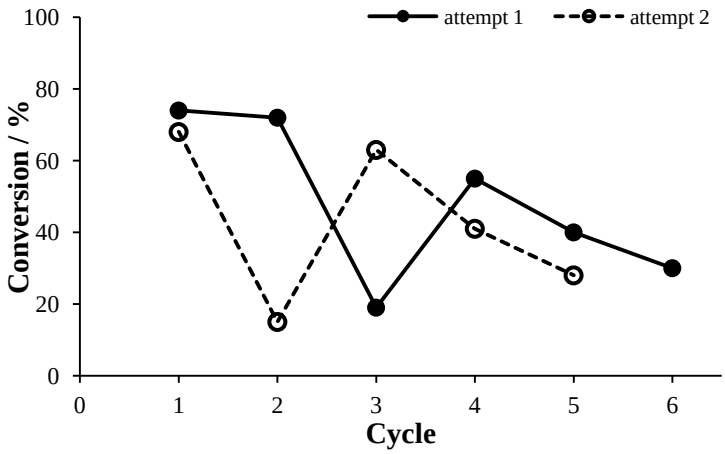

Figure 5.12. Recycling efficiency of CS(2) over multiple catalytic cycles, carried out at 1 mol% loading and 25 °C

It was hypothesized that the presence of residual organic solvent (in different amounts) may have caused the observed recycling efficiency. The presence of organic solvents in the reaction may reduce the efficiency of substrate uptake due to enhanced solubility of reagents in the surrounding medium. A similar effect has previously been shown by Mase *et al.* where high catalytic activity was observed in water due to the formation of a concentrated organic phase.[14] However, upon addition of an organic solvent, increased solubility of the reagents and support were observed eliminating the concentrating effects of the confined organic phase.

To further confirm this effect, reactions were carried out in the presence of a selection of organic co-solvents; and uniformly reached considerably lower conversions than reactions catalyzed in its absence (Table 5.4) verifying that the presence of a co-solvent, (a good solvent for the core and aldol reagents) has a negative effect on the catalytic activity of the nanogels. We attribute this effect to the increased solubility of reagents in the surrounding solution which reduces the efficiency of the hydrophobic concentrator effect, as well as potential blocking of the core reactive sites by solvent.

Table 5.4. The catalytic activity of CS(2) nanogels in the presence of a co-solvent

Entry	Co-solvent	% organic	Catalyst loading / mol%	Conv.[a] / %	*anti/syn* ratio[a]	ee[b] / %
1	Et_2O	20	1	16	97/3	95
2	Et_2O	33	1	15	95/5	95
3	EtOAc	20	1	28	97/3	20
4	$CHCl_3$	20	1	17	95/5	21
5	-	-	1	79	97/3	99

[a] Determined by ^{1}H NMR spectroscopy (400 MHz, $CDCl_3$) after 24 hours, reactions carried out in triplicate
[b] Determined by chiral HPLC, ChiralPak IA 80:10:10 hexane:propan-2-ol:ethanol, 1 mL.min^{-1}

Interestingly, after complete removal of both the organic co-solvent and water, the catalytic efficiency of CS(2) in water was retained after re-suspension and catalysis in 100% water. If a co-solvent was added to a third catalytic cycle, a drop in activity was once again observed (Figure 5.13). These results suggest complete removal of residual organic solvents from the nanogel solution is vital in order to maintain high activity over multiple catalytic cycles.

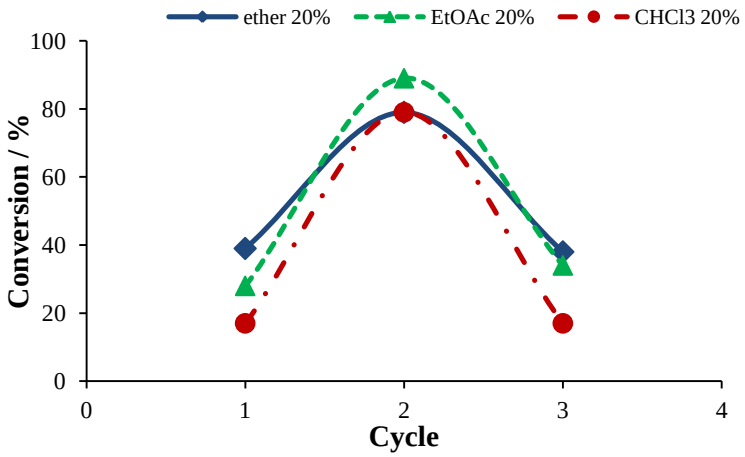

Figure 5.13. Catalytic activity of CS(2) nanogels where cycle 1 and 3 were carried out in the presence of co-solvent but cycle 2 in pure water, reactions carried out at 1 mol% and for 24 hours

With this in mind, a second recycling protocol was developed and evaluated, involving complete removal of water and re-dispersion of the dry nanogels into fresh nanopure water. We were delighted to find that this new protocol was highly successful, reflected in the high conversions and enantioselectivities maintained over five cycles for CS(2) nanogels (Figure 5.14). This recycling protocol was therefore used to investigate the recycling efficiency of the CS(15) and CSC(15) nanogels.

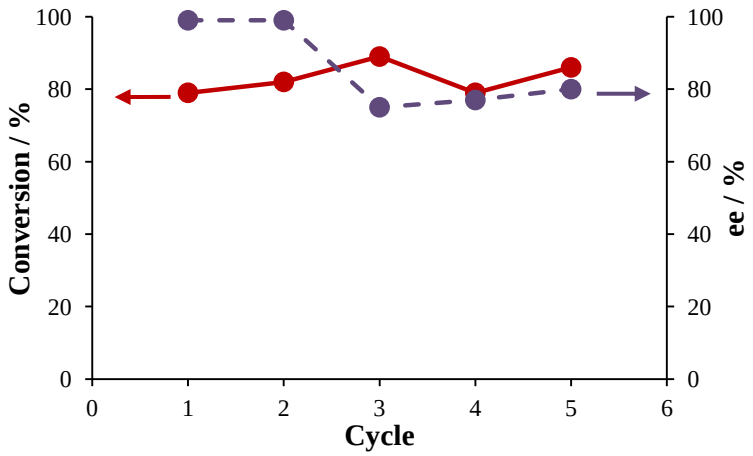

Figure 5.14. Recycling efficiency of CS(2) using the new recycling protocol, catalysis carried out at 1 mol% loading and 25 °C

5.4.5.2. Recycling efficiency of CS(15) and CSC(15)

The recycling efficiency of CS(15) and CSC(15) was first compared at 1 mol% loading and 25 °C, following the second recycling protocol. As mentioned above, this involved the complete removal of all solvent and re-dispersion into water. For CS(15) and CSC(15) a total of five catalytic cycles were carried out (Figure 5.15 and Table 5.5) and for the first three cycles, comparable results were found. However, in cycle 4 and 5, particularly in the case of CS(15) a dramatic drop in conversion and enantioselectivity was observed. This perhaps suggests CS(15) nanogels were not efficiently restored after reach cycle (Table 5.5). The higher enantioselectivity observed for the last two cycles is attributed to the low conversions achieved and is therefore considered insignificant.

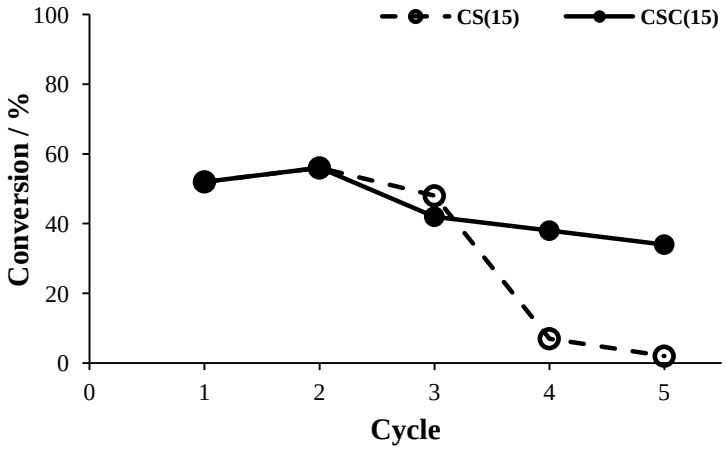

Figure 5.15. The catalytic efficiency of CS(15) and CSC(15) nanogels over multiple cycles carried out at 1 mol% loading and 25 °C

The same dramatic decrease in activity was not observed for CSC(15), though a small decrease in conversion was observed for each subsequent cycle. No significant difference in enantioselectivity was observed throughout the five cycles (Table 5.5). CSC(15) showed considerably greater recycling potential which may be attributed to the

linear polymer chains providing improved re-dispersability in water (see below, Figure 5.17, Figure 5.18, Figure 5.19) .

Table 5.5. The catalytic activity and selectivity of CS(15) and CSC(15) over multiple cycles carried out at 25 °C and 1 mol% loading

Catalyst	Cycle	Conv.[a] / %	*anti/syn* ratio[a]	ee[b] / %
CS(15)	1	52	97/3	95
	2	56	95/5	82
	3	48	97/3	80
	4	7	-	90
	5	2	-	94
CSC(15)	1	52	95/5	90
	2	56	98/2	89
	3	42	97/3	85
	4	38	98/2	89
	5	34	92/8	93

[a] Determined by ^{1}H NMR spectroscopy (400 MHz, $CDCl_3$) after 24 hours, reactions carried out in triplicate
[b] Determined by chiral HPLC, ChiralPak IA 80:10:10 hexane:propan-2-ol:ethanol, 1 mL.min^{-1}

The recycling potential of CSC(15) was further investigated at higher catalyst loading to limit loss in activity through loss of nanogels in each cycle. Unfortunately, a similar decrease in activity with catalytic cycle was observed for CSC(15) even at 2 mol% loading (Figure 5.16, Table 5.6). Importantly, relatively high enantioselectivity was maintained throughout the 6 cycles. The recovery and reuse of these nanostructures are certainly promising though further improvements can be made to extend the number of high yielding catalytic cycles.

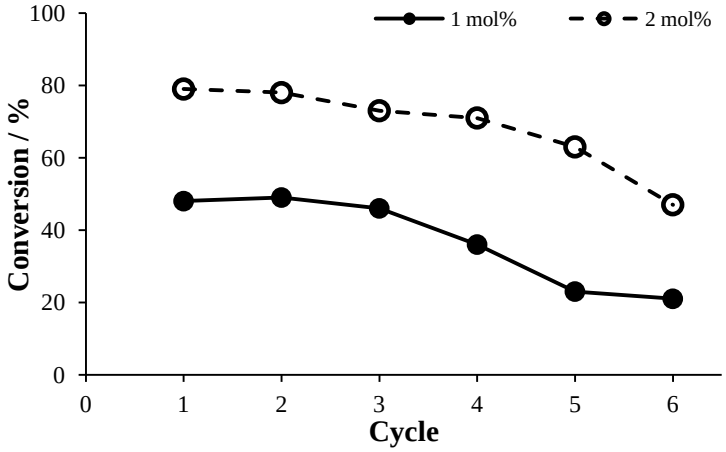

Figure 5.16. The conversion achieved by CSC(15) nanogels over 6 catalytic cycles carried out at 1 and 2 mol% loading and 25 °C

Table 5.6. The catalytic efficiency of CSC(15) nanogels over multiple catalytic cycles, carried out at 25 °C and at 1 and 2 mol% loading

Catalyst loading / mol%	Cycle	Conv.[a] / %	*anti/syn* ratio[a]	ee[b] / %	TON[c]
1	1	48	95/5	95	48
	2	49	97/3	85	49
	3	46	98/2	89	46
	4	35	96/4	92	35
	5	23	96/4	96	23
	6	21	96/4	96	21
2	1	79	97/3	95	40
	2	78	98/2	94	39
	3	73	97/3	91	37
	4	71	97/3	92	36
	5	63	97/3	91	32
	6	47	97/3	87	24

[a] Determined by ^{1}H NMR spectroscopy (400 MHz, $CDCl_3$) after 24 hours, reactions carried out in triplicate
[b] Determined by chiral HPLC, ChiralPak IA 80:10:10 hexane:propan-2-ol:ethanol, 1 mL.min^{-1}
[c] Defined as the moles of substrates converted into product by one mole of catalyst at a given time (in this case 24 hours)

5.4.5.3. Characterization of recovered nanogels

The successful re-dispersion of CS(15) and CSC(15) nanogels was investigated by DLS, both before and after catalysis, in which case the nanogels were recovered, dried and re-dispersed in nanopure water and further characterized. In both cases the D_h prior to and after catalysis were comparable at 5 °C: CS(15) 133 nm (PDI = 0. 138) and 132 nm (PDI = 0.182), CSC(15) 142 nm (PDI = 0.142) and 123 nm (PDI = 0.174) (Figure 5.17).

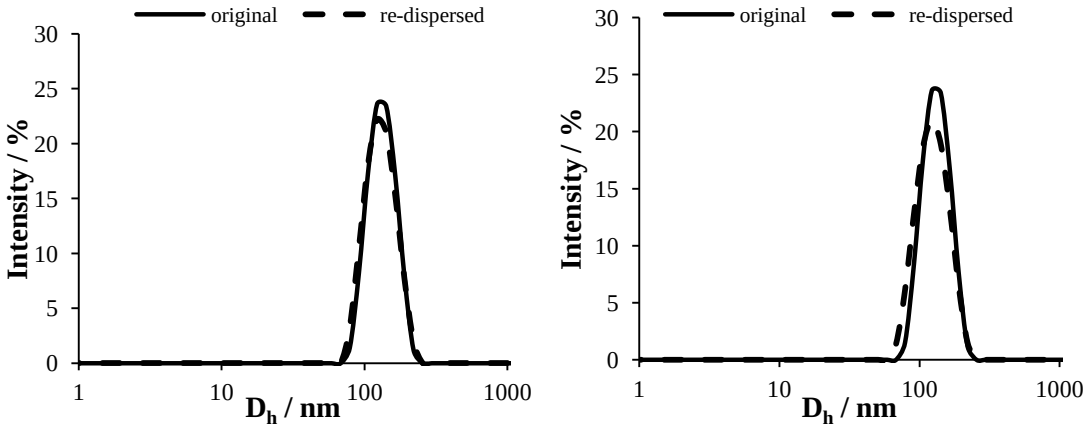

Figure 5.17. DLS traces of nanogels before catalysis and after recovery and re-dispersion, CS(15) D_h = 133 and 132 nm (left) and CSC(15) D_h = 142 and 123 nm (right) at 5 °C

As well as comparable particle size, the thermo-responsive property was also retained in both nanogels after recovery and re-dispersion: CS(15) 30 nm (PDI = 0.130) and 33 nm (PDI = 0.170) and CSC(15) 29 nm (PDI = 0.123) and 34 nm (PDI = 0.168) (Figure 5.18), The attraction and advantage of these systems is their ease of recovery and successful re-dispersion in water.

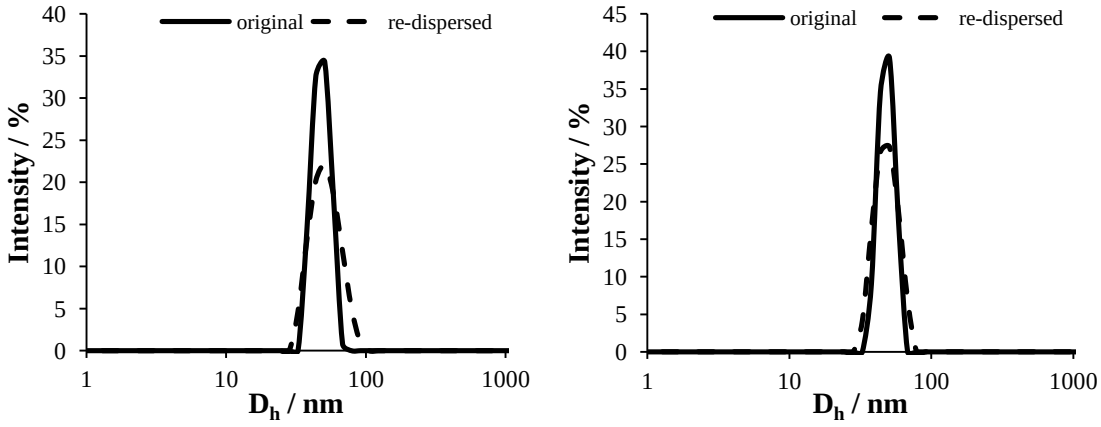

Figure 5.18. DLS traces of nanogels before catalysis and after recovery and re-dispersion, CS(15) D_h = 30 and 33 nm (left) and CSC(15) D_h = 29 and 34 nm (right) at 40 °C

CS(15) and CSC(15) nanogels recovered after the 5th catalytic cycle was again recovered, re-dispersed. Some large particles were observed for both nanogels, a change from 70 nm (PDI = 0. 120) before the first catalytic cycle to 68 nm (PDI = 0.260) after the 5th cycle was observed for CS(15) at 25 °C. For CSC(15) a change from 88 nm (PDI = 0.209) to 92 nm (PDI = 0.161) was observed. A population of much larger particles (or aggregated particles) was observed in both cases (Figure 5.19). Even though larger particles were observed for both nanogels, the more superior re-dispersibility observed for CSC(15) may explain the more efficiency recovery and reuse observed.

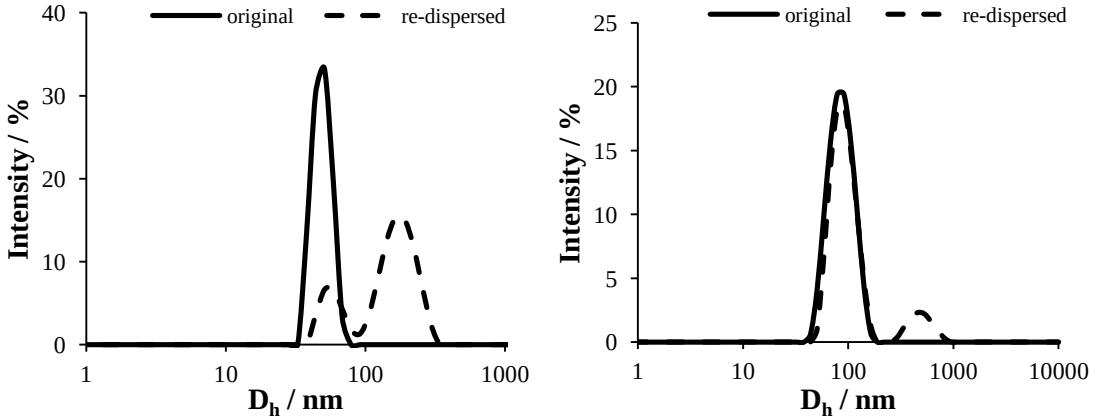

Figure 5.19. DLS traces of nanogels recovered after the 5th catalytic cycle at 25 °C, left: CS(15) D_h = 70 nm (original), 68 nm (re-dispersed), right: CSC(15) D_h = 88 nm (original), 92 nm (re-dispersed)

5.4.6. Synthesis and characterization of CSC with longer PNIPAM corona

CSC nanogels with double the length of PNIPAM corona chains were synthesized to investigate the possibility of completely shutting off catalytic activity at elevated temperatures. The CSC nanogels were synthesized according to the procedure previously described (and detailed below in the experimental section), with E15.05 as the hydrophobic core. These CSC nanogels will be referred to as CSC(15)2 with the number in brackets indicating the core DoF and 2 to the longer PNIPAM corona.

D_h of the initial core E15.05 was determined to be 36 nm (PDI = 0.142) at 25 °C and 121 nm (PDI = 0.110) for the corresponding CSC(15)2 supporting the successful addition of the shell/corona (Figure 5.20). Spherical structures were observed in dry-state TEM, with a D_{av} of 44 ± 8 nm (Figure 5.21). Again, the D_{av} observed by TEM are smaller than those found by DLS which is attributed to the shrinking of the sample upon removal of water, during TEM sample preparation.

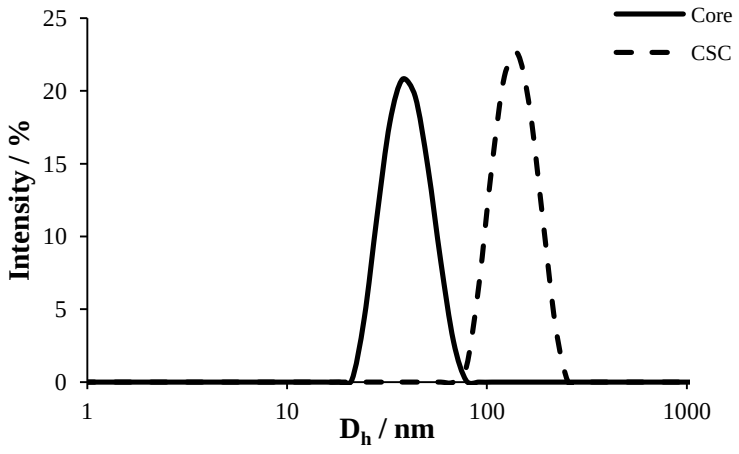

Figure 5.20. D_h of initial E15.05 core and the corresponding CSC(15)2, 36 nm (PDI = 0.142) and 121 nm (PDI = 0.110) respectively, determined at 25 °C

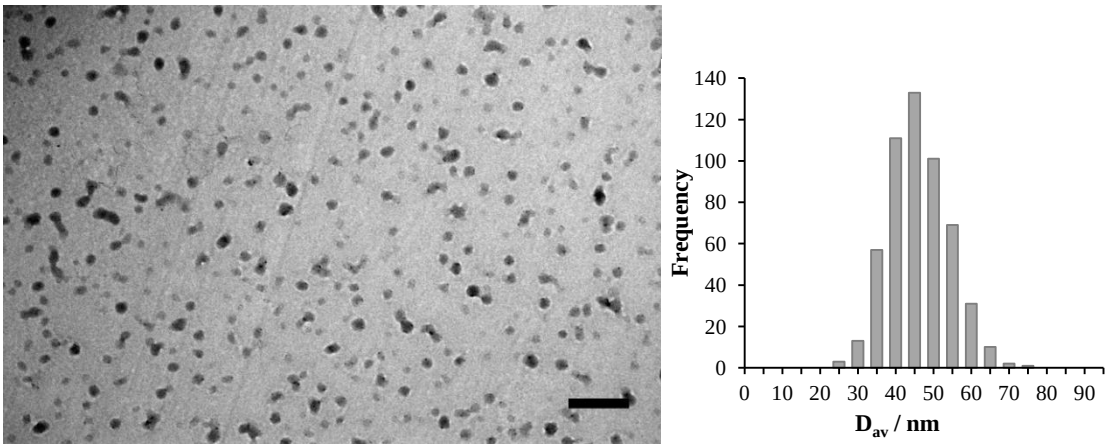

Figure 5.21. Representative unstained TEM image of CSC(15)2, D_{av} = 44 ± 8 nm, scale bar is 300 nm

Two more significant transition temperatures were found for CSC(15)2 when the change in D_h with temperature was investigated, one at 22 °C and the other at 30 °C, as determined by the D_h *vs* temperature curve (Figure 5.22). We attribute to two transition temperatures to the separate and individual collapse of the cross-linked PNIPAM and linear PNIPAM corona. We propose two transition temperatures are observed for CSC(15)2 but not CSC(15) as a result of the longer PNIPAM chains in CSC(15)2 making the difference between shell and corona more apparent. We hypothesized that the collapse of the longer PNIPAM chains will more efficiently block access to the core at elevated temperature resulting in a significant reduction or maybe even complete shutdown of the catalytic activity. The additional smaller transition observed at lower temperature (approx. 10 °C) may be attributed to PNIPAM present within the shell causing some shrinking of the particles even at this temperature.

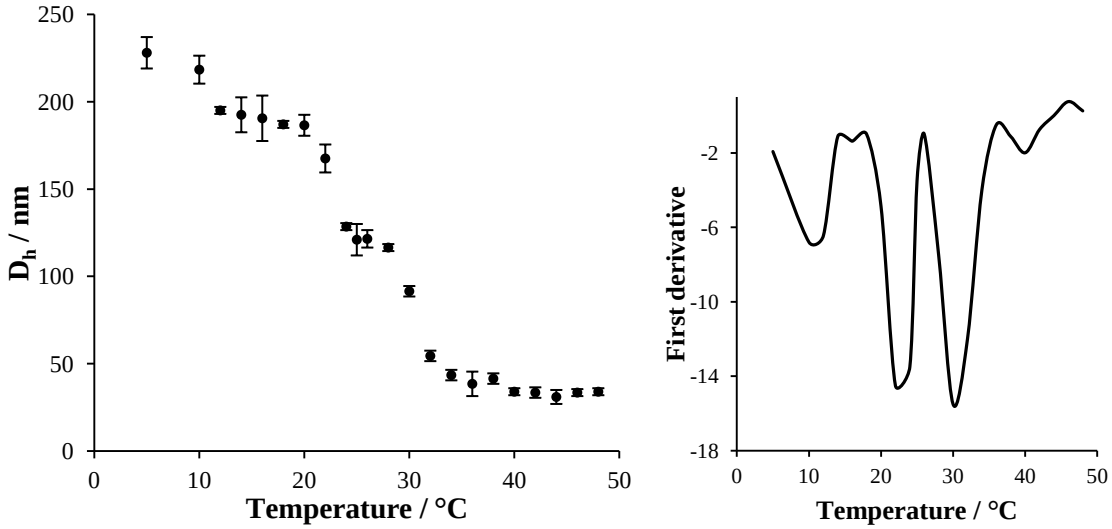

Figure 5.22. The change in D_h of CSC(15)2 with temperature and the first derivative showing two major transition temperatures, 22 and 30 °C

5.4.7. Catalytic efficiency of CSC(15)2

Catalysis was carried out at 1 mol% loading and at 4, 25 and 40 °C where particle D_h was 228, 121 and 34 nm respectively. Interestingly, a complete shutdown in activity was not observed at 40 °C and the activity at 25 °C showed considerable lower activity than previously observed (Figure 5.23).

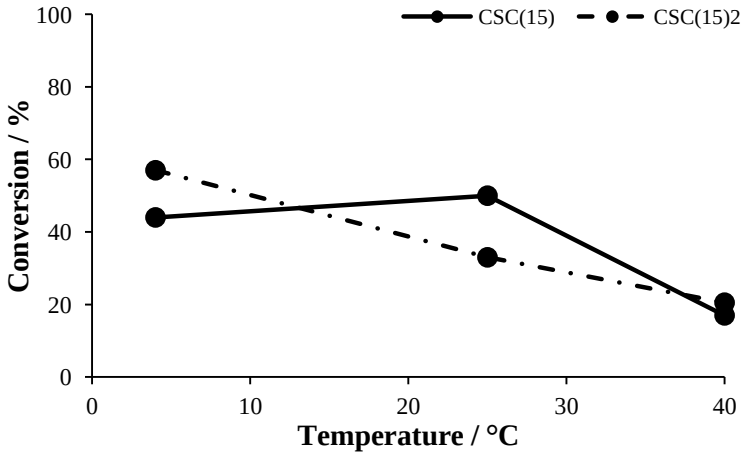

Figure 5.23. The catalytic activity of CSC(15) and CSC(15)2 at three different temperatures, carried out at 1 mol%

We propose this is a direct effect of the two transition temperatures observed for CSC(15)2, where the first transition temperature was as low as 22 °C. This suggests that a significant amount of PNIPAM has already collapsed at 25 °C resulting in restricted access explaining the lower activity observed (Table 5.7).

Table 5.7. Catalytic activity and selectivity of CSC(15)2 at 1 mol% loading and three temperatures

T / °C	D_h / nm	Conv.[a] / %	*anti/syn* ratio[a]	ee[b] / %
4	222	59	98/2	88
25	121	23	98/2	87
40	34	22	98/2	84

[a] Determined by ^{1}H NMR spectroscopy (400 MHz, $CDCl_3$) after 24 hours, reactions carried out in triplicate
[b] Determined by chiral HPLC, ChiralPak IA, 80:10:10 hexane:propan-2-ol:ethanol, 1 mL.min^{-1}

5.4.8. Control reactions

A number of background reactions using E15.05 were carried out to investigate the influence of temperature on the non-temperature-responsive core. One of the main objectives was to examine the temperature influence on the catalyst enantioselectivity and whether the presence of a PNIPAM shell may help conserve catalyst selectivity at elevated temperatures. Firstly, no significant difference in D_h, attenuation or count rates were observed for E15.05 at the three reaction temperatures confirming the core was not thermo-responsive and stable at these temperatures (Figure 5.24).

T / °C	D_h / nm	PDI
5	30 ± 5	0.128
25	30 ± 3	0.142
40	28 ± 5	0.135

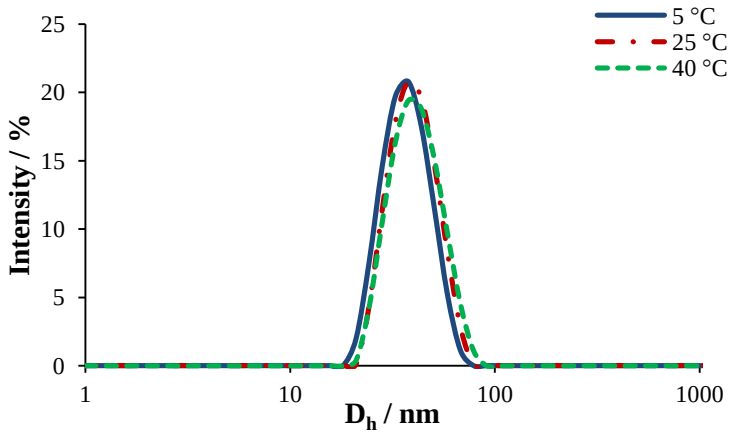

Figure 5.24. D_h of the hydrophobic nanogel E15.05 at a range of temperatures

Catalysis was carried out at two different loadings, 1 and 8.5 mol% to provide a direct comparison to reactions catalyzed by CS(15) and CSC(15) as well as the hydrophobic nanogels discussed in chapter 3. As expected, an increase in catalytic activity with increasing temperature was observed at both loadings (Figure 5.25). Interestingly, high *anti/syn* ratios were achieved at both loadings and all three temperatures but a dramatic drop in enantioselectivity was observed at 40 °C, at both loadings achieving only 40 and 26% ee (Table 5.8, entries 3 and 6). We rationalize that the low enantioselectivity is a direct result of catalyst degradation and/or reduced stability of key transitions states at elevated temperatures.[55-57] This truly highlights the advantage of our CS type nanostructures where PNIPAM acts as a protective shell.

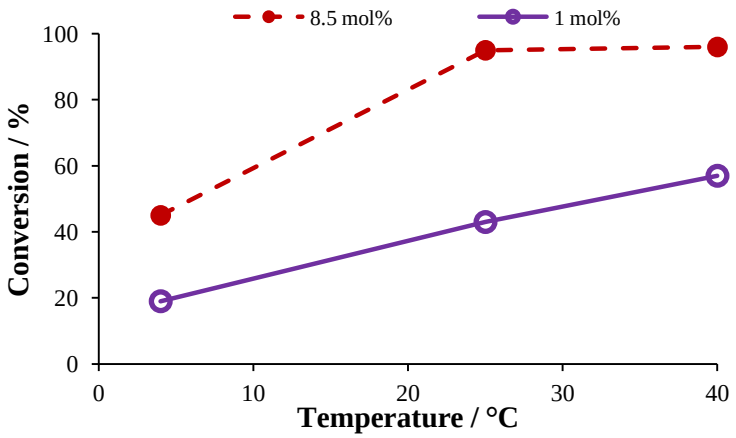

Figure 5.25. Catalytic activity of E15.05 at 1 and 8.5 mol% loading and a selection of temperatures

Table 5.8. The catalytic activity and selectivity of E15.05 at 1 and 8.5 mol% loading at a selection of temperatures

Entry	T / °C	D_h[a] / nm	Catalyst loading / mol%	Conv.[b] / %	*anti/syn* ratio[b]	ee[c] / %
1	4	28	8.5	45	98/2	97
2	25	30	8.5	95	97/3	96
3	40	30	8.5	96	98/2	26
4	4	28	1	19	96/4	97
5	25	30	1	43	97/3	89
6	40	30	1	57	96/4	40

[a] Determined by DLS
[b] Determined by ^{1}H NMR spectroscopy (400 MHz, $CDCl_3$) after 24 hours, reactions carried out in triplicate
[c] Determined by chiral HPLC, ChiralPak IA, 80:10:10 hexane:propan-2-ol:ethanol, 1 mL.min^{-1}

5.4.9. Catalytic dependency on core DoF

5.4.9.1. Synthesis and characterization of CS with low core DoF

CS nanogels consisting of a hydrophobic with 5 wt% DoF and PNIPAM shell was synthesized according to the procedure previously described above. Successful addition of the PNIPAM shell was confirmed DLS (Figure 5.26) with an increase in D_h from 19 to 64 nm at 25 °C. These CS nanogels will be referred to as CS(5).

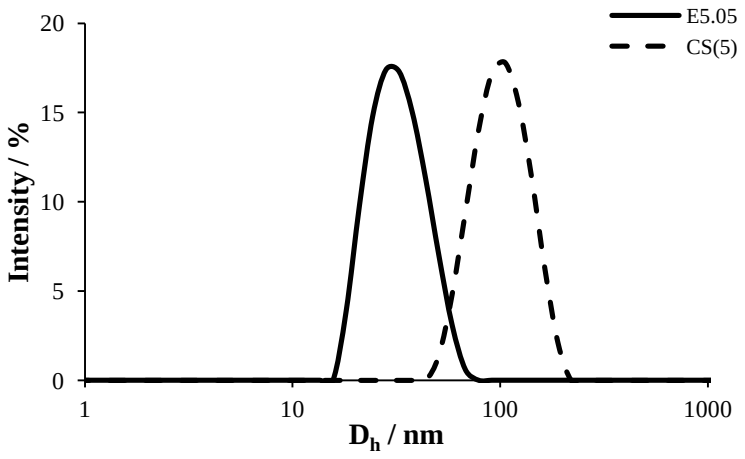

Figure 5.26. Change in D_h upon addition of PNIPAM shell to E5.05, at 25 °C

As previously mentioned, dry-state TEM was unable to confirm addition of PNIPAM shell on previous nanogels as water was removed during the drying process causing the PNIPAM shell to shrink. Interestingly, significantly larger D_{av} (49 ± 9 nm) compared to the core was observed for CS(5) even in the dry-state (Figure 5.27).

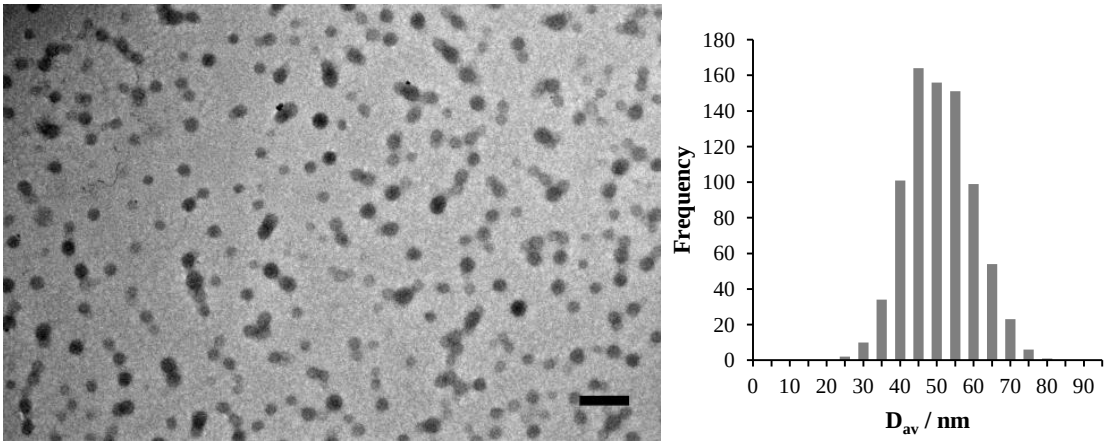

Figure 5.27. Representative dry-state TEM image of CS(5), D_{av} = 49 ± 9 nm, scale bar is 200 nm

The thermo-responsive property of CS(5) was examined by monitoring the change in D_h with temperature by DLS. As expected, a decrease in D_h was observed with increasing temperature as PNIPAM shrinks by expelling water from the cross-linked network (Figure 5.28).

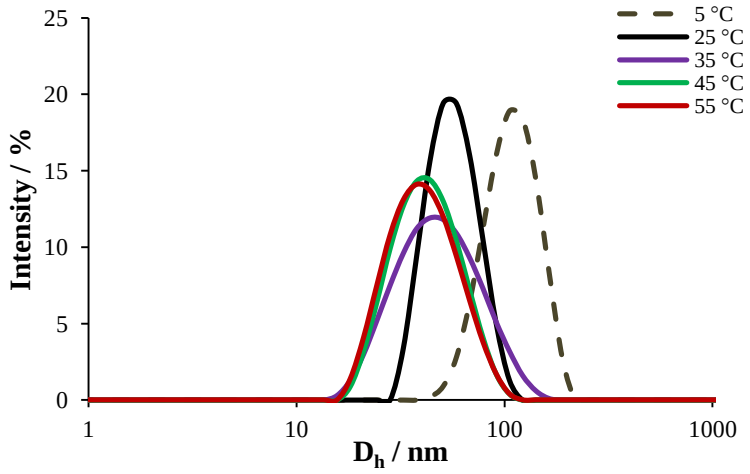

Figure 5.28. Change in D_h with temperature of CS(5) nanogels, by DLS

A sharp change in particle size was observed between 20 and 35 °C indicating a dramatic change in the nature of the PNIPAM shell. The D_h then continued to shrink reaching a final D_h of 16 nm at 65 °C. The transition temperature (27 °C) was then determined using the first derivative of the D_h against temperature curve (compare 30 °C for CS(15)) (Figure 5.29).

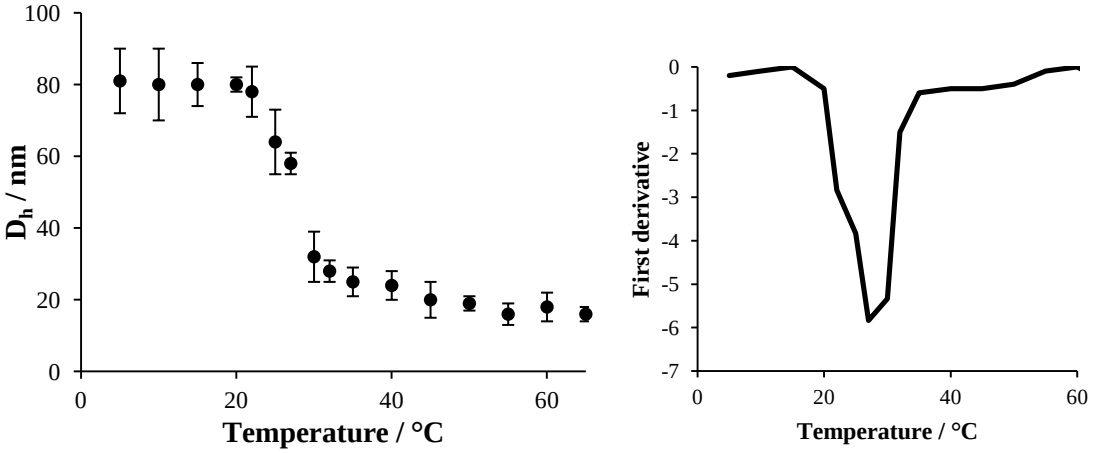

Figure 5.29. Change in D_h with temperature where the transition temperature was determined to be 27 °C

5.4.9.2. Catalytic efficiency and recyclability of CS(5) nanogels

The catalytic efficiency of CS(5) in the model aldol reaction at 4, 25 and 40 °C was determined and compared to CS(15). D_h of CS(5) at 25 and 40 °C were found to be relatively comparable to those of CS(15), 64 *vs* 70 nm and 24 *vs* 30 nm. The most significant difference in size was observed at 4 °C where CS(15) was considerably larger, 133 nm compared to 81 nm for CS(5) (52 nm difference). In fact, this is also the temperature where the most significant difference in activity was observed, 15 *vs* 76% conversion for CS(15) and CS(5) respectively (Figure 5.30). Interestingly, CS(5) outperforms CS(15) at all three temperatures despite a drop in activity at 40 °C.

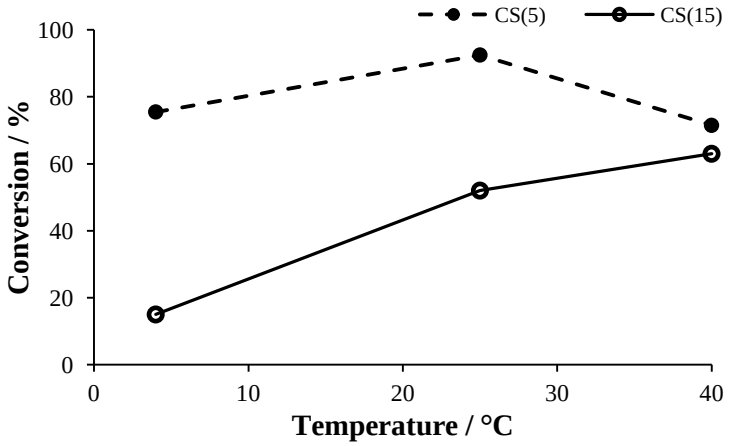

Figure 5.30. Catalytic dependency of CS(5) nanogel on temperature at 1 mol% loading, compared to CS(15)

Both CS nanogels showed high enantioselectivity at 25 °C (Table 5.9, 96 *vs* 95% ee, compare to entry 2 in Table 5.2). At 4 and 40 °C CS(5) showed significantly lower enantioselectivity compared to CS(15) and as low as 75% ee was observed for CS(5), considerable lower than previously observed for any CS nanogel (Table 5.9).

Table 5.9. The activity and selectivity of CS(5) at different temperatures, catalyzed at 1 mol% loading

T / °C	D_h[a] / nm	Conv.[b] / %	*anti/syn* ratio[b]	ee[c] / %
4	81	76	98/2	75
25	64	93	97/3	96
40	24	72	95/5	87

[a] Determined by DLS
[b] Determined by ^{1}H NMR spectroscopy (400 MHz, $CDCl_3$) after 24 hours, reactions carried out in triplicate
[c] Determined by chiral HPLC, ChiralPak IA, 80:10:10 hexane:propan-2-ol:ethanol, 1 mL.min^{-1}

As detailed in chapter 3, different concentrations of nanogels are required to achieve the same catalyst loading as a result of the difference in core DoF. In other words, less CS(15) nanoreactors are required to make up 1 mol% loading compared to CS(5) as

each reactor is functionalized with more catalyst. Thus, we attribute the difference in catalytic efficiency between CS(5) and CS(15) to the difference in nanoreactor concentration (Figure 5.31).

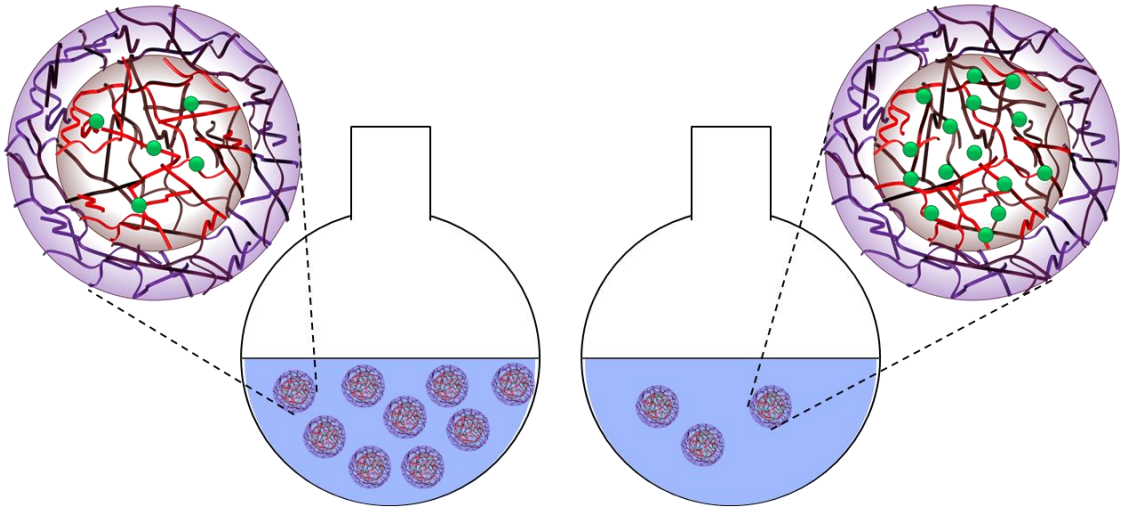

Figure 5.31. Schematic representation of the difference in nanogel concentration required for a 1 mol% reaction when catalyzed by CS(5) (left) and CS(15) (right)

The recycling potential of CS(5) at 1 mol% loading and 25 °C was investigated following the recycling procedure previously detailed. The first four cycles were incredibly efficient, with insignificant differences in both the activity and more importantly the enantioselectivity (Figure 5.32). However, a significant drop from 86% to 60% conversion was observed in the fifth catalytic cycle, though high enantioselectivity was maintained.

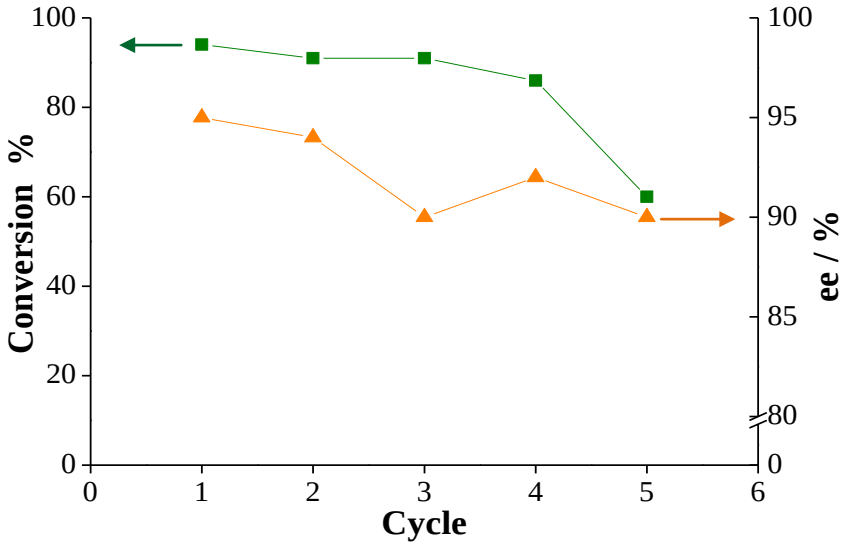

Figure 5.32. Recycling efficiency and selectivity of CS(5) over five catalytic cycles

The recycling results suggests CS(5) is overall the more efficient system (Table 5.10). Moreover, CS(5) shows better recycling compared to CSC(15) which is also superior to CS(15). It is possible that the catalytic moieties are better protected in CS(5) compared to both CS(15) and CSC(15) due to the low DoF and as a result greater core hydrophobicity.

Table 5.10. The recycling efficiency of CS(5) at 1 mol% loading and 25 °C

Cycle	Conv.[a] / %	*anti/syn* ratio[a]	ee[b] / %
1	94	97/3	95
2	91	95/5	94
3	91	95/5	90
4	86	97/3	92
5	60	95/5	90

[a] Determined by ^{1}H NMR spectroscopy (400 MHz, $CDCl_3$) after 24 hours, reactions carried out in triplicate
[b] Determined by chiral HPLC, ChiralPak IA, 80:10:10 hexane:propan-2-ol:ethanol, 1 mL.min^{-1}

5.4.9.3. Synthesis and characterization of CSC with low core DoF

To further confirm the results observed for CS(5) and CS(15) in both activity and recyclability, a similar comparison was carried out for CSC nanogels. Thus, CSC(5) was synthesized with a hydrophobic PEMA core (5 wt% DoF and 0.5 wt% CLD), PNIPAM (0.5 wt% CLD) shell and PNIPAM corona using the procedure previously described. The resulting CSC(5) nanogels were characterized by DLS and dry-state TEM. Again, we were not able to use cryo-TEM to confirm the addition of the shell, and only the change in D_h by DLS was used to validate the addition of shell/corona (Figure 5.33).

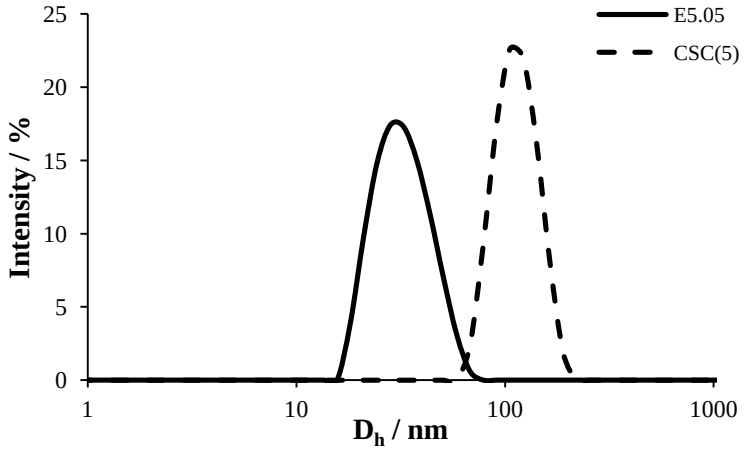

Figure 5.33. Change in D_h of CSC(5) upon addition of PNIPAM shell and corona, increase from 27 nm to 87 nm at 25 °C

DLS was once again used to investigate the thermo-responsive property of CSC(5) by monitoring the change in D_h with temperature (Figure 5.34). The first derivative of the D_h against temperature plot was used to determine the transition temperature, 26 °C (Figure 5.34). This is comparable to the transition temperature of CSC(15) (27 °C) (Figure 5.7). Moreover, CSC(5) and CSC(15) showed similar D_h at 25 °C, 87 and 88 nm respectively.

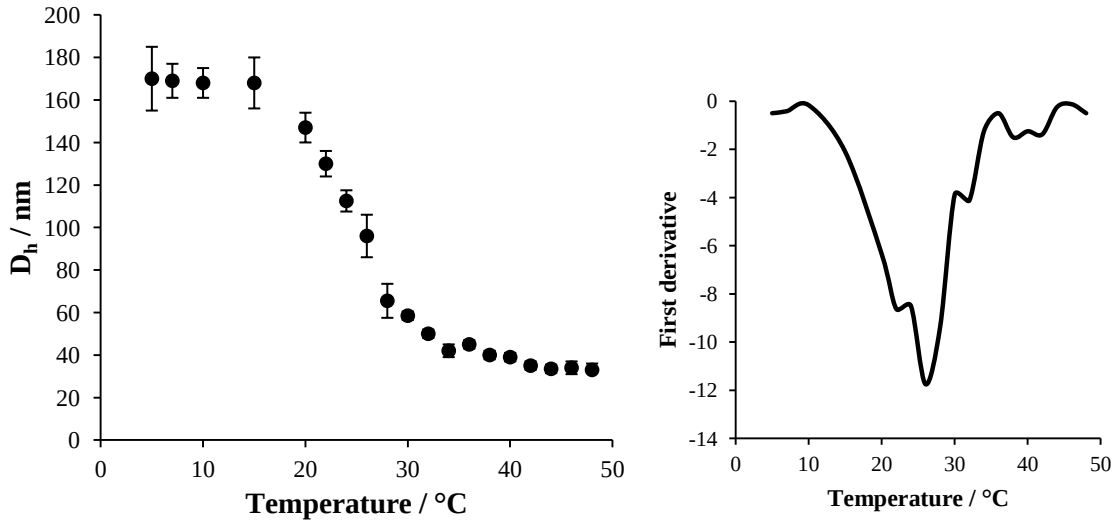

Figure 5.34. Change in D_h with temperature of CSC(5) and a transition temperature of 26 °C

Although dry-state TEM cannot be used to confirm addition of PNIPAM shell/corona, it suggests the nanostructures are spherical with D_{av} of 49 ± 9 nm (Figure 5.35).

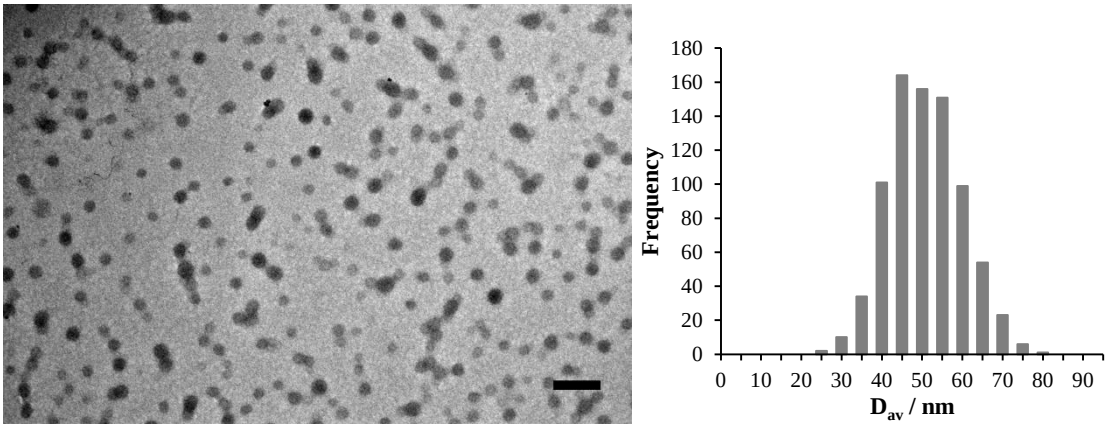

Figure 5.35. Representative unstained TEM image of CSC(5), D_{av} = 49 ± 9 nm, scale bar is 200 nm

5.4.9.4. Catalytic efficiency and recyclability of CSC(5)

The catalytic efficiency of CSC(5) and CSC(15) at 4, 25 and 40 °C in the model aldol reaction were compared (Figure 5.36 and Table 5.11). Our previous hypothesis

regarding the collapse of PNIPAM shell/corona and its influence on nanogel activity was further confirmed by the drop in activity observed at 40 °C for CSC(5). At 4 and 25 °C, CSC(5) outperforms CSC(15) reaching higher conversions after 24 hours. This supports our hypothesis that CS(5) outperformed CS(15) as a result of the higher concentration of nanoreactors used in each catalysis reaction and highlights the importance of nanoreactor design where modifications to parameters such as DoF may be utilized to tailor properties of the resulting nanoreactor.

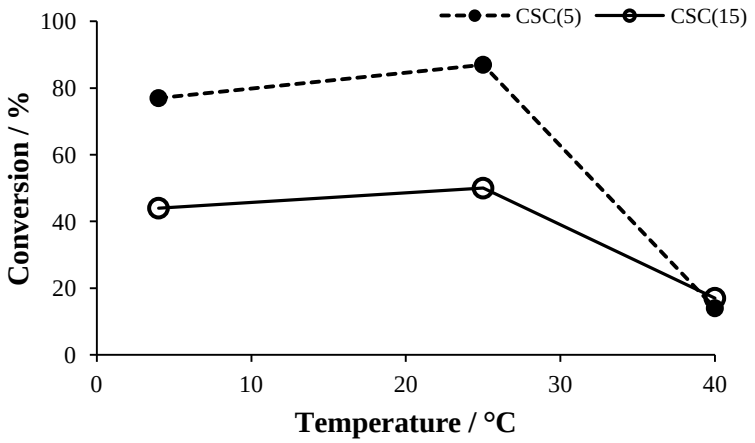

Figure 5.36. The catalytic activity of CSC(5) and CSC(15) at different temperatures, carried out at 1 mol% loading

Table 5.11. The catalytic activity of CSC(5) at different temperatures and 1 mol% loading

T / °C	D_h[a] / nm	Catalyst loading / mol%	Conv.[b] / %	*anti/syn* ratio[b]	ee[c] / %
4	178	1	77	97/3	85
25	87	1	87	97/3	96
40	39	1	14	98/2	91

[a] Determined by DLS
[b] Determined by ^{1}H NMR spectroscopy (400 MHz, $CDCl_3$) after 24 hours, reactions carried out in triplicate
[c] Determined by chiral HPLC, ChiralPak IA, 80:10:10 hexane:propan-2-ol:ethanol, 1 mL.min^{-1}

The recycling potential of CSC(5) at 1 mol% loading and 25 °C was investigated following the recycling procedure previously described. High conversions were

obtained over the first 5 cycles followed by a drop in conversion from 65 to 34% in the final two cycles which was interestingly not accompanied by a significant change in enantioselectivity (Figure 5.37). Thus, CS(5) and CSC(5) nanogels are able to maintain high enantioselectivities throughout multiple cycles despite the observed drop in catalytic activity.

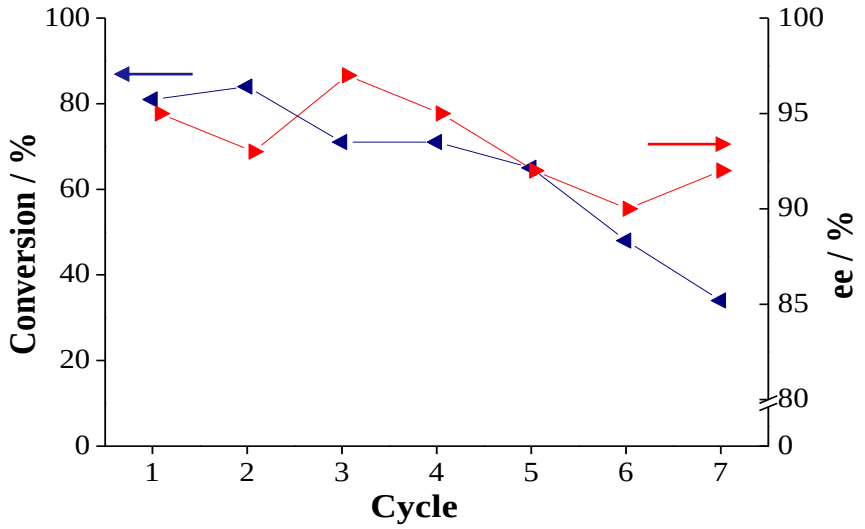

Figure 5.37. Recycling efficiency of CSC(5) over 7 catalytic cycles

Table 5.12. The recycling efficiency of CSC(5) carried out at 25 °C and 1 mol% loading

Cycle	Conv.[a] / %	*anti/syn* ratio[a]	ee[b] / %
1	81	97/3	95
2	84	97/3	93
3	71	96/4	97
4	71	97.3	95
5	65	96/4	92
6	48	96/4	90
7	34	96/4	92

[a] Determined by ^{1}H NMR spectroscopy (400 MHz, $CDCl_3$) after 24 hours, reactions carried out in triplicate
[b] Determined by chiral HPLC, ChiralPak IA, 80:10:10 hexane:propan-2-ol:ethanol, 1 mL.min^{-1}

5.4.10. Catalytic dependency on core hydrophobicity

5.4.10.1. Synthesis and characterization of CS nanogels with PMMA core

CS nanogel consisting of a hydrophobic PMMA (15 wt% DoF, 0.5 wt% CLD) core and PNIPAM (0.5 wt% CLD) shell was synthesized according to the previously detailed two step procedure. A change in D_h from 26 nm (PDI = 0.210) to 57 nm (PDI = 0.080) at 25 °C confirmed the successful addition of the PNIPAM shell (Figure 5.38). Dry-state TEM (Figure 5.39) was used to confirm the spherical morphology of the CS(M15) nanogels, D_{av} = 34 ± 7 nm.

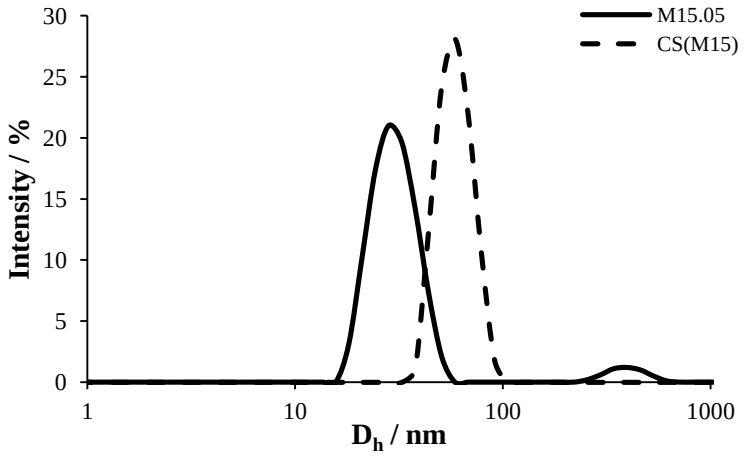

Figure 5.38. Change in D_h upon addition of PNIPAM shell to original E15.05 nanogel at 25 °C, from 26 to 57 nm

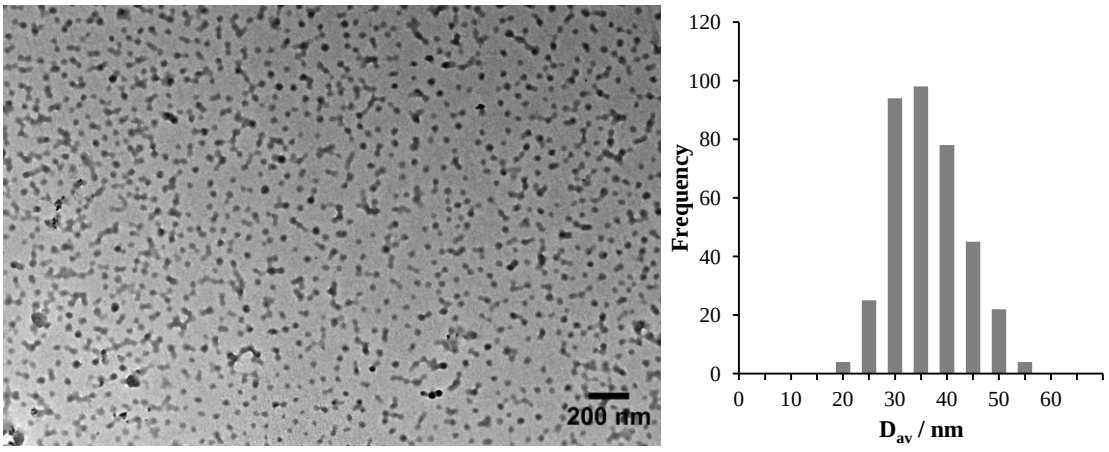

Figure 5.39. Representative unstained TEM image of CS(M15) nanogels, D_{av} = 34 ± 7 nm

As expected, a decrease in D_h was observed with increasing temperature confirming the thermo-responsive property of CS(M15) (Figure 5.40). However, the sharp transition previously observed with the EMA based CS and CSC nanogels was not observed. Instead, CS(M15) showed a steady and gradual decrease in D_h with temperature. A gradual increase in mean count rate was observed with increasing temperature (and hence decreasing D_h). This is not unexpected considering the more compact nature of the collapsed aggregate. Moreover, a decrease in particle PDI was observed confirming a narrower particle size distribution. The difference in the shape of the D_h *vs* temperature graph compared to its EMA cored equivalence may be explained by considering the slightly more hydrophilic nature of MMA. It is possible some water is trapped closer to the MMA core (compared to EMA) and is therefore less readily removed from nanogel as the shell shrinks. However, this cannot be confirmed without further investigations with core-shell structures containing a more hydrophobic core. Nevertheless, the D_h of CS(M15) at the temperatures of interest, 4, 25 and 40 °C were determined to be 127, 57 and 32 nm respectively.

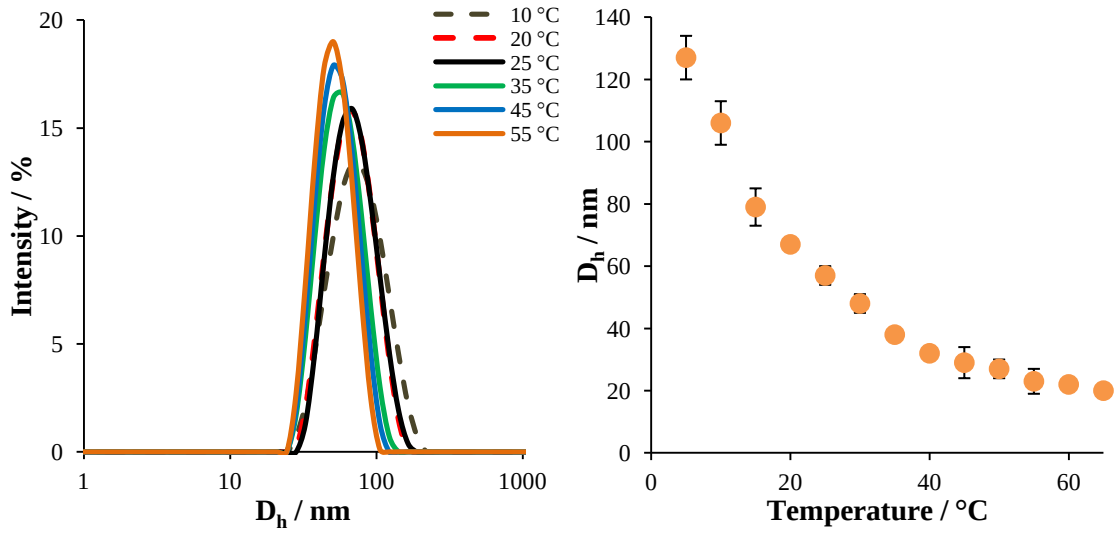

Figure 5.40. Change in D_h with temperature for CS(M15) nanogels

5.4.10.2. Catalytic efficiency and recyclability of CS(M15)

The catalytic efficiency of CS(M15) at a range of temperatures were compared to CS(E15). As both nanogels were functionalized with the catalyst to the same degree, the concentration of nanoreactors required to make up 1 mol% loading will be comparable. As expected, an increase in activity was observed with increasing temperature. Unexpectedly, CS(M15) showed greater catalytic activity than CS(E15) at 1 mol%, in the studied temperature range (Figure 5.41). This is in contrast to the activity observed for M15.05 (53% conv., *anti/syn* 98/2, 67% ee) and E15.05 (95% conv., *anti/syn* 98/2, 97% ee) in the absence of the PNIPAM shell. This suggests the PNIPAM shell has a considerable effect on the catalytic activity of the catalyst containing hydrophobic nanogel core.

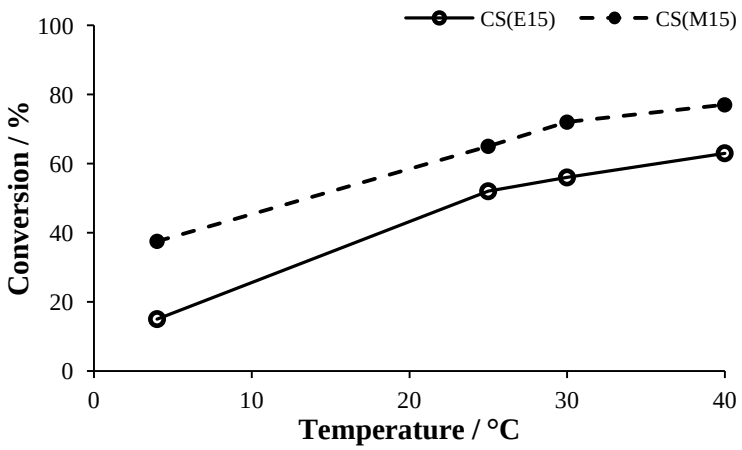

Figure 5.41. The catalytic activity of CS(M15) and CS(E15) at 1 mol% and different temperatures

Interestingly, CS(M15) showed low enantioselectivity at temperatures below and above 25 °C (Table 5.13, entries 1 and 4). A drop in ee was observed even by a 5 °C increase in reaction temperature from 25 to 30 °C (from 98 to 89%) which was not accompanied by a large increase in conversion. Most significant is the drop in ee to 35% at 4 °C for

CS(M15) compared to the 90% ee observed for CS(E15) at the same temperature. This was not unexpected as low ee has previously been associated with M15.05. In chapter 3 we proposed this was an effect of the increased hydrophilic content linked to catalyst DoF. This effect was supported by an increase in ee with increasing hydrophobicity around the catalytic sites, by substitution of MMA to EMA and addition of a hydrophobic shell. Thus, we attribute the low ee at 4 °C to the swollen nature of the PNIPAM shell which decreases its ability to efficiently protect the core from the surrounding water. This is supported by an increase in enantioselectivity with increasing temperature (Table 5.13), where PNIPAM is comparatively more hydrophobic. This highlights the enantioselective dependency on nanogel hydrophobicity.

Table 5.13. The catalytic activity of CS(M15) at 1 mol% catalyst loading and different temperatures

Entry	T / °C	D_h[a] / nm	Conv.[b] / %	*anti/syn* ratio[b]	ee[c] / %
1	4	127	38	98/2	35
2	25	57	65	97/3	98
3	30	48	72	96/4	89
4	40	32	77	95/5	70

[a] Determined by DLS
[b] Determined by ^{1}H NMR spectroscopy (400 MHz, $CDCl_3$) after 24 hours, reactions carried out in triplicate
[c] Determined by chiral HPLC, ChiralPak IA, 80:10:10 hexane:propan-2-ol:ethanol, 1 mL.min^{-1}

The recyclability of CS(M15) was investigated following the recycling procedure previously discussed, at 25 °C. Only small differences in activity and enantioselectivity were observed over the first four catalytic cycles (Table 5.14). A small drop in activity was then observed in the 5th cycle which was accompanied by a small drop in enantioselectivity. Thus, the CS(M15) nanogels performed extremely consistently over the first five catalytic cycles before a significant drop in activity was noted. More

importantly, the enantioselectivity remained high throughout the six cycles (Table 5.14). Thus, CS(M15) and CS(E15) show similar recyclabilities over 4-5 catalytic cycles. These results are indeed encouraging and improvements may be made to further increase the number of catalytic cycles that may be carried out before losses in activity and enantioselectivity are observed.

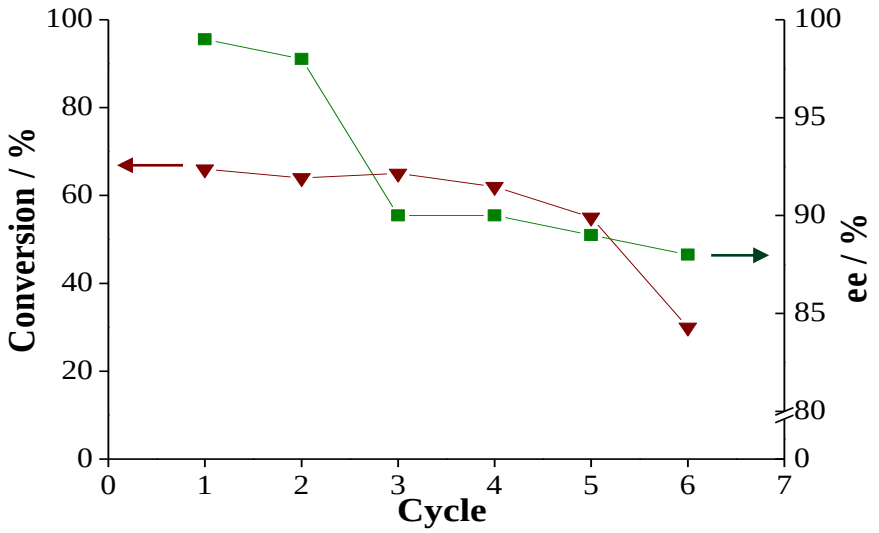

Figure 5.42. Recycling activity and selectivity of CS(M15) over multiple cycles, at 1 mol% loading and 25 °C

Table 5.14. Recyclability of CS(M15) over 6 cycles, catalyzed at 1 mol% loading and 25 °C

Cycle	Conv.[a] / %	*anti/syn* ratio[a]	ee[b] / %
1	66	97/3	99
2	64	97/3	98
3	65	96/4	90
4	62	96/4	90
5	55	96/4	89
6	30	95/5	88

[a] Determined by ^{1}H NMR spectroscopy (400 MHz, $CDCl_3$) after 24 hours, reactions carried out in triplicate
[b] Determined by chiral HPLC, ChiralPak IA, 80:10:10 hexane:propan-2-ol:ethanol, 1 mL.min^{-1}

5.5. Conclusion

Recyclable CS and CSC nanogels were successfully synthesized *via* a seeded precipitation polymerization of NIPAM. The nature of the shell was found to have a significant effect on the catalytic activity of the hydrophobic nanogel core as a result of the thermo-responsive property of the PNIPAM shell. The collapse of PNIPAM at elevated temperatures was found to increase the catalytic activity of nanogels with CS morphology which was attributed to the increased hydrophobic nature of the CS nanogels. The collapse of the linear PNIPAM corona chains on the other hand were found to block substrate access to the catalytic core resulting in a dramatic drop in the catalytic activity of the CSC nanogels. Further increasing the length of the PNIPAM corona resulted in poor catalytic activity at temperatures as low as 25 °C. Interestingly, a decrease in nanogel core DoF was accompanied by an enhancement in catalytic activity. This was attributed to the use of a higher concentration of nanogels highlighting the importance of nanogel/nanoreactor design. CSC nanogels showed greater recyclability compared to the CS nanogels, which is most likely associated with the linear polymer chains allowed easy re-dispersibility in water.

5.6. Experimental

5.6.1. Materials

NIPAM was recrystallized from methanol and stored at 4 °C. 4-Nitrobenzaldehyde was filtered through a silica column prior to use. All other reagents were used as received from Sigma-Aldrich without further purification.

5.6.2. Instrumentation

^{1}H NMR spectra were recorded at 400 MHz on a Bruker DPX 400 FT-NMR spectrometer using deuterated solvents. Chemical shifts are reported as δ in parts per

million relative to $CHCl_3$ (7.26 ppm) or CD_3OD (3.31 ppm) as the internal standard. Dialysis tubing was purchased from Spectrum labs with MW cut off of 6-8 and 12-14 kDa. HPLC analysis was performed on a Varian 920-LC on a chiral column, Chiralpak IA (150 mm × 4.6 mm × 5 µm) with guard cartridge (Chiralpak 5 µm) purchased from Chiral Technologies Europe. Hydrodynamic diameters (D_h) and size distributions of nanogels were determined by DLS on a Malvern Zetasized Nano ZS instrument operating at 25 °C with a 4 mW He-Ne 633-nm laser module. Measurements were made at a detection angle of 173° (back scattering) and the data was analyzed using Malvern DTS 6.20. All determinations were made in triplicate (with 12 runs recorded for each measurement). TEM samples were prepared by drop deposition onto copper/carbon grids that had been treated with oxygen plasma to increase surface hydrophilicity and examined with a transmission electron microscope (JEOL TEM-2100), operating at 200 kV. Micrographs were collected at magnifications varying from 30 K to 100 K and calibrated digitally.

5.6.3. Synthesis of L-proline functionalized methacrylate monomer

A representative procedure for the synthesis of the L-proline functionalized methacrylate monomer[58] (**3.3**) is given in Chapter 3.

5.6.4. Synthesis of L-proline functionalized hydrophobic nanogels

A representative procedure for the emulsion polymerization[36] of hydrophobic L-proline functionalized nanogels is given in Chapter 4.

5.6.5. Synthesis of CS nanogels with PNIPAM shell

A representative procedure for the synthesis of the CS nanogels is as follows: the hydrophobic nanogels synthesized in the previous step were used as seeds in a seeded emulsion polymerization reaction.[36-39] The hydrophobic seeds (25 mL) were submerged

in a pre-heated oil bath at 70 °C under nitrogen. In a separate reaction mixture, SDS (0.018 g) was dissolved in water (25 mL) and stirred under nitrogen. The shell forming monomer, NIPAM (0.220 g), the cross-linker *N,N'*-methylenebisacrylamide (bis, 1.3 mg, CLD 0.5 wt%) and the initiator, KPS (2.5 mg) were then added to the SDS/water solution. This polymerization mixture was then slowly added to the heated seed solution, at a rate of 25 $mL.h^{-1}$ using a syringe pump. Once the addition was completed, nitrogen was bubbled through the polymerization reaction for an additional 10 minutes. The polymerization was then left to stir at 70 °C for 12 hours. The final CS nanogels were purified *via* dialysis against nanopure water (MW cut off 12-14 kDa). The amount of NIPAM used in the polymerization was based on the mass of the original hydrophobic core where CS nanogels with double the mass were synthesized. Hence, the mass of the core is equal to the mass of the shell which in theory also doubles the radius of the particles.

5.6.6. Synthesis of CSC nanogels with PNIPAM shell and corona

The core-shell-corona nanogels were synthesized in a one-pot-two-step reaction where the first step involved the formation of a small cross-linked NIPAM shell and second step the growth of linear NIPAM polymers from the cross-linked NIPAM shell. The first step was carried out following the procedure explained above for synthesis of CS nanogels. In a similar fashion, the seed nanogel particles (25 mL) was heated at 70 °C and bubbled with nitrogen. However, instead of making a single pot containing all the NIPAM monomer and cross-linker, the monomer was separated into two reaction mixtures. The first mixture, used to synthesize the cross-linked shell consisted of NIPAM (0.110 g), Bis (0.5 mg, 0.5 wt%), SDS (0.009 g), KPS (2.5 mg) and water (12.5 mL). This solution was added slowly to the heated seed particles, under nitrogen and allowed to proceed for 20 minutes.

The second pot of polymerization mixture consisted of the remaining NIPAM monomer (0.110 g), SDS (0.009 g) and water (12.5 mL). No additional initiator was added, as this allows NIPAM to react with the active radicals present in the shell from the first polymerization process. As no cross-linker was present in the second monomer solution, linear NIPAM polymer chains will result, forming the corona layer. The CSC nanogels were purified *via* dialysis against nanopure water (MW cut off 12-14 kDa).

5.6.6.1. Monitoring growth of shell and corona by DLS

The CSC nanogel synthesis was set up as described above. An aliquot was withdrawn from the polymerization after 10 min, diluted with nanopure water, filtered (through a 0.45 µm filter) and analyzed by DLS at 5 °C. Aliquots were then withdrawn at 5 min intervals. After a similar D_h had been observed for 30 min of consecutively withdrawn aliquots, the second step of the polymerization was initiated (corona synthesis). The first aliquot was withdrawn after 5 min and then at 10 min intervals for 45 min. The polymerization was allowed to proceed for an additional 12 hours after which is was quenched by cooling to RT and exposure to air. The resulting CSC nanogels were purified *via* dialysis against nanopure water (MW cut off 12-14 kDa).

5.6.7. Aldol reaction: a representative procedure

4-Nitrobenzaldehyde (0.038 g, 0.25 mmol, 1 eq) was dissolved in cyclohexanone (0.104 mL, 1 mmol, 4 eq) and mixed with the functionalized nanogel (0.0025 mmol, 1 mol%). The reaction mixture was homogenized by vigorous shaking and allowed to stir at the desired temperature for 24 hours. The reaction was quenched *via* the addition of diethyl ether (Et_2O) which was used to extract the product from the nanogel core. The nanogels remained in the aqueous phase, as the NIPAM shell is insoluble in Et_2O. Extraction was carried our numerous times until the aqueous phase was no longer yellow. The organic phases were then combined, dried *in vacuo* and the crude product characterized by ^1H

NMR spectroscopy determining the reaction conversion and product diastereomeric *anti/syn* ratio. The crude product was then filtered through a small column of silica and the product enantiomeric excess (*ee*) determined by chiral HPLC (ChiralPak IA, 80:10:10 hexane:propan-2-ol:ethanol, 1.0 $mL.min^{-1}$.

(S)-2-((R)-hydroxyl-(4-nitrophenyl)methyl)-cyclohexan-1-one: ^{1}H NMR (400 MHz, $CDCl_3$): δ = 1.19-2.57 (8H, m, C**H**$_2$), 4.00 (1H, s, O**H**), 4.82 (1-xH, d, J = 4.5 Hz, C**H**, anti), 5.41 (xH, C**H**, syn), 7.44 (2H, d, J = 8.6 Hz, Ar-**H**), 8.15 (2H, d, J = 8.6 Hz, Ar-**H**). ^{13}C NMR (400 MHz, $CDCl_3$): δ = 24.9, 27.0, 36.5, 42.0, 57.0, 74.0, 123.7, 127.9, 147.3, 148.5, 213.3. ESI-MS found: 272.1 ($M+Na^+$) $C_{13}H_{15}NO_4$; expected 249.10. Chiral HPLC: minor enantiomer t_R = 12.4 min, major enantiomer t_R = 18.3 min. This compound has been fully characterized by others.[13, 52, 59-61]

5.6.8. Recycling protocol

5.6.8.1. Protocol 1

The first catalytic cycle was carried out as previously described. The reaction was quenched *via* the addition of diethyl ether (Et_2O) and the two phased mixture was shaken to extract the aldol product from the nanogel core. Et_2O was then removed and the aqueous system further extracted by Et_2O, and this process was repeated until the extracted Et_2O was no longer colour (yellow from the product and starting aldehyde). The combined Et_2O layers were dried and the crude product characterized by ^{1}H NMR spectroscopy. Residual Et_2O in the remaining aqueous solution was removed *via* a flow of air. A new batch of reagents was subsequently added to the stirring nanogel solution and a second cycle was allowed to proceed. The same work-up procedure was applied after each cycle.

5.6.8.2. Protocol 2

Similarly, Et_2O was added to both quench the reaction and for extraction of products from the nanogel core. Multiple extractions were carried out until the Et_2O was no longer coloured, which was then dried and analyzed by ^1H NMR spectroscopy. The remaining aqueous phase was completely dried and re-dispersed into fresh nanopure water. The white colour of the dry polymer indicated all aldol product and unreacted starting reagents had been successfully extracted from the nanogels. After re-dispersion, the nanogel was stirred in the fridge overnight and then allowed to equilibrate in room temperature, under constant stirring. In a second cycle, 4-nitrobenzaldehyde (0.038 mg, 1 eq) was dissolved in cyclohexanone (0.104 mL, 4 eq) and added to the recovered and re-dispersed nanogel solution and homogenized by vigorous shaking. After 24 hours, the same work-up/recovery procedure was applied.

5.7. References

1. J.-H. Ryu, S. Jiwpanich, R. Chacko, S. Bickerton and S. Thayumanavan, *J. Am. Chem. Soc.*, 2010, **132**, 8246.

2. D. C. González-Toro, J.-H. Ryu, R. T. Chacko, J. Zhuang and S. Thayumanavan, *J. Am. Chem. Soc.*, 2012, **134**, 6964.

3. Y. Koda, T. Terashima, A. Nomura, M. Ouchi and M. Sawamoto, *Macromolecules*, 2011, **44**, 4574.

4. J. Xu, G. Chen, R. Yan, D. Wang, M. Zhang, W. Zhang and P. Sun, *Macromolecules*, 2011, **44**, 3730.

5. T. Terashima, A. Nomura, M. Ito, M. Ouchi and M. Sawamoto, *Angew. Chem. Int. Ed.*, 2011, **50**, 7892.

6. T. Terashima, A. Nomura, M. Ouchi and M. Sawamoto, *Macromol. Rapid Commun.*, 2012, **33**, 833.

7. Y. Liu, Y. Wang, Y. Wang, J. Lu, V. Piñón and M. Weck, *J. Am. Chem. Soc.*, 2011, **133**, 14260.

8. B. Helms, S. J. Guillaudeu, Y. Xie, M. McMurdo, C. J. Hawker and J. M. J. Fréchet, *Angew. Chem. Int. Ed.*, 2005, **44**, 6384.

9. P. Cotanda, A. Lu, J. P. Patterson, N. Petzetakis and R. K. O'Reilly, *Macromolecules*, 2012, **45**, 2377.

10. B. Helms, C. O. Liang, C. J. Hawker and J. M. J. Fréchet, *Macromolecules*, 2005, **38**, 5411.

11. P. Cotanda and R. K. O'Reilly, *Chem. Commun.*, 2012, **48**, 10280.

12. D. Enders, M. R. M. Hüttl, C. Grondal and G. Raabe, *Nature*, 2006, **441**, 861.

13. M. Gruttadauria, F. Giacalone, A. Mossuto Marculescu, P. Lo Meo, S. Riela and R. Noto, *Eur. J. Org. Chem.*, 2007, **28**, 4688.

14. N. Mase, Y. Nakai, N. Ohara, H. Yoda, K. Takabe, F. Tanaka and C. F. Barbas, *J. Am. Chem. Soc.*, 2005, **128**, 734.

15. D. E. Bergbreiter, *Catal. Today*, 1998, **42**, 389.

16. D. E. Bergbreiter, P. L. Osburn and C. Li, *Org. Lett.*, 2002, **4**, 737.

17. C. N. Urbani and M. J. Monteiro, *Macromolecules*, 2009, **42**, 3884.

18. S. Li, Y. Ge, A. Tiwari, S. Wang, A. P. F. Turner and S. A. Piletsky, *J. Catal.*, 2011, **278**, 173.

19. Z. Ge, D. Xie, D. Chen, X. Jiang, Y. Zhang, H. Liu and S. Liu, *Macromolecules*, 2007, **40**, 3538.

20. R. Ma and L. Shi, *Macromol. Biosci.*, 2010, **10**, 1397.

21. S. Li, Y. Ge, A. Tiwari and S. Cao, *Small*, 2010, **6**, 2453.

22. H. Zhang, L. Ding, Y. Chen, W. Yang and J. Deng, *J. Polym. Sci., Part A: Polym. Chem.*, 2012, **50**, 4415.

23. S. Li and S. Gong, *J. Phys. Chem. B*, 2009, **113**, 16501.

24. S. F. M. van Dongen, W. P. R. Verdurmen, R. J. R. W. Peters, R. J. M. Nolte, R. Brock and J. C. M. van Hest, *Angew. Chem. Int. Ed.*, 2010, **49**, 7213.

25. A. K. Diallo, E. Boisselier, L. Liang, J. Ruiz and D. Astruc, *Chem. Eur. J.*, 2010, **16**, 11832.

26. J. C. Park, H. J. Lee, J. Y. Kim, K. H. Park and H. Song, *J. Phys. Chem. C*, 2010, **114**, 6381.

27. Y. Lan, L. Yang, M. Zhang, W. Zhang and S. Wang, *ACS Appl. Mater. Interfaces*, 2009, **2**, 127.

28. J. Gaitzsch, D. Appelhans, L. Wang, G. Battaglia and B. Voit, *Angew. Chem. Int. Ed.*, 2012, **51**, 4448.

29. N. Giuseppone and J.-F. Lutz, *Nature*, 2011, **473**, 40.

30. T. Mes, R. van der Weegen, A. R. A. Palmans and E. W. Meijer, *Angew. Chem. Int. Ed.*, 2011, **50**, 5085.

31. R. Biswas, N. Maillard, J. Kofoed and J.-L. Reymond, *Chem. Commun.*, 2010, **46**, 8746.

32. Y. Lu, J. Yuan, F. Polzer, M. Drechsler and J. Preussner, *ACS Nano*, 2010, **4**, 7078.

33. S. Li, Y. Ge and A. P. F. Turner, *Adv. Funct. Mater.*, 2011, **21**, 1194.

34. D. Valade, Y. Jeon, S. Kessel and M. J. Monteiro, *J. Polym. Sci. A Polym. Chem.*, 2012, **50**, 4762.

35. G. Wei, W. Zhang, F. Wen, Y. Wang and M. Zhang, *J. Phys. Chem. C*, 2008, **112**, 10827.

36. B. R. Saunders, H. M. Crowther and B. Vincent, *Macromolecules*, 1997, **30**, 482.

37. I. Berndt and W. Richtering, *Macromolecules*, 2003, **36**, 8780.

38. C. D. Jones and L. A. Lyon, *Macromolecules*, 2000, **33**, 8301.

39. T. E. Kristensen, F. K. Hansen and T. Hansen, *Eur. J. Org. Chem.*, 2009, **3**, 387.

40. I. Varga, T. Gilányi, R. Mészáros, G. Filipcsei and M. Zrínyi, *J. Phys. Chem. B*, 2001, **105**, 9071.

41. N. Welsch, M. Ballauff and Y. Lu, *Chemical Design of Responsive Microgels*, 2011, 234, 129, Springer Berlin Heidelberg.

42. H. G. Schild, *Prog. Polym. Sci.*, 1992, **17**, 163.

43. T. Hellweg, C. D. Dewhurst, W. Eimer and K. Kratz, *Langmuir*, 2004, **20**, 4330.

44. J. P. Patterson, A. M. Sanchez, N. Petzetakis, T. P. Smart, I. I. I. T. H. Epps, I. Portman, N. R. Wilson and R. K. O'Reilly, *Soft Matter*, 2012, **8**, 3322.

45. Y. Lu, A. Wittemann, M. Ballauff and M. Drechsler, *Macromol. Rapid Commun.*, 2006, **27**, 1137.

46. H. Iwamura, D. H. Wells, S. P. Mathew, M. Klussmann, A. Armstrong and D. G. Blackmond, *J. Am. Chem. Soc.*, 2004, **126**, 16312.

47. N. S. Ieong, K. Brebis, L. E. Daniel, R. K. O'Reilly and M. I. Gibson, *Chem. Commun.*, 2011, **47**, 11627.

48. J. J. Crassous, M. Ballauff, M. Drechsler, J. Schmidt and Y. Talmon, *Langmuir*, 2006, **22**, 2403.

49. S. Lv, L. Liu and W. Yang, *Langmuir*, 2009, **26**, 2076.

50. A. Balaceanu, Y. Verkh, D. E. Demco, M. Möller and A. Pich, *Macromolecules*, 2013, **46**, 4882.

51. J. C. Park, J. U. Bang, J. Lee, C. H. Ko and H. Song, *J. Mater. Chem.*, 2010, **20**, 1239.

52. F. Giacalone, M. Gruttadauria, P. L. Meo, S. Riela and R. Noto, *Adv. Synth. Catal.*, 2008, **350**, 2747.

53. S. Calogero, D. Lanari, M. Orrù, O. Piermatti, F. Pizzo and L. Vaccaro, *J. Catal.*, 2011, **282**, 112.

54. Y.-X. Liu, Y.-N. Sun, H.-H. Tan, W. Liu and J.-C. Tao, *Tetrahedron: Asymmetry*, 2007, **18**, 2649.

55. J. Ribas-Arino, M. A. Carvajal, A. Chaumont and M. Masia, *Chem. Eur. J.*, 2012, **18**, 15868.

56. S. Bahmanyar and K. N. Houk, *J. Am. Chem. Soc.*, 2001, **123**, 12911.

57. M. B. Schmid, K. Zeitler and R. M. Gschwind, *Chem. Sci.*, 2011, **2**, 1793.

58. T. E. Kristensen, K. Vestli, M. G. Jakobsen, F. K. Hansen and T. Hansen, *J. Org. Chem.*, 2010, **75**, 1620.

59. D. Font, C. Jimeno and M. A. Pericas, *Org. Lett.*, 2006, **8**, 4653.

60. N. Zotova, A. Franzke, A. Armstrong and D. G. Blackmond, *J. Am. Chem. Soc.*, 2007, **129**, 15100.

61. A. J. A. Cobb, D. M. Shaw, D. A. Longbottom, J. B. Gold and S. V. Ley, *Org. Biomol. Chem.*, 2005, **3**, 84.

Conclusions

As a result of the advances made in polymerization techniques, a range of well-defined nanostructures with multiple functionalities in any desired morphology can now be readily synthesized. This allows us to directly attach the desired functionality onto a polymer scaffold and carry out organic reactions in water with high efficiency as a result of hydrophobic and concentrator effects. The successful incorporation of the catalytically active amino acid L-proline into a number of polymer scaffolds, including self-assembled polymer micelles and cross-linked nanogels was presented in this thesis. Their application as nanoreactors for organic reactions in water has been evaluated using a model asymmetric aldol reaction. Their ability to sequester organic and hydrophobic molecules from the surrounding aqueous media was demonstrate by the high catalytic activity observed at significantly lower catalyst loading than previously reported by the unsupported catalyst in organic media. Furthermore, by introducing a thermo-responsive shell, readily recyclable nanoreactors were achieved with interesting temperature dependent activity. We have also shown that we can tailor the catalytic activity of our nanoreactors by tuning the concentration of hydrophobic material in the reaction, allowing more reagents to be sequestered from the surrounding environment.

We believe that recent advances in polymer technology have allowed us to, with great control and efficiency, synthesize well-defined nanoreactors with any desired functionality for a range of reactions. Hopefully in the future we can extend these synthetic systems to include the structural complexity of natural systems.

I. Appendix: Collaborative Work

Work undertaken with Professor Michael Monteiro, Australian Institute for Bioengineering and Nanotechnology, University of Queensland, Brisbane, Australia

This work was published in ACS Macro Letters under the heading 'Thermoresponsive Polymer-Supported L-Proline Micelle Catalysts for the Direct Asymmetric Aldol Reactions in Water'

ACS Macro Lett., **2013**, 2, 327-331, doi: 10.1021/mz4000943

The self-assembly of thermo-responsive block copolymers containing L-proline moieties as catalytic nanoreactors was investigated and applied to the catalysis of a model aldol reaction. Poly(*N*-isopropylacrylamide) (PNIPAM) exhibits a lower critical solution temperature (LCST), below which it is water soluble and above which it is not. As a result of this thermo-responsive property, a temperature-dependent self-assembly process can be achieved when PNIPAM is used as the core-forming segment in a block copolymer.

To this end, a block copolymer with a permanently hydrophilic block, poly(dimethacrylamide) (PDMA), and a thermo-responsive block, PNIPAM containing L-proline functionalities was synthesized using reversible addition-fragmentation chain transfer (RAFT) polymerization (Scheme I.1).

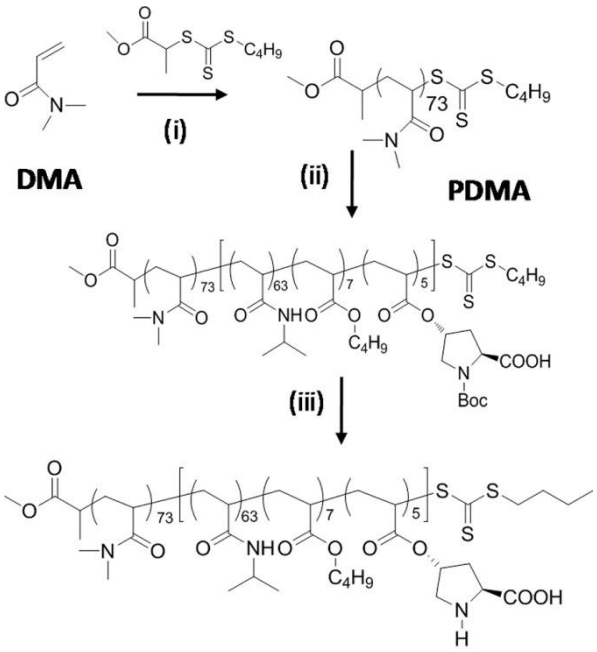

Scheme I.1. (i) Synthesis of PDMA, (ii) synthesis of block copolymer containing L-proline moieties and (iii) deprotection of Boc protected L-proline to yield catalytically active thermo-responsive block copolymer

Upon self-assembly of the synthesized copolymer, micelles approximately 15-20 nm in size were formed at temperatures above the LCST (> 25 °C) with the catalytic motifs contained within the hydrophobic PNIPAM core (Figure **I.1**). The self-assembly temperature was tailored by incorporating butyl acrylate (BuA) units into the PNIPAM block.

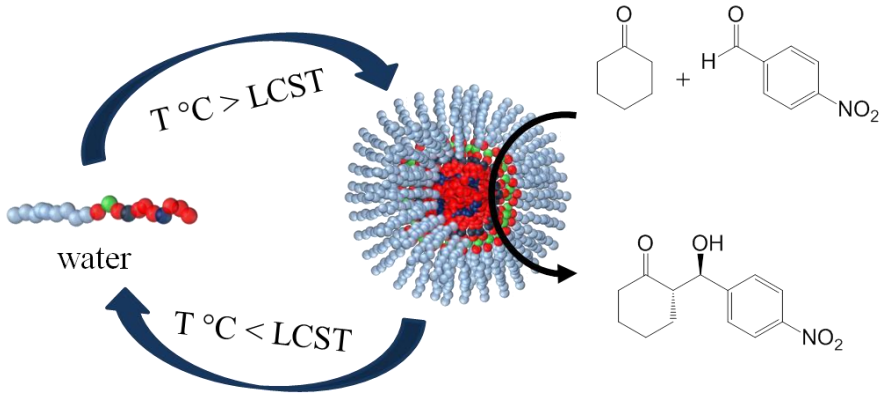

Figure I.1. **Self-assembly of PDMA-*b*-P(NIPAM-*co*-BuA-*co*-ProA) at temperatures above the LCST of PNIPAM, micelle catalyzed asymmetric aldol reaction and subsequent disassembly of micelles below LCST**

The catalytic activity, with respect to a model aldol reaction, of the polymer micelles (10 mol% catalyst loading, LCST ~35 °C) was investigated over a series of temperatures: (a) 25 °C in the absence of micelles, (b) 35 °C at the start of micellization, (c) 40 °C during micellization and finally (d) 50 °C above the LCST of the micelles. High catalytic activity was achieved in the presence of the micelles (80-95% conversion, 96% *ee*). Comparatively lower conversions were observed at 25 °C, which was attributed to the absence of micelles (53% conversion, 96% *ee*). The importance of the hydrophobic pocket presented upon self-assembly was further highlighted by the fact that less than 6% conversion was achieved when catalysis was accomplished by the fully hydrophilic PDMA-*b*-P(DMA-*co*-ProA), at elevated temperatures.

The recycling efficiency of micelle system was also investigated; this was achieved by lowering the temperature to completely disassemble the micelles and resulting in precipitation of the aldol product in near pure form. The product was collected by centrifugation and the polymer-containing aqueous solution reused in additional catalytic cycles. Although small losses in conversions were observed after five catalytic cycles, the selectivity remained high and represents an elegant solution to the use and reuse of organocatalysts in aqueous media.